Institut für Experimentelle und Klinische Pharmakologie und Toxikologie
der Medizinischen Fakultät der Universität des Saarlandes

Dissertation

GENETISCHE STRATEGIEN ZUR UNTERSUCHUNG KÖRPERHOMÖOSTASE KONTROLLIERENDER HYPOTHALAMISCHER ZELLPOPULATIONEN IN DER MAUS

vorgelegt von
Philipp Wartenberg
geboren am 12. Januar 1986
in Mainz, Deutschland
2021

zur Erlangung des akademischen Grades des Doktors der Naturwissenschaften

Department of Pharmacology and Toxicology Saarland University School of Medicine

Dissertation

GENETIC STRATEGIES TO DISSECT HYPOTHALAMIC CELL POPULATIONS CONTROLLING BODY HOMEOSTASIS IN MICE

submitted by
Philipp Wartenberg
born on the 12th of January 1986
in Mainz, Germany
2021

In partial fulfilment of requirements for the degree of Doctor of Philosophy

Tag der Promotion:	27.10.2021
Dekan:	Prof. Dr. M. Menger
Berichterstatter:	Prof. Dr. U. Boehm
	Prof. Dr. F. Kirchhoff
	Prof. Dr. S. Urbschat
Tag der Abgabe der Dissertation:	04. März 2021

Zusammenfassung

Der Hypothalamus, lokalisiert im Diencephalon in der Nähe der Eminentia mediana (ME) und der Hypophyse, steuert die Körperhomöostase und die Fertilität durch die Freisetzung von Hormonen und die Integration von Rückmeldungen aus der Peripherie. Um diese Körperachsen, wie die sexuell dimorphe Hypothalamus-Hypophysen-Gonaden-Achse (HPG-Achse), zu koordinieren, besteht der Hypothalamus aus zahlreichen Zelltypen, die jeweils ein spezifisches Repertoire an Proteinen exprimieren. Die Ionenkanalfamilie der Transient-Receptor-Potential (TRP)-Kanäle ist essentiell für diese Koordinierung und ist in zahlreichen Organen exprimiert. Die TRP-Expressionsmuster im Gesamtorganismus, vor allem aber im Hypothalamus, sind von großem Interesse, aber zuverlässige Daten mit zellulärer Auflösung fehlen aus unterschiedlichen Gründen. TRP-Kanäle sind in der Membran lokalisiert, werden posttranslational glykosyliert und zeigen in der Regel ein eher niedriges Expressionsniveau. Dies erschwert die epitopgerichtete Antikörperproduktion und den Nachweis auf RNA-Ebene, gerade auch im Hypothalamus. Reportermäuse, die diese Zellpopulationen mit einem Fluoreszenzfarbstoff markieren, können genutzt werden, um diese Schwierigkeiten zu umgehen. Um die TRP-Expression im Hypothalamus zu untersuchen und für jeden TRP-Kanal die spezifischen Zelltypen zu identifizieren, habe ich die neu generierten TRPM5- TRPM6-, TRPV6-, TRPA1-, TRPML3-, TRPC2-, TRPC4- und TRPC5-τGFP Reportermäuse und iDISCO-Clearing verwendet. Eine Subpopulation von Tanyzyten im dritten Ventrikel exprimiert TRPM5 und stehen potenziell im bidirektionalen Austausch mit dem Blutkreislauf über ihre Fasern welche in Richtung der fenestrierten Endothelzellen in der ME projizieren. Zusätzlich zu den Tanyzyten identifizierte ich TRPM5 sowie TRPC5- und TRPA1 Zellen in der Pars tuberalis in engem Kontakt mit Blutgefäßen. Interessanterweise wird TRPV6 nicht im Gehirn exprimiert, während TRPM6 in jedem Blutgefäß der Blut-Hirn-Schranke zu finden ist. TRPC4 wurde in Perizyten identifiziert, welche ihre Fasern um Blutgefäße wickeln, und τGFP-Expression wurde in Fasern in der ME von TRPC2-Reporter Tieren gefunden. Diese Fasern stehen in engem Kontakt mit fenestrierten Blutgefäßen im posterioren Teil der ME, was darauf hindeutet, dass diese Fasern hier terminieren. Diese Fasern haben ihren Urpsrung in akut TRPC2 exprimierenden Neuronen im paraventrikulären Nukleus (PVN), die ventro-lateral in die ME projizieren. Eine kleine Subpopulation dieser Neurone exprimiert ebenfalls Corticotropin-Freisetzendes-Hormon (CFH), aber Ablation oder synaptisches silencing von TRPC2 Neuronen hatte keinen Einfluss auf den Adrenocorticotropin (ACTH)-Spiegel. Die Aktivierung von TRPC2 Neuronen führte zu erhöhten luteinisierendem Hormon (LH) und follikelstimulierendem Hormon (FSH) Spiegeln. Dies deutet auf eine mögliche Rolle der TRPC2 Neuronen bei der Regulation der Hormonfreisetzung in der ME hin. Die HPG-Achse wird durch Sexualhormone, wie z. B. Östrogen, in sexuell dimorpher Weise gesteuert. Das geschwindigkeitsbestimmende Enzym für die Östrogensynthese ist Aromatase. Um zu verstehen, wie Östrogen die sexuelle Differenzierung beeinflusst, habe ich die Aromatase-Expression während der embryonalen und pränatalen Entwicklung untersucht. Hierzu nutzte ich ebenfalls eine Cre-Reportermaus, die die Aromatasezellen mit τGFP markiert. Aromataseneurone waren erstmals am Embryonaltag 13,5 (E13,5) sichtbar und nahmen bis E16,5 in ihrer Anzahl dramatisch zu. Bei der Geburt zeigte sich ein ausgeprägter sexueller Dimorphismus im Nucleus arcuatus (Arc). Hier wird Aromatase nur in männlichen Tieren exprimiert. Die Mehrheit der Östrogenrezeptor (ÖR) exprimierenden Neurone ist Aromatase negativ. Dies deutet darauf hin, dass Aromataseneurone entweder in den Gonaden oder im Gehirn synthetisiertes Testosteron in Östrogen umwandeln können, um die Neuronenaktivität über ÖR-abhängige parakrine Mechanismen zu regulieren. Um diese Hypothese zu testen, haben wir in Zusammenarbeit mit der Gruppe von Prof. Erik Hrabovszky wholecell-Patch-Clamp Experimente an Kisspeptin Neuronen im Arc durchgeführt. Diese

Neurone sind östrogen-sensitiv und Aromatase-negativ. Testosteron reduzierte die Erregbarkeit der Kisspeptin-Neuronen um ~50% und die Applikation des Aromatase-Inhibitors Letrozol oder des ÖR-Inhibitors ICI182780 verhinderte diesen Effekt vollständig. Meine Ergebnisse liefern detaillierte räumlich-zeitliche Informationen über die Entwicklung von Aromatase-Neuronen. Außerdem heben sie einen neuartigen parakrinen Mechanismus hervor, durch den Aromataseneurone die Aktivität verschiedener neuronaler Populationen, die ÖRs exprimieren, regulieren.

Abstract

The hypothalamus, located in the diencephalon, close to the median eminence (ME) and the pituitary gland controls body homeostasis by the release of hormones and integration of periphery feedback. To orchestrate these body axes, such as the sexually dimorphic hypothalamus-pituitary-gonadal axis (hpg-axis), the hypothalamus consists of numerous cell populations, each expressing a specific repertoire of proteins. The ion channel family of transient receptor potential (TRP) channels is essential for this orchestration and is widely expressed in the body. TRP-expression patterns with cellular resolution are of great interest, especially in the hypothalamus, but detection is challenging due to multiple reasons. TRP channels are membrane-bound proteins, posttranslationally glycosylated and their expression levels are generally rather low. This makes epitope-directed antibody production and detection at the RNA level with cellular resolution difficult, unfortunately including the hypothalamus. Reporter mice which label these cell populations with a fluorescent marker, are an elegant tool to overcome these caveats. To investigate TRP expression in the hypothalamus and to identify the individual cell type for each TRP channel, I utilized the newly generated TRPM5, TRPM6, TRPV6, TRPA1, TRPML3, TRPC2, TRPC4 and TRPC5 τGFP-reporter mice and iDISCO clearing. TRM5 is expressed in a subpopulation of tanycytes at the floor of the third ventricle, having access to blood-borne cues via processes extended towards diaphragmed endothelial fenestrations, potentially mediating bidirectional communication between the cerebrospinal fluid and the blood. In addition to tanycytes, I identified TRPM5, and also TRPC5 and TRPA1 cells in the pars tuberalis in close contact with blood vessels. Interestingly, TRPV6 is not expressed in the brain, whereas TRPM6 was found in every blood vessel of the blood brain barrier (BBB). TRPC4 was identified in pericytes, wrapping their processes around blood vessels and τGFP expression was found in fibers in the ME of TRPC2 reporter animals. These fibers are in close contact with fenestrated blood vessels in the posterior ME, indicating that these fibers terminate here. I identified the origin of these fibers in acutely TRPC2 expressing neurons in the paraventricular nucleus (PVN), projecting ventro-latterally into the ME. A subset of these neurons co-express corticotropin-releasing-hormone (CRH), but ablation or silencing of TRPC2 neurons did not have an effect on adrenocorticotropin (ACTH) levels. Activation of TRPC2 neurons resulted in increased luteinizing hormone (LH) and follicle-stimulating hormone (FSH) levels. This shows a potential role of TRPC2 neurons in mediating hormone release in the ME. The hpg-axis is controlled by sex steroids, such as oestrogen, in a sexually dimorphic manner. The rate-limiting enzyme for oestrogen synthesis is aromatase. To gain a better understanding how oestrogen impacts sexual differentiation, I investigated aromatase expression through embryonic and prenatal development. To address this question, I capitalized on a Cre reporter mouse which labels aromatase cells with τGFP. Aromatase neurons were first visible at embryonic day 13.5 (E13.5) and dramatically increased in number by E16.5. At birth I revealed a prominent sexual dimorphism in the arcuate nucleus (Arc). Here, aromatase is only expressed in male animals. The majority of oestrogen receptor (ER)-expressing neurons were devoid of aromatase. This indicates that aromatase neurons can convert gonadal and/or brain-born testosterone to oestrogens to regulate neuron activity via ER-dependent paracrine mechanisms. To test this hypothesis we collaborated with the group of Prof. Erik Hrabovszky to perform whole-cell-patch-clamp experiments on kisspeptin neurons in the Arc. These neurons are oestrogen sensitive and are not co-expressing aromatase. Testosterone reduced kisspeptin neuron firing by ~50% and bath application of the aromatase inhibitor Letrozole or the ER-inhibitor ICI182780 entirely prevented this effect. My study provides detailed spatio-temporal information on aromatase neuron development and highlights a novel paracrine mechanism whereby aromatase neurons regulate the activity of distinct neuronal populations expressing ERs.

Für den Krümel

Contents

1 Introduction

The hypothalamus, located in the diencephalon, close to the median eminence (ME) and the pituitary gland controls body homeostasis by the release of hormones and receives feedback from the periphery. To orchestrate these body axes, such as the sexually dimorphic hypothalamic-pituitary-gonadal axis (hpg-axis), the hypothalamus, in contrast to the hippocampus or cerebellum, consists of heterogeneously groups of multiple unique neuronal clusters (D. W. Kim *et al.*, 2020), each expressing a specific repertoire of proteins including ion channels. The ion channel family of transient receptor potential (TRP) channels are essential for controlling body axes and are widely expressed, but their body-wide expression patterns at a cellular resolution is still largely unclear. Investigation of their expression is challenging. Antibodies against TRP channels are difficult to produce because TRP channels are located in the membrane and posttranslationally glycosylated. This blocks most of the epitopes needed for specific antibody binding. Due to low expression levels, mRNA detection with *in situ* hybridisation to gain a cellular resolution is difficult. One strategy to overcome this caveat is to generate reporter mice which reliable label TRP-expressing cells with a fluorophore. These reporter animals can be used for body-wide mapping of TRP-expressing cell populations.
Sex steroids, such as oestrogen, are in control of gender typical behaviours, fertility and sexual differentiation in early development, rendering the hpg-axis sexually dimorphic. Oestrogens are synthesized from androgens, such as testosterone by the enzyme aromatase, located in the membrane of the endoplasmic reticulum. This localization and low expression levels, especially during embryogenesis, makes mapping of aromatase expression with antibodies or *in situ* hybridization difficult. Reporter mice in combination with binary genetic strategies labelling the cells with a fluorophore overcome these caveats and enable the investigation of the onset of aromatase expression and its influence on sexual differentiation.

1.1 Binary genetic strategies for cell labelling

Genetically modified mouse models are a powerful tool to visualize and manipulate specific cell populations. Two different strategies are used for this purpose, transgenic mouse lines and knock-in mouse lines. Transgenic mouse lines are generated by microinjection of DNA (plasmids or bacterial artificial chromosome containing a transgene and regulatory elements) into a zygote pronucleus where the DNA integrates randomly into the genome, often at numerous sites. A downside to this approach is, that expression of the transgene can be influenced by the local chromatin structure and it can also have unwanted effects at the locus of integration. This can result in either inappropriate levels of transgene expression or the observation of phenotypes in the resulting mouse line which can complicate subsequent analyses.
Knock-in mice are generated by gene targeting, facilitating targeted integration of foreign DNA into the genome via homologous recombination into a specific locus. Transgenes are directly controlled by regulatory elements within a specific locus, resulting in faithful transgene expression under endogenous promotor activity. This is a huge advantage over transgenic animals. For visualization of cell populations of interest, the Cre/loxP system offers an elegant approach. This system facilitates the generation of mouse lines containing a combination of alleles by simple breedings. Knock-in mice express Cre under the control of an endogenous promotor, such that Cre reflects the expression pattern of the desired gene of interest. These mice can be bred to reporter mice that contain Cre-dependent genetic elements. These elements are often under the control of a ubiquitously active promotor such as within the ROSA26 (R26) locus. Through gene targeting, these Rosa-mice contain

an additional gene (for example a fluorescence protein) that is only expressed when the Cre-dependent stop cassette is removed. This cassette is a strong transcriptional stop signal flanked by loxP sites. These sites are recognized by Cre and after Cre-mediated removal of the floxed STOP signal, allow expression of the transgene. An important characteristic of this approach is that cells are labelled throughout their lifetime, even when the Cre-expressing locus is no longer active. This facilitates consistent expression of reporter genes and identifies every cell that has previously expressed the gene of interest. This is particular useful for proteins that are difficult to detect such as TRP channels and aromatase. By using this binary genetic approach to express reporter genes in these cells, they can be reliably visualized and further manipulated (Figure 1).

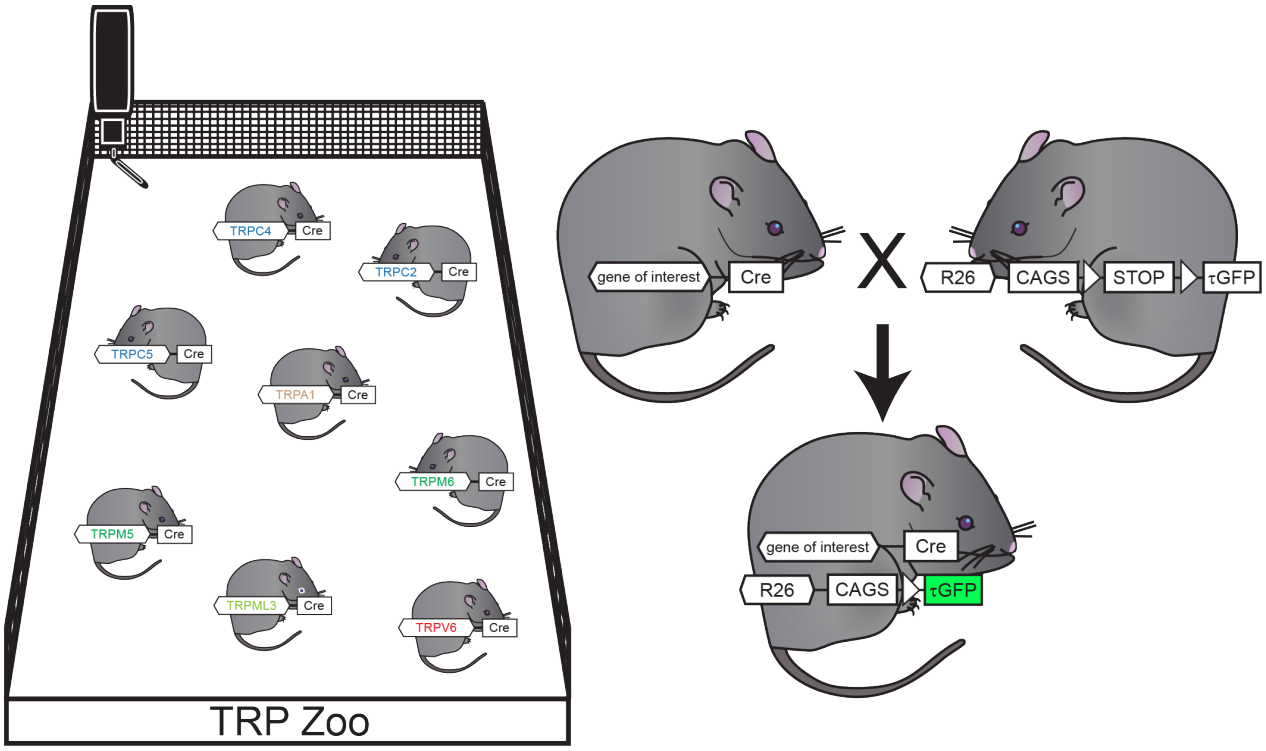

Figure 1: The Cre-Zoo. Cre-driver lines used in this thesis on the left. Breeding these different Cre drivers with the enhanced-ROSA26/τGFP (eR26-τGFP) reporter mouse line enables mapping of expression with cellular resolution on a body-wide scale. Cre removes the stop signal in the *ROSA26* locus by interacting with the two loxP sites flanking the stop signal.

1.2 Transient receptor potential channels

The TRP channel superfamily is one of the largest ion-channel families consisting of 28 members divided into seven subfamilies. They were first discovered in Drosophila melanogaster by Minke, Wu and Pak in 1975 (Minke *et al.*, 1975), observing an abnormal behavioural phenotype in response to light in a mutant strain of flies. Their electroretinogram showed a transient receptor potential to constant light and this is the origin of the name TRP. The seven subfamilies include TRPC (canonical), TRPV (vanilloid), TRPM (melastatin), TRPP (polycystin), TRPML (mucolipin), TRPA (ankyrin) and TRPN (NOMPC-like). The subfamilies show a sequence homology of 30% to 47% between subfamilies and up to 90% between members of the same subfamily. All TRP channels share the same structure of 6 transmembrane domains which form a homotetrameric channel complex with N- and C-termini which are located in the cytosol (Figure 2). The voltage-sensing region is formed by the transmembrane domains one to four and the pore is established between transmembrane domains five and six (Liedtke *et al.*, 2007).

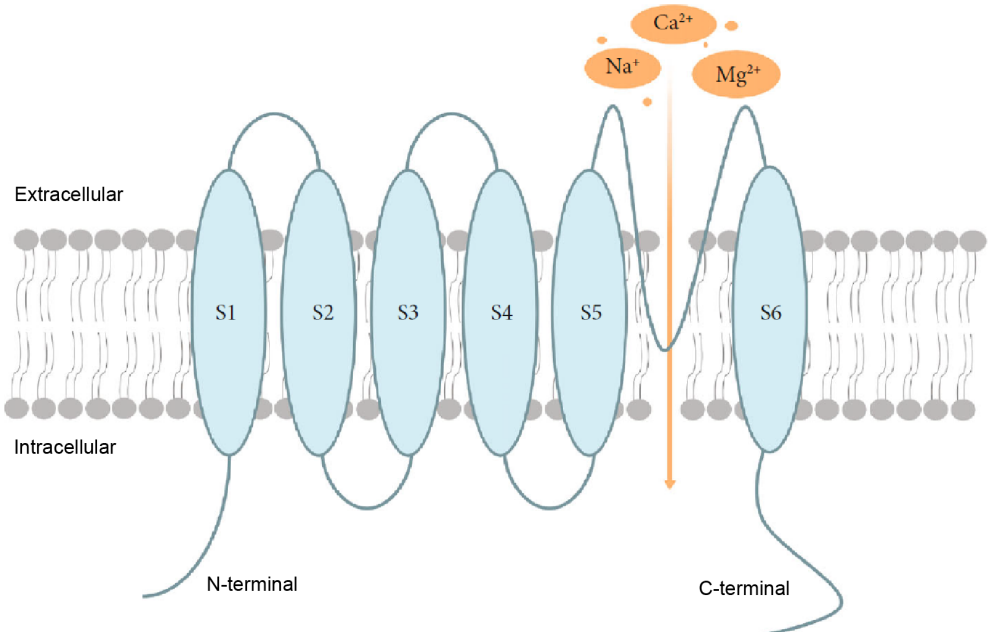

Figure 2: Schematic representation of TRP channels. TRP channels consist of 6 transmembrane domains and variable intracellular N- and C-termini, with a reentry loop that forms a pore located between S5 and S6. As cation channels, this structure constitutes an influx pathway mostly for Ca^{2+}, Na^{+}, and Mg^{2+}. Figure legend and figure reproduced from Ostrowski *et al.*, 2020.

TRP channels show permeability to both monovalent and divalent cations. They present multiple activation methods such as ligand binding, voltage, changes in temperatures and modifications of nucleophilic residues (Bernd Nilius and Owsianik, 2011). TRP channels are expressed in a variety of organs and display a plethora of functions. They function as cellular sensors and are involved in ion homeostasis and regulation of intracellular signalling, mostly by providing entry pathways for Ca^{2+}. It is not surprising that human diseases are linked to dysfunctions within TRP channels. For example TRPC4 mutations are linked to severe pulmonary arterial hypertension (Alzoubi *et al.*, 2013), TRPM4 mutations lead to cardiac conduction disease (Kruse *et al.*, 2009) and malfunction in TRPML1 causes a dysregulation of lysosome function (Bach, 2005).
TRP channels are located in the plasma membrane, form complexes with other TRP channels and are often

posttranslationally glycosylated. This makes antibody production difficult, as they need to bind to channel-specific epitopes for detection and are expressed at low levels, which makes RNA detection difficult. Despite these problems, most expression data are either based on RNA detection or antibody stainings and many of these studies lack cellular resolution and have often only focused on one organ. Reporter mice are an elegant tool to overcome all these caveats and enable investigation of TRP channel populations and their role in body homeostasis. For this purpose multiple new Cre-driver lines were established for TRPM5, TRPM6, TRPV6, TRPA1, TRPML3, TRPC2, TRPC4 and TRPC5, enabling mapping of body-wide TRP expression. These TRP channels are introduced in the next paragraphs with a focus on known expression data, mostly lacking cellular resolution, highlighting the need for body-wide mapping with cellular resolution.

1.2.1 The chemosensory specialist TRPM5

TRPM5 is a member of the melastatin subfamiliy. The sequences of mouse and human TRPM5 display about 80% sequence homology (Ullrich *et al.*, 2005). TRPM5 and its close relative TRPM4, are gated by a voltage-dependent increase in Ca^{2+} and they are impermeable for Ca^{2+} ions but selective for the monovalent cations K^+, Na^+,Cs^+ and Li^+ (Guinamard *et al.*, 2011). The Ca^{2+} origin for TRPM5 activation is either a result from receptor-mediated intracellular store release or extracellular Ca^{2+} influx. TRPM5 expression in the liver, the heart, kidney, spleen, brain, lung and the testes has been detected by Northern blot (Enklaar *et al.*, 2000). RT-PCR experiments revealed expression in the stomach, intestine, prostate, pancreas and pituitary (Fonfria *et al.*, 2006).

The role of TRPM5 in taste transduction has been described in great detail. Taste perception consists of five modalities: sweet, umami, salty, bitter and sour (Jayaram Chandrashekar *et al.*, 2006). Type II taste receptor cells (TRC) express TRPM5 and are responsible for the processing of sweet, bitter and umami tastants (Zhang *et al.*, 2003). They are organized as taste buds in papillae of the tongue and palate epithelium. Co-expressed with TRPM5 are TAS1Rs (responsible for umami and sweet taste detection), TAS2Rs (responsible for bitter taste detection), PLCβ2 and the heteromeric G-protein gustducin (Pérez, Margolskee, *et al.*, 2003). TRPM5 is activated by the following cascade; after activation of the respective taste GPCR, the Gα subunit and G$\beta\delta$ subunit are released into the cytosol. The G$\beta\delta$ subunit interacts with phospholipase C (PLC), cleaving phosphatidylinositol 4,5-biphosphate (PIP2) into inositol-1,4,5-triphosphate (IP3) and diacylglycerol (DAG). IP3 binds to its receptor on the endoplasmic reticulum membrane and triggers Ca^{2+} release from the endoplasmic reticulum (Roper, 2007). This Ca^{2+} concentration rise opens TRPM5, leading to Na^+ influx and depolarization of the cell (Pérez, Huang, *et al.*, 2002). TRPM5 KO mice display a strong reduction or no response at all to sweet, bitter and umami tastants but still show responses to sour and salty tastants (Philippaert *et al.*, 2017). The expression pattern of TRPM5 makes it tempting to speculate that the taste cascade is functional in tissues other than the tongue. TRPM5, together with other elements of the taste transduction pathway, were identified in a subset of solitary chemosensory cells (SSCs) in the olfactory, respiratory and digestive epithelia which are involved in the detection and processing of chemical cues in mice and rats (Tizzano *et al.*, 2011). Pathway components were also found in the choroid plexus and in areas of the brain stem in the rat, where they play a role in sensing chemicals of the cranial extracellular fluids (Tomás *et al.*, 2016). TRPM5 is expressed in mature olfactory sensory neurons (OSNs) of mice in the ventral and lateral part of the olfactory epithelium (Pyrski *et al.*, 2017) and is involved in sensing pheromones (Oshimoto *et al.*, 2013).

In the intestine, TRPM5 is expressed in brush and tuft cells, together with other receptors of the taste pathway

(Bezençon *et al.*, 2008). Taste receptors in these cells detect compounds released by parasites and trigger type 2 immune response in the gut (Howitt *et al.*, 2016). TRPM5 and gustducin double KO animals have impaired type 2 immune responses following gut infection, highlighting the function of TRPM5 in the gut. TRPM5 is expressed in the islets of Langerhans in the pancreas. Here, TRPM5 plays a role in glucose-stimulated insulin secretion. In the classical activation model, glucose enters the cell by diffusion or GLUT-2 transporters. Metabolized glucose triggers a rise in the ATP to ADP ratio. Rising ATP levels close ATP-sensitive K^+-channels, leading to Ca^{2+} influx through the opening of voltage-gated Ca^{2+} channels and the release of internally stored Ca^{2+}. This concentration increase activates TRPM5 and insulin is secreted (Emily R. Liman, 2010). This model was verified in TRPM5 KO animals. Islets from KO animals showed significant reduction in the glucose-induced Ca^{2+} activity and subsequent insulin release. KO animals had a reduced glucose clearance in both intraperitoneal and oral glucose tolerance tests when compared to WT animals (Colsoul *et al.*, 2010).

1.2.2 TRPM6 regulates Mg^{2+} homeostasis

Within the TRPM family, TRPM6 and TRPM7 share a unique kinase function in their ion channel domain (Schlingmann *et al.*, 2007) and are selective for Ca^{2+} and Mg^{2+} (Nadler *et al.*, 2001). TRPM6 is an essential component of Mg^{2+} resorption in the kidney and the intestine. Increased Mg^{2+} in the diet leads to increased TRPM6 mRNA in the intestine (Groenestege *et al.*, 2006). TRPM6 function in Mg^{2+} resorption in the intestine is highlighted by the discovery of a TRPM6 loss-of-function mutation in patients with a form of hereditary hypomagnesemia called hypomagnesemia with secondary hypocalcemia (HSH). Symptoms include a defect in intestinal Mg^{2+} absorption and cerebral convulsions due to profound hypomagnesemia early in infancy. TRPM6 expression in human tissue was also found in the testis and in lung leukocytes and also in mouse embryos by Nothern-blot analysis (Walder *et al.*, 2009), where TRPM6 is involved in the neural tube closure (Chubanov *et al.*, 2016).

1.2.3 TRPV6 is needed for sperm maturation

TRPV6 maintains the Ca^{2+} balance in the body, is a highly Ca^{2+}-permeable channel which is constitutively open and located in the apical membrane of endothelial cells. TRPV6 has a broad expression pattern with mRNA found in the intestine and kidney (Wu *et al.*, 2011), as well as the placenta, epididymis and exocrine tissue like the pancreas (Wissenbach *et al.*, 2001). Despite the fact that TRPV6 is a key channel in Ca^{2+} absorption in many tissues and is important for bone mineralization, Ca^{2+} absorption is not completely abolished in the absence of TRPV6 (Benn *et al.*, 2008). The channel is inactivated by a Ca^{2+}-dependent feedback mechanism and its activity is linked to PI(4,5)P2 levels, with decreasing concentrations corresponding to decreased channel activity (Thyagarajan *et al.*, 2008). In the placenta, Ca^{2+} absorption is an important function. TRPV6 is expressed in trophoblasts and syncytiotrophoblasts in the placenta (Wissenbach *et al.*, 2001). In TRPV6 KO fetuses the maternal-fetal $_{45}Ca^{2+}$ transport is decreased by 40% and Ca^{2+} levels in the blood are reduced (Suzuki *et al.*, 2008). TRPV6 is also expressed in the fetal labyrinth, the yolk sac and the maternal part of the placenta. TRPV6 KO in dams lead to an impaired Ca^{2+} uptake in trophoblasts and reduced Ca^{2+} content in the placenta and in the embryo. The offspring is smaller, has a lower body weight and has less calcified femurs compared to offspring of WT mothers. These phenotypes unravel the essential role of TRPV6 in Ca^{2+} transport between the mother and the embryo. TRPV6 also plays a major role in male fertility, as male KOs show a severely reduced fertility (Bianco *et al.*, 2007). This impaired fertility in KO males is due to TRPV6's essential role in Ca^{2+}

absorption in the epididymis. TRPV6 reduces the luminal Ca^{2+} levels needed for normal sperm maturation (Weissgerber *et al.*, 2011). A TRPV6 knock-in mouse carrying an amino acid mutation which produces a channel incapable of Ca^{2+} transport (B. Nilius *et al.*, 2001), displays a 50% reduction of caudal sperm due to impaired TRPV6 function in the apical membrane of epididymal epithelia.

1.2.4 TRPA1 is a potential cold sensor

The transient receptor potential ankyrin (TRPA) subfamily, named due to its 14 to 18 ankyrin repeats, is comprised of Ca^{2+}-permeable non-selective cation channels, and contains only one member, TRPA1. TRPA1 is expressed in sensory neurons, peptidergic and non-peptidergic neurons in primary afferents (Bernd Nilius and Flockerzi, 2014) and in non-neuronal cell types like epithelial and hair cells. Analysis of primary cell cultures from human tissues revealed TRPA1 expression in Islets of Langerhans and other sensory cell types (Bernd Nilius and Flockerzi, 2014). TRPA1 is activated by a wide variety of noxious external stimuli such as intense cold, reactive chemical species and endogenous signals associated with cell damage and is involved in pain and inflammation. Chemical activators are plenty, for example isothiocyanates from mustard oil, wasabi and horseradish (Jordt *et al.*, 2004) and intracellular Ca^{2+} (Doerner *et al.*, 2007).
Cold can activate mouse TRPA1 in a Ca^{2+}-independent manner (Sawada *et al.*, 2007) and heterologously expressed human TRPA1 is activated by both cold and heat. Despite the plethora of pharmacological studies regarding TRPA1, only one channelopathy was described so far, in contrast to many of the other TRP channels. Familial Episodic Pain Syndrome (FEPS) is a rare autosomal dominant disease and manifests already in infancy. It is characterized by episodes of incapacitating upper body pain that can spread into the abdomen and the legs, triggered by fasting and physical stress (Kremeyer *et al.*, 2010). TRPA1 also plays a crucial role in the physiology of migraine (Demartini *et al.*, 2017). TRPA1-activating compounds trigger migraine and anti-migraine agents act by down-regulating the activity of this channel (Benemei *et al.*, 2017). It was shown that migraine is triggered by oxidative stress, mainly mediated by TRAP1 (Borkum, 2018). TRPA1 is involved in tooth pain and inflammation. Hypersensitivity to cold is a main feature of dental pulp inflammation. TRPA1, along with other TRP channels such as TRPM8, are expressed in trigeminal branches which innervate the orodental system. These branches detect and transduce noxious and non-noxious thermal stimuli. Because these TRP channels are expressed in the sensory nerves that innervate the tooth, they may contribute to pain sensation in inflammatory teeth (C.-K. Park *et al.*, 2006).

1.2.5 TRML3 is involved in lysosomal exocytosis

The TRPML family consists of the three mammalian genes TRPML1 (*MCOLN1*), TRPML2 (*MCOLN2*) and TRPML3 (*MCOLN3*), which form heterodimers with each other (Zeevi *et al.*, 2009). TRPML3 is Ca^{2+} permeable (Cuajungco *et al.*, 2008) and TRPML3 mRNA was found in different organs including the thymus, lung, kidney, spleen, eye (Samie *et al.*, 2009) and also in the brain and the pancreas (Bernd Nilius and Flockerzi, 2014). The protein was detected in hair cells of the cochlea (Nagata *et al.*, 2008), melanocytes of the skin (Xu *et al.*, 2007) and in the olfactory system using TRPML3 antibodies (Castiglioni *et al.*, 2011). These antibody studies revealed that TRPML3 is located in a population of membrane-bound vesicles along the endocytosis and exocytosis pathway in late endosomal and lysosomal (LEL) compartments (Castiglioni *et al.*, 2011) and in early endosomes (EE) (H. J. Kim *et al.*, 2009). Mutations in TRPML3 are linked to the varitint-waddler disease in humans (Di Palma *et al.*, 2002). A mutation in mouse TRPML3 replicates the phenotype of deaf-

ness, circling behaviour, and pigmentation defects (Di Palma *et al.*, 2002). The vast majority of expression data regarding TRPML3 in both human and mice, were gathered with RT-PCR and lack cellular resolution. Only few studies using antibodies against the channel which were also tested in KO conditions but the low expression level complicates reliable channel detection.

1.2.6 The TRPC familiy

The TRPC family comprises seven members (TRPC1 to TRPC7) and were the first discovered mammalian TRP channels due to their similarity to TRP channels in Drosophila melanogaster. TRPC channels are permeable for monovalent cations including Na^+ and Ca^{2+} (Tang *et al.*, 2018). TRPC channels are activated by DAG, after initial activation of G-protein coupled receptors. TRPC2, C3, C6 and C7 are activated in this way but C1, C4 and C5 are insensitive to DAG and are activated by an increase in external and internal Ca^{2+} levels (Schaefer *et al.*, 2000). Opening of TRPC channels increases intracellular Ca^{2+} concentrations to prolong and enhance depolarization (DeHaven *et al.*, 2009). In addition, TRPC channel activation leads to the activation of voltage gated calcium channels involved in neuronal firing patterns (Bröker-Lai *et al.*, 2017). TRPC4 and TRPC5 also interact with Gi2 in addition to Gq. TRPC4 is widely expressed in human tissue (Clapham *et al.*, 2005) and its expression in mice was shown by RT-PCR, *in situ* hybridization and Northern and Western blot in the brain, eye, heart, lung, spleen, liver, pancreas and intestine (Bernd Nilius and Flockerzi, 2014). The vast majority of these studies do not use *in situ* hybridization to detect TRPC4 and are therefore lacking cellular resolution. TRPC5 expression is observed in the brain of both humans and mice by RT-PCR and in mice also detected with antibodies but antibody specificity is debated. In the periphery, TRPC5 expression is found in the liver, heart and kidney (Bernd Nilius and Flockerzi, 2014).

1.2.7 TRPC2 and it's role in the olfactory system in mice

The sense of smell, together with the sense of taste, are important mechanisms to detect the outside world and react accordingly with a specific behaviour. The olfactory system is specialised in the detection of odorants and pheromones, translating these into electrical signals in the brain to regulate specific hard wired behaviour, such as fleeing from a predator, social behaviour and mating. The olfactory system can be divided into four different organs. The vomeronasal organ (VNO), the main olfactory epithelium (MOE), the septal organ (SO) and the Grüneberg ganglion. Odorants are detected in the MOE, located in the roof of the posterior nasal cavity. OSNs in the MOE project into the olfactory bulb, which is located at the most anterior part of the telencephalon. OSNs express a class of GPCRs, the odorant receptors. The main components of the odorant transduction pathway are the G-protein olfactory subunit (Golf), adenylyl cyclase type III (ACIII) and olfactory cyclic nucleotide-gated channel subunit 1 (OCNC1) (Berghard *et al.*, 1996). This class of genes is the biggest gene family in mice and humans with more than 1000 genes per species (Godfrey *et al.*, 2004). The OSNs are bipolar neurons containing both sensory dendrites and one long axon projecting into a specific glomerulus in the olfactory bulb. The olfactory bulb is connected to a large variety of other brain regions which control behaviour including the anterior olfactory nucleus (AON), piriformcortex (PC), olfactory tubercle (OT), postero-lateral cortical amygdaloid nucleus (PLCN), and anterior cortical nucleus (ACN) (Li *et al.*, 2015).
In 1813 the VNO was described for the first time by the anatomist L. Jacobson as a secretory organ in the nose. The VNO is a bilaterally symmetrical, cylindrical organ encased in a bony capsule on the anterior nasal septum and contains vomeronasal sensory neurons (VSNs) that differ in their pattern of activation and receptor compo-

sition from the OSNs. The VSNs express two classes of G-protein receptor genes, Vmn1r and Vmn2r, similar to bitter taste receptors (J. Chandrashekar *et al.*, 2000) and project to the accessory olfactory bulb (AOB). Mitral cells in the AOB, detect the electrical signal from the VSNs and project to the vomeronasal amygdala (Jia *et al.*, 1997). This brain region contains different nuclei including the bed nuclei of the accessory olfactory tract, the stria terminalis and the posteromedial cortical and medial nuclei of the amygdala (Halpern, 1987), and is known as the 'neuroendocrine hypothalamus', due to its role in controlling hormone release from the pituitary. Chemosignals can either be volatile; processed in the MOE, or non-volatile; handled in the VNO. Pheromones, small molecules used by animals to detect predators, attract mating partners and social communication are in general non-volatile cues. In mammals, pheromones have long-lasting effects through altering the endocrine status as well as short term-effects on behaviour. The VNO is essential in pheromone detection as evidenced by the effects of surgical ablation of the VNO (VNX). VNX completely abolishes sexual behaviour in male hamsters (Robertson *et al.*, 1997) and in mice leads to reduction of mounting frequency (Beynon *et al.*, 2002). The detection of pheromones and the appropriate response is encoded by V1Rs and V2Rs and depends on TRPC2. TRPC2 is a pseudogene in humans and great apes (Vannier *et al.*, 1999) and is activated by a GPCR/IP3 pathway or by release of Ca^{2+} endoplasmic reticulum storage (Vannier *et al.*, 1999). The channel is located in VSN microvilli, the site of pheromone detection (E. R. Liman *et al.*, 1999) and TRPC2 ablation in VSNs impairs pheromone-evoked responses (Stowers *et al.*, 2002 and Leypold *et al.*, 2002). The cascade starts with GPCR activation, which triggers a PLC-dependent cascade which cleaves PIP2 into IP3 and DAG. DAG activates TRPC2 and the depolarization occurs (Figure 3).

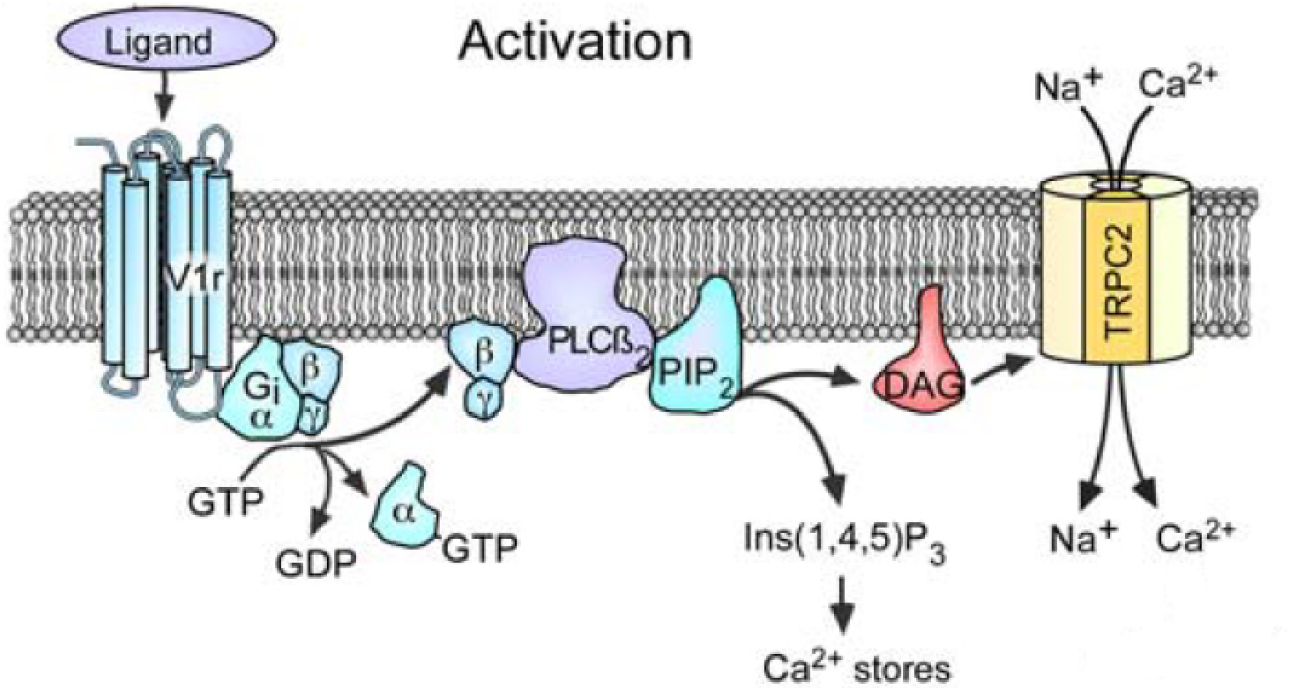

Figure 3: Schematic representation of TRPC2 activation in the VSNs. G-Protein subunits are GTP-dependent cleaved into the α and $\beta\gamma$ subunits and PLC is activated. PIP2 is cleaved into IP3 and DAG, DAG is interacting with TRPC2 and is opening the channel. Figure legend and figure reproduced from Zufall *et al.*, 2005.

TRPC2 KO females show normal sexual behaviour, whereas KO males mount male and female animals with a similar rate (Stowers *et al.*, 2002 and Leypold *et al.*, 2002). Male-male aggression and maternal aggression is impaired in KO animals (Leypold *et al.*, 2002 and Kimchi *et al.*, 2007) and in one KO strain, females displayed male-like sexual behaviour (Kimchi *et al.*, 2007). TRPC2 mRNA was initially found only in VSNs (E. R. Liman *et al.*, 1999) and functional TRPC2 in VSNs is required for displaying normal aggressive and sexual behaviour. Later, TRPC2 mRNA and protein was detected in OSNs in the MOE (Omura *et al.*, 2014) and TRPC2 fibers were found to innervate the AOB and a subset of glomeruli.

1.3 The blood brain barrier, brain windows and the paraventricular nucleus

Blood vessels transport blood throughout the body and use fenestrations for the delivery of oxygen, nutrients and the clearance of waste. The blood brain barrier (BBB) is a mix of different cell types, called the neurovascular unit. Non-fenestrated blood vessels regulate molecule transport between the central nervous system (CNS) and the vascular system. The microvascular endothelial cells of the BBB are 40% less thick than endothelial cells in muscles and in contrast to other epithelial cells are connected by tight junctions, prohibiting free passage of small molecules into the CNS (Westergaard *et al.*, 1973). Specialized transporters regulate the entry of nutrients and lipophilic molecules into and waste out of the brain (Mittapalli *et al.*, 2010). The BBB vessels are surrounded by a basement membrane, providing a docking point for signalling molecules and an additional barrier. Astrocytes of the BBB provide a communication system between neurons and the vascular system by ensheathing either neuronal processes or blood vessels (Abbott *et al.*, 2006). Pericytes of the BBB are embedded in the basement membrane and wrap their processes around the vascular tube regulating blood flow in response to neuronal activity and immune cell infiltration. The ratio of pericytes to endothelial cells in the CNS is between 1:1 and 3:1, which is much higher compared to the rest of the body where the ratio is 100:1 (Shepro *et al.*, 1993).

Brain windows, a BBB free area, provide a fast, barrier free communication between the vascular system and hormone-releasing neuronal fibers. Brain windows include the ME, the perivascular space of the portalvessels and the subarachnoid space (Rodríguez *et al.*, 2010). The ME is located below the third ventricle in the tuberal region of the hypothalamus and neurosecretory axons release their content here or project towards the neuropituitary to release their content (Clasadonte *et al.*, 2018). Vesicle-associated protein 1 (PV-1) homodimers form the fenestrations allowing free passage of molecules smaller than 1 kDa into the ME milieu by simple diffusion (Stan *et al.*, 1999). How is free diffusion between the CNS and the ME prevented? The ME is tightly closed to the CNS and the cerebrospinal fluid (CSF) by tanycytes, specialized glial cells in the mature brain lining the floor of the third ventricle. Tanycytes have single, long process and can be separated into four groups depending on their localization along the third ventricle (Mazzuca, 1974). α1-tanycytes project into the ventromedial and dorsomedial nucleus, α2-tanycytes into the Arcuate nucleus (Arc), β1-tanycytes into the latero-external part of the ME and the Arc and β2-tanycytes, located at the floor of the third ventricle, project to the base of the ME onto the portal capillary system (Figure 4). β-tanycytes are connected by tight junctions and establish the barrier between the ME the CNS and the CSF (Mullier *et al.*, 2010).

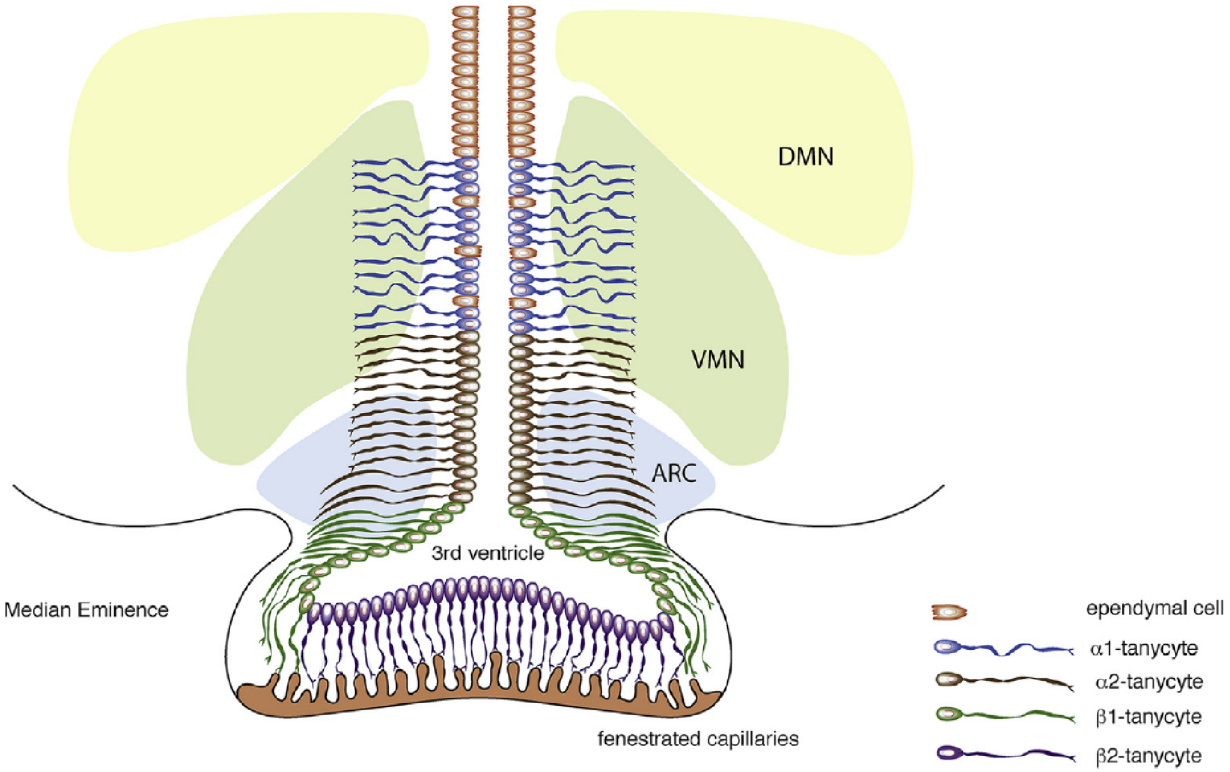

Figure 4: Distribution of different tanycyte subtypes along the third ventricular surface. The dorso-ventral organization of tanycytes and ependymal cells in relation to the ME is illustrated here. β2-tanycytes are the most ventral tanycytes, they are in contact with the fenestrated capillaries of ME and the third ventricle CSF that they isolate from free diffusion of blood-borne signals. Just dorsal to these, β1-tanycytes perform the same barrier function for the arcuate nucleus. α1 and α2 tanycytes are present dorsally to β cells. ARC = arcuate nucleus, VMN = ventro-medial nucleus, DMN = dorso-medial nucleus. Figure legend and figure reproduced from Rizzoti *et al.*, 2017.

The paraventricular nucleus (PVN) is located at the top of the third ventricle in close apposition to the dorsomedial nucleus. It is highly vascularized and contains magnocelluar oxytocin (OXT) and arginine-vasopressin (AVP) neurons projecting into the neuro-pituitary. OXT is released during suckling, sexual stimulation and stress (Jong *et al.*, 2015) and OXT receptors are expressed in the uterus and the brain (Hidema *et al.*, 2016). Physiological functions of AVP, often expressed together with OXT, are reduced food intake (Yoshimura *et al.*, 2017), blood glucose regulation and locomotor activity (Tsunematsu *et al.*, 2008). In addition, the PVN contains parvocellular corticotropin-releasing hormone (CRH) neurons, thyrotropin-releasing hormone (TRH) neurons and a second population of AVP neurons projecting into the ME. CRH triggers adrenocorticotropin (ACTH) release from the pituitary and activates further glucocorticoid release (McEwen, 2007) which then inhibits CRH expression in the PVN neurons (Watts *et al.*, 2004). TRH is expressed as a pre-protein (ppTRH) which is then post-translationally converted into TRH (Lechan *et al.*, 1986) and activates the thyroid gland.

1.4 Tissue clearing

The major increase in the use of mouse models with fluorescently labelled tissues in the last decades and the improvement in microscope technology has increased the knowledge of how the nervous system communicates with the periphery. Connectivity was mainly investigated in organ sections due to limitations in light penetration depth into whole organs. Tissue clearing together with light sheet and confocal microscopes enable the visualization of whole organs with cellular resolution. Three different tissue clearing approaches are available: hydrophobic, hydrophilic and hydrogel-based methods (Tainaka *et al.*, 2016). All approaches remove lipids (delipidation), pigments (decolourization) and calcium phosphate (decalcification) and match the refractive index (RI) of the organ to the imaging medium to minimize light scattering during the imaging process. Hydrophobic tissue clearing methods use organic solvents and reach a near complete transparency of intact organs quickly (Vigouroux *et al.*, 2017). DISCO-based methods initially dehydrate the organ to remove water, a source of light scattering and then use organic solvents to match the RI to the imaging medium (Susaki *et al.*, 2016). Different water-soluble reagents are used in hydrophilic tissue clearing methods to achieve transparency. These reagents form hydrogen bonds with proteins and water within the organ which preserves the structure and the endogenous fluorescence. Multiple different methods are in use, FocusClear which uses X-ray contrast agents and detergents (Y.-C. Liu *et al.*, 2003), Sca*le* uses urea and expands the tissue (Richardson *et al.*, 2015), See Deep brain (seeDB) uses fructose (Ke *et al.*, 2013) and urea is used by CUBIC for clearing. Cleared lipid extracted acryl hybridized rigid immunostaining/*In situ* hybridization compatible tissue hydrogel (CLARITY) is a hydrogel-based method developed by Deisseroth, Chung and colleagues (Chung *et al.*, 2013). Hydrogel removes lipids and minimizes the loss of biomolecules and structural damage. The main downside of CLARITY is its toxicity and the time required for clearing. Caveats of the other methods are that hydrophilic methods try to preserve the endogenous fluorescence but have high background fluorescence and in DISCO based methods the tissue must be stained for visualization of fluorescence.

1.5 The hypothalamic-pituitary-gonadal axis

The hpg-axis regulates fertility, puberty and sexual behaviour. Gonadotropin releasing hormone (GnRH) is released in a gender-specific and age-dependent manner from the hypothalamus into the portal veins in the ME (Constantin, 2011) and acts on target cells in the pituitary, namely the gonadotropes, triggering the release of luteinizing hormone (luteinizing hormone (LH)) and follicle-stimulating hormone (follicle-stimulating hormone (FSH)) (Jeong *et al.*, 2006). LH and FSH are transported in the blood to the gonads, where they activate respective receptors to maintain gametogenesis (Sofikitis *et al.*, 2008) and regulate testosterone and oestrogen synthesis (Yang *et al.*, 2015). In females, LH and FSH govern ovarian cyclicity and regulate the oestrus cycle which lasts 24-32 days in humans and 4-5 days in rodents (Fleetwood *et al.*, 1983). FSH is indispensable for oocyte maturation and induces the LH surge leading to ovulation. Varying amounts of each of the steroid hormones are released into the circulation depending on the current position with the cycle, creating a tightly regulated interplay between these numerous factors to provide the effect necessary at each time point (Baird *et al.*, 1975). In males, LH and FSH regulate spermatogenesis and testosterone production within the gonads (O'Shaughnessy, 2014). These sex hormones are then transported back to the hypothalamus were they regulate the pulsatile release of LH and FSH and the appropriate sexual behaviour (Constantin, 2011) (Figure 5).

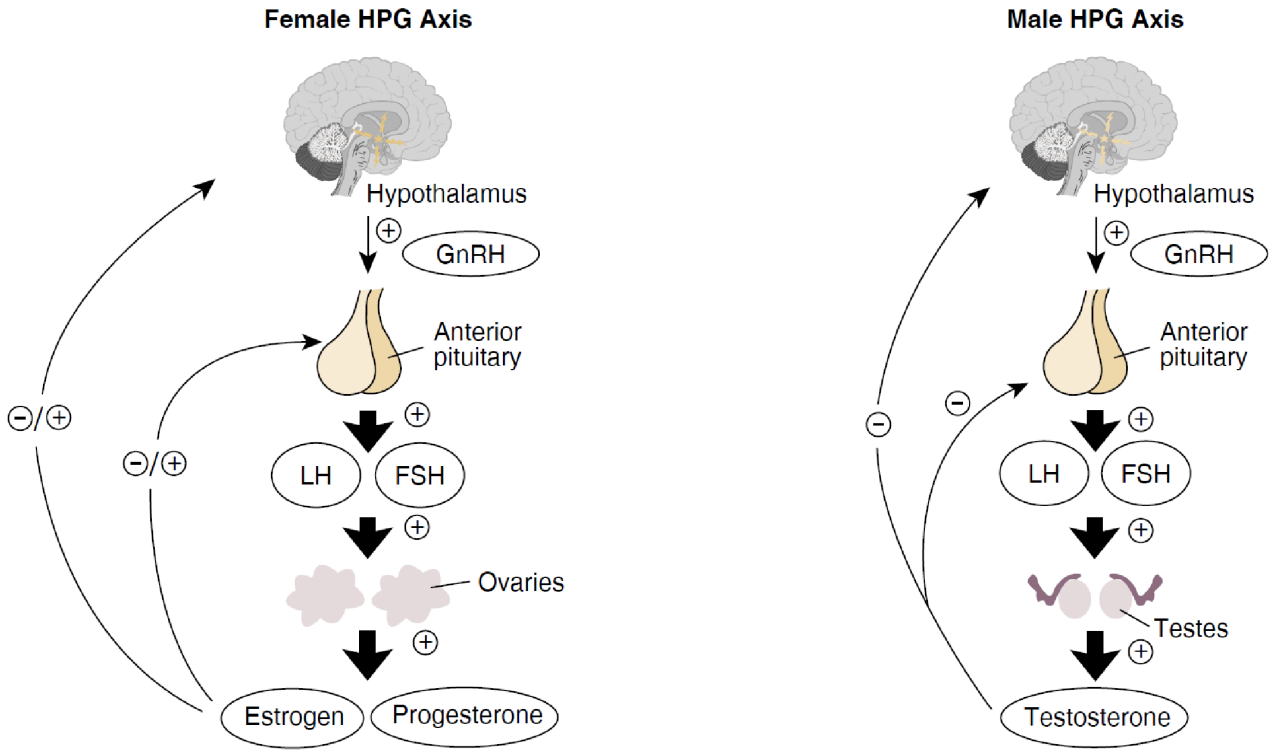

Figure 5: Schematic representation of the hpg-axis. The hypothalamus secretes GnRH which acts on the pituitary gland. In response to this stimulus, the pituitary gland releases gonadotropins (i.e., LH and FSH). LH and FSH in women stimulate the ovaries to produce estrogens and progesterone. Depending on the phase of the menstrual cycle, those hormones act back on the hypothalamus and pituitary gland in either a stimulatory or inhibitory manner. In men, LH stimulates the testes to release testosterone, which feeds back on the hypothalamus and pituitary. Figure legend and figure reproduced from Hiller-Sturmhöfel *et al.*, 1998.

GnRH release is controlled by kisspeptin, encoded by the *Kiss1* gene, acting on the G-protein-coupled receptor GPR54 in GnRH neurons (Ohtaki *et al.*, 2001). Kisspeptin signalling via Gpr54 controls reproductive physiology, shown by Gpr54 loss-of-function mutations in humans and knockout of the Gpr54 gene in mice which both results in delayed puberty due to hypogonadotropic hypogonadism (Seminara *et al.*, 2003). Two major kisspeptin neuron populations are found in the Arc and the anteroventral periventricular nucleus (AVPV). Arc kisspeptin neurons impinge onto GnRH processes at the ME, suggesting a role in modulating GnRH release into the hypophyseal portal circulation (Yip, Boehm, *et al.*, 2015). The AVPV kisspeptin population is sexually dimorphic. Female mice display ~ 10 times more AVPV kisspeptin neurons than males and the AVPV population is established around the time of puberty (Clarkson *et al.*, 2006).
Oestrogen has different effects on the AVPV and ARC kisspeptin neurons. In the Arc, oestrogen decreases kisspeptin mRNA whereas in the AVPV it increases kisspeptin expression (Smith *et al.*, 2006). These effects are mediated by oestrogen receptors (ERs). ERα, the main ER, is expressed in both Arc and AVPV kisspeptin neurons (Smith *et al.*, 2006). ERα signalling can be mediated via classical oestrogen response element (ERE) signalling or via ERE-independent mechanisms. A mouse model with abolished ERE signalling revealed that positive feedback on the hpg-axis is mediated by ERE signalling, as is the oestrogen-dependent upregulation of kisspeptin expression in the AVPV (Gottsch *et al.*, 2009), while the inhibiting effects of oestrogen are ERE independent (Glidewell-Kenney *et al.*, 2007). ERα signaling in kisspeptin neurons plays a key role in puberty onset and oestrus cyclicity in females. Mice with a conditional KO of ERα in kisspeptin neurons show precocious puberty, never establish a stable cycle and are infertile (Mayer, Acosta-Martinez, *et al.*, 2010) while ablation of kisspeptin neurons in adult mice also results in infertility (Mayer and Boehm, 2011). Further analysis of these conditional knockout mice demonstrated that positive feedback is mediated by ERα signalling in kisspeptin neurons but the inhibitory effect of oestrogen is not impaired (Dubois *et al.*, 2015). Recent work highlighted the different functions of the AVPV and Arc kisspeptin populations in their ERα signalling pathway. Mice with a conditional KO of ERα only in AVPV kisspeptin neurons display normal cycles but impaired LH surges while KO in Arc neurons leads to disrupted cyclicity (Wang *et al.*, 2019). The kisspeptin/GnRH system is established during development. Kisspeptin promoter activity can be detected at embryonic day (E13.5) in the ARC (Kumar, Freese, *et al.*, 2014 and Kumar, Periasamy, *et al.*, 2015) together with initial Gpr54 promoter activity (Knoll *et al.*, 2013), exclusively in GnRH neurons in both males (Kumar, Periasamy, *et al.*, 2015) and females (Kumar, Freese, *et al.*, 2014). Together with the first expression of the two genes, kisspeptin neurons become oestrogen sensitive as the first ERα expression occurs in both genders, with the majority of kisspeptin neurons expressing ERα (Kumar, Freese, *et al.*, 2014 and Kumar, Periasamy, *et al.*, 2015). This onset indicates a functional kisspetin-to-GnRH communication in the embryo, long before puberty onset. This early connectivity is reduced in older animals and only subpopulations of Arc (~23%) and AVPV (~36%) kisspeptin neurons are communicating with GnRH neurons (Kumar, Candlish, *et al.*, 2015).
The kisspeptin/GnRH system is functional early in embryonic development and is oestrogen sensitive. What is the source of oestrogen and what is the impact of oestrogen on the sexual differentiation of populations such as the AVPV kisspeptin neurons? This is discussed in the next chapter.

1.6 Aromatase and sexual differentiation of the brain

The P450 superfamily is present in all life forms from prokaryotes to plants and mammals. A key role of this superfamily is the oxidative transformation of endogenous and exogenous molecules (Ortiz de Montellano *et al.*, 2002). Aromatase (*Cyp19a1*) is a member of this family and irreversibly converts androgens such as androstenedione and testosterone into the estrogens oestrone and estradiol, respectively (Biegon *et al.*, 2012). Aromatase is expressed in a wide variety of tissues, including the gonads, brain, skin, bones, liver and placenta (E. R. Simpson *et al.*, 1994). Mutations in this enzyme cause at least two human diseases, both extremely rare with less then 100 patients worldwide. The aromatase deficiency syndrome is caused by a single nucleotide mutation in exon 9. Female homozygous patients present with ambigous genitalia, fusion of posterior scrotolabial folds and pseudo hermaphrodism (Jones *et al.*, 2007). They develop follicular cysts (Belgorosky *et al.*, 2003), delayed bone ageing and a tall stature (Mullis *et al.*, 1997). Patients fail to undergo normal puberty (Mullis *et al.*, 1997) but this can be treated with oestrogen (Evan R. Simpson, 2004). Males, on the other hand, are diagnosed later in life, undergo normal puberty and are very tall in stature (Carani *et al.*, 1997). The second syndrome, the aromatase excess syndrome, is characterized by aromatase overexpression due to a mutation in the 5'-end of the gene (Stratakis *et al.*, 1998). The phenotype manifests itself before puberty onset with a stronger phenotype in males. Males show feminisation with prepubertal or peripubertal gynecomastia (Hemsell *et al.*, 1977) and advanced bone age (Tanner *et al.*, 1966), resulting in a short stature (Berkovitz *et al.*, 1985). Female patients show precocious thelarche, macromastia, short stature and increased uterine volume (Martin *et al.*, 2003), while fertility is not affected (Martin *et al.*, 2003). Aromatase is also involved in oestrogen-related cancers such as breast, ovary and prostate cancer, which are often treated with aromatase inhibitors (C. Gao *et al.*, 2014).

Male and female hormonal milieus differ and are regulated by the hpg-axis. The developmental fate of the gonads is already established very early in embryogenesis in a hormone-independent mechanism. The gene *SRY* on the Y chromosome is sufficient to initiate testis development (Koopman *et al.*, 1991). In later developmental stages, the gonads establish gender-specific hormonal milieus to either masculinize and defeminize or feminize the brain in an oestrogen-dependent way. This time window is called the critical period and is different from species to species but a common feature is the high sensitivity of the brain to steroids. Gender-specific apoptosis is used to reduce cell numbers and these changes persist into adult life. Two different hypotheses were postulated to explain how the brain differentiates. The organizational/activation hypothesis was postulated in 1959 and is based on observations in guinea pigs (PHOENIX *et al.*, 1959). Removal of the gonads during the critical period in males, prevents male sexual behaviour in adults. Interpretation of this phenomenon is that male brain development needs steroids from the gonads and the female brain is the default state of brain development and occurs also in the absence of gonadal steroids. When the organizational/activation hypothesis was tested in rats, females were masculinized when injected with testosterone during the critical period. As controls, female rats were injected with oestrogen and surprisingly their brains were masculinized and oestrogen was even more effective then testosterone. Injecting the non-aromatizable androgen dihydrotestosterone (DHT), which acts on androgen receptors, did not masculinize the brain (Whalen *et al.*, 1981). This was explained by the discovery that aromatase is expressed in the brain (Lephart, 1996) and this led Naftolin in 1975 (Naftolin *et al.*, 1975) to postulate the aromatization hypothesis which was later expanded by others (Vreeburg *et al.*, 1977). According to this hypothesis, testosterone is converted to oestrogen in the brain and masculinizes the brain. But oestrogen is not only needed in males for normal development but also in the female. Female littermates of aromatase null

mice have impaired sexual behaviour and do not have a normal estrus cycle, indicating that oestrogen produced by aromatase is also needed for proper female development (J. Bakker *et al.*, 2003). The placenta produces large amounts of oestrogen that can pass through the placenta-embryo-barrier by diffusion. The embryos are protected from maternal oestrogen by α-fetoprotein which is synthesized in the placenta (Julie Bakker *et al.*, 2006) and the embryo syntheses oestrogen itself via aromatase. What are the mechanisms used by the brain for this sexual differentiation?

The brain is, depending on the gender, either masculinized, defeminized or feminized. A readout for sexual differentiation is the sexual behaviour in adults. This behaviour is determined by the hormonal milieu during the critical period and the hormonal milieu in adulthood when the behaviour is displayed. During the critical period, oestrogen must be provided in neonates and testosterone in adults to show normal male behaviour and females need protection from circulating oestrogens during the critical period and oestrogen and progesterone in adult life for normal female behaviour. How does the developing brain manage these criteria for normal masculinization, feminization and defeminization? The major cellular mechanism influenced by oestrogen in the critical period is apoptosis. Depending on the gender and the brain region, oestrogen either initiate apoptosis or prevents it. Examples include the higher vocal center (HVC) in male song birds, where oestrogen protects the neurons from apoptosis resulting in a nucleus which is larger in males compared to females (Burek *et al.*, 1997). In rats, the preoptic area (POA) is bigger in males compared to females and cells in female rats begin to die at postnatal day 7 (P7) and can no longer be detected by P10. Oestrogen or androgen treatment during the critical period protects females from cell loss in this nucleus (Rhees *et al.*, 1990). In the AVPV, a nucleus which is larger in females than in males, oestrogen triggers apoptosis in male animals (Simerly *et al.*, 1997). Another cellular mechanism influenced by oestrogen is neurite growth and synaptic patterning (Calizo *et al.*, 2000). Oestrogen can induce neurite growth in organotypic explant cultures from the POA, the hypothalamus and the cerebral cortex when bathed in oestrogen (Toran-Allerand, 1976). But does a masculinization of the brain always leads to defeminization? An elegant study tested this with the use of prostoglandin PGE2 which influences dendrite density in the POA in an oestrogen-dependent manner (Amateau *et al.*, 2004). COX-2, an immediate early response gene is the limiting enzyme in the synthesis of PGE2. Treating rats with a COX-2 inhibitor during the critical period decreased the dendrite density in males to female levels and treated females showed no reduction and a male-like pattern. Adult males treated this way during the critical period, do not display male behaviour but adult females, when provided with testosterone, show typical male behaviour. When the COX-2 inhibitor-treated males were given estradiol as adults, because they have female-like brains, they did not show any sexual behaviour. Treated females on the other hand were able to show male or female behaviour depending on the hormone treatment they received. This shows that masculinization is not equal to a defeminization, but that these two processes are independent of each other (Todd *et al.*, 2005).

Oestrogen is required during the critical period for normal development but the ontogeny of aromatase expression in the brain and gonads as well as which brain regions first become sensitive to steroid hormones are unknown. Detailed brain mapping in embryos has been complicated by the fact that aromatase is difficult to detect at the mRNA level due to its low expression and antibodies against aromatase are not reliable due to its localization in the membrane of the endoplasmic reticulum. Reporter mice can help to overcome these caveats and can provide many details in the process of masculinization, defeminization or feminization of the brain.

1.7 Scientific aims of my study

Aim 1:
Mapping of TRP expression throughout the body with special emphasis on the hypothalamus utilizing TRP-reporter mice. Developing a TRP-Atlas

Aim 2:
Reporter mouse-assisted identification of TRP-expressing cells in the median eminence using 3D reconstruction

Aim 3:
Characterisation of TRPC2 neurons in the central nervous system

Aim 4:
Functional characterization of aromatase expression in the embryonic and perinatal murine brain

2 Material and Methods

2.1 Materials

2.1.1 General Materials

Chemicals were mainly bought from Sigma, VWR or Roth. Molecular weight standards and PCR reagents were obtained from Bioline. All buffers and media were made with deionized water (ddH_2O) and autoclaved (20 min, 121°C) or filtered with 0.22 μm Millex-GP sterilizing filters (Thermo Fischer).

Table 1: List of used kits.

Kit name	supplier
RNeasy Mini Kit™	Qiagen (#74106)
Superscript III	Invitrogen (#18080-044)
Maxima First Strand cDNA Synthesis Kit for RT-QPCR	Thermo Fischer (#K1642)
Tyramide Signal Amplification biotin Kit	PerkinElmer (#NEL700001KT)
Luminex Kit (pituitary hormones)	Merk (#MPTMAG-49K)
ACTH ELISA kit	MyBiosource (#MBS720035)
MyTaq Red mix, 2x	Bioline (#BIO-25044)

Table 2: List of used genotyping primers.

Primer name	Sequence (from 5' to 3' end)
ArIC-IRES-Cre FW	AGGATGACTCTGGTCAGAGATACCTG
ArIC-IRES-Cre RV	GCTGTAGAACTCTAGCAGGAGACC
ArIC-IRES-Cre WT FW	CTTGCACCCAAATGAGGACAGG
TRPC2-IRES-Cre FW	CTGCCCATGTGCTGGTTCAC
TRPC2-IRES-Cre RV	TGCTTCTCTGGCCTCCTAGC
TRPC2-IRES-Cre neo- FW	AACTAAACTGGTCGAGCGATGG
TRPM5-IRES-Cre FW	AGGCCACTGTTCCTTAGTGTCC
TRPM5-IRES-Cre RV	GCTCCCGAATAGATGCCAAAGAC
TRPM5-IRES-Cre neo- FW	GGTCGAGCGATGGATTTCCG
TRPA1-IRES-Cre FW	GCACAGTTACCTGGTGCAGAAC
TRPA1-IRES-Cre RV	GGGTGAGGTTGCAGGAACTAGG
TRPA1-IRES-Cre neo- FW	TCCGTAACCTGGATAGTGAAACAGG
TRPC4-IRES-Cre FW	AGGTGGTGGTGGAAGACACC
TRPC4-IRES-Cre RV	TTGCCTGCCCAGAGCACTA
TRPC4-IRES-Cre neo- FW	AACTAAACTGGTCGAGCGATGG

continued on next page

continued from previous page

Primer name	Sequence (from 5' to 3' end)
TRPC5-IRES-Cre FW	TGGCAGGACATCCGCTATTC
TRPC5-IRES-Cre RV	GGGTCACCTCTGAGAACAGG
TRPC5-IRES-Cre neo- FW	CCGTCTCTGGTGTAGCTGATG
TRPM6-IRES-Cre FW	AAGCCTGATGTCCAGTCCACC
TRPM6-IRES-Cre RV	CCAGGGAGGTCCACATTGTAAAG
TRPM6-IRES-Cre neo- FW	GGTCGAGCGATGGATTTCCG
e*ROSA26* FW	GGAAGCACTTGCTCTCCCAAAG
e*ROSA26* RV	GGGCGTACTTGGCATATGATACAC
e*ROSA26* WT RV	CTTTAAGCCTGCCCAGAAGACTC
ROSA26 FW	GGAAGCACTTGCTCTCCCAAAG
ROSA26 RV	AACCACTGGAAAGACCGCGAAG
ROSA26 WT RV	CTTTAAGCCTGCCCAGAAGACTC
ROSA26 FW	GGAAGCACTTGCTCTCCCAAAG
ROSA26 RV	AACCACTGGAAAGACCGCGAAG
e*ROSA26* RV	GGGCGTACTTGGCATATGATACAC
ROSA26 WT RV	CTTTAAGCCTGCCCAGAAGACTC
Cre FW	GCGGTCTGGCAGTAAAAACTATC
Cre RV	GTGAAACAGCATTGCTGTCACTT

The enhanced *ROSA26* PCR is used for e*R26*-τGFP and *eR26*-DREAAD. *Rosa26* PCR primers are used for *ROSA26*-DTA and *ROSA26*-iDTR. The multi-PCR primers are used for standard genotyping. This PCR tests for the presence of Cre, the normal and enhanced ROSA allel independent of the specific Cre driver or reporter mouse (Table 2).
For genotyping PCR reactions, the following protocol for a 12.5 μl reaction was used:

MilliQ	up to 12.5 μl
2x MyTaq Red mix	6.25 μl
Primer (2.5 pM)	0.25 μl each
DNA	1 μl

Table 3: List of used RT primers.

Primer name	Sequence (from 5' to 3' end)
Aromatase RT FW	TCGGCATGCATGAGAACGGCA
Aromatase RT RV	CAGGGCCCGTCAGAGCTTTCAT
Cyp11a1 RT FW	TTCCTTTGAGTCCATCAGCA
Cyp11a1 RT RV	CACTGGTGTGGAACATCTGG

continued on next page

continued from previous page

Primer name	Sequence (from 5' to 3' end)
Cyp17a1 RT FW	TTCGCCTGGGTACCACAACTGC
Cyp17a1 RT RV	TAGAGTCACCATCTGGGGCCGA
TRPC2 RT FW	GCACCACCTGCCGCTATTTC
TRPC2 RT RV	TCGTTGAAATTGCCTAGCTTCTCG

For reverse transcriptase PCR reactions, the following protocol for a 12.5 μl reaction was used:

MilliQ	up to 12.5 μl
2x MyTaq Red mix	6.25 μl
Primer	0.25 μl each
cDNA	1 μl

Table 4: List of buffers and stock solutions.

buffer	composition
20X PBS	3 M NaCl 161 mM Na_2HPO_4 39 mM KH_2PO_4 adjust pH to 7.4
50X TAE	242 g Tris 57.1 ml acidic acid 100 ml 0.5 M EDTA ph 8.0
ear lysis buffer	50 mM Tric-HCl (pH 7.5-8.0) 100 mM NaCl 0.2% NP-40 0.2% Tween-20 1 mM EDTA 100 mg/ml proteinase K just before use
tail lysis buffer	100 mM Tris 5 mM EDTA 0.2% SDS 200 mM NaCl 100 mg/ml proteinase K just before use
4% Paraformaldehyd (1l)	dilute 40g PFA in 60°C H_2O for 20 min add 2 to 3 drops of 10M NaOH until visible clear cool down to 4°C and add 50 ml 20x PBS
Tris-NaCl-Tween 20 (TNT)	0.1 M Tris pH 7.5 0.15 M NaCl

continued on next page

continued from previous page

buffer	composition
	0.05% Tween 20
PBS-Tween 20 (PBST)	0.05% Tween 20 in 1x PBS
PBS-Carrageenan (vegetable non-gelling gelatin) (1l)	heat H_2O to 40°C dissolve 5 g Carrageenan in small increments under constant stirring ON filter the final solution
blocking solution	10% donkey serum 3% BSA 0.03% TX-100 in 1x PBS
iDISCO blocking solution	0.2% gelatine 0.5% TX-100 or 1% TX-100 depending on tissue size in 1x PBS
Hoechst solution (for nuclear stain)	5 μg/ml Hoechst 33258 dye in PBS, pH 7.4

Table 5: List of primary antisera.

Antiserum	Host	conc.	Manufacturer
GFP	chicken	1:1000	Invitrogen (#A10262)
GFP	rabbit	1:1000	Invitrogen (#A11122)
GFP	rabbit	1:10000 (for iDISCO)	Invitrogen (#A6455)
ERα	rabbit	1:1000	Millipore (#06-935)
Kisspeptin	rabbit	1:500	Millipore (#AB9754)
Luteinizing hormone	guinea pig	1:500	National Hormone & Peptide Programm (#AFP344191)
Follicle stimulating hormone	guinea pig	1:500	National Hormone & Peptide Programm (#AFP1760191)
Growth hormone	rabbit	1:500	National Hormone & Peptide Programm (#AFP2631058)

continued on next page

continued from previous page

Antiserum	**Host**	**conc.**	**Manufacturer**
Prolactin	rabbit	1:500	National Hormone & Peptide Programm (#AFP65191)
Adrenocorticotropic hormone	rabbit	1:500	National Hormone & Peptide Programm (#AFP71111591)
Thyrotropin-releasing hormone	rabbit	1:500	National Hormone & Peptide Programm (#AFP2665563)
Olfactory marker protein	goat	1:1000	FUJIFILM (#544-10001)
Oxytocin	rabbit	1:1000	Immunostar (#20068)
Argenin/Vasopressin	rabbit	1:1000	Novus (#NB100-65214)
Tyrosin-Hydroxylase	rabbit	1:1000	Abbexa (#abx005909)
Corticotropin releasing hormone	rabbit	1:1000	Immunostar (#20084)
Somatostatin	rabbit	1:1000	Immunostar (#20067)
Thyrotropin releasing hormone	rabbit	1:1000	Invitrogen (#AB152)
CD-31	goat	1:1000 (for normal IHC) 1:5000 (for iDISCO)	R&D Systems (#AF3628)
PV-1	chicken	1:1000 (for normal IHC) 1:2500 (for iDISCO)	kindly provided by Prof. Philippe Ciofi Neurocentre Magendie, INSERM Unit 862, University of Bordeaux, France
Vimentin	chicken	1:2500 (for iDISCO)	GeneTex (#GTX30668)
HA-taq	chicken	1:1000	ThermoFischer (#GW22511)
Calcitonin	rabbit	1:1000	abcam (#ab8553)

Table 6: List of secondary antisera.

Antiserum	Host	conc.	Manufacturer
chicken 488	goat	1:500	Invitrogen (#A11039)
rabbit Cy5	donkey	1:500	Jackson Immuno Research (#711-175-152)
goat Cy2	donkey	1:500	Jackson Immuno Research (#705-225-147)
goat Cy3	donkey	1:500	Jackson Immuno Research (#705-165-147)
chicken 488	donkey	1:500	Jackson Immuno Research (#703-545-155)
chicken Cy3	donkey	1:500	Jackson Immuno Research (#703-465-155)
rabbit biotinylated	donkey	1:500	Vector Labs (#VEC-BA-1000)
streptavidin Cy5	-	1:500	Jackson Immuno Research (#016-170-084)

2.2 Methods

2.2.1 Mouse lines

Animal care and experimental procedures were approved by the Ethical Committees for animal use of the Saarland University or University of Hungary. Mice were kept under a 12 hour light/dark cycle with food and water *ad libitum*. Animals undergo operation procedures or animals for timed pregnancies were kept under a reversed 12 hour light/dark cycle with food and water *ad libitum*.

Table 7: List of used mouse lines.

mouse line	description
ArIC/e*R26*-τGFP	Cre recombinase is expressed under the control of the Aromatase promotor, cuts out the stop signal in the ROSA-locus and enables constitutive τGFP expression.
TRPC2IC/e*R26*-τGFP	Cre recombinase is expressed under the control of the TRPC2 promotor, cuts out the stop signal in the ROSA-locus and enables constitutive τGFP expression.

continued on next page

continued from previous page

mouse line	**description**
TRPC2IC/*R26*-DTA	Cre recombinase is expressed under the control of the TRPC2 promotor, cuts out the stop signal in the ROSA-locus and enables constitutive expression of diphteria toxin which kills the cell.
TRPC2IC/*R26*-TeNT	Cre recombinase is expressed under the control of the TRPC2 promotor, cuts out the stop signal in the ROSA-locus and enables constitutive expression of Tetanus toxin light chain GFP fusion which prevents vesicular release.
TRPC2IC/e*R26*-DREADD	Cre recombinase is expressed under the control of the TRPC2 promotor, cuts out the stop signal in the ROSA-locus and enables constitutive expression of a DREADD-HA tag fusion protein and a nuclear guided iRFP protein linked by a 2A-linker.
TRPM5IC/e*R26*-τGFP	Cre recombinase is expressed under the control of the TRPM5 promotor, cuts out the stop signal in the ROSA-locus and enables constitutive τGFP expression.
TRPA1IC/e*R26*-τGFP	Cre recombinase is expressed under the control of the TRPA1 promotor, cuts out the stop signal in the ROSA-locus and enables constitutive τGFP expression.
TRPC4IC/e*R26*-τGFP	Cre recombinase is expressed under the control of the TRPC4 promotor, cuts out the stop signal in the ROSA-locus and enables constitutive τGFP expression.
TRPC5IC/e*R26*-τGFP	Cre recombinase is expressed under the control of the TRPC5 promotor, cuts out the stop signal in the ROSA-locus and enables constitutive τGFP expression.
TRPM6IC/e*R26*-τGFP	Cre recombinase is expressed under the control of the TRPM6 promotor, cuts out the stop signal in the ROSA-locus and enables constitutive τGFP expression.
KP-ZsGreen	Kiss1-Cre transgenic animals (Yeo et al 2016) bred to the Gt(ROSA)26Sor_CAG/LSL_ZsGreen1 Tm indicator strain (The Jackson Laboratory, JAX No. 007906) to mark kisspeptin cells with GFP

2.2.2 Genotyping

Routine genotyping was performed by technical assistants within the laboratory. Using 100 μl ear lysis buffer crude genomic DNA was extracted form ear biopsies by incubation at 55°C overnight under agitation. For embryonic gender PCR, biopsies were incubated in 500 μl tail lysis buffer and incubated at 55 °C over night with agitation. On the next day the samples were centrifuged for 10 min at 17000 x g at RT. The supernatant was added to 500 μl isopropanol and mixed. Samples were centrifuged at 17000 x g for 5 min at RT and the supernatant was removed. 200 μl 70% Ethanol were added and centrifuged for 5 min at 17000 x g at RT. The supernatant was removed, the pellet dried and resuspended in 100 μl H_2O.
1 μl of extracted DNA was used for the PCR reaction. Samples were placed in a Bio-Rad T100 thermal cycler with the appropriate annealing temperature (see Table 2) and standard program. 12.5 μl of the amplified samples were loaded on a 1% agarose/TAE gel (4 μl ethidium bromide per 100 μl agarose gel) alongside with a molecular weight ladder (Hyperladder 100 bp, Bioline). The gel was run at 130 V for 45 minutes. Bands were visualized using a Herolab E.A.S.Y. Doc Plus geldocumentation system.

2.2.3 Perfusion

Animals were deeply anaesthetized with a mix of ketamine (200 mg/kg)/xylazin (32mg/kg). When the animal showed no more reflexes, the fur was wetted with ethanol and the chest opened with scissors to expose the heart. A cut was made in the right atrium and a needle placed in the left ventricle. PBS was used to remove the blood followed by ice cold 4% PFA. The used volume of solutions was depending on the age of the animal. After perfusion organs of interest were harvested and post-fixed in 4% PFA on ice for two to three hours.

2.2.4 Preparation of embryonic tissue

Pregnant mice were anaesthetized and sacrificed, the embryos removed, washed in ice-cold 1X PBS and immersed in 4% PFA on ice overnight. Whole embryos (E12.5 and E13.5) or only embryo heads (E16.5 and E18.5) were then transferred to 30% sucrose and kept at 4°C until they sank down. The embryos were frozen in optimal cutting solution (Leica) by snapfreezing tissue in an isopentan bath cooled by Ethanol with dry-ice and 14 μm sagittal sections were prepared using a cryostat.

2.2.5 Decalcification

After perfusion and post-fixation bone containing tissue were decalcified by immersing in a 0.5 M EDTA solution at 4°C until bone tissue became decalcified enough to perform cryosectioning.

2.2.6 OCT embedding and cryosectioning for non embryonic tissue

For cryosectioning, fixed tissue was immersed in 18% sucrose at 4°C over night or until the tissue sank down. After cryoprotection, tissues were kept in OCT freezing medium (Leica Microsystems) for 2 to 3 hours. For freezing a glass box was submerged in a bath of ethanol with dry ice and filled with isopentane. Tissues were transferred into embedding molds (Thermo Fischer) with fresh OCT and rapidly frozen in an isopentan bath cooled by Ethanol with dry-ice. Tissues were stored at -80°C until cryosectioning.

All tissues were prepared as series of five (Boehm *et al.*, 2005). Brain, embryos, pituitary and nose tissues were sectioned at 14 μm, other organs were sectioned with 10 μm thickens. Sections were stored at -80°C until usage.

2.2.7 Activation of DREADD

For activation of DREADD in the TRPC2IC/eR26-DREADD animals, 5 μg/kg CNO (Tocris) was injected intraperitoneally and blood was collected 25 min, 1 hour or 2 hours after injection.

2.2.8 Stereotactic injection

Animals were anaesthetized with 5% isoflurane mixed with oxygen and then transferred to a stereotaxic injection apparatus (Stoelting Co.) and injected with Caprofen (5 mg/kg, s.c.) and a local injection of 5% Lidocain and 0.25% Bupicacain. Anaesthetized mice were maintained under 2% isoflurane. The sculpt was shaved and opened with a scalpel along the midline to expose the skull. The tissue was cleaned with 3% H_2O_2. According to the lateral ventricle coordinates given in the Franklin and Paxinos Atlas (Franklin and Paxinos, 2001), one or two holes were drilled into the cranium using a dentist drill, depending in the number of injection sides. With a Hamilton microlitre syringe, 30 μg/μl colchicine (Sigma) was injected with the help of collaboration partners, into the lateral ventricle (-0.70 mm posterior, 1.15 mm lateral and 2.10 mm ventral to bregma) with a injection rate of 0.1 μl/min. After the operation mice were transferred into their homecage and perfused two days later.

2.2.9 Hematoxylin and Eosin (H&E) staining

Cryosections were washed shortly in PBS to rehydrate the tissue followed by a washing step in ddH_2O. Sections were then stained with Mayer's hematoxylin (Morphisto) for 6 minutes, rinsed in lurk warm running tap water for 6 minutes, incubated for 6 minutes in Eosin (Morphisto) and dehydrated through an alcohol gradient (2x 70%, 2x 96%, 2x 100%) and finished with two washes in Xylol. Slides were mounted with DePeX (Serva).

2.2.10 Immunohistochemistry-immunofluorescence (IHC-IF)

For standard IHC, cryosections were washed 3 times in 1x PBS followed by 1 hour incubation at room temperature in blocking solution (see Table 4). Sections were then incubated in primary antisera at 4°C over night. For concentrations of the specific primary antiserum see Table 5. When multiple primary antisera were used, sections were washed three times in PBST after the incubation with the first primary antiserum, followed by incubation in the second primary antiserum. Antisera were diluted in PBS-Carrageenan or PBS. After primary antiserum incubation, sections were washed three times in PBST and incubated in appropriate secondary antisera for two hours at room temperature. Secondary antisera were diluted in PBS-Carrageenan. For concentrations and detailed information see Table 6. When multiple secondary antisera were used, sections were washed in PBST after each secondary antiserum before incubating sections in the next one. After secondary antiserum incubations sections were washed in PBST and incubated for 5 minutes in Hoechst-Solution for nuclear staining. Sections were washed in PBST and coverslips were mounted with mounting medium Fluoromount-G (Southern Biotech).
For streptavidin-based staining, the same protocol was used as above. After the secondary antiserum incubation, (biotinylated) sections were washed with PBST and incubated for 1 hour in streptavidin Cy5.

TSA amplification protocol was used for the visualization of the HA-tag in TRPC2IC/e*R26*-DREADD animals. Slides were washed three times in PBS, incubated for 10 min in 0.5% TX-100, washed in TNT and blocked in TNB-blocking solution (provided in the kit). Sections were incubated in primary antisera overnight at 4°C and left for 2 hours at RT on the following morning. Slides were washed in TNT and incubated in biotinylated secondary antiserum recognizing the host of the first antiserum for two hours at RT, followed by three washes in TNT and incubation in 1:100 streptavidin (SA)-conjugated horseradish peroxidase (SA-HRP, provided in the kit) for 30 min at RT. Slides were washed three times in TNT and incubated for exactly 10 min in 1:50 TSA and washed three times in TNT. For visualization of the primary antiserum, slides were incubated in streptavidin Cy5. Nuclei were stained with Hoechst.

2.2.11 Kawamoto bone sectioning

For the preparation of non-decalcified bone samples, the Kawamoto method was used Kawamoto *et al.*, 2014. In short, after perfusion the bone is kept in 4% PFA overnight and is then immersed in 30% sucrose overnight. Bones were frozen in OCT and 6 μm thick sections were collected on cryofilm and transferred onto a glass slide.

2.2.12 Blood sample preparation for Luminex and ELISA

For preparation of plasma, animals were decapitated and blood was collected in pre-cooled EDTA coated tubes. Samples were immediately centrifuged for 20 min at 4°C at 4.300 rpm. The plasma in the supernatant was aliquoted and frozen at -80°C until used in either Luminex or ELISA.

2.2.13 Reverse transcription PCR

For the preparation of total RNA from embryonic tissue, total RNA from E13.5 embryo heads was isolated with the RNeasy Mini Kit (Qiagen) according to the manufacturer's instructions and the RNA concentration was measured using a Nanodrop. cDNA was synthesized from total RNA with Superscript III (Thermo Fischer) according to manufacturer's instructions. RT-PCR reactions with Primers against Cyp11a1, Cyp17a1 and Cyp19a1 were performed with MyTaq Red mix (Bioline).
For preparation of total RNA to perform RT-PCR for TRPC2 and Cre, total RNA was isolated from brain samples containing the PVN with the RNeasy Mini Kit (Qiagen) according to the manufacturer's instructions and the RNA concentration was measured using a Nanodrop. cDNA was synthesized from total RNA with the Maxima First Strand cDNA Synthesis Kit (Thermo Fischer) according to manufacturer's instructions. RT-PCR reactions with primers against TRPC2 and Cre were performed with MyTaq Red mix (Bioline).

2.2.14 iDISCO clearing and staining

Animals were perfused with standard the perfusion protocol. Brains were removed and post-fixed for three hours in 4% PFA on ice. If sections were used for iDISCO staining, brains were sectioned on a vibratome (Leica) with a thickness of 350 μm. For the following protocol only antiserum, incubation times were different when whole brains or tissues were used.
After post-fixation, tissue were dehydrated in progressively higher concentrations of Methanol in 1x PBS (20%, 40%, 60%, 80% and two times 100%) for one hour each. Tissues were incubated overnight at 4°C

in 66% Dichlormethane (DCM) / 33% Methanol. On the next day tissues were washed multiple times in 100% Methanol, chilled at 4°C and incubated overnight in 5% H_2O_2 in Methanol at 4°C protected from light. Samples were rehydrated and blocked in iDISCO blocking solution (see Table 4) for 3 to 4 days at room temperature. Tissues were incubated in primary antisera (see Table 5) for 1 week (sections) or 2 weeks (whole organs) at 37°C. After incubation in primary antisera, tissues were washed multiple times during the day at room temperature in 1x PBS + 1% Triton X-100 and overnight at 4°C. The next day, tissues were incubated in secondary antisera (see Table 6) for one week at 37°C. After secondary antisera incubation tissues were washed in 1x PBS + 1% Triton X-100 multiple times during the day at room temperature and one final time overnight at 4°C.
For clearing tissues were dehydrated the same way as before and incubated in 66% DCM / 33% Methanol overnight at 4°C. The next day tissues were incubated in 100% DCM for two hours. Tissues were transferred in 100% Dibenzylether (DBE) for two hours for clearing. To finalize the clearing, tissues were transferred into fresh 100% DBE and stored until imaging in glass bottles.

2.2.15 Cell counting

Neurons were manually counted in every fifth section using the ImageJ Cell Counter plugin. τGFP and hormone-producing neurons were counted based on positively stained cytoplasm and ERα and c-Fos cells were counted based on nuclear signal. Counted numbers were multiplied by 2.5 to estimate the total number of neurons per brain (Boehm, Zou, & Buck, 2005). Fiber density was qualitatively determined and grouped in four different categories based on intensity.

2.2.16 ERα distance measurements

Distances between τGFP-positive, but ERα-negative neurons and τGFP-negative/ERα-positive cells were calculated with the line tool in the Zen-Blue software (Zeiss). Randomly chosen cells from three different animals per age and sex group were included in the calculation.

2.2.17 Fiber distance measurments

For distance calculation of TRPC2 fibers to the blood vessels of the ME, different Imaris tools were used. First, the fluorescence signals were transformed into Imaris surfaces using the surface tool of Imaris. Only fluorescence signals inside the ME were used to build the surface. With Imaris, the distance of the τGFP surface to the blood vessel surface was calculated.

2.2.18 Electrophysiology

The following methods were used by Imre Farkas in the lab of Prof. Eric Hrabovszky , Laboratory of Reproductive Neurobiology, Institute of Experimental Medicine, Budapest, Hungary, to perform the electrophysiology experiments. Male KP-ZsGreen mice (P4-7) were sacrificed by decapitation in deep isoflurane anesthesia. The heads were immersed in ice-cold low-Na cutting solution bubbled with carbogen (a mixture of 95% O_2 and 5% CO_2) and the brains were removed rapidly from the skull. The cutting solution contained the following (in mM): saccharose 205, KCl 2.5, $NaHCO_3$ 26, $MgCl_2$ 5, NaH_2PO_4 1.25, $CaCl_2$ 1, glucose 10. Hypothalamic blocks were dissected, and 200 μm-thick coronal slices were prepared with a VT-1000S vibratome (Leica Microsystems, Wetzlar, Germany) in the ice-cold oxygenated cutting solution. Slices including the arcuate

nucleus (ARC) were transferred into artificial cerebrospinal fluid (aCSF) containing (in mM): NaCl 130, KCl 3.5, $NaHCO_3$ 26, $MgSO_4$ 1.2, NaH_2PO_4 1.25, $CaCl_2$ 2.5, glucose 10 and allowed to equilibrate for 1 h. The aCSF was bubbled with carbogen and the temperature was allowed to decrease slowly from 33°C to room temperature.
Recordings were carried out in carbogenated aCSF at 33°C, using an Axopatch-200B patch-clamp amplifier, a Digidata-1322A data acquisition system, and a pCLAMP 10.4 software (Molecular Devices Co., Silicon Valley, CA, USA). The patch electrodes (OD = 1.5 mm, thin wall; WPI, Worcester, MA, USA) were prepared with a Flaming-Brown P-97 puller (Sutter Instrument Co., Novato, CA, USA). Electrode resistance was 2–3 MΩ. The intracellular pipette solution contained (in mM): K-gluconate 130, KCl 10, NaCl 10, HEPES 10, MgCl2 0.1, EGTA 1, Mg-ATP 4, Na-GTP 0.3. pH=7.2-7.3 with KOH. Osmolarity was adjusted to 300 mOsm with D-sorbitol. To eliminate any direct androgen receptor-mediated response to testosterone, the androgen receptor blocker flutamide (1 μM; Tocris; Bristol, UK) was included in the intracellular pipette solution. Once the whole-cell patch-clamp configuration was achieved, the intracellular milieu was allowed to reach an equilibrium for 15 min before the recording was started. To eliminate indirect transsynaptic actions of testosterone, spike-mediated neurotransmitter release was blocked in all experiments by the addition of the GABAA-R blocker picrotoxin (100 μM, Tocris) and the glutamate-receptor blocker kynurenic-acid (2 mM, Sigma) to the aCSF 10 min before recording. KP-ZsGreen neurons of the ARC were visualized with a BX51WI IR-DIC microscope (Olympus Co., Tokyo, Japan) placed on an antivibration table (Supertech Ltd., Hungary-Switzerland) using a brief illumination at 470 nm and an epifluorescent filter set. Firing was recorded in current-clamp mode with a holding current of 0 pA. Following a 5-min control recording period, aCSF was replaced with aCSF containing 50 nM testosterone (similar to the male serum T concentration and the recording continued for 10 additional minutes. Other measurements were carried out in the presence of the aromatase-inhibitor Letrozole (100 nM, Tocris) or the broad-spectrum estrogen-receptor antagonist ICI182,780 (Faslodex, 1 μM, Tocris). The blockers were added to the aCSF 15 min before testosterone (i.e. 10 minutes before the control recording started) and were present throughout the recording. In some measurements, Letrozole was applied intracellularly (100 nM), together with flutamide (1 μM) to eliminate endogenous aromatase activity that might occur within kisspeptin neurons. Each neuron served as its own control when drug effects were evaluated.

2.2.19 Mass spectometry for TRPV6

The following methods were used by Dr. Claudia Fecher-Trost in the lab of Prof. Veit Flockerzi, to perform the mass spectometry analysis of TRPV6 protein in different mouse tissues. TRPV6 enrichment by antibody-based affinity purification from mouse tissue: 100 μg of antigenic peptide-purified TRPV6 antibodies (ab429, polyclonal or 20C6, monoclonal) were covalently coupled to magnetic M-280 tosyl-activated beads (Invitrogen) as described before or 10 μg of monoclonal and polyclonal purified TRPV6 antibodies were preincubated with 50 μl of a (1:1) mixture of protein A/G Dynabeads (Invitrogen) in RIPA buffer (150 mM NaCl, 50 mM Tris HCl, pH 8.0, 5 mM EDTA, 1% Nonidet P40, 0.1% SDS, 0.5% Na-deoxycholate, pH 7.4 including protease inhibitors). 100 mg to 500 mg freshly isolated or snap frozen (-80 °C) adult mouse tissue were shredded in 1-5 ml RIPA buffer with an ultraturrax, homogenized with a glass teflon potter and incubated for 45 min at 4°C. After ultracentrifugation (100.000 x g, 45 min at 4°C) the supernatant was incubated with the TRPV6 antibodies bound to magnetic beads for 16 h at 4°C. The beads were collected with a magnetic rack and washed five times with 1 ml RIPA buffer. Proteins were eluted with 50 μl denaturing sample buffer (final concentration:

60 mM Tris HCl, pH 6.8, 4% SDS, 10% glycerol including 0.72 M β-mercaptoethanol) at 60°C for 20 min and separated on NuPAGE™4%-12% gradient gels. MS sample treatment with tryptic in gel digest was described before.

Nano-LC-ESI-MS/MS measurements and raw data analysis: Tryptic peptide extracts were analyzed by nano LC-ESI-MS/MS (Ultimate 3000 RSLC nano system coupled to an LTQ Orbitrap Velos Pro, all ThermoScientific, TF, Dreieich, Germany). Peptides were trapped on a C18 trap column (100 μm x 2 cm, Acclaim PepMap, ThermoScientific) and separated on a reversed phase column (nano viper Acclaim PepMap capillary precolumn, and Acclaim Pep Map, 75 μm x 50 cm, ThermoScientific) at a flow rate of 200 nl/min with buffer A (water and 0.1% formic acid) and B (90% acetonitrile and 0.1% formic acid) using gradient 1 (4 to 55% buffer B in 30 min; 55 to 90% B in 6 min) or gradient 2 (4 to 55% buffer B in 56 min; 55 to 90% B in 7 min). The effluent of the chromatography was directly sprayed into the mass spectrometer through a coated silica electrospray emitter (PicoTipEmitter, 15 μm, New Objective, Woburn, MA, USA) and ionized at 2.2 kV. MS spectra were acquired in a data-dependent mode. For the collision induced dissociation (CID) MS/MS top10 method (gradient 1 and 2), full scan MS spectra (m/z 300–1700) were acquired in the Orbitrap analyzer using a target value of 106. The 10 most intense peptide ions with charge states $\rangle 2$ were fragmented in the high-pressure linear ion trap by low-energy CID with normalized collision energy of 35%. Fragmented peptides were analysed by using MASCOT algorithm and Proteome Discoverer 1.4 software (ThermoScientific). Peptides were matched to tandem mass spectra by Mascot version 2.4.0 (Matrix Science, London, UK) by searching an SwissProt database (version 2018_05, species mouse, number of protein entries 16.992). MS2 spectra were matched with a mass tolerance of 7 ppm for precursor masses and 0.5 Da for fragment ions. We used tryptic digest, and allowed for up to two missed cleavage sites. Carbamidomethylation of cysteine was set as a fixed modification and deamidation of asparagine and glutamine, acetylation of protein N-terminus and lysine and oxidation of methionine were set as variable modifications.

2.2.20 Softwares and microscopes

ZenBlue Software (Zeiss) or AxioVsion (Zeiss) were used to acquire images from cryosections from the AxioVision SlideScanner (Zeiss) or Imager.M2 Epifluorescence microscope (Zeiss). ZenBlack (Zeiss) was used to acquire images from iDISCO cleared brain sections with a LSM 710 confocal microscope (Zeiss) or SIM-microscope (Zeiss). The Lavision Software was used to acquire images from whole cleared organs with light sheet microscopy in the lab of Paolo Giacobini (aff) with the help of Gaeten Ternier. ImageJ was used for cell counting and ZenBlue for ERα distance measurements. Imaris (Bitplain) was used for 3D reconstruction of the iDISCO cleared samples and the calculation of the tanycyte and fiber distance measurements.

2.2.21 Statistical methods

All data for the cell counting and distance measurments are presented as the mean ± SEM. Two-tailed unpaired Student's t tests were used to determine statistical significance in these experiments. Following statistics were used for the electrophysiological experiments performed by Dr. Imre Farkas. All data are presented as the mean ± SEM. Patch-clamp recordings were stored and analyzed off-line. Event detection was performed using the Clampfit module of the PClamp 10.4 software (Molecular Devices Co., Silicon Valley, CA, USA). Firing rates within the 10-min treatment periods were presented and then illustrated in the bar graphs as percentages of the firing rate of the 5 min control periods that is all experiments were self-controlled in each neuron. Two-tailed

unpaired Student's t tests were used to determine statistical significance in each group of these percentage firing rate data. These percentage data characterizing the different treatment groups were then compared by ANOVA, followed by Tukey's post-hoc test. Statistical differences were considered significant at $p < 0.05$.

3 Results

3.1 Whole mouse body mapping of TRP reporter mice

To investigate TRP channel expression on a body-wide scale at cellular resolution I developed a dissecting and imaging pipeline, capitalising on the expertise from Prof. Krasteva-Christ (Institute of Anatomy and Cell Biology, Saarland University School of Medicine, Homburg, Germany) for assistance in developing organ-specific dissection protocols. After organ collection and staining, sections were imaged with the Zeiss slidescanner and images uploaded to the TRP-Atlas. The TRP-Atlas is a database for TRP-expression profiles in the mouse for adult and juvenile animals of both genders (Figure 6).

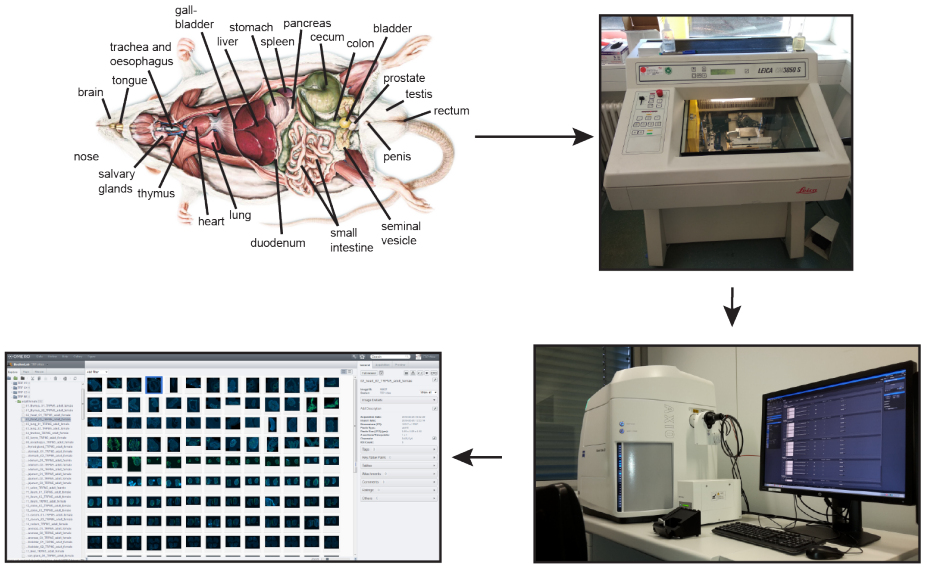

Figure 6: Pipeline for the TRP-Atals. After dissection of organs, cryostections were prepared and stained. Tissue was imaged with the Zeiss slidescanner and selective pictures uploaded into the TRP-Atlas. The atlas is a reference atlas for TRP expression in organs of adult and juvenile animals of both gender.

The development of the organisational structure and image collection forms a part of this thesis. Multiple new TRP Cre-driver lines were developed within the transregional collaborative research centre 152 and I have mapped the expression in these driver lines to delineate TRP channel expression with a cellular resolution on a body-wide scale. I have mapped expression in TRPC2, TRPC4, TRPC5, TRPM5, TRPM6, TRPML3 and TRPV6 Cre-driver lines. The mapping for some of these lines was performed by multiple people under my supervision and TRPV6 mass spectrometry data were generated for specific organs. Following people participated partially in this mapping. The mass spectrometry experiments for TPRV6 were performed and analysed by Dr. Claudia Fecher-Trost in the group of Prof. Veit Flockerzi and the results generously shared with me. TRPV6 mapping and analysis was performed by Femke Lux and me together. TRPA1 organ mapping was performed by Hannah Rill as her Bachelor thesis, TRML3 organ mapping was performed by Barbara Spix from the group of Prof. Christian Grimm at the LMU Munich and TRPM6 organ mapping was performed by Anna Erbacher from the group of Prof. Thomas Gudermann at the LMU Munich, all three under my supervision. I perfused the animals and dissected the organs for the mapping in TRPA1, TRM6 and TRPML3 reporter mice, Hannah, Anna and Barbara sectioned and stained the organs respectively and we analysed the data together. Several of these results have already been published or are in the process of being reviewed (see page 134).

The gustatory channel TRPM5 is expressed throughout the body. I confirmed TRPM5 expression in a subset of cells in the islet of Langerhans, brush cells in the respiratory and gustatory system and in the taste buds. I observed TRPM5 expression in nearly all organs of the body at variable amounts (Table 8, page 104, appendix). TRPV6 is expressed in organs involved in Ca^{2+} resorption. We found TRPV6 expression in the thyroid gland in a subset of cells of the cuboidal thyrocytes, forming the spherical follicles which contain the prohormones thyroglobulin and iodine. Because the thyroid gland is releasing the thyroid hormones triiodothyronine (T3), thyroxine (T4) and calcitonin, which is involved in the regulation of the Ca^{2+} serum levels, we did a co-staining with an anti-serum against calcitonin. TRPV6 cells are not co-expressing calcitonin and serve a different function than the calcitonin cells (Figure 7).

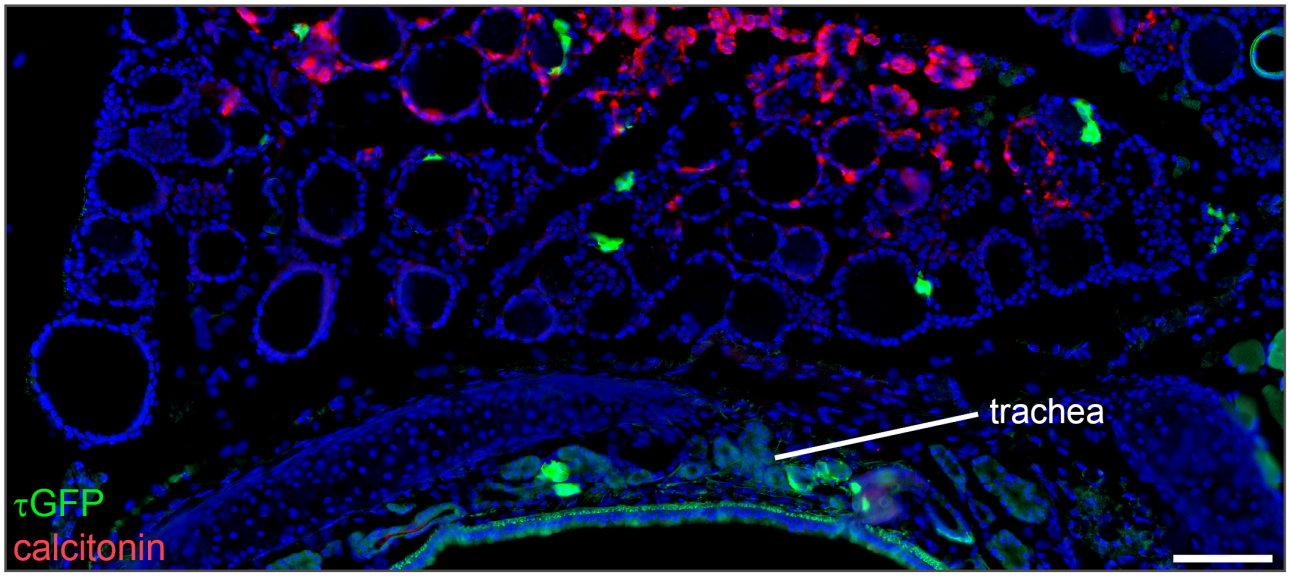

Figure 7: TRPV6 is expressed in a subset of cells in the thyroid gland. Reporter gene expressing cells (green) in the thyriod gland of TRPV6IC/eR26-τGFP do not co-express calcitonin (red). The TRPV6 cells seem to not be involved in the calcium sensing function of the thyriod gland. In the bottom half of the picture τGFP expressing cells in the trachea are shown. Nuclear counterstain in blue. Scalebar: 100 μm.

In the salivary gland, caecum, pancreas, uterus, epididymis and prostate Dr. Claudia Fecher-Trost showed TRPV6 protein with mass spectrometry and we identified the cell types expressing TRPV6 in these organs (Figure 52, page 111, appendix; Figure 53, page 112, appendix; Figure 54, page 113, appendix; Figure 55, page 114, appendix; Figure 56, page 115, appendix; Figure 57, page 116, appendix and Table 12, page 105, appendix). Interestingly, TRPV6 expression in the pancreatic acinar cells is age dependent with nearly all acinar cells in adult animals being TRPV6 positive, in stark contrast to juvenile animals (Figure 54, page 113, appendix). We identified a TRPV6 cell population in enamel secreting high prismatic epithelial cells but not in the teeth itself (Figure 51, page 110, appendix). Expression in a subset of enamel cells was also observed in the TRPA1 reporter mouse. In contrast to TRPV6, τGFP expression was also found in the teeth (Table 10, page 106, appendix). I identified a similar pattern in the TRPC4 and TRPC5 reporter animals, with TRPC5 revealing the highest cell numbers out of the three reporter lines (Figure 8). With these results a collaboration with Prof. Katharina Zimmermann (Klinik für Anästhesie, Universität Erlangen-Nürnberg, Erlangen, Germany) was initiated and resulted in the identification of TRPA1 and TRPC5 as cold sensors in odontoblasts (Bernal *et al.*, 2021 in press). We found TRPML3 to be predominantly expressed in immune cells. Large TRPML3 population were observed in immune cell producing tissues like the thymus and spleen. In addition we also

identified τGFP-positive cells in the lung and in OSNs and VSNs. Surprisingly, most, if not all OSNs seem to be TRPML3 positive (Figure 58, page 117, appendix and Table 11, see page 107, appendix). TRPM6 in the periphery was mainly found in the lung and despite the known role of the channel in intestine, we only observed a minor population in the small and large intestine (Table 12, page 108, appendix). I observed τGFP expression in TRPC2 reporter in a large population of OSNs and in all VSNs. I did not observe any expression in other organs in the periphery (Table 13, page 109, appendix). Organ mapping results are summarized in Figure 9.

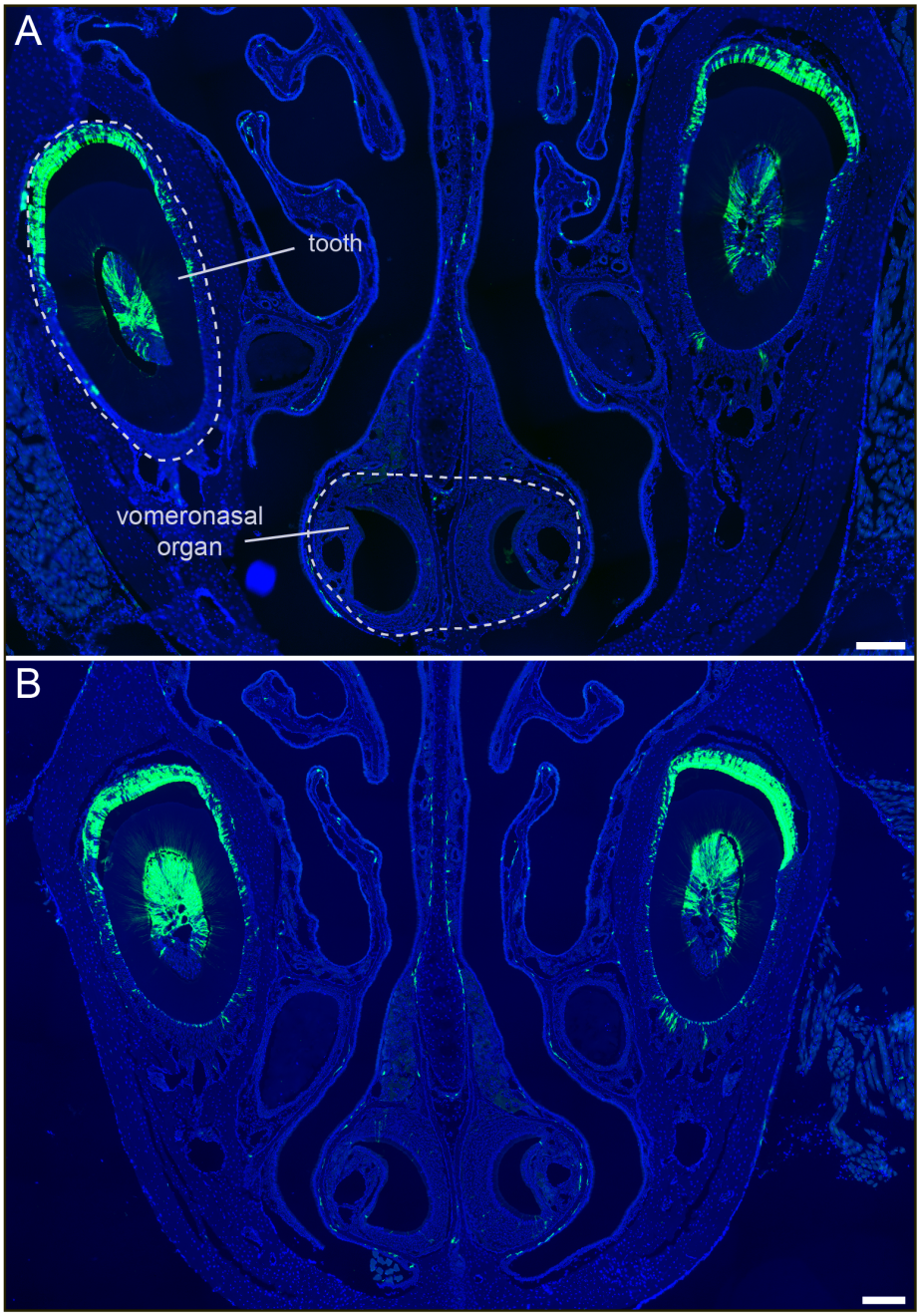

Figure 8: TRPC4 and TRPC5 are expressed in teeth. (A) τGFP expression was observed in enamel secreting cells and cells in the teeth in the TRPC4IC/eR26-τGFP animals. No expression was observed in the VSNs. (B) A similar pattern was identified in the TRPC5IC/eR26-τGFP animals. In these animals the amount of reporter gene expressing cells in the teeth seemed increased compared to TRPC4. Nuclear counterstain in blue. Scalebar: 100 μm.

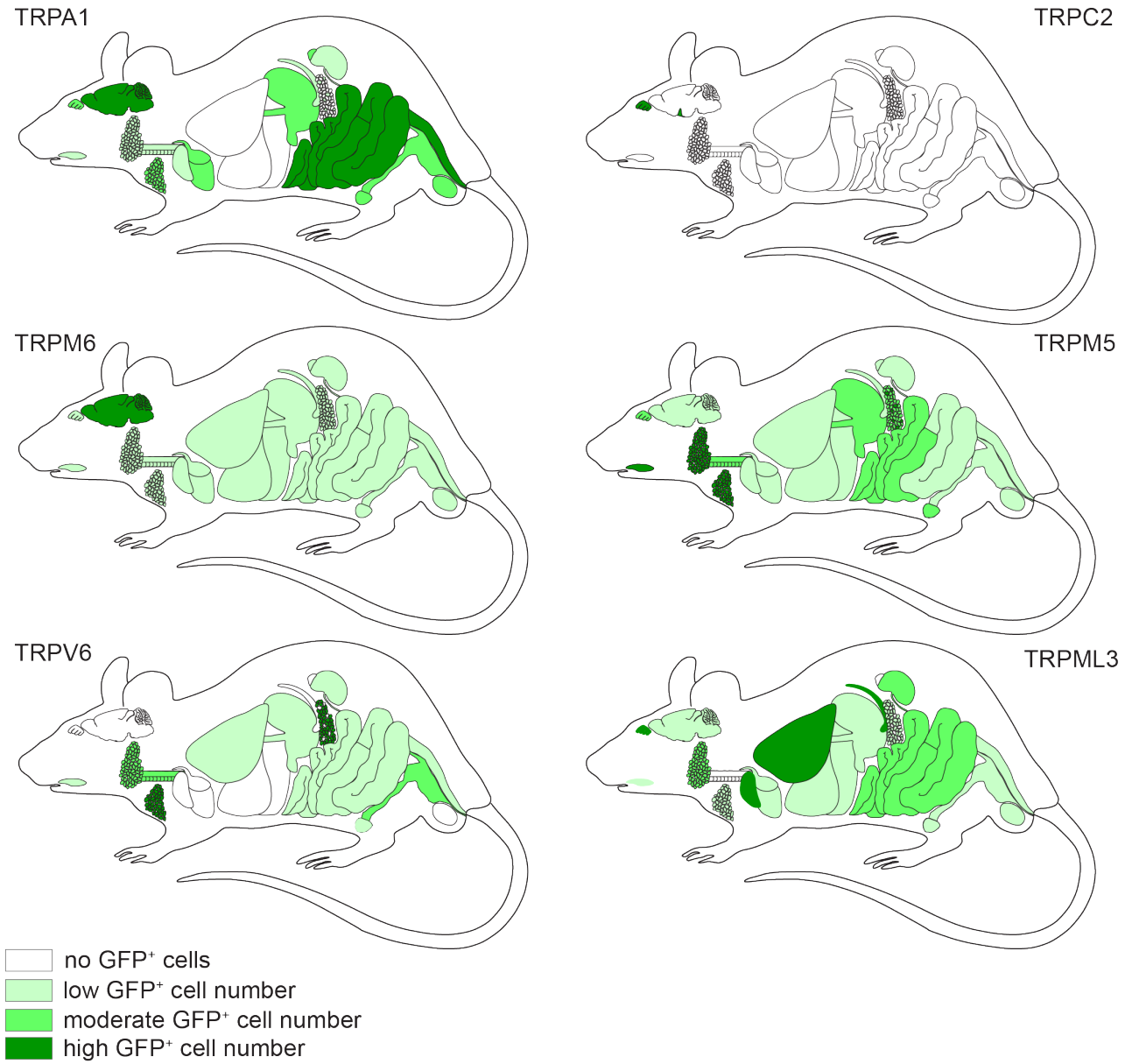

Figure 9: Summary of the TRP organ mapping. TRPA1 was mainly observed in the CNS and in the intestine. TRPC2 was only found in the olfactory tissue, pituitary and brain. TRPM6 expression was observed in the vascular system of the brain and to different degrees throughout the body. TRPM5 was observed throughout the whole body and cell number was organ dependent. No expression was observed in the brain of TRPV6 reporter animals. The pancreas and epididymis displayed high amounts of τGFP expressing cells. Most τGFP expressing cells in the TRPML3 reporter animals were observed in the VSNs, OSNs and in the lung.

In the brain all investigated TRP channels are expressed (with the exception of TRPV6) in different cell types and brain regions. TRPA1 was found in cortical neurons and interestingly, only in the curvature of blood vessels, at least in the cortex (Figure 10). In 3D-reconstructed brains of TRPM6 reporter mice I revealed that most, if not all of vascular endothelial cells in the CNS express τGFP and most of the ependymal cell population is positive (Figure 11). In the hypothalamus, the control centre of body homeostasis, I identified reporter gene expression driven by different TRP reporter mice in a large variety of cell types in the Arc and ME. TRPM5 driven reporter gene expression was observed in a subset of tanycytes lining the floor of the third ventricle (Figure 13 A). In the TRPM6 reporter mouse τGFP was identified in blood vessels and in ependymal cells in the wall of the ventricle. Interestingly, no signal was observed in the ME (Figure 13 B). Only fibers were found in the ME in TRPC2 reporter mice (Figure 13 C). This TRPC2 CNS expression will be described in more detail below. TRPC4 and TRPC5 driven reporter gene expression was observed in similar cells types. In the ME I observed dense fiber innervation and also τGFP+ cells in close contact to the vascular system at the base of the ME (Figure 13 D and E). TRPA1 was expressed in neurons in the ventrolateral part of the ventrolateral hypothalamic nucleus, the dorsomedial hypothalamic nucleus and the medial posterior part of the Arc with few fibers. In the ME TRAP1+ cells are in close contact with a subset of blood vessels. I identified a large variety of TRP channels expressed in the Arc and in the ME in different cell types. This highlights an important role of TRP channels in the control of body homeostasis (Figure 12).

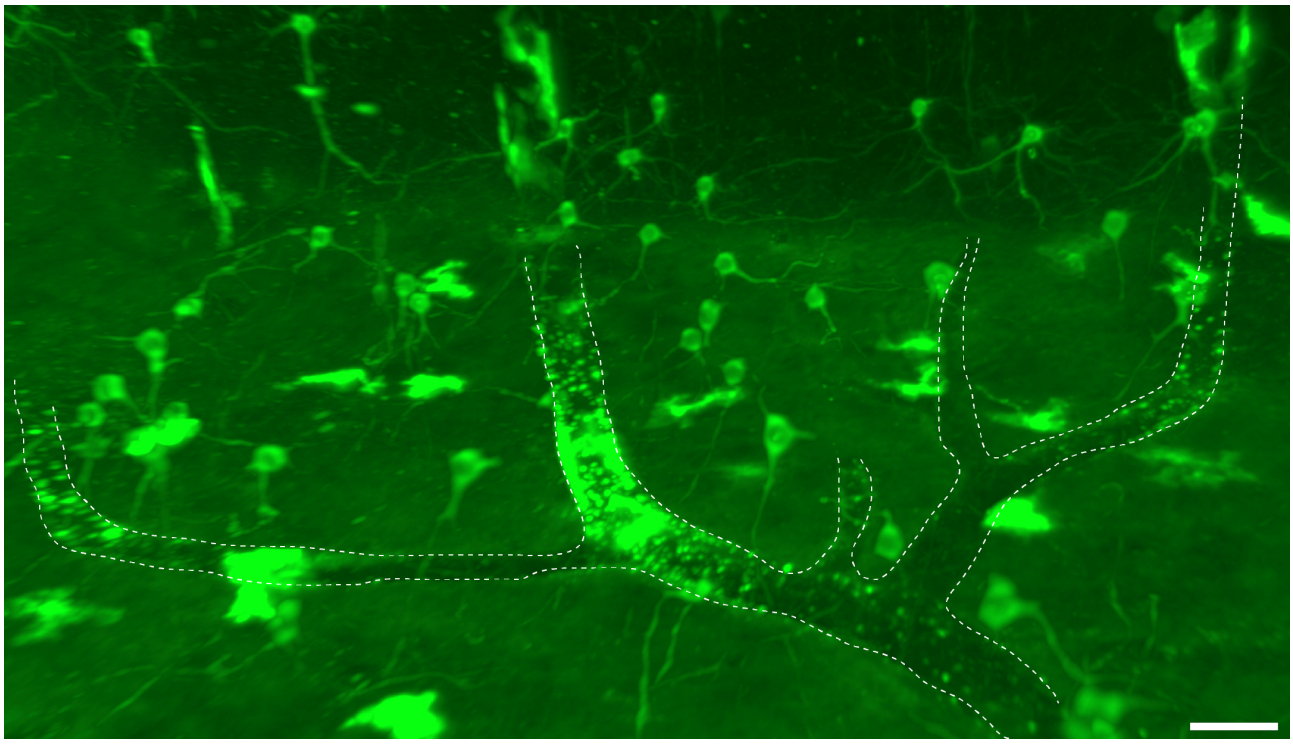

Figure 10: TRPA1 is expressed in curvature of CNS vessels. In the cortex TRPA1 is expressed in a subset of neurons and in the curvature of blood vessels (vessel indicated by stitched line). Scalebar: 50 μm.

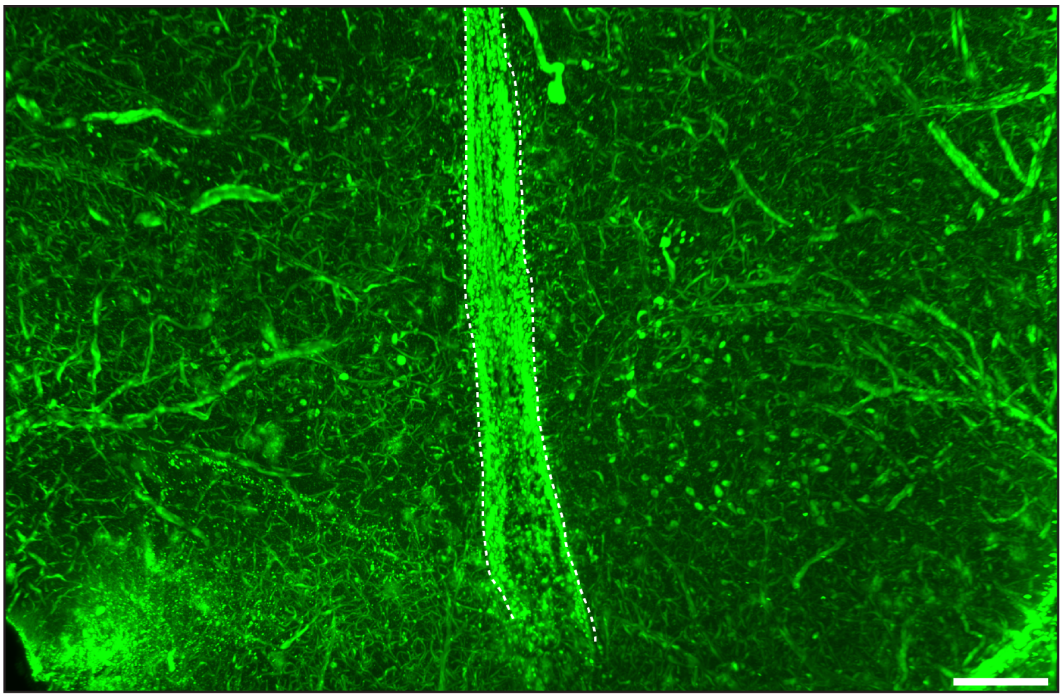

Figure 11: TRPM6 is expressed in the vascular CNS system. iDISCO cleared images revealed that all CNS blood vessels express TRPM6. A large population of ependymal cells lining the 3V (stitched line) were found to be τGFP positive. Scalebar: 100 μm.

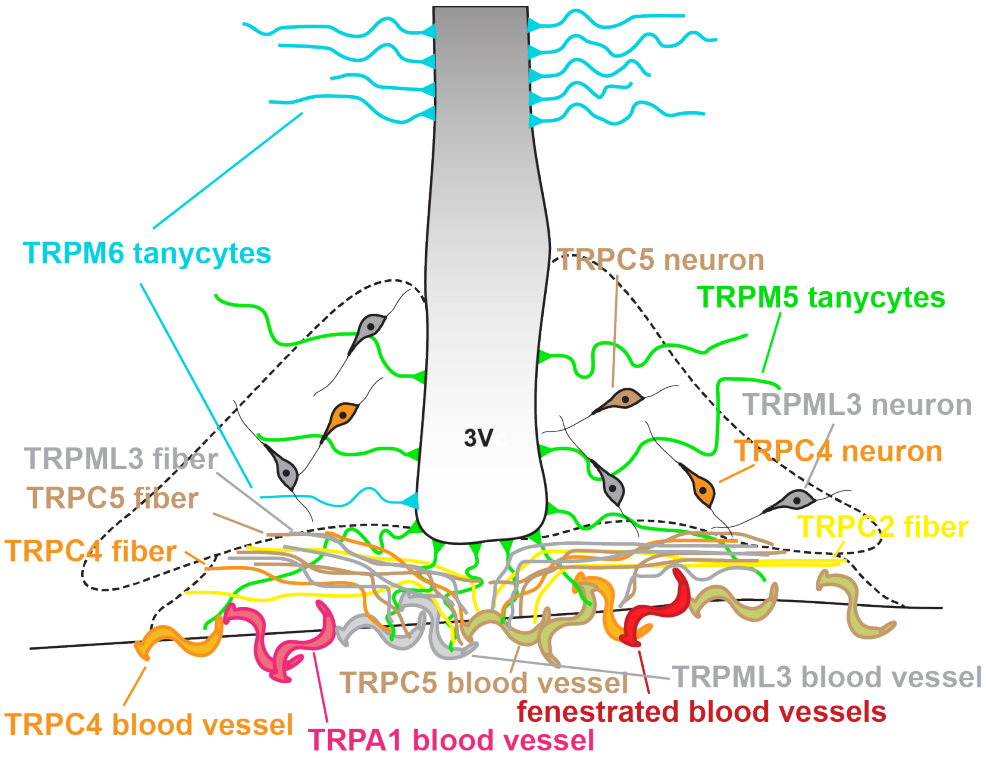

Figure 12: Summary of TRP channel expression in the Arc and ME. TRPM5 expressing cells were only observed in a subset of tanycytes. TRPM6 was only observed in the vascular system of the Arc and in few tanycytes and ependymal cells. TRPML3 expressing cells were found in a subset of blood vessels in the ME and neurons in the Arc. TRPC4 and TRPC5 showed a similar pattern with expression in subsets of neurons, fibers and blood vessels. TRPC2 was only observed in fibers.

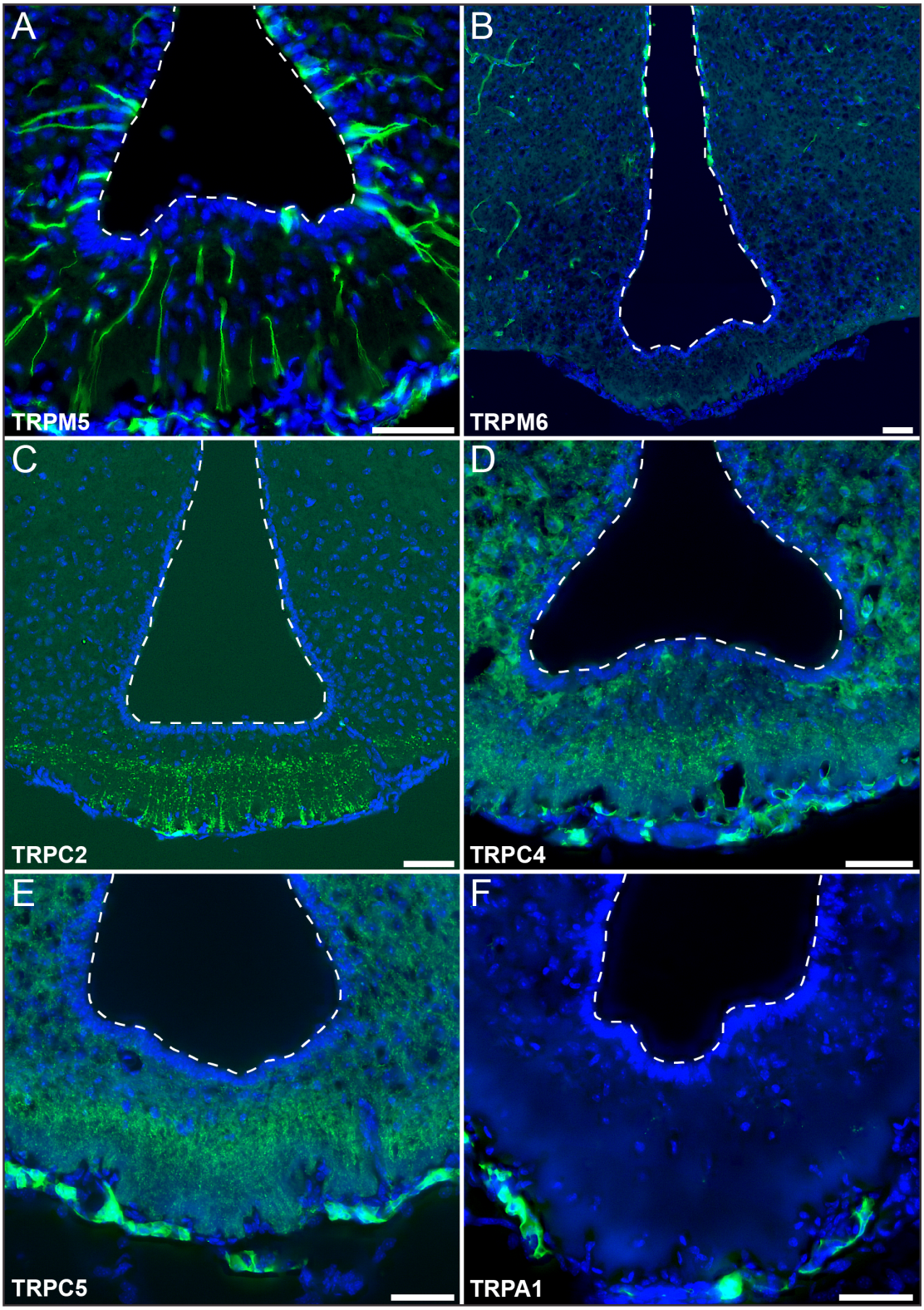

Figure 13: TRP channels are differently expressed in the ME. (A) TRPM5 driven reporter gene expression was found in tanycytes at the floor of the third ventricle projecting to the bottom of the ME. (B) In TRPM6 reporter animals no GFP-expression was found in the ME. (C) τGFP in TRPC2-IRES-Cre animals was found in neuronal fibers, potentially terminating in the ME. (D) TRPC4 was found in multiple cells types of the ME. GFP was found in neuronal fibers and cells in close apposition to the vascular system at the bottom of the ME. (E) The GFP pattern for TRPC5 is similar to that of TRPC4. (F) TRPA1 driven reporter gene expression was only found at the bottom of the ME in close apposition to the vascular system. Scalebars: 50 μm. Dotted line indicates 3V.

3.2 TRP channels in the 3D-reconstructed ME

I utilized iDISCO clearing to further characterize TRP channel expression in the ME and Arc in regards to their morphology and interaction with the vascular system of the ME.

Within the ME, TRPM5 cells were mainly confined to the walls of the third ventricle, indicating that these cells are tanycytes. I found most TRPM5 tanycytes at the floor of the third ventricle. Their cell bodies constitute the wall of the third ventricle and their ventral projections reach the surface of the ME surrounding the CD31-positive blood vessels of the hypothalamo-hypophyseal portal plexus (Figure 14 A and B). Based on their distribution, laterally facing the ventromedial arcuate nucleus and infundibular sulcus and medially the ME, most TRPM5 tanycytes are of the β1- and β2-subtypes. Co-labelling for the tanycytic marker vimentin revealed that the M5 tanycytes constitute a specific subpopulation of the whole tanycyte population due to the presence of numerous single-labeled vimentin profiles (Figure 14 C). TRPM5 tanycytes seem to be homogeneously distributed both mediolaterally and rostrocaudally. I traced the projections of individual TRPM5 tanycytes and observed the classic morphology of successive branching into smaller processes forming brush-like distal profiles (Figure 14 D - G). Most of these projections form endfeet in close vicinity to CD31-positive capillary vessels (Figure 14 D and F). I also found M5 tanycyte processes branching and terminating in capillary-free portions of the ME parenchymal surface (Figure 14 E and G). Next I determined whether TRPM5 tanycytes terminate around permeable, fenestrated capillary vessels responsible for bidirectional brain-to-blood exchanges in BBB-free areas. Because endothelial fenestrations in the ME are diaphragmed, I used an antiserum against the integral diaphragm protein PV-1 (Figure 14 H - J). I then performed immunostaining for PV-1 on cleared brain sections prepared from the reporter mice and found that TRPM5 tanycytic processes terminate at a variable distance from PV-1-positive capillaries, and as close as 0.5 μm based on measurements by SIM microscopy (Figure 14 J). Taken together, these data suggest that the M5 tanycytes have access to blood-born cues.

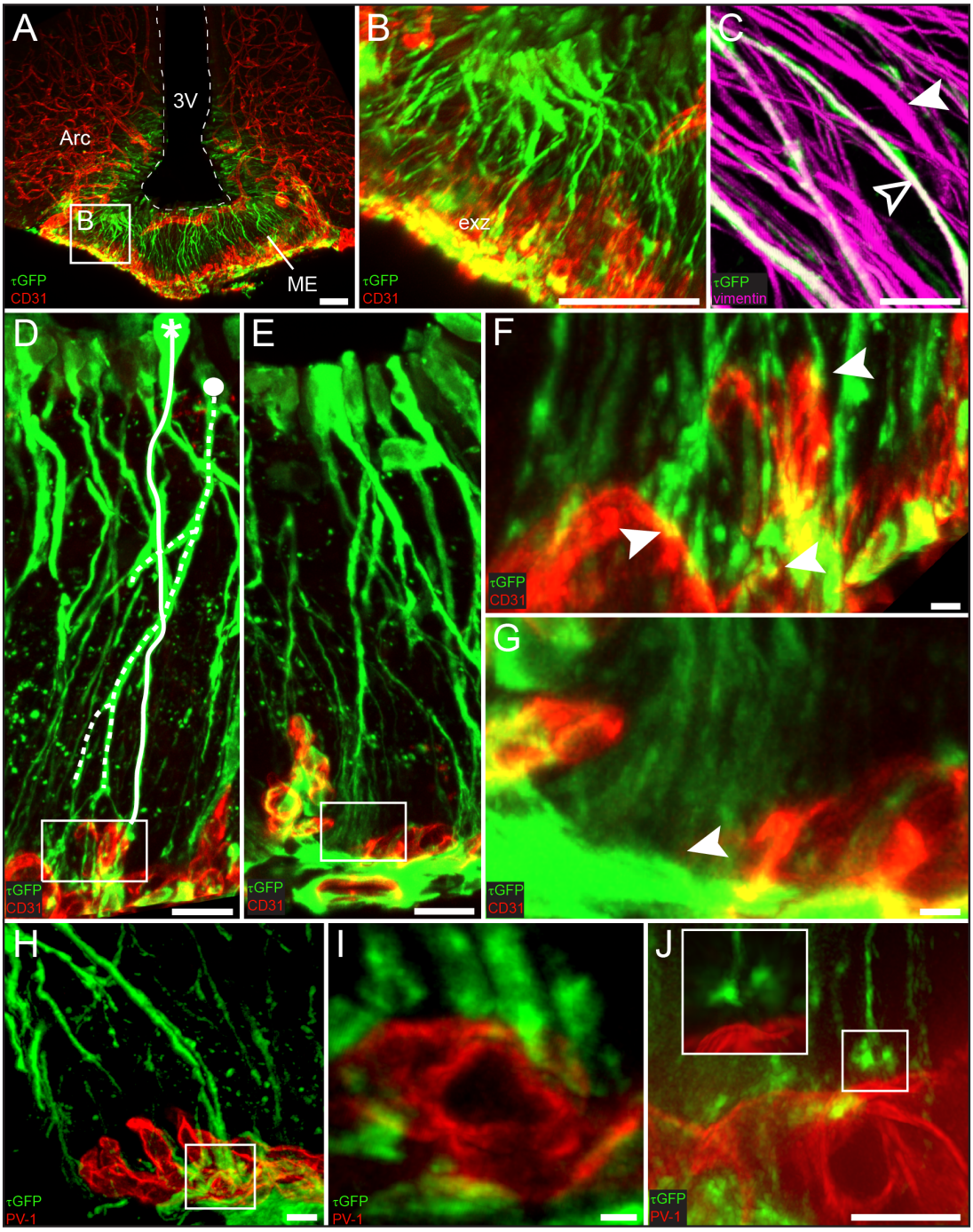

Figure 14: iDISCO cleared and 3D-reconstructed images of the ME from TRPM5-IC/eR26-τGFP mice immunolabeled for GFP (green), the endothelial marker CD31 (red), the endothelial permeability marker PV-1 (red), or the tanycyte marker vimentin (magenta). (A) M5 tanycytes are located in the floor of the third ventricle (3V) at the level of the ventromedial arcuate nucleus (ARC) and ME. (B) enlarged from the box in A, shows the elongated morphology of the M5 tanycytes projecting to the ME external zone (exz) near the capillary vessels. (C) Not all Vimentin-positive profiles are simultaneously GFP-labeled (filled arrowheads), demonstrating that TRMP5-expression delineates a specific subpopulation of tanycytes (unfilled arrowheads). (D-G) Fine architecture of the M5-tanycytes. (D, detailed in F) Two individual M5 tanycytes (marked by solid and dotted lines) form branched processes with endfeet in close apposition (arrowheads) to capillary vessels. (E, detailed in G) Other M5 tanycytes terminate at the parenchymal surface away from capillary vessels (arrowheads). (H-J) M5 tanycytes terminate near permeable microvessels, either with endfeet covering the microvessels (H, detailed in I) or seen at a distance using SIM miroscopy (J and enlarged box). Scalebars: 50 μm (A, B, C and E); 30 μm (D and H); 10 μm (F and G); 5 μm (I and J).

To better visualize the TRPM5 signal in the ME, I prepared a cleared section of the intact ME imaged from ventral to dorsal. In this orientation I could identify a new TRPM5 expressing cell type in the ME. These cells are located in the pars tuberalis, clustering around blood vessels. Due to their localization these cells are only visible as a thin GFP signal in coronal sections. These cells were not observed outside the vascular system of the ME and are not restricted to fenestrated blood vessels, indicated by their localisation on PV-1 negative vessels (Figure 15).

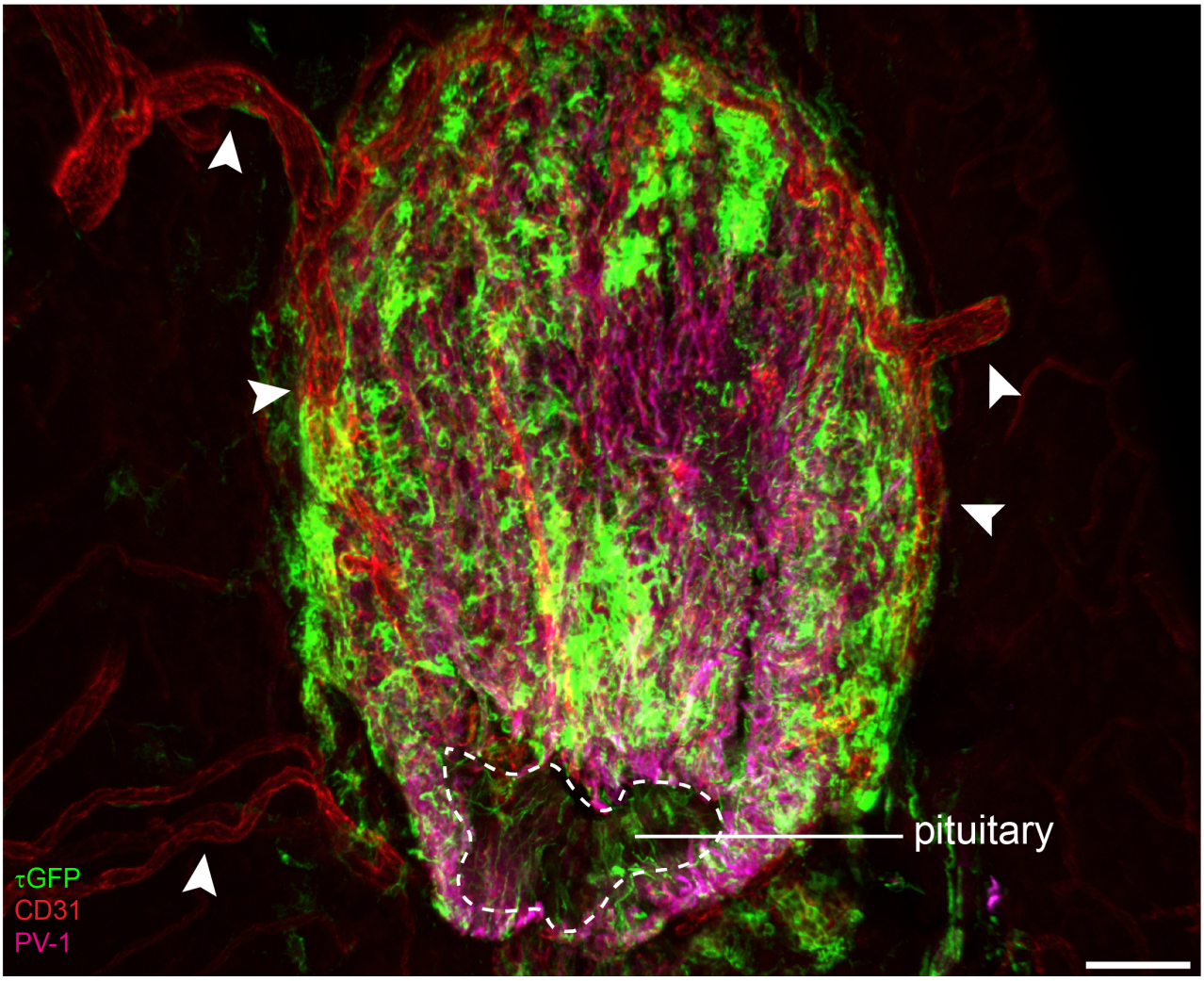

Figure 15: TRPM5 (green) is expressed in cells covering the bottom the the ME. Image of the complete ME from ventral to dorsal. In this orientation a new TRPM5 expressing cell type was revealed. These cells are located in the pars tuberalis and cover both fenestrated (magenta) and non-fenestrated (red, arrowheads) blood vessels. These cells are restricted to the pars tuberalis. Scalebars: 50 μm.

τGFP signal in TRPC2 reporter mice in the ME was restricted to neuronal fibers. These fibers are in close contact with fenestrated capillaries in the floor of the ME but the distance to the vascular system seem to vary depending on Bregma position. In more anterior parts of the ME the majority of TRPC2 fibers are on average 44.03 μm away from the vascular system (Figure 16 A). In the posterior part of the ME, fibers gather around fenestrated blood vessels and are on average only 10.33 μm away from the vascular system (Figure 16 B).

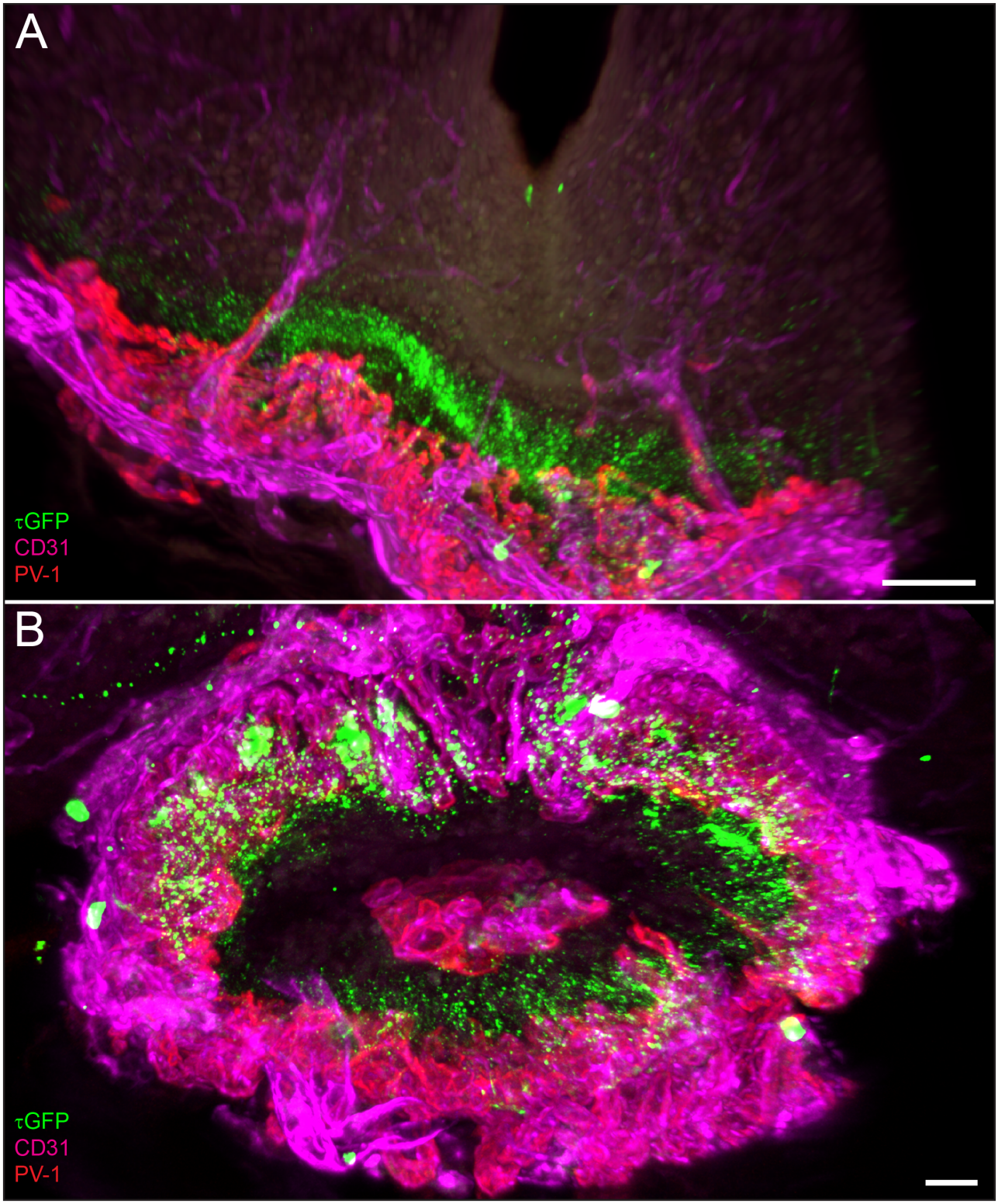

Figure 16: Distance between TRPC2 neuronal fibers and blood vessels is region dependent in the ME. (A) In more anterior parts of the ME the majority of TRPC2 fibers display an increased distance to the capillary system (magenta and red), compared to the posterior part where TRPC2 fiber seem to terminate close to fenestrated blood vessels (B). Scalebars: 50 μm.

In the Arc and the ME, TRPC4-driven reporter gene expression was observed in fibers and vascular endothelial cells but the majority of τGFP signal was observed in cells that resemble pericytes in their morphology. These cells are compromised of a cell body in close contact to blood vessels with two long projections wrapping around blood vessels in the Arc and also on fenestrated blood vessels in the ME (Figure 17).

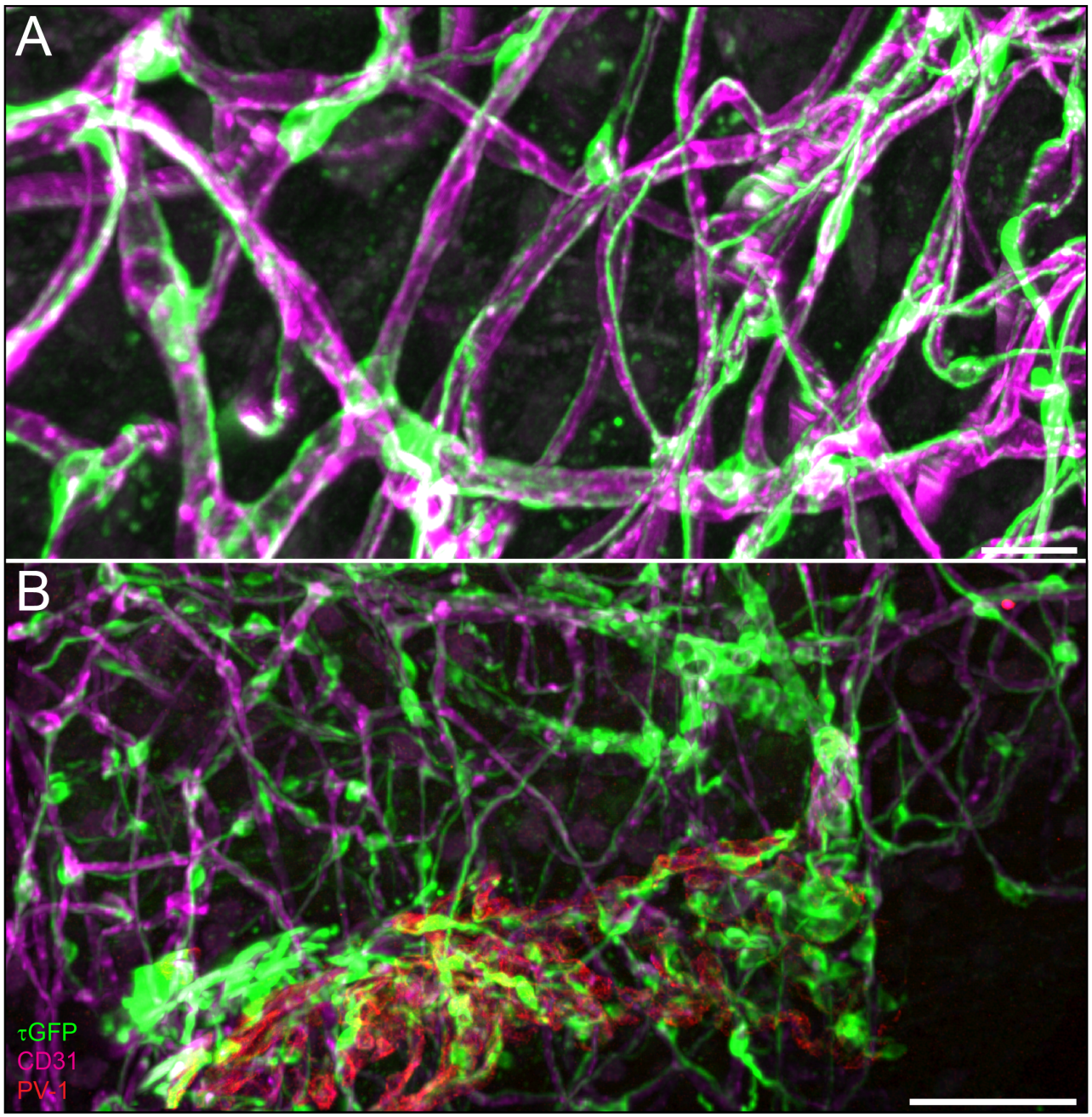

Figure 17: TRPC4 (green) is expressed in pericytes in the Arc and ME. (A) In 3D-reconstructed images τGFP was identified in cells which are in close contact to blood vessels (magenta). These cells display two long projections along the blood vessels, indicating that these cells might be pericytes. (B) TRPC4 driven reporter gene expression was observed in cells resembling pericytes in close contact with fenestrated blood vessels (red) in the ME. In addition τGFP expression was also identified in a subset of non-fenestrated blood vessels (red). Scalebars: A: 50 μm, B: 200 μm.

Besides the expression in neuronal fibers in the ME and neurons in the Arc, I observed TRPC5-driven reporter gene expression in cells in the pars tuberalis (Figure 18). These cells are morphological similar to the cells found in TRPM5 reporter mice and cells of these types were also observed in the pars tuberalis of TRPA1 reporter mice (Figure 19). TRPA1 and TPRC5 cells occupy a similar location at the borders of the ME while the TRPM5 cells seem to be more heterogeneously distributed.

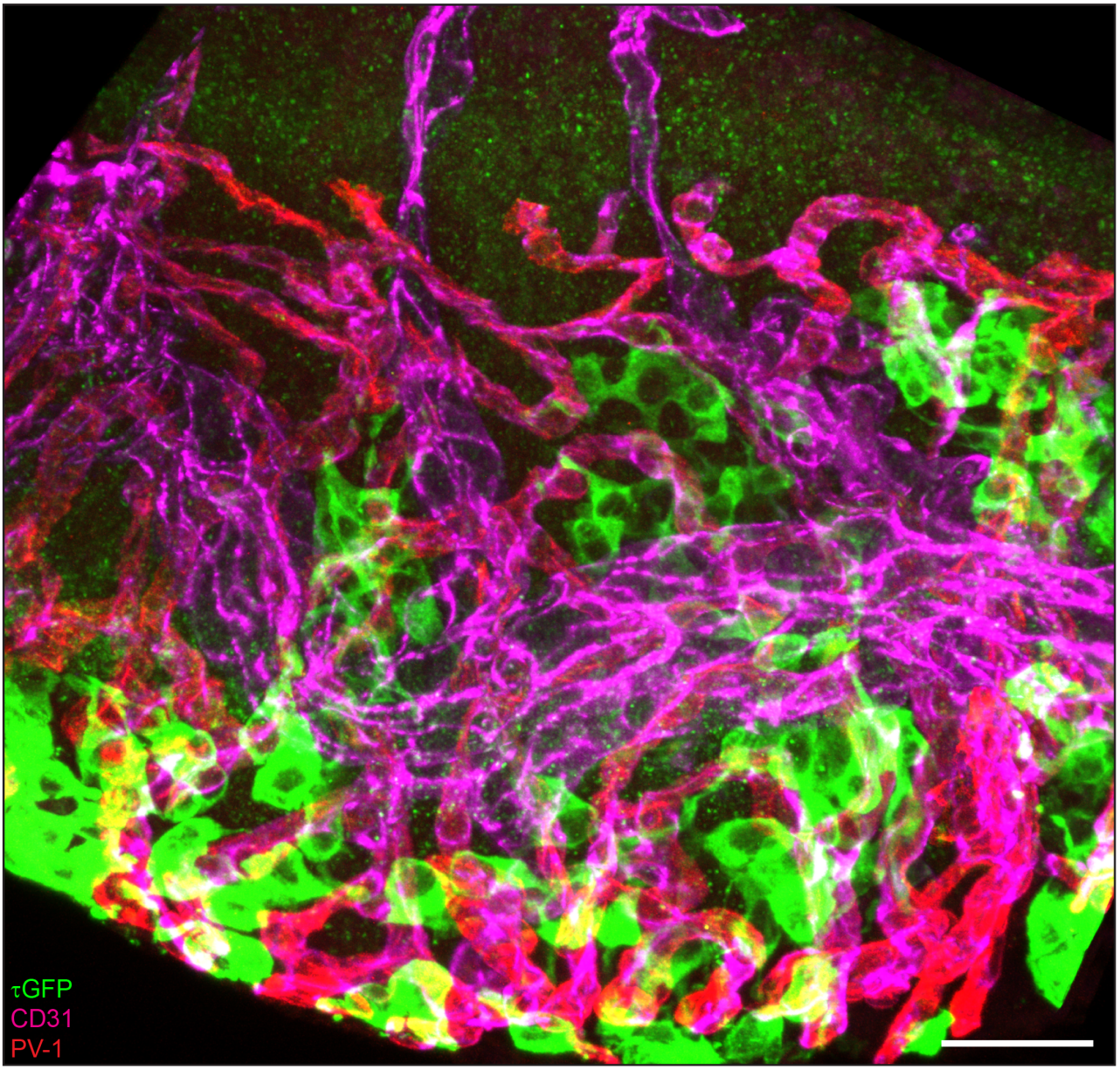

Figure 18: TRPC5 is expressed in cells lining the pars tuberalis. Reporter gene expression in cleared TRPC5 reporter MEs was identified in cells that resemble the TRPM5 cells in the pars tuberalis. These cells are in close contact with fenestrated (red) blood vessels in the ME. τGFP signal was also observed in fibers innervating the ME. Scalebars: 100 μm.

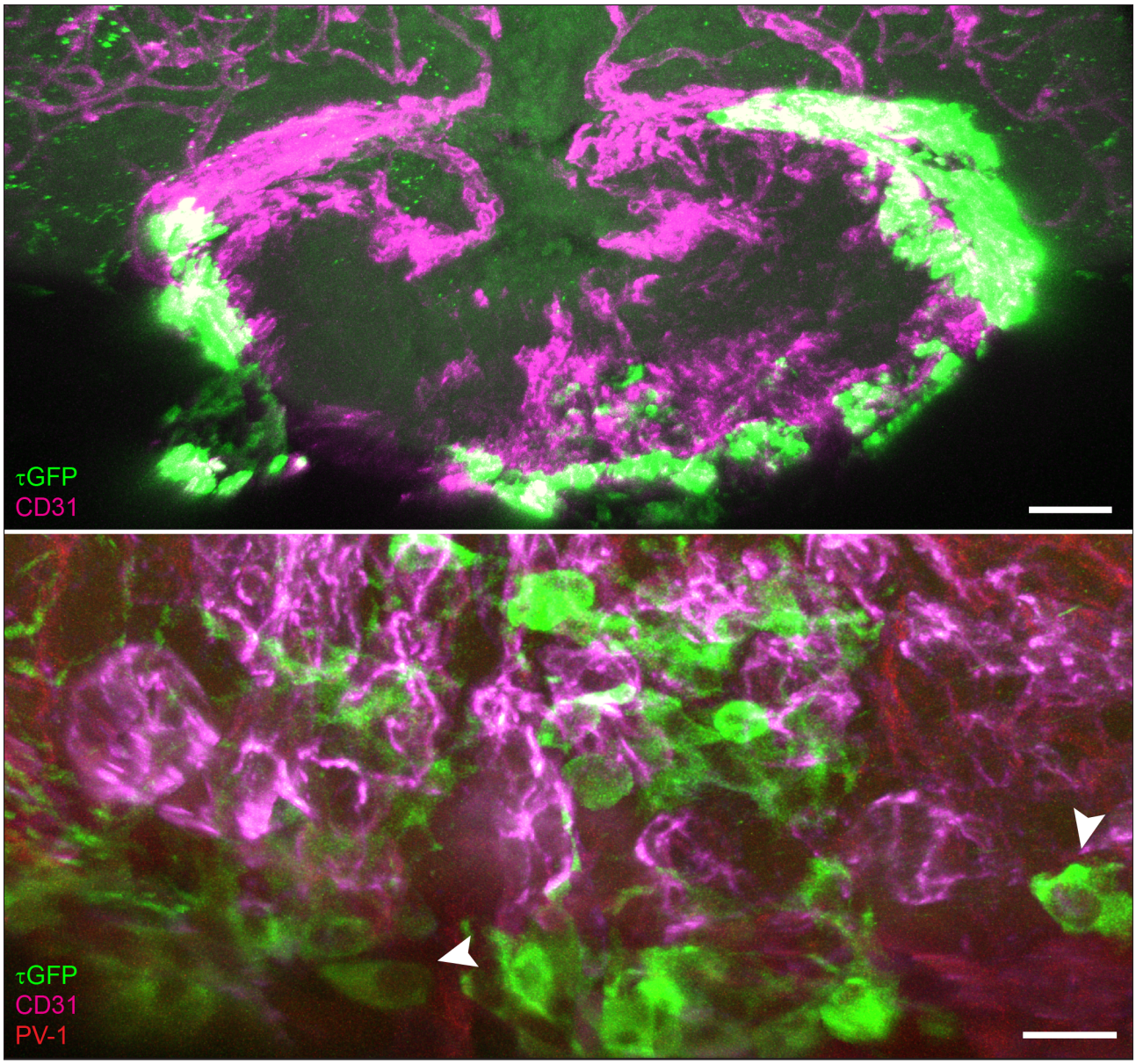

Figure 19: TRPA1 was found in a subset of cells in the pars tuberalis (arrowheads). Like in TRPM5 and TRPC5 reporter animals, these cells are in close contact with the vascular system. Scalebars: 50 μm.

These findings revealed that TRP channels are expressed in different cell types in the ME brain window and the expression patterns vary also between members of the same subfamily. My results indicate that for a more precise morphological analysis cleared and 3D-reconstructed MEs show benefits compared to thin cryosections.

3.3 TRPC2 in the CNS

TRPC2 was reported to be only expressed in vomeronasal sensory neurons in the VNO and recently shown to be also expressed in the MOE. With the new TRPC2IC/eR26-τGFP mouse I confirmed the expression in the olfactory system (Figure 20). In addition, I revealed TRPC2 expression in a small group of pituitary cells and in a population of PVN neurons in the hypothalamus (Table 13, page 109, appendix). I investigated if the TRPC2 cell population in the pituitary is part of the hormone producing cells, somatotropes, corticotropes, thyrotropes, gonadotropes or lactotropes. To identify these cell populations I performed stainings against LH/FSH, ACTH, growth hormone (GH), thyroid-stimulating hormone (TSH) and Prolactin. Staining against these pituitary hormones revealed that the TRPC2 cells are not part of the gonadotrope cell population and staining against ACTH showed that the reporter gene expressing cells are ACTH negative. I also did not observe any colocalization between TRPC2 and prolactin or TSH expressing cells. Very few TRPC2 cells were also expressing GH, but compared to the total number of GH-expressing cells this colocalized population seems negligible (Figure 21). In the brain I found TRPC2 to be expressed in some non neuron cells throughout the brain which resemble glia and astrocytes in shape. Heavy fiber innervation of glomeruli from the nose sensory neurons was found.

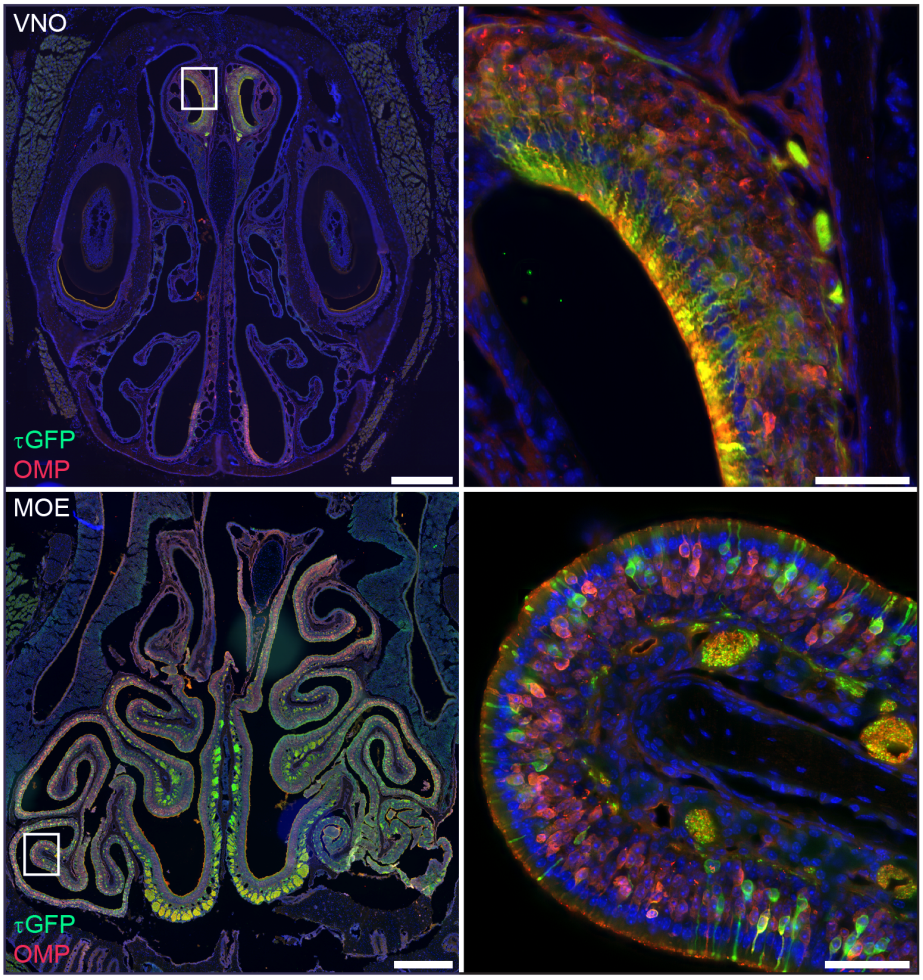

Figure 20: TRPC2 is expressed in all VSNs and a large amount of OSNs. (A) VSNs, marked by the expression of OMP (red) are all positive for τGFP. (B) Magnified image of the region indicated in (A). (C) A subset of OMP+ OSNs (red) expressed the reporter gene. (D) Magnified image of the region indicated in (C). Nuclearstein in blue. Scalebars: 500 μm overview, 50 μm inset.

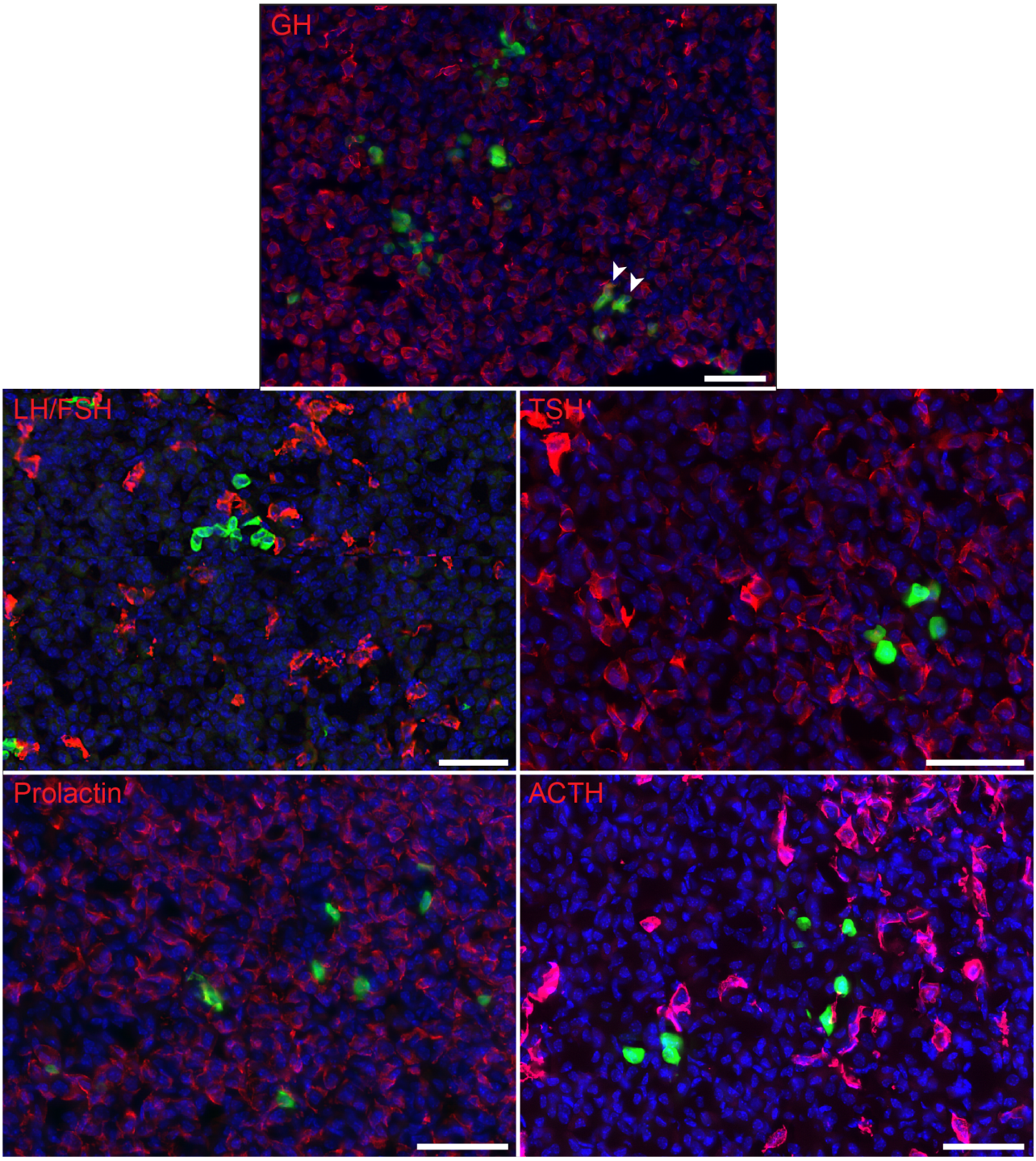

Figure 21: TRPC2 pituitary cells are not hormone releasing cells. Costainings against τGFP and the pituitary hormones LH/FSH, TRH, Prolactin, ACTH and GH revealed that only very few TRPC2 are also expressing GH (arrowheads) and were negative for any other hormone. Scalebars: 50 μm.

3.3.1 Projection pattern of TRPC2 neurons

τGFP expression in the TRPC2IC/eR26-τGFP animals was observed in a small population of PVN neurons with around 450 neurons per animal. This was the only observed neuronal signal. Most neurons were observed in the medial parvocellular subdivision of the PVN. I performed RT-PCR experiments with primers against TRPC2 and confirmed acute TRPC2 expression in PVN neurons(Figure 22). Next, I investigated if the neuronal fibers observed in the ME originate from this neuronal population. Fibers are projecting ventro-laterally out of the PVN along the lateral hypothalamus (Figure 23 A) until they reach the bottom of the lateral hypothalamus and project in the direction of the midline (Figure 23 B) where fibers from both hemispheres merge together in the ME (Figure 23 C). This indicated that the fibers from the TRPC2 neurons in the PVN terminate in the ME.

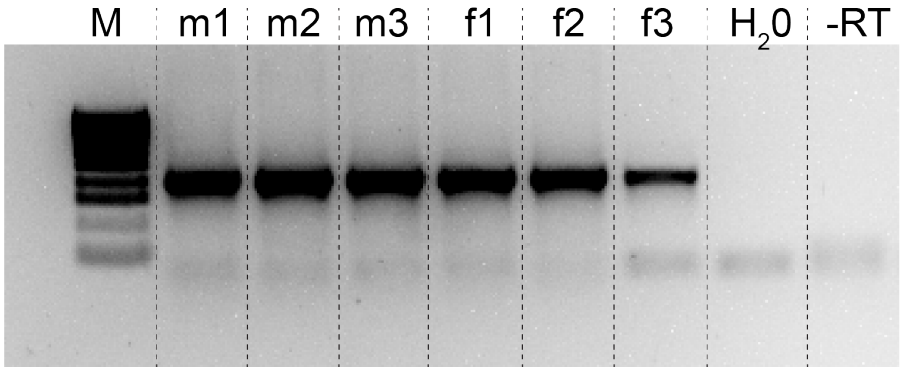

Figure 22: TRPC2 is acutely expressed in PVN neurons. In three males and three females a TRPC2-specific band (295 bp) was observed. No band was found in the water and -RT control..

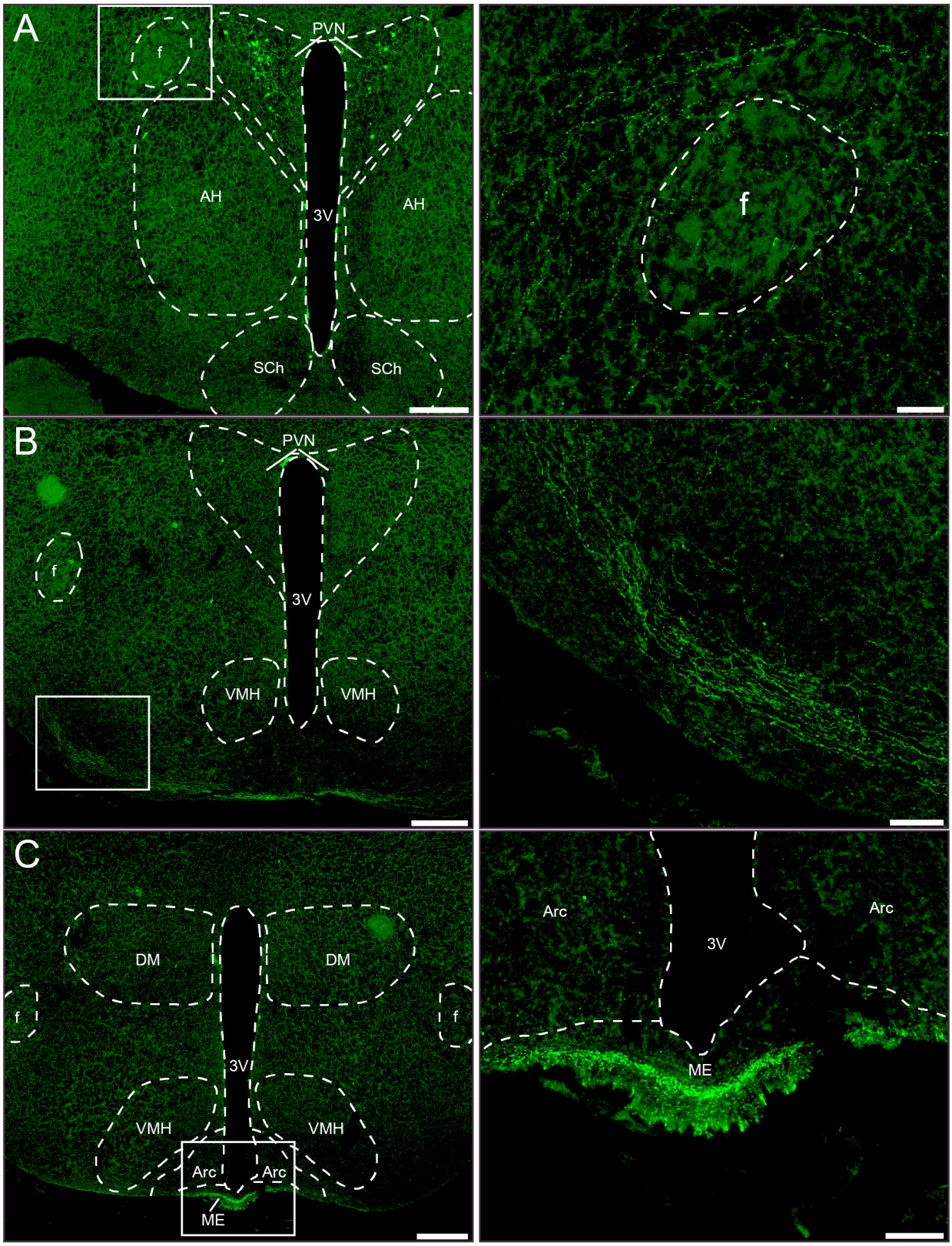

Figure 23: Fibers from TRPC2 PVN neurons project ventro-laterally into the ME. (A) TRPC2 fibers project ventro-laterally passing the fornix along the lateral hypothalamus. (B) Fibers reach the bottom of the lateral hypothalamus and fibers from both hemispheres merge along the midline (C) Fibers end in the ME. PVN: paraventricular nucleus; 3V: third ventricle; Arc: arcuate nucleus; DM: dorsomedial nucleus; VMH: ventromedial hypothalamus; ME: median eminence; f: fornix; AH: anterior hypothalamic area; SCh: suprachiasmatic nucleus. Scalebars: 200 μm overview, 100 μm inset.

3.3.2 Hormonal identity of TRPC2 PVN neurons

The neurons in the paraventricular nucleus can be separated into magnocellular neurosecretory neurons (Oxytocin and Vasopressin) projecting into the pituitary and parvocellular neurosecretory neurons (corticotropin-releasing hormone, vasopressin and thyrotropin-releasing hormones) projecting into the ME. I performed costainings against these hormones to identify the hormonal identity of PVN neurons. Because I did not observe any fibers in the neuropituitary, the TRPC2 PVN neurons could not be magnocellular neurons. Costaining against oxytocin and vasopressin also confirmed this assumption because no TRPC2 neurons were colocalized with either of the two hormones (Figure 24 and Figure 25). I also performed stainings against tyrosin hydroxylase (TH), CRH, somatostatin (SST) and TRH. I did not observe any colocalization of any of these hormones with τGFP neurons (Figure 24) and only minor colocalization of TRPC2 and CRH in fibers of the ME (Figure 25). Because these hormones are quickly transported from the somata to the synaptic release point in the ME it is not possible to detect the peptides in all neurons with immunofluorescence. To be able to still use immunofluorescence as a detection method in the PVN TRPC2IC/eR26-τGFP animals were injected with colchicine in the lateral ventricle to prevent the transport out of the somata. In these animals I found that the hormone neuron number is drastically increased compared to the non-injected animals. I observed no colocalization between TRPC2 and OXT, TRH, SST, AVP and TH but TRPC2 was only colocalizing with CRH. Only a minor subset of TRPC2 and an even smaller subset of CRH neurons are double positive (Figure 26). These experiments revealed that a subpopulation TRPC2 PVN neurons coexpress CRH. The majority of TRPC2 neurons were not postive for any of the classical PVN hormones.

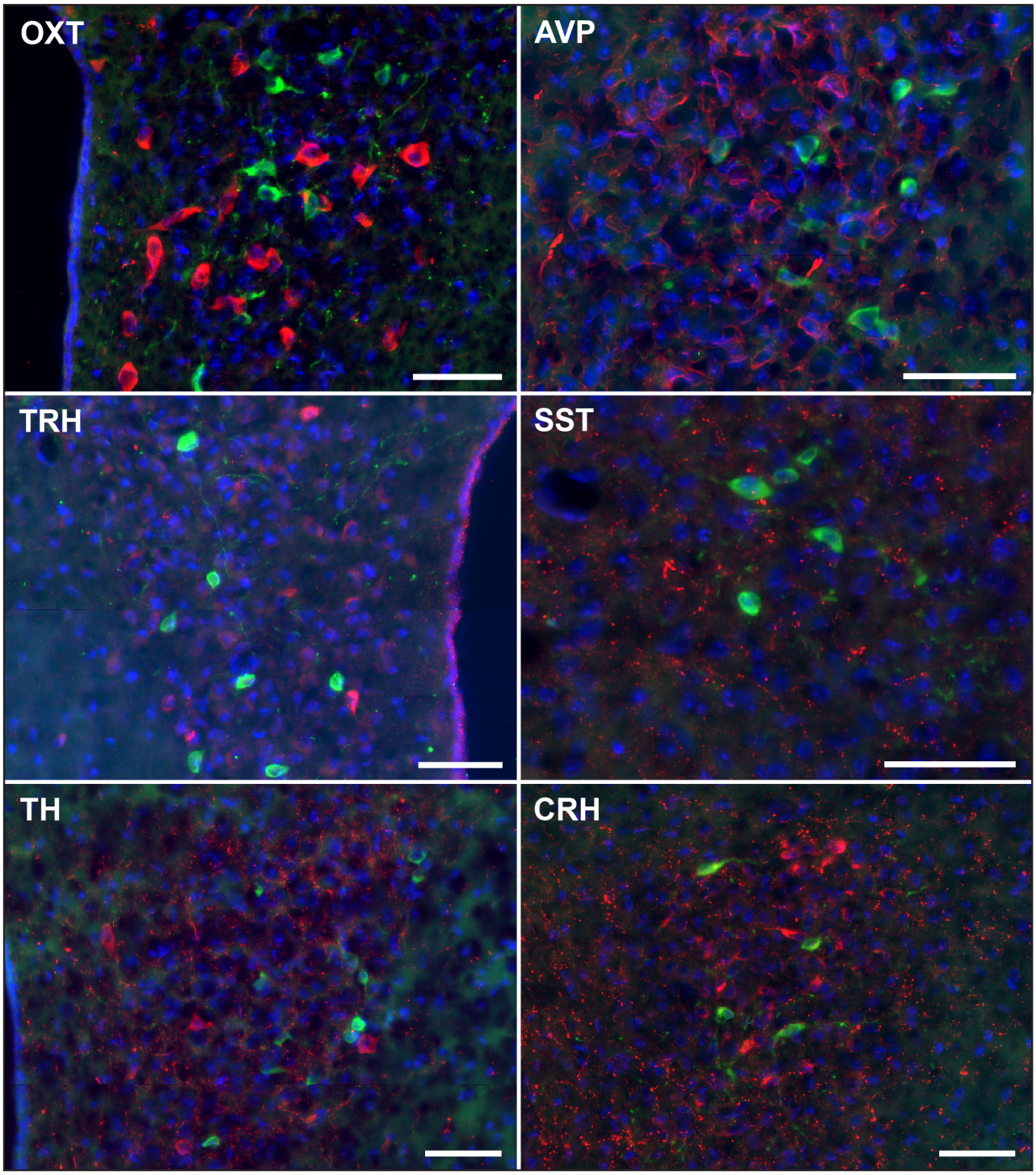

Figure 24: TRPC2 neurons are not expressing PVN hormones. Costainings for oxytocin (OXT), vasopressin (AVP), thyroxin-releasing-hormone (TRH), somatostatin (SST), tyrosin hydroxylase (TH) and corticotropin-releasing-hormone (CRH) and τGFP revealed no colocalization. Scalebars: 50 μm.

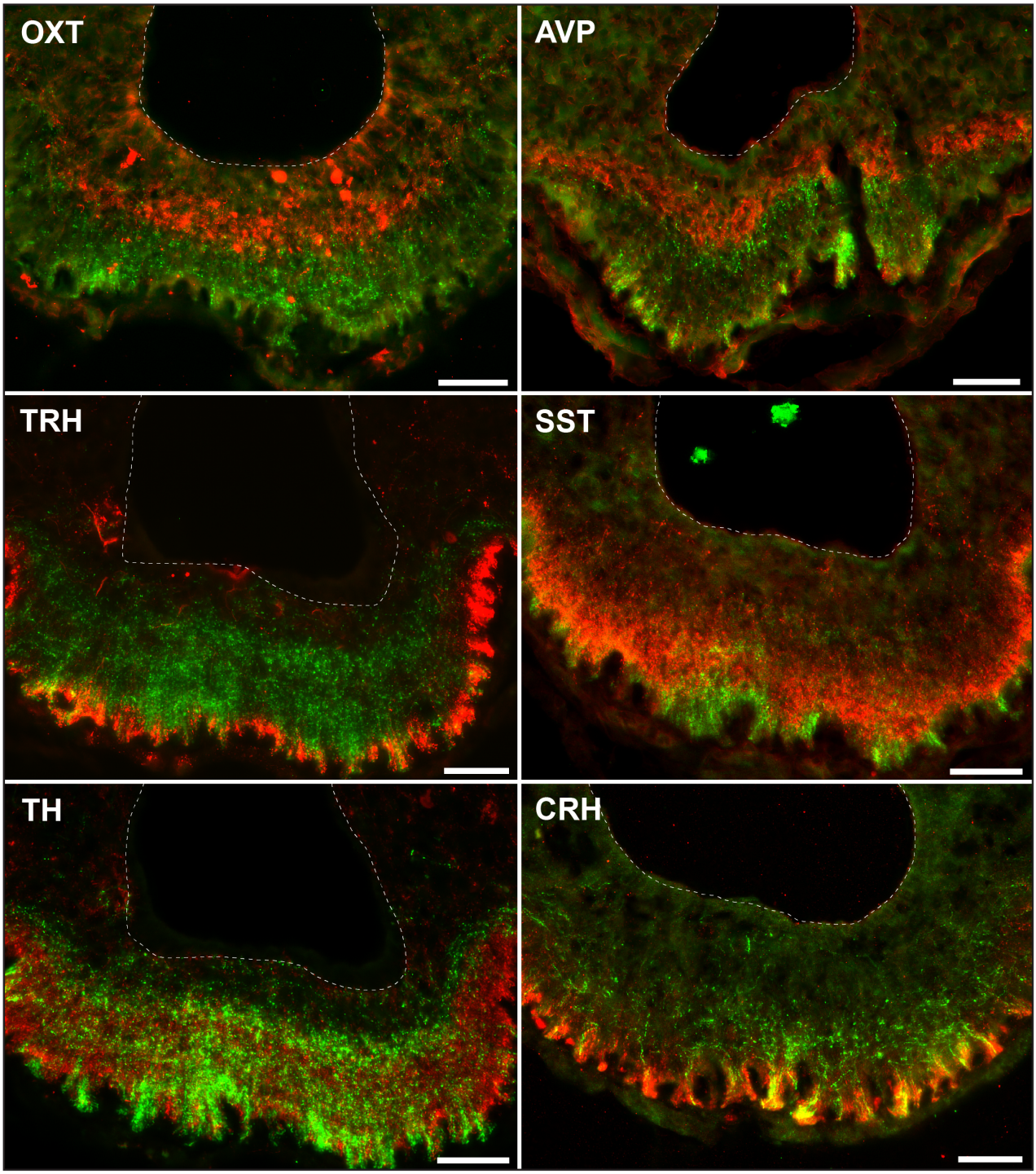

Figure 25: TRPC2 fibers only colocalize with a subset of CRH fibers. Costainings in the ME against PVN hormones revealed no colocalization between TRPC2 and PVN hormonal fibers with the exception of a small subset of CRH fibers. Scalebars: 50 μm.

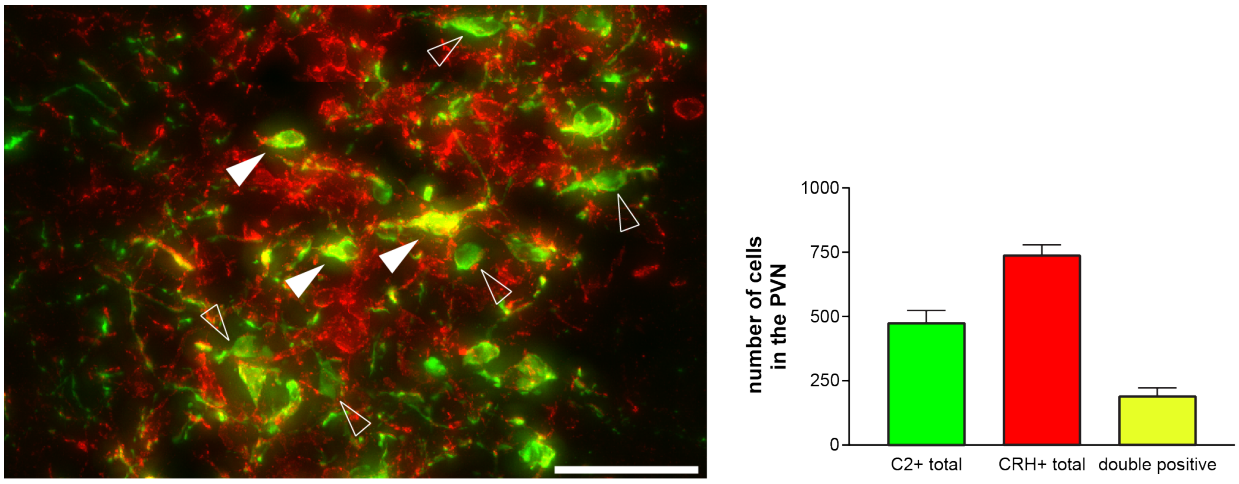

Figure 26: A small subset of CRH neurons expresses TRPC2. After colchicine injection, a subset of τGFP neurons also expresses CRH. Filled arrowheads indicate double positive neurons, unfilled arrowhead indicate CRH negative τGFP neuron. Only 190.8 ± 53.64 neurons are double positive of 475.8 ± 83.27 total TRPC2 neurons and 732.5 ± 79.41 of total CRH neurons. Scalebar: 50 μm.

3.3.3 TRPC2 neurons have only a minor impact on hormone levels

To investigate the impact of TRPC2 neurons on hormone release from the pituitary, I utilized TRPC2IC/eR26-DREAAD animals. In these animals a designer receptor exclusively activated by designer drug (DREADD) is expressed after initial Cre-expression. This channel is linked to an HA-tag and also expresses the nucleus-directed fluorescence marker iRFP. I performed staining against the HA-tag to verify faithful expression of the channel in TRPC2 PVN neurons (Figure 27). I injected Clozapine N-oxide (CNO) in these animals to activate TRPC2 via the artificial G-protein coupled pathway and measured the impact of this activation on pituitary hormones. No statistical difference was observed in all investigated hormones 25 minutes after injection between Cre-positive and Cre-negative controls (Figure 28). Also no differences in hormone concentration was observed between the 1 hour, the 2 hour and the uninjected control group for ACTH, TSH, Prolactin and GH (Figure 28). FSH concentrations were higher 1 or 2 hours after injection of CNO in DREADD expressing animals when compared to uninjected control animals (Figure 28). LH levels in the blood were statistically higher 2 hours after injection in DREADD animals when compared to controls but not after 1 hour (Figure 28). These results show that TRPC2 PVN neurons might have an effect on the LH/FSH secretion by enhancing the release. Due to small animal numbers these results have to be treated with caution.

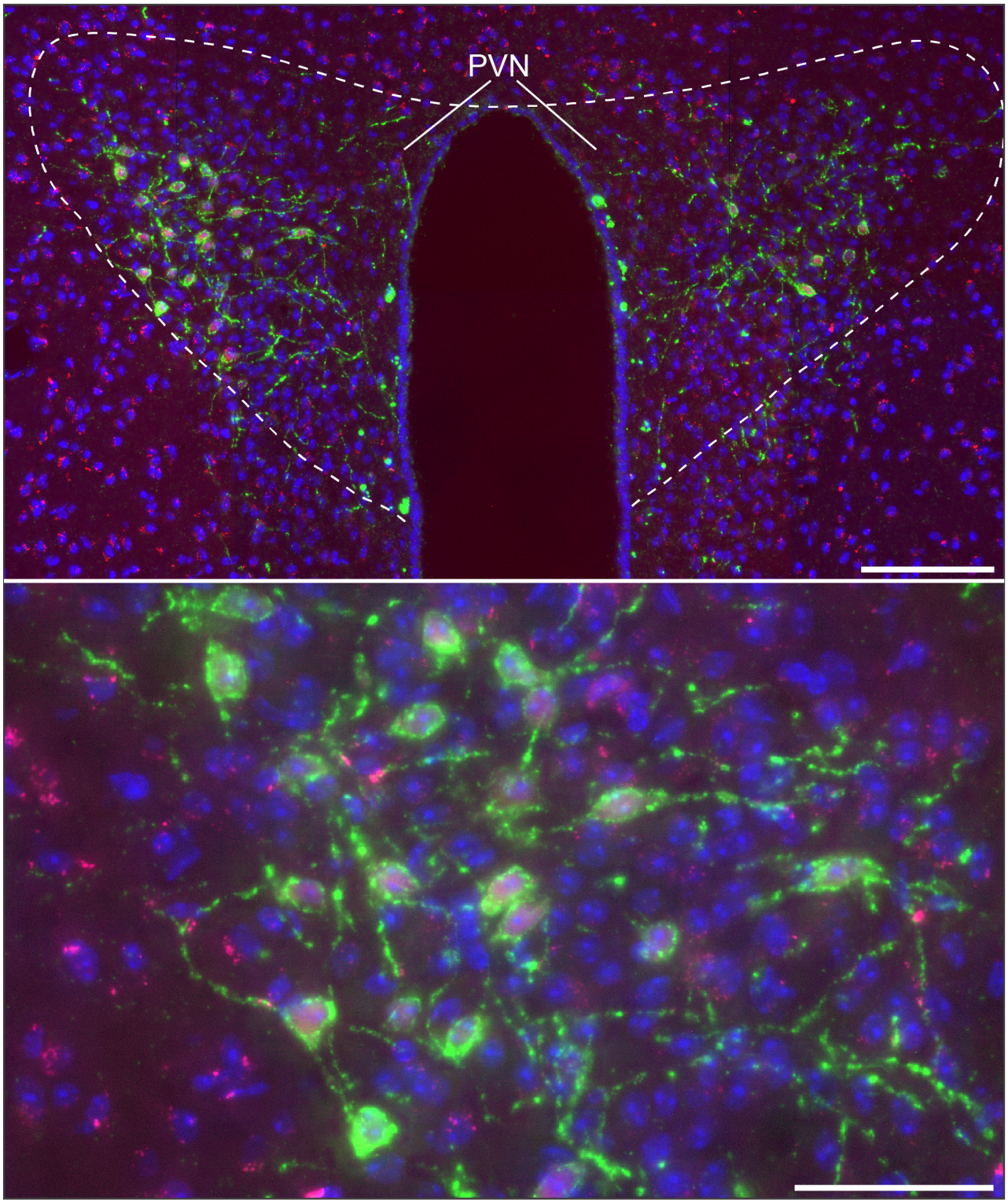

Figure 27: Designer receptor exclusively activated by designer drug (DREADD) channel is faithfully expressed in TRPC2 neurons. Overview picture shows HA-tag signal in green and iRFP in red. Bottom panel shows magnified area from top. Scalebars: 100 μm (top), 20 μm (bottom).

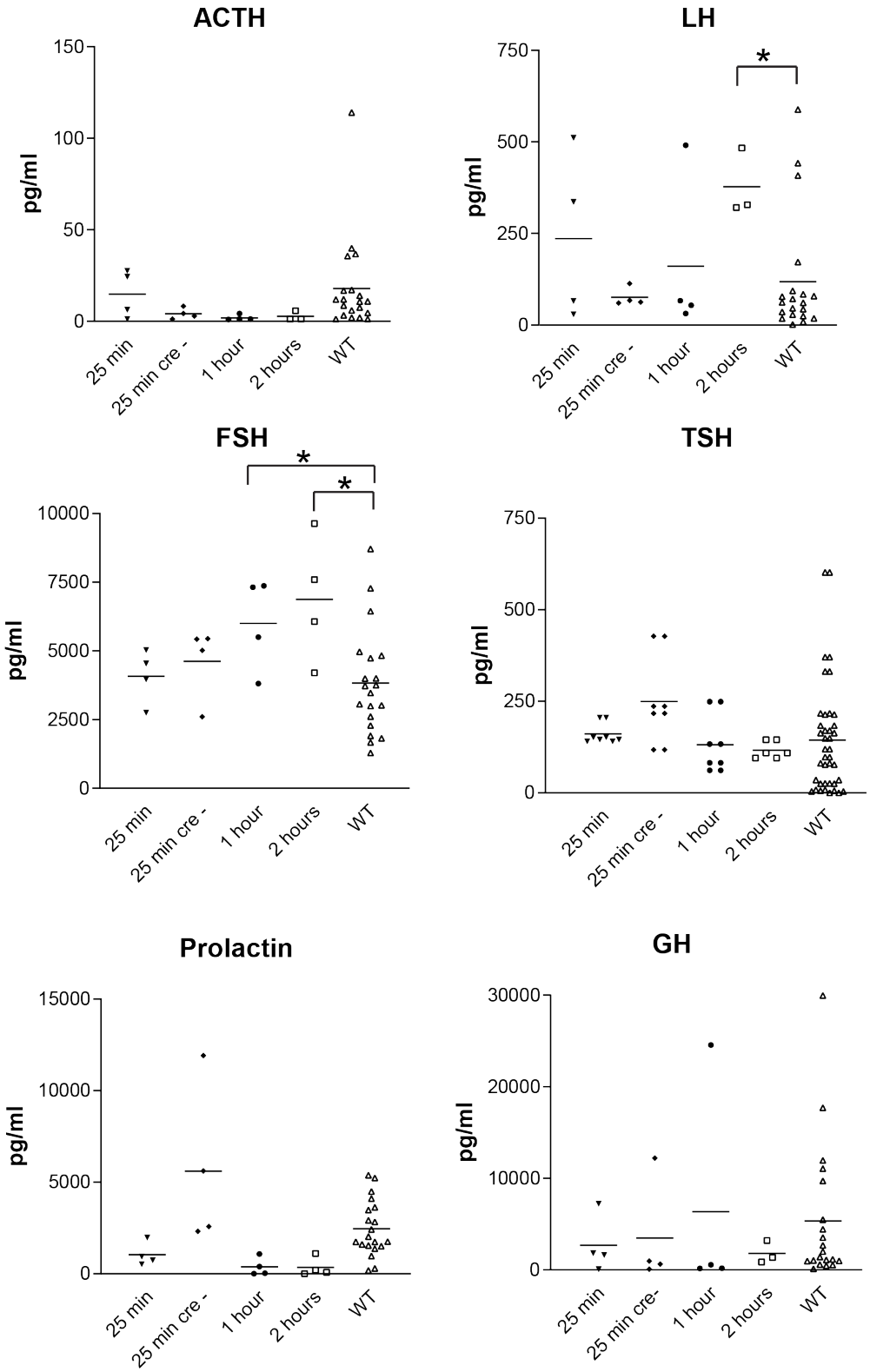

Figure 28: Only LH and FSH levels change after DREADD activation. ACTH, TSH, Prolaction and GH are not statistically different in all groups analysed. 1 or 2 hours after activation, FSH levels are increased in CNO injected DREADD animals compared to uninjected wild type animals (1 hour vs WT p-value: 0.0485, 2 hour vs WT p-value: 0.0103). LH levels were only increased in the 2 hour group compared to control animals (p-value: 0.0148)..

To investigate the impact of the TRPC2/CRH double positive neurons on ACTH levels I chronically silenced the TRPC2 neurons by expressing tetanus toxin in these neurons. In these TRPC2IC/R26-TeNT animals, tetanus toxin is expressed from the *ROSA26* locus and blocks vesicular release. In a second animal model (TRPC2IC/R26-DTA) TRPC2 neurons were ablated by the expression of diphtheria toxin A (DTA) after cre recombination in these cells. After injecting animals with PBS to induce stress due to the injection, I harvested the blood and measured ACTH plasma levels. I did not detect a significant difference between wild type (WT) animals and the chronical silenced or ablated group (Figure 29). These result indicate that the TRPC2 PVN population has no impact on ACTH release from the pituitary.

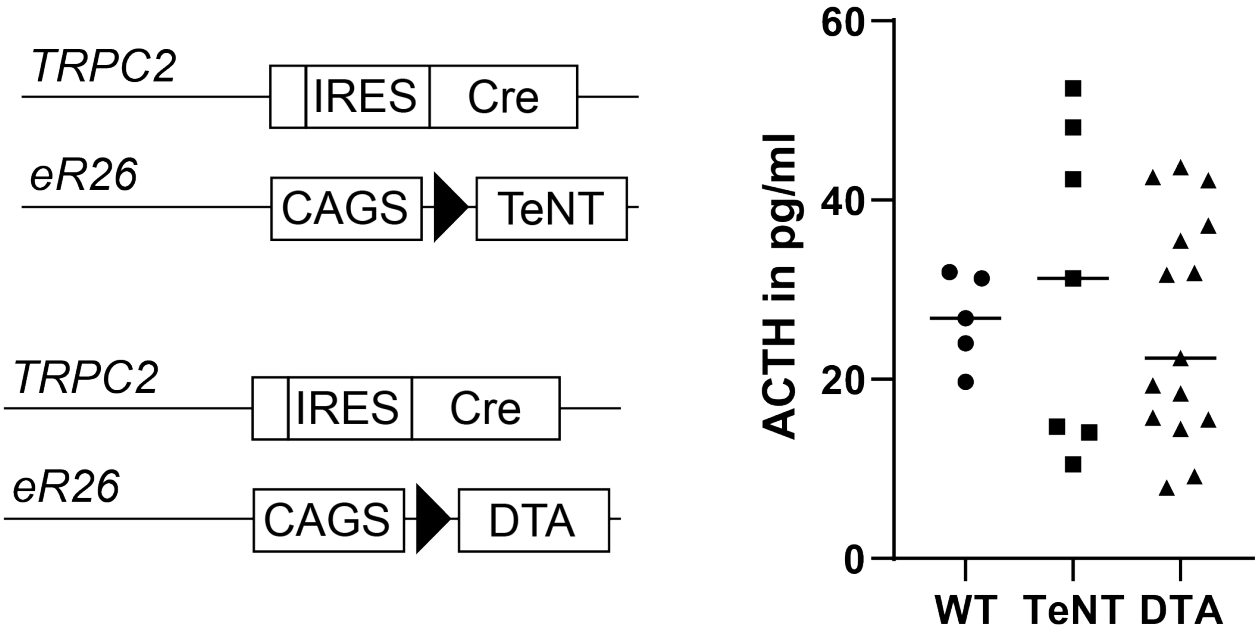

Figure 29: Chronical silencing or ablation of TRPC2 neurons has no impact on ACTH release. On the left, breeding schemes for the TRPC2IC/R26-TeNT and TRPC2IC/R26-DTA animals are shown. Graph shows results of ACTH level measurement in the blood of silenced and ablated animals compared to WT animals. No significant difference in ACTH levels was detected.

These findings highlight the power of reporter mouse lines for investigating subpopulation in control of body homeostasis. The binary genetic approach is an elegant tool to visualize cell population in which the gene of interest is expressed at low levels or antibodies are difficult to produce as shown here for TRP channels. Aromatase is also involved in the control of body homeostasis through synthesis of oestrogen and no reliable antibodies are available. I investigated the onset of aromatase expression in the embryonic brain and the influence of aromatase neurons on parts of the hpg-axis.

3.4 Aromatase is expressed in the embryonic mouse brain

To identify aromatase neurons in the developing mouse brain, I generated reporter mice in which aromatase-expressing cells are labelled with τGFP (ArIC/eR26-τGFP). The τGFP fusion protein is actively shipped down axonal microtubuli visualizing both aromatase-positive perikarya and their projections. While I did not find fluorescent signal in either male or female brains at embryonic day 12.5 (E12.5; Figure 30). I detected τGFP+ cells at E13.5 (Figure 30). The fluorescent signal was restricted to two distinct forebrain nuclei, the preoptic area and the stria terminalis, respectively, with more aromatase neurons in the medial preoptic area (46.0 ± 5.6 τGFP+ cells in males; 48.8 ± 14.9 cells in females, see Table 14, page 117, appendix) than in the stria terminalis (17.5 ± 4.2 cells in males; 23.1 ± 6.3 cells in females; n = 4-5 animals, see Table 14, page 117, appendix). Both nuclei also contained some τGFP+ fibers in close apposition to the labelled somata. I next performed RT-PCR for the Cyp19a1 gene (catalyzing both the conversion of androstendione to oestrone and of testosterone to estradiol) on whole brain mRNA prepared from E13.5 mouse brains. Cyp19a1 mRNA was readily detected in all tested individuals, confirming aromatase expression at this age. I also analyzed expression of the Cyp11a1 (converting cholesterol to pregnolone) and Cyp17a1 genes (converting pregnolone to 17-alpha-hydroxypregnolone and to 17-alpha-hydroxypregnolone-dehyroepiandrosterone, DHEA), respectively. All 3 Cyp enzymes tested were expressed at E13.5, suggesting *de novo* steroid hormone synthesis in the embryonic murine brain (Figure 31).

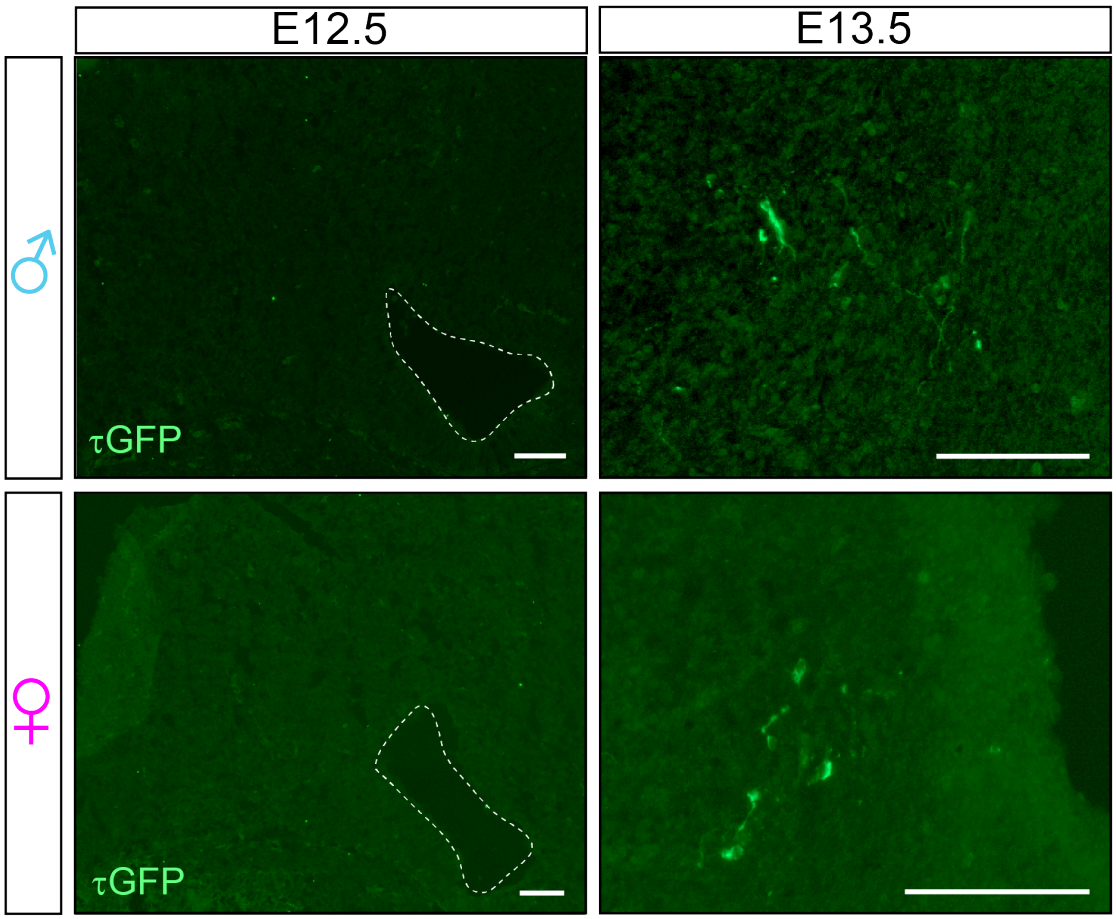

Figure 30: In E12.5 male embryos no τGFP signal was detected in the brain. The onset of aromatase expression occurs at E13.5 in the medial preoptic area and the stria terminalis. In both developmental stages the medial preoptic area is shown. No gender differences were detected. Scalebar, 50 μm..

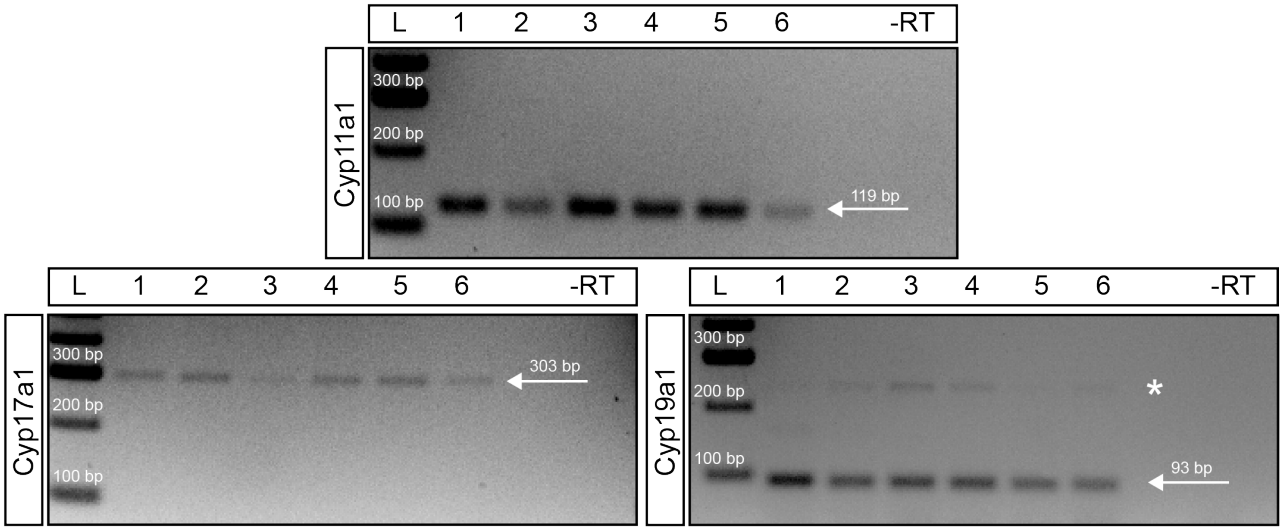

Figure 31: RT-PCR of E13.5 embryos. Cyp11a1 band at 119 base pairs, Cyp17a1 band at 303 base pairs, Cyp19a1 band at 93 base pairs. Bp = base pairs, asterisk: unspecific bands.

3.4.1 Development of an aromatase neural network *in utero*

The total number of aromatase neurons increased dramatically throughout embryonic brain development (E13.5: 63.5 ± 6.2 vs. E16.5: 3921 ± 380.4 vs. E18.5: 6073 ± 324.1 τGFP cells in males (n = 3-5 animals) and E13.5: 56.3 ± 12.9 vs. E16.5: 3330 ± 262.2 vs E18.5: 6583 ± 458.5 cells in females (n = 3-4 animals), see Table 15, page 117, appendix and Table 16, page 118, appendix). Strikingly, aromatase was exclusively expressed in distinct nuclei in the hypothalamus and the amygdala/stria terminalis at all stages analysed.

At E16.5, most aromatase neurons were located in the medial amygdaloid nucleus (1047.5 ± 88.8 cells in males, 839.3 ± 83.8 cells in females) and in the medial preoptic area (1070.8 ± 178 cells in males, 996.8 ± 70.3 cells in females, n = 3 animals) (Figure 32). Both nuclei contained dense τGFP+ fibers as well (Figure 32 unfilled arrowheads). Additional aromatase neurons were located in the cortical amygdaloid nucleus and in the optic tract. I also identified fluorescent somata and dense fibers in the stria terminalis, the bed nucleus of the stria terminalis, the ventromedial and the dorsomedial nuclei, the paraventricular nucleus and the medial tuberal nucleus. A few aromatase neurons were located in the lateral preoptic and the lateral hypothalamic areas, respectively. At E18.5 (Figure 32), aromatase expression started in the amygdalohippocampal area (135.8 ± 39.3 cells in males, 150 ± 45.1 cells in females, n = 3 animals). Only sparse τGFP+ fibers were observed in the amygdalohippocampal area and the cortical amygdaloid nucleus. In contrast, both the optic tract and particularly the medial amygdaloid nucleus contained dense fluorescent fibers, decorating almost the entire nucleus (Table 16, page 118, appendix). Aromatase neurons and fibers in the hypothalamus remained restricted to the nuclei identified at E16.5, with somewhat increased cell numbers (Table 16, page 118, appendix). Most aromatase neurons were found in the medial preoptic area with 2722.5 ± 123.5 cells in males and 2885 ± 217.4 cells in females (n = 3 animals). This individual nucleus also showed the highest increase in aromatase cell numbers when compared to E16.5 animals. The medial tuberal nucleus, the lateral hypothalamic and the lateral preoptic areas only contained sparse fluorescent fibers, whereas all other τGFP+ nuclei displayed dense τGFP+ fibers. The stria terminalis contained particularly dense fluorescent fibers comparable to the medial amygdaloid nucleus (Table 16, page 118, appendix and Figure 33). Importantly, no sexual dimorphism in the aromatase expression pattern was observed in any nucleus at any embryonic developmental stage analyzed.

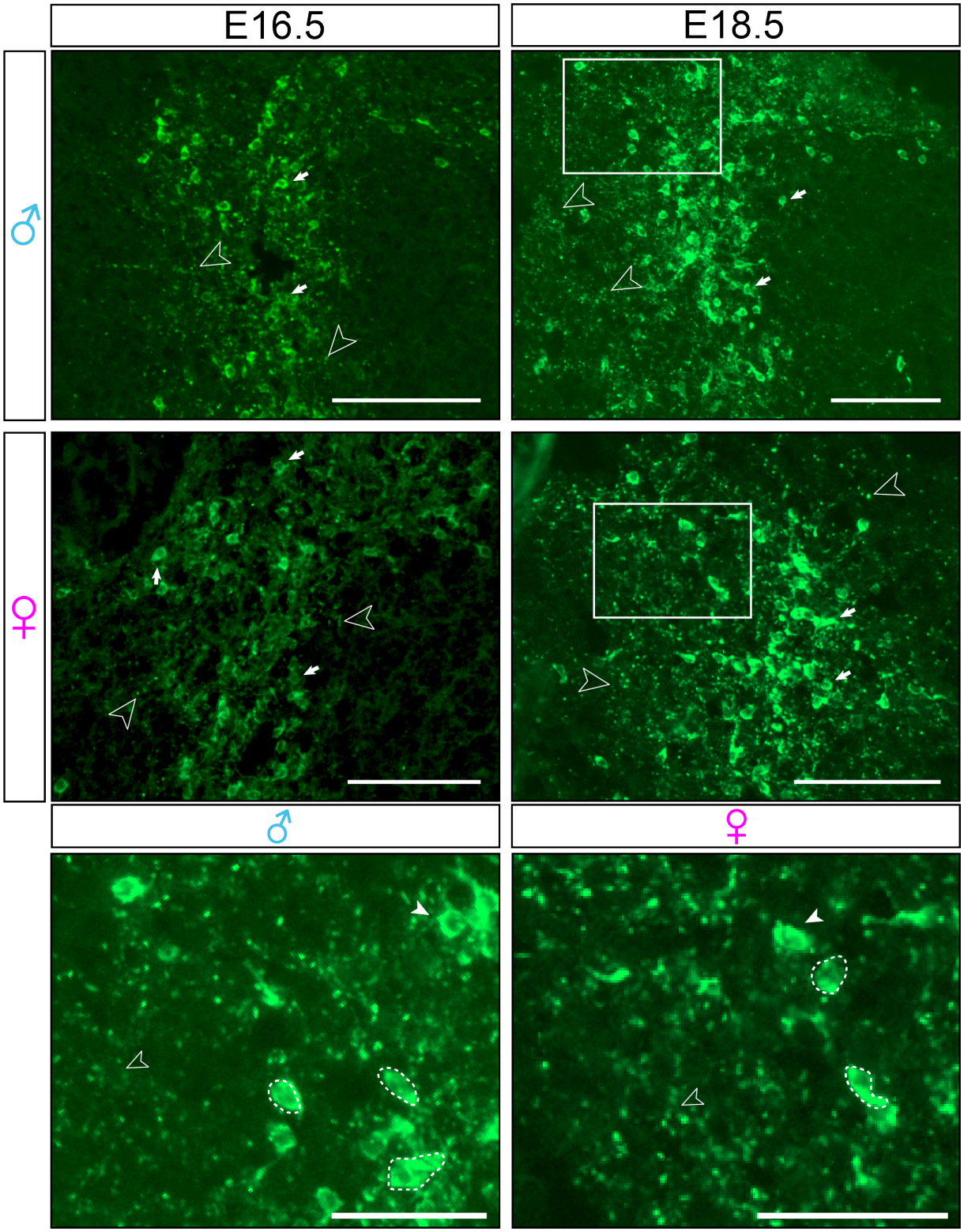

Figure 32: At E16.5 more nuclei express τGFP compared to younger animals and the overall cell number is increasing, but expression stayed restricted to nuclei of the hypothalamus and the amygdala. Male embryos at the age of E18.5 display τGFP expression in the same nuclei as in E16.5, but the overall cell number was increased. Filled arrowheads marking neurons and non-filled arrowheads marking fibers. In females no differences in the τGFP expression pattern were detected compared to males. In both developmental stages the medial preoptic area is shown. Filled arrowheads marking neurons and non-filled arrowheads marking fibers. Magnified overview of the area indicated in above. Dotted line is outlining neurons. Dotted line is outlining neurons. Scale bars, 100 μm (overview), 50 μmm (insets).

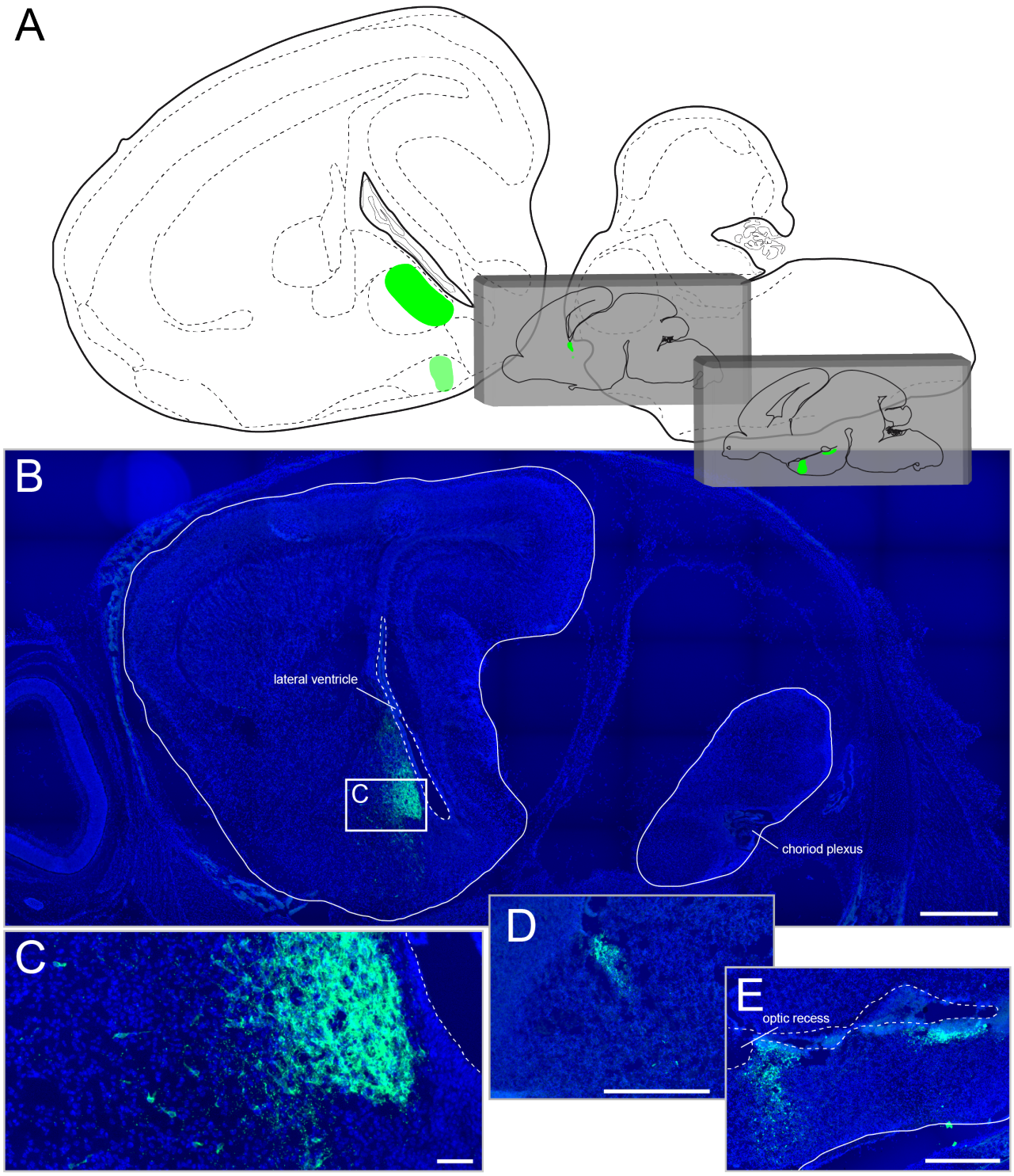

Figure 33: Overview over E18.5 GFP expression. (A) Schematic overview over the GFP expression in E18.5. GFP was only found in the amygdala and the hypothalamus. (B) Dense GFP signal was found in the amygdala close to the lateral ventricle. (C) Magnified image of the area indicated in B. (D) A smaller GFP population was found in the stria terminalis. (E) GFP population found in the hypothalamus. Nuclear counterstain in blue. Scalebars, B, D and E: 500 μm, C: 50 μm.

3.4.2 Oestrogen-sensitive neural circuitry in the embryonic mouse brain

Aromatase, kisspeptin, GPR54/kisspeptin receptor and ERα expression all start at E13.5 in the male and female murine brain, suggesting temporal orchestration and raising the possibility, that locally produced neurosteroids impinge onto oestrogen-sensitive neural circuits in the embryonic mouse brain. I first asked whether aromatase neurons in the developing murine brain are themselves sensitive to oestrogen providing an autocrine feedback mechanism. To do this, I immunolabeled sections prepared from ArIC/eR26-τGFP brains with antibodies against ERα). I did not detect immunofluorescence signals for ERα in E12.5 embryos (Figure 36 and Figure 37), consistent with previous reports (Kumar et al., 2014; Kumar et al., 2015). While ERα immunoreactivity was readily detected in multiple nuclei at E13.5 (Figure 34), it did not colocalize with aromatase neurons in either sex (Figure 36 and Figure 37 and Table 18, page 120, appendix and Table 19, page 121, appendix). At E16.5, I found that 14.7% ± 0.6% of all aromatase neurons expressed ERα in males (14.8% ± 0.7% in females) (n = 3 animals). While I did not observe ERα expression in most hypothalamic aromatase neurons, some colocalization between aromatase and ERα signals was detected in the amygdala, the optic tract and the stria terminalis (Table 20, page 121, appendix and Table 21, page 122, appendix). The medial tuberal nucleus exhibited the highest colocalization rate (57.1% ± 12% in males, 44.4% ± 3.2% in females) but contained only few aromatase neurons Table 20, page 121, appendix and Table 21, page 122, appendix). Vice versa, the medial preoptic area with the highest number of aromatase neurons only showed a low rate of colocalization (11.4% ± 1.6% in males, 7.6% ± 3.2 in females). Overall colocalization between aromatase neurons and ERα in the brain remained at similarly low rates at E18.5 (14% ± 0.5% of aromatase neurons in males, 16.7% ± 1.3% in females; Table 22, page 122, appendix and Table 23, page 123, appendix). Interestingly, although I did observe intense ERα staining in the optic tract and MPOA, I found that hardly any τGFP+ somata or fibers are innervating the ERα population, indicating that oestrogen is acting in a paracrine way (Figure 35). Taken together, these data suggest little autocrine action of oestrogen in the embryonic male and female mouse brain. At birth I observed similar patterns (Table 24, page 124, appendix and Table 25, page 125, appendix).

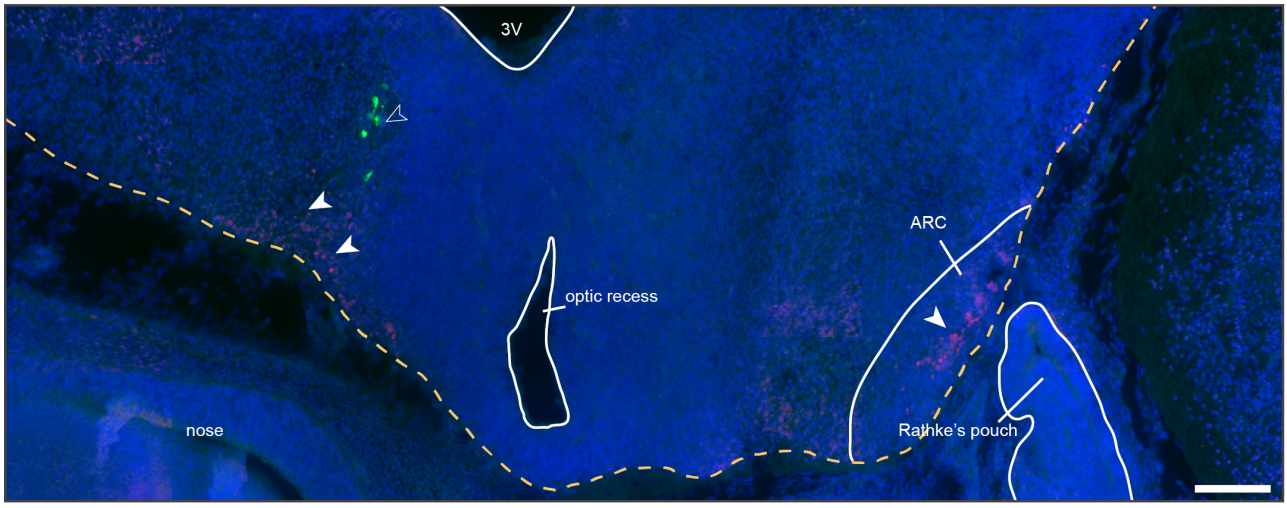

Figure 34: Aromatase neurons do not colocalize with ERα neurons in E13.5 old animals. Unfilled arrowhead indicates τGFP neurons in the medial preoptic area. Filled arrowheads indicate ERα expressing neurons. In the ARC ERα neurons were detected but no aromatase neurons were in close apposition. 3V = third ventricle. Nuclear counterstain in blue. Scalebar, 100 μm.

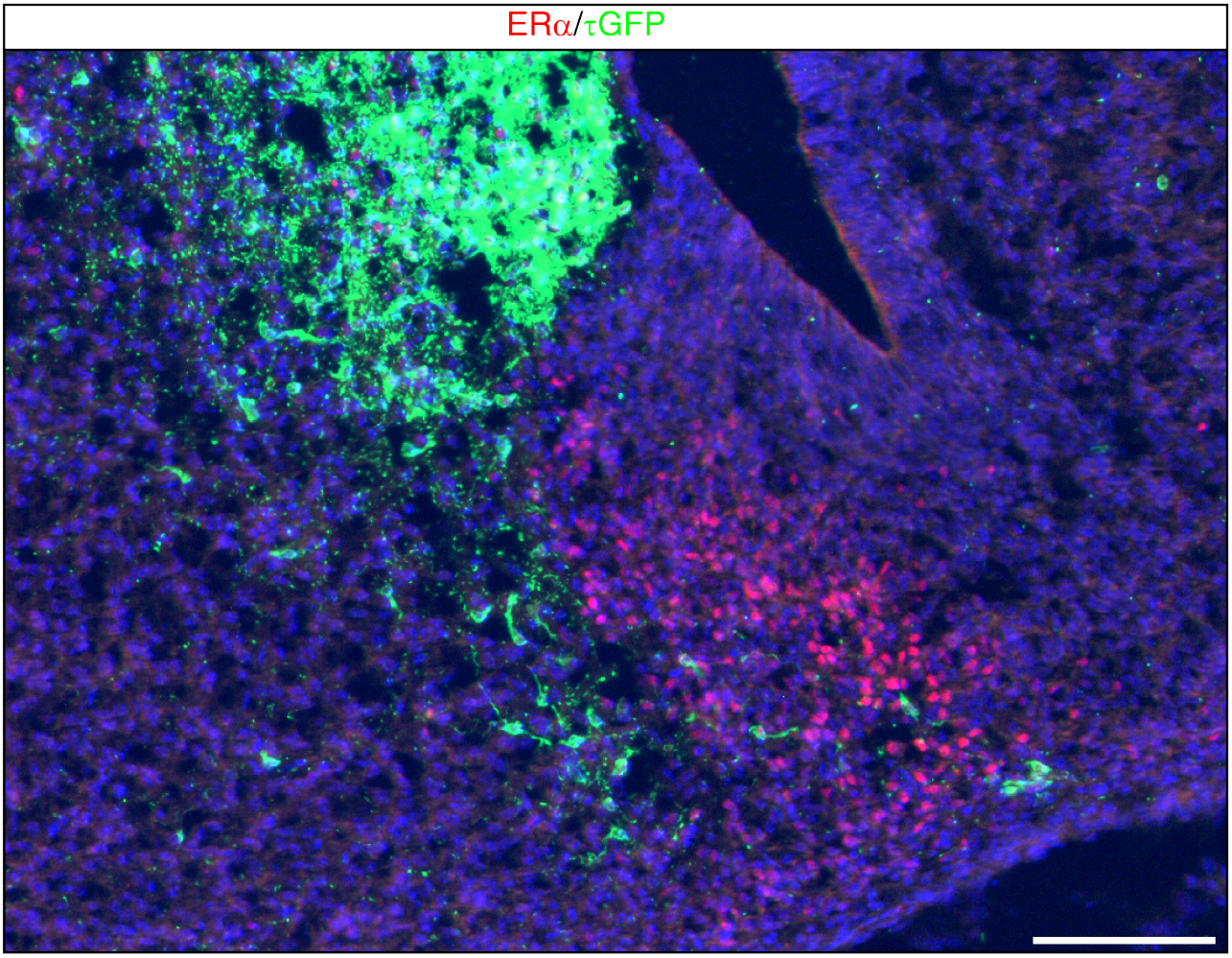

Figure 35: Aromatase neurons are in close apposition to ERα neurons in the amygdala. In E18.5 old animals τGFP expressing neurons in the amygdala are in close apposition to ERα expressing neurons, but rarely colocalize. Nuclear counterstain in blue Scalebar, 100 μm.

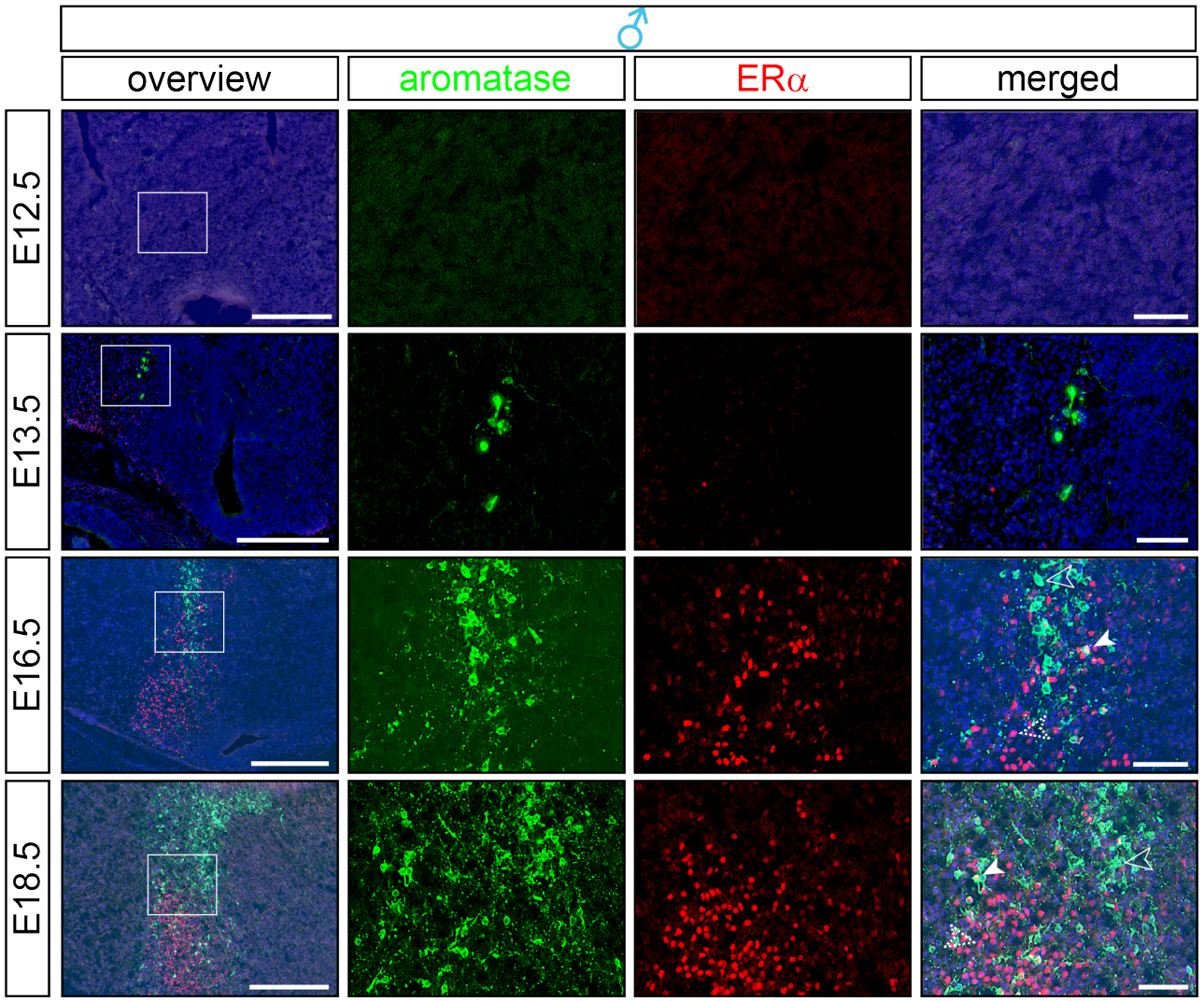

Figure 36: τGFP is rarely colocalized with ERα in males. Double immunofluorescence for ERα (red) and τGFP (green) of sagittal sections through the head of male ArIC/eR26-τGFP embryos at different ages. Shown is the medial preoptic area of male embryos at different ages as an example region with strong τGFP, and ERα signal. Neither τGFP nor ERα is expressed at E12.5. Onset of ERα expression coincides with the expression of τGFP in male embryos. However ERα is expressed in nuclei with no detectable τGFP expression (like the ARC) or ERα expressing cells are not τGFP positive when they are expressed in the same nucleus. In older embryos ERα is coexpressed with τGFP in the same neurons. In nearly all τGFP expressing nuclei a small subset of τGFP+ cells also coexpresses ERα. The overall coexpression value stays below 20% in both E16.5 and E18.5 animals. Some nuclei express ERα but are τGFP negative and other nuclei express both τGFP and ERα but these cells do not colocalize. Merged images and overview also display nuclear counterstain in blue. Unfilled arrowhead marks Aromatase neuron, dotted unfilled arrowhead marks ERα positive neuron and filled arrowhead marks double positive neuron. Scalebars, A: 250 μm (overviews), 50 μm (insets).

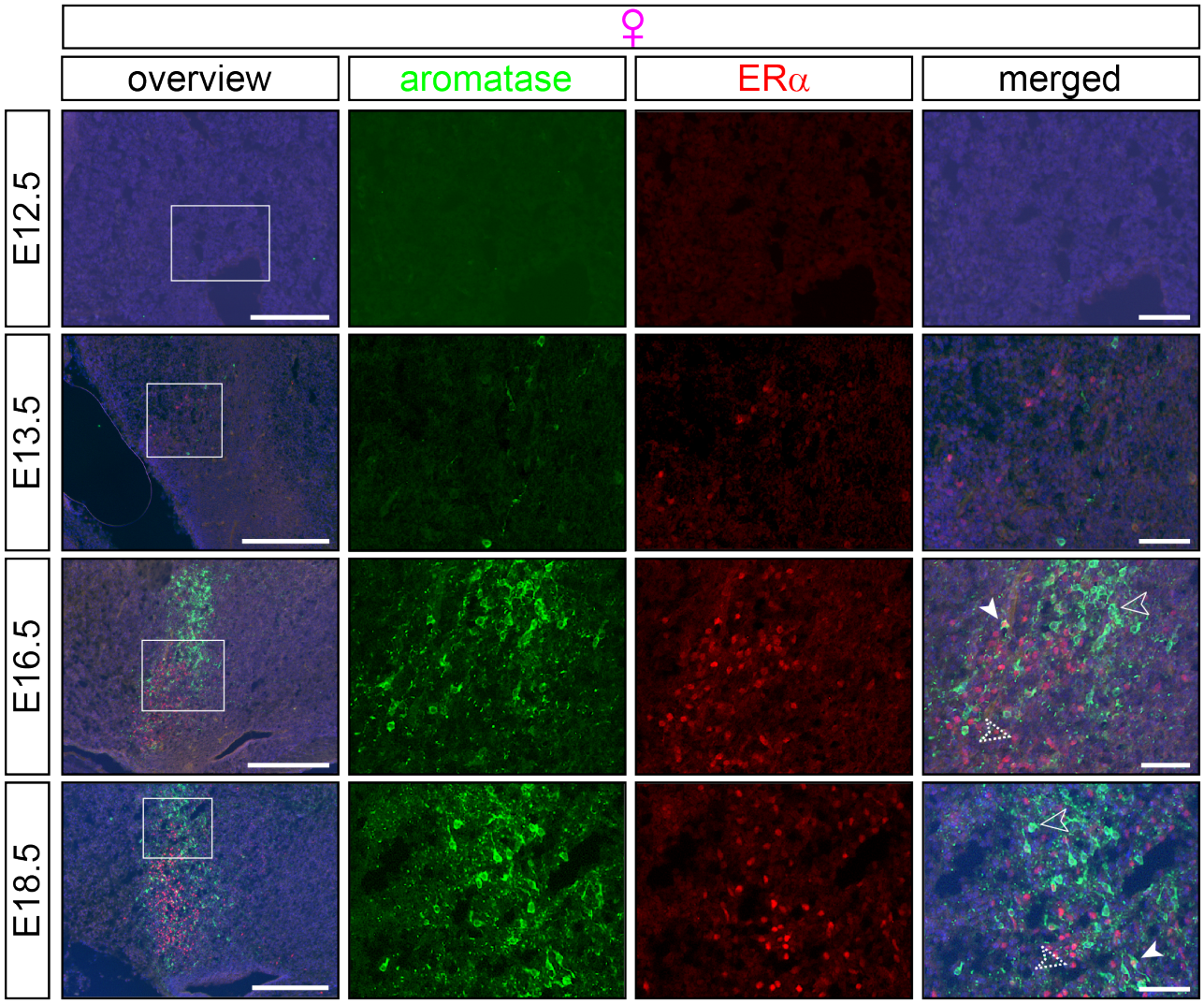

Figure 37: τGFP and ERα rarely colocalized in the female embryo brain. Double immunofluorescence for ERα (red) and τGFP (green) of sagittal sections through the head of female ArIC/eR26-τGFP embryos at different ages. Shown is the medial preoptic area of female embryos at different ages as an example region with strong τGFP and ERα signal. τGFP and ERα were found in the same nucleus but are rarely colocalized in all developmental stages. Merged images and overview also display nuclear counterstain in blue. Unfilled arrowhead marks Aromatase neuron, dotted unfilled arrowhead marks ERα positive neuron, and filled arrowhead marks double positive neuron. Scale bars, 250 μm (overview), 50 μm (inset).

3.4.3 Most aromatase neurons are in close apposition to oestrogen receptor α neurons in the embryonic mouse brain

I next investigated the spatial relationship between aromatase neurons and oestrogen-sensitive neurons in the developing mouse brain and determined the mean distance between these neurons in the medial preoptic area of the hypothalamus. I found average distances corresponding to 2-3 cell diameters between aromatase and ERα neurons (61.4 μm in males and 50.9 μm in females at E13.5, 44.6 μm in males and 38.9 μm in females at E16.5, 55.2 μm in males and 50.1 μm in females at E18.5). Similar distances were determined in the medial amygdaloid nucleus (26.4 μm in males and 25.9 μm in females at E16.5, 47.4 μm in males and 42.9 μm in females at E18.5). Taken together, these data demonstrate that most aromatase neurons are in close apposition to estrogen receptor α neurons in the embryonic mouse brain and raise the possibility that estrogen acts in a

paracrine way in these nuclei (Figure 38 and Figure 39).

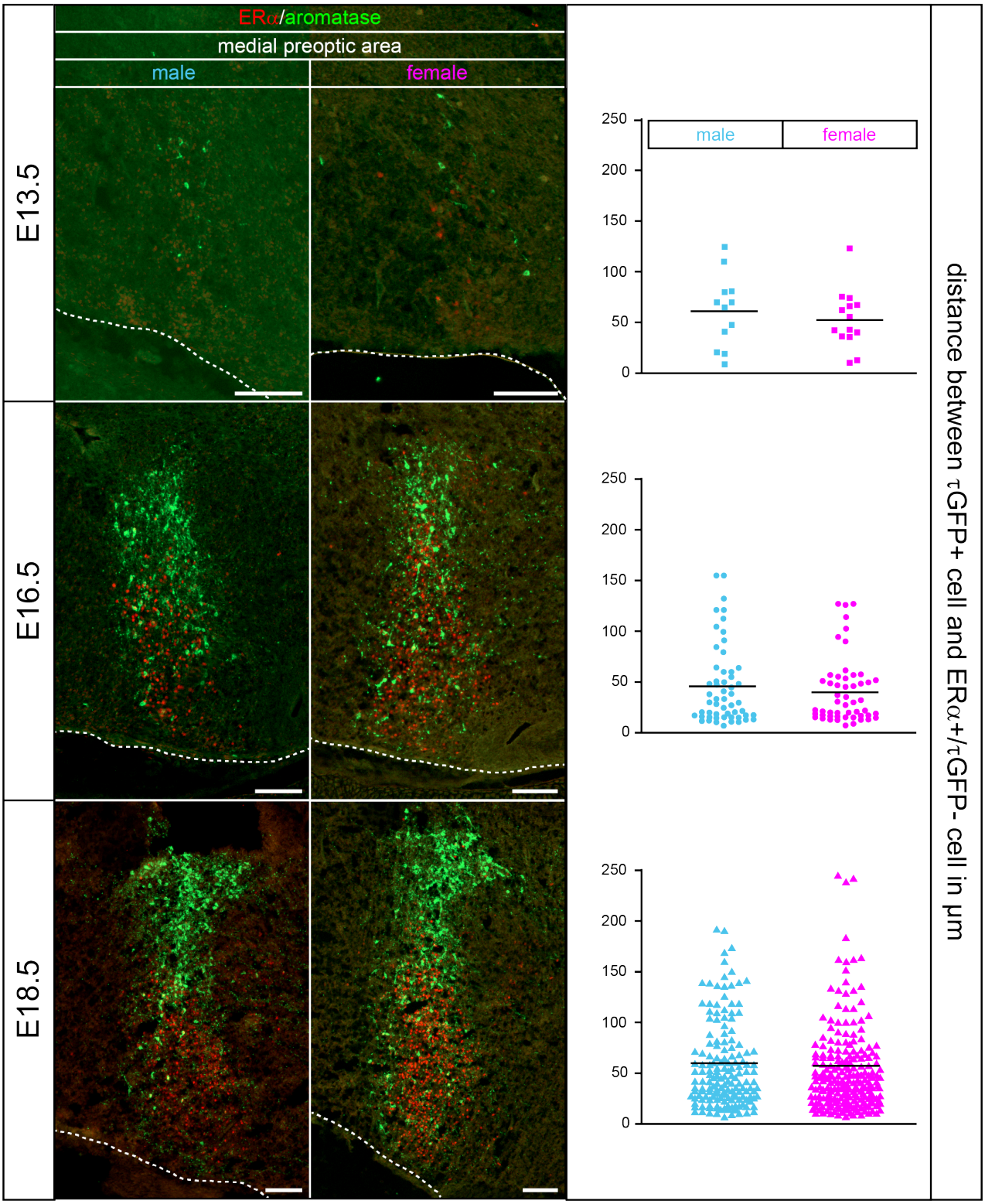

Figure 38: Aromatase expressing and ERα expressing cells are in close apposition in the MPOA. In E13.5 old animals no co-expression of τGFP and ERα was observed, but the two populations are in close contact in the MPOA (top fluorescence picture). In E16.5 old embryos colocalisation was observed but the majority of ERα cells is aromatase negative but in close apposition (middle fluorescence picture). In E18.5 embryos the same correlation was observed but total cell number was increased (bottom fluorescence picture). The graphs on the right side show the distance between the two populations and their mean for all ages analysed. Scalebars: 100 μm.

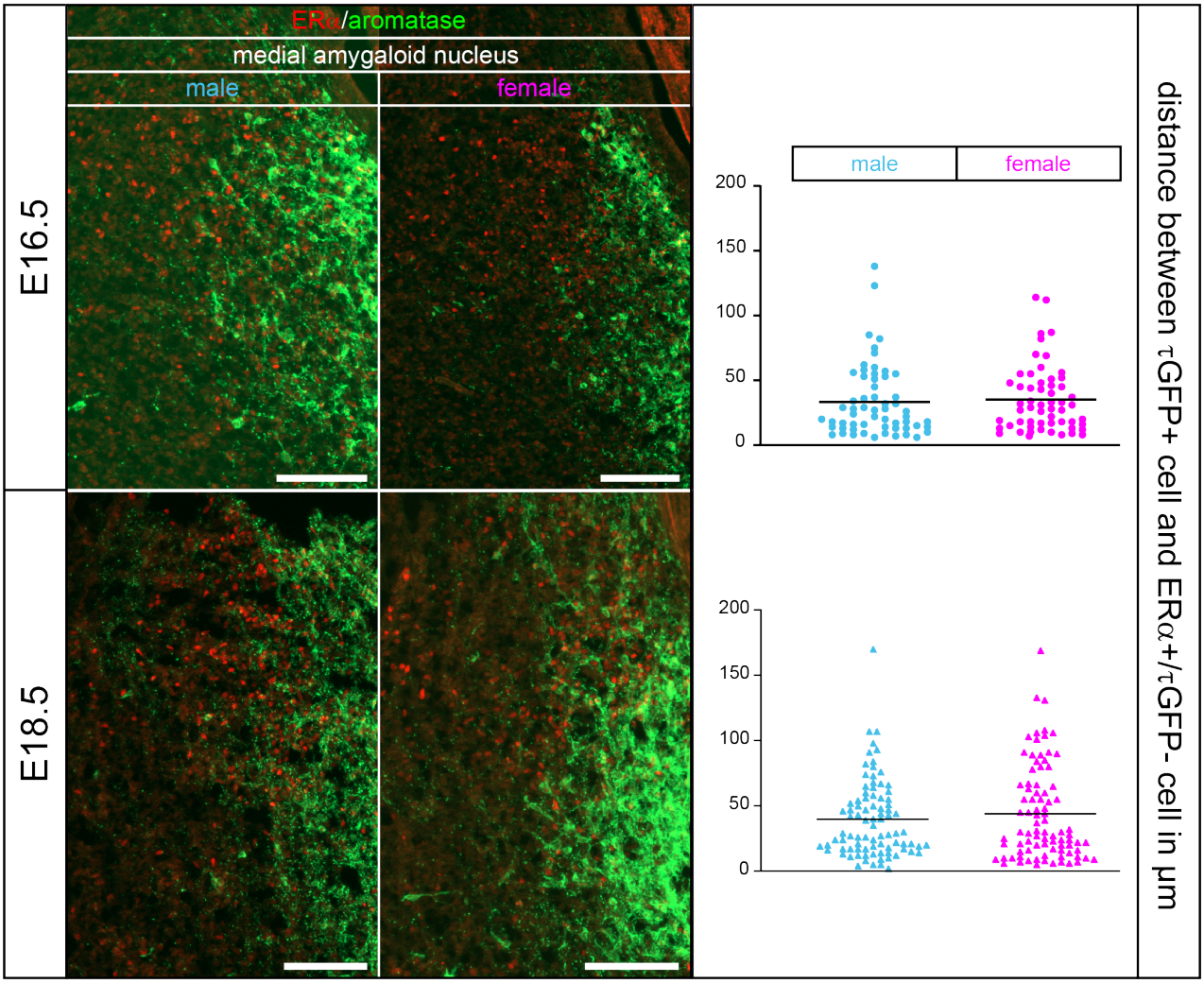

Figure 39: Aromatase expressing and ERα expressing cells are in close apposition in the medial amygdaloid nucleus. In both ages only a minor fraction of neurons expressed both τGFP and ERα. The vast majority of single positive cells were in close apposition with no difference between ages. In older animals the total cell number was increased. The graphs on the right side show the distance between the two populations and their mean for all ages analysed. Scalebars: 100 μm.

3.4.4 Aromatase expression in the arcuate nucleus begins at birth and is sexually dimorphic

Kisspeptin neurons are restricted to the arcuate nucleus of the hypothalamus until puberty and express ERα. I therefore next analysed the spatial relationship between aromatase neurons and arcuate kisspeptin neurons at birth. To do this, I stained brains sections prepared from ArIC/eR26-τGFP brains with antibodies against kisspeptin. While I did not detect aromatase neurons in the arcuate nucleus in either male or female brains throughout embryonic development (Figure 40), this changed at birth. At P0, I found a prominent cluster of τGFP+ neurons in the male arcuate nucleus (176 ± 64.1 τGFP+ cells, n = 3 animals; Figure 41 and Table 17, page 119, appendix). Overall colocalization between aromatase neurons and ERα in the arcuate nucleus (88.1 ± 37.2 ERα/τGFP+ cells corresponding to 40.8% ± 4.8% of the total τGFP+ cell population in males, n = 4 mice). Strikingly, this aromatase neuron cluster was notably absent in the female arcuate nucleus, demonstrating sexually dimorphic aromatase expression in this area of the hypothalamus at birth. I next stained brains sections prepared from ArIC/eR26-τGFP brains with antibodies against kisspeptin. While none of the arcuate aromatase neurons expressed kisspeptin (Figure 42 A and B), these two neuronal subtypes were always in the immediate vicinity of each other.

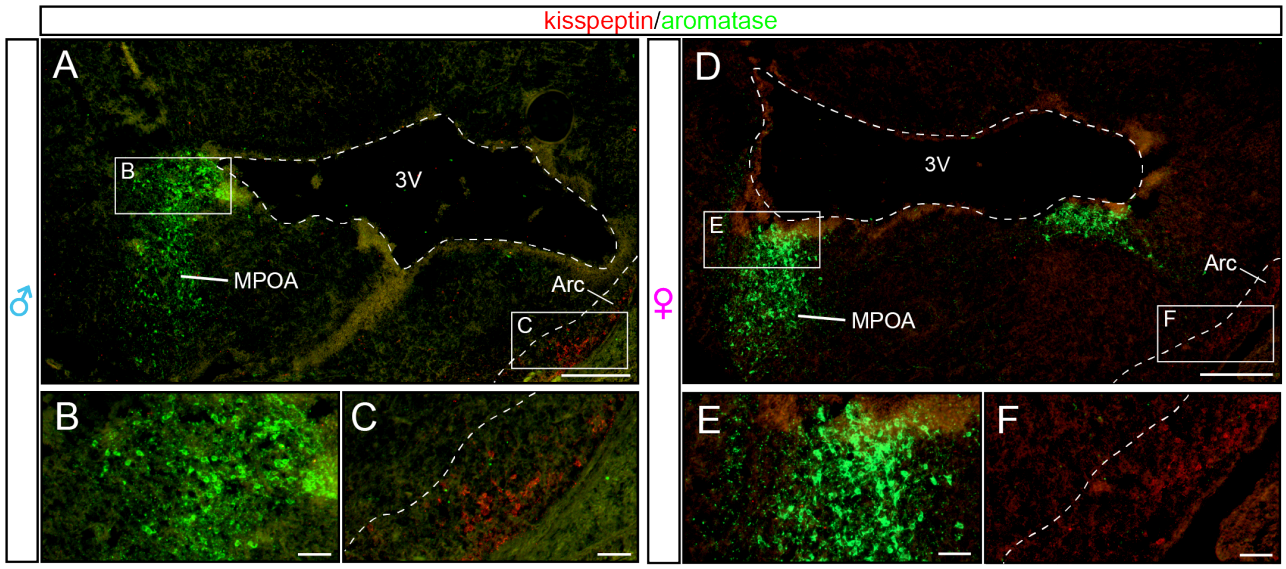

Figure 40: Aromatase is expressed in distinct nuclei of the hypothalamus and amygdala in E18.5 animals. (A - F) Double immunofluorescence with antiserum against kisspeptin (red) and τGFP (green) revealed that aromatase is not expressed in the embryonic ARC regardless of sex. (A), Sagittal section through the hypothalamus of a E18.5 old male embryo. (B), strong τGFP expression was observed in the medial preoptic area. (C), τGFP signal was absent in the ARC. Kisspeptin (red), exclusively expressed in the ARC in embryos was present. (D - E) The expression pattern of τGFP and kisspeptin in the female are similar to that in males. Scale bars, (A - F) 250 μm (overview), 50 μm (inset).

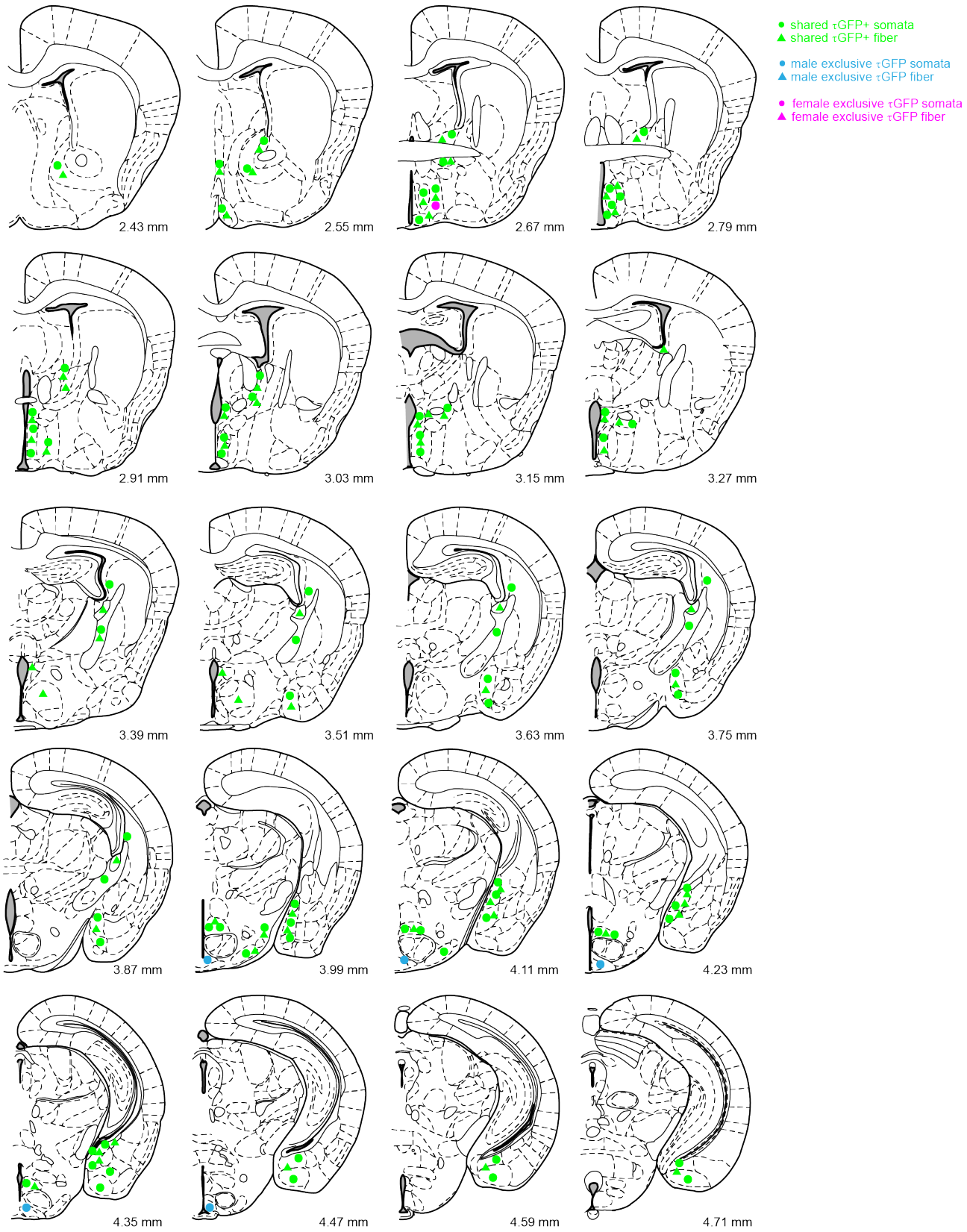

Figure 41: Summary of τGFP expression in P0 male and female brain. The expression of τGFP is shown from the first to bregma point with reporter gene to the last bregma point with reporter gene expression. Circles represent cell bodies and triangles represent fibers. In green signals shared by both genders, in blue male exclusive and in pink female exclusive cell or fiber populations.

3.4.5 Testosterone inhibits arcuate kisspeptin neurons via paracrine mechanisms requiring estrogen production by aromatase neurons

I hypothesized that aromatase neurons in the developing brain generate estrogens from brain-born and/or circulating androgens, and estrogens regulate the activity of the adjacent estrogen receptor expressing kisspeptin neurons via paracrine mechanisms. To test this hypothesis, Dr. Imre Farkas from the group of Prof. Erik Hrabovszky, Laboratory of Reproductive Neurobiology, Institute of Experimental Medicine, Budapest, Hungary, used electrophysiology on acute brain slice preparations from newborn (P4-P7) male mice with genetically labeled kisspeptin neurons. Whole-cell patch-clamp experiments were carried out in current-clamp mode to record firing of Kisspeptin-ZsGreen (KP) neurons. Indirect transsynaptic actions of T were eliminated by including picrotoxin and kynurenic acid in the aCSF. Further, presence of the androgen receptor (AR) antagonist flutamide (100 nM) in the electrode solution was used to also block any AR-mediated direct response of the recorded kisspeptin neuron to testosterone. As most kisspeptin neurons showed no spontaneous activity, a 10 pA depolarizing current was applied during the entire recording period to induce and maintain firing. Firing of kisspeptin neurons (n = 27) was typically irregular with frequent burst-like patterns and 3-5 minute-long-oscillations between peaks and nadirs. This observation fitted well with the activity patterns reported for adult mice. Mean firing rate during the 5-min control period was 2.26 ± 0.54 Hz (n = 7) which decreased significantly following testosterone administration at 50 nM to 54.1 ± 15.3% of the control rate (Figure 42 C and H). Neuronal activity started to decline 3.4 ± 1.1 min after testosterone supplementation of the aCSF. A washout effect was reflected by the slow increase in neuronal activity 15-20 min after testosterone treatment was suspended (Figure 42 D and H). The reduced firing rate of KP neurons in response to testosterone treatment resembled the estrogen response of adult KP neurons. This resemblance and the absence of detectable aromatase signal in kisspeptin neurons raised the possibility that testosterone requires conversion to estradiol by aromatase neurons to inhibit kisspeptin neuron firing. Therefore, we replicated the above experiment with both testosterone and the aromatase inhibitor Letrozole (100 nM) in the aCSF. Following a 5-min control period with Letrozole in the artificial cerebrospinal fluid (aCSF), the recording was continued for 10 min in the presence of testosterone. Preincubation of the slice with Letrozole completely prevented the effect of testosterone on KP neuron firing (112.0 ± 8.16% of the control value 1.8 ± 0.48 Hz, Student' t-test, p=0.2029, n=6) (Figure 42 E and second column in H). This observation indicated that testosterone needs to be converted to estradiol by aromatase in order to act on ERs in KP neurons. Indeed, testosterone was unable to alter kisspeptin neuron activity in the presence of the ER inhibitor ICI182,780 (108.5 ± 16.92% of the control value 1.8 ± 0.21 Hz, Student's t-test, p=0.632, n=8) (Figure 42 F and 3rd column in H). To rule out that testosterone is converted to estradiol by this low level of aromatase and to prove that testosterone acts mostly indirectly on kisspeptin neurons via paracrine mechanisms, Letrozole (100 nM), in addition to flutamide, was added to the electrode solution and then, the effect of testosterone re-assessed. Testosterone application in this study resulted in a significant decrease in kisspeptin neuron firing (57.9 ± 9.39% of the control value 1.9 ± 0.31 Hz, Student's t-test, p=0.0029, n=8) (Figure 42 G and 4th column in H), which was similar to the effect of testosterone alone (Figure 42 1st column in H). This observation indicated that endogenous aromatase has only minor, if any contribution to the testosterone effect on kisspeptin neuron firing; therefore, the mechanism whereby testosterone acts on kisspeptin neurons is mostly paracrine. The firing rates of the different treatment groups were significantly different by ANOVA (p=0.0055) followed by Tukey's post-hoc test. Analysis of the control periods (before testosterone) with ANOVA followed by Tukey's post-hoc test showed that ICI182,780 or intra/extracellular Letrozole alone

did not alter the firing rate (ANOVA, p=0.8286).

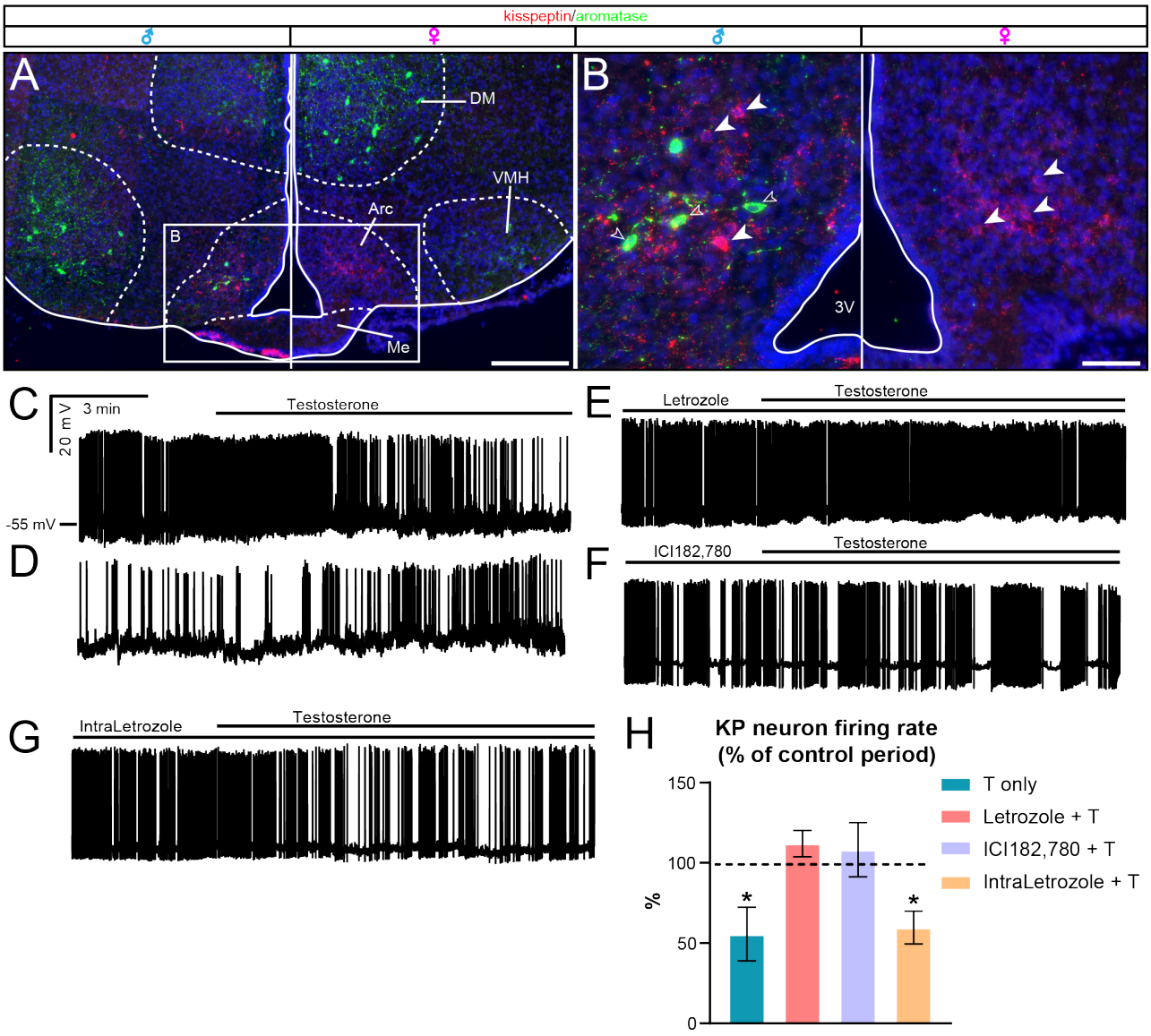

Figure 42: Locally synthesised oestrogen reduces kisspeptin firing rate. (A) Reporter gene expression was only detected in the male Arc of ArIC/eR26-τGFP after birth. These aromatase cells do not colocalize with kisspeptin neurons. No reporter gene was observed in females. (B) Magnified image of the area indicated in (A). The representative traces in (C - G) were recorded from kisspeptin neurons of the Arc. (C) Firing rate decreased in response to testosterone administration. (D) The effect of testosterone could be washed out slowly. (E) Supplementation of the extracellular solution with Letrozole prevented the action of testosterone. (F) The ER-antagonist ICI182,780 also abolished the action of testosterone. (G) Intracellular administration of Letrozole showed no antagonistic effect, unlike its extracellular use. (H) Bar graph reveals that testosterone reduces kisspeptin neuron firing rate to the 54% of the control value. This action is entirely prevented by prior bath application of the aromatase inhibitor Letrozole (2nd column) or the ER-inhibitor ICI182,780 (3rd column). Estradiol is not derived from the recorded kisspeptin neurons because Letrozole in the electrode solution (IntraLetrozole) does not interfere with testosterone actions (4th column). * = p $\langle$ 0.05 by Student's t tests. Scalebars: 100 μm.

4 Discussion

Genetic approaches are powerful in gaining access to cell types and genes of interest that are otherwise hard to detect. Cre reporter mice enable mapping of body-wide expression patterns with cellular resolution. This is needed in particular for genes that are hard to detect with other methods like mRNA detection or antibodies. Whole body KO animals were used to investigate the role of proteins on body homeostasis, but interpretation of the resulting phenotypes are difficult without the knowledge of the expression pattern in all organs and cell types. In addition, KO animals have other caveats. There is no temporal or spatial control over the knocked-out gene and compensation for the KO during development need to be considered. This is especially true for the investigation of TRP channels. These channels are hard to detect on the mRNA level due to their low expression and antibodies are difficult to develop because TRP channels are membrane bound proteins and are post-translationally glycosylated, making the access to epitopes for antibody detection challenging. To overcome these difficulties, multiple new Cre driver lines were developed within the TRR152 for the investigation of body homeostasis and its control centre, the hypothalamus. This brain region orchestrates homeostasis by integrating feedback from the periphery and the release of hormones to regulate different organ functions. This is controlled via the hpg-axis to regulate fertility and sexual behaviour, as well as other axes such as the hypothalamus-pituitary-adrenal gland axis (hpa-axis), to control corticosteroid concentrations and the hypothalamus-pituitary-thyriod gland axis (hpt-axis), to regulate thyroid hormone levels in the blood.
The ME is the brain window that connects the hypothalamus and the periphery. Multiple different cell types work together to maintain a barrier to the CNS and control the exchange of molecules in both directions. Fenestrated blood vessels allow the flow of compounds in both directions, while tanycytes form a barrier between the CSF, CNS and the ME and also transport molecules from the ME into other areas of the brain like the PVN and the Arc. Microglia and astrocytes take part in the communication between axons and other cell types. In addition to these cell types in the ME, hormone homeostasis regulating cells are also found in the pars tuberalis between the ME and pituitary. Investigation of different TRP Cre-driver lines revealed that TRP channels are expressed in different cell types in the ME (Figure 43). TRP channels play a crucial role in body homeostasis and my results indicate that these channels are not only expressed in peripheral organs but also in different cell types in the ME where they might orchestrate body functions in the hypothalamus.
Cre-driver lines can be bred to a large variety of *ROSA26* (R26) strains to not only visualize cell populations trough the use of a fluorescent reporter such as GFP, to investigate Ca^{2+} signalling within these cells using the R26-GCaMP3 reporter mouse or to manipulate them in different ways such as ablating cell populations with a temporal and spatial resolution, by injecting diphtheria toxin (DT) in the region of interest in R26-iDTR animals. Using R26-DREADD animals, cell populations can be activated under temporal control, while CRISPR-Cas in cas9-expressing R26 animals allows for the KO of genes in subpopulation of cells after delivering the guide-RNA with the help of adeno-associated viruses (AAV) . With the R26-TeNT line tetanus toxin light chain fused to GFP is cre-dependently expressed and blocks the vesicular release (Figure 44).

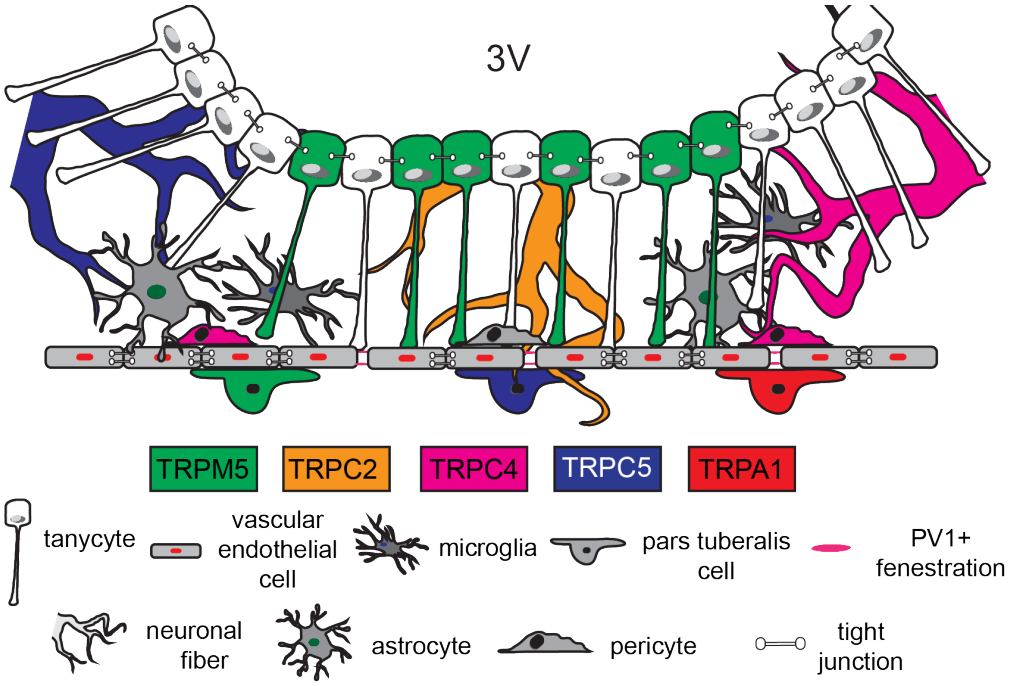

Figure 43: Summary of TRP channel expression in the ME. TRPM5 was found in a subset of tanycytes and cells in close contact with the blood vessel system in the pars tuberalis. TRPC2 was only observed in fibers innervating the ME. TRPC4 was identified in pericytes, blood vessels and fibers. TRPC5 was observed in fibers and cells of the pars tuberalis, TRPA1 only in pars tuberalis cells.

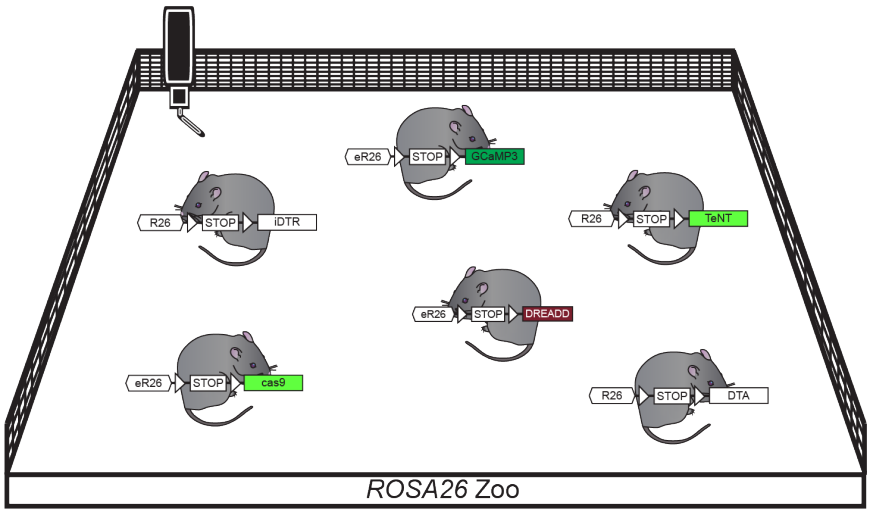

Figure 44: The *ROSA26* zoo. Different R26 lines can be bred to Cre-driver lines for specific manipulation of subpopulations after initial Cre-mediated removal of the stop signal. In the R26-DTA lines Cre-expressing cells are ablated after removal of the stop signal by the expression of diphtheria toxin A. To ablate cells in the R26-iDTR mouse, diphtheria toxin must be injected and binds to its receptor to initiate ablation. Ca^{2+} signalling can be investigated in the R26-GCaMP3 animals by expression of the Ca^{2+} indicator GCaMP3 after Cre-mediated recombination. Synaptical silencing occurs in the R26-TeNT animals by the expression of the tetanus toxin light chain fused to GFP by blocking the vesicular release machinery. By breeding Cre-drivers to the R26-DREADD line cre-expressing cells can be activated by the injection of CNO and subsequent activation of the G-protein coupled DREADD receptor. In R26-cas9 animals the CRIPR/cas-system can be used by AAV mediated delivery of guide-RNAs to knock out genes only in cells were Cre was expressed.

4.1 TRPM5 tanycytes communicate with fenestrated blood vessels

The chemosensation specialist TRPM5 is expressed in taste buds and in OSNs (Kusumakshi *et al.*, 2015 and Pyrski *et al.*, 2017). I confirmed these expression patterns in the organ mapping and also revealed that TRPM5 is expressed only in few taste buds in juvenile animals. During the suckling phase it could be hypothesized that there is no need for animals to distinguish between tastants and TRPM5 is only required during taste transduction. Further experiments during the weaning phase are needed to investigate the onset of TRPM5 expression in the taste buds more thoroughly. In the respiratory system the taste pathway senses "bitter" substances such as bacterial quorum sensing molecules and subsequent TRPM5-mediated activation of these cells leads to the release of acetylcholine (Krasteva-Christ *et al.*, 2015). We observed intense reporter gene expression in different organs in smooth muscle cells. Smooth muscle cells are depolarized by an increase in intracellular Ca^{2+} and TRPM4 is activated downstream of this signalling (Earley, 2013). As TRPM4 and TRPM5 are closely related, TRPM5 might serve a similar function during the depolarization of smooth muscle cells in many organs. In addition to TRPM5+ pancreatic islets and the well documented function of TRPM5 in insulin secretion we also observed a subset of acinar cells expressing TRPM5. These cells secrete digestive enzymes by exocytosis in a Ca^{2+}-dependent mechanism (Williams, 2010). A hypothetical role for TRPM5 in these cells is depolarization of the acinar cells subsequent to GPCR activation resulting in increased intracellular Ca^{2+} concentration and opening of other voltage gated ion channels leading to exocytosis.
In the CNS we observed reporter gene expression in the choroid plexus. The cells of the choroid plexus are involved in CSF production and controlling the exchange of signalling molecules between the CSF and the vascular system. Other TRP channels are also expressed in the choroid plexus, such as TRPV4 and TRPM3. TRPV4 is involved in osmotic regulation and TRPM3 in ion and water transport. TRPM5 might have a similar function or may be involved in subsequent release of signalling molecules like ATP, into the CSF. In general, organ mapping of TRPM5IC/e*R26-τ*GFP reporter mice revealed expression mainly in cells involved in chemosensation. To further investigate the role of the choroid plexus TRPM5 cells in signal transduction, GCamP reporter mice can be used to provide a readout of responses to different signalling molecules such as ATP. In addition, TRPM5 channel modulators and calcium imaging will help to investigate the role of TRPM5 in the control of CSF composition.
TRPM5 expression was also found in a subset of β-tanycytes at the floor of the third ventricle. Tanycytes, besides their barrier function, are also chemosensation cells and organize exchange between the CNS, CSF and the vascular system. These cells control body homeostasis, for example through conversion of T4 into its active form T3 or reproductive physiology by physically inhibiting GnRH release in the ME (Parkash *et al.*, 2015). In iDISCO-cleared tissues I observed that only a subset of TRPM5+ tanycytes also express the tanycyte marker vimentin, making this a small population of tanyctes in which the taste transaction pathway might be functional. The formation of endfeet in close contact with fenestrations in the ME makes it tempting to speculate about the function of the TRPM5 tanycytes. The iDISCO images revealed that the cell bodies of M5 tanycytes form multiple clusters, making it less likely that they have a major impact on barrier function but rather in sensing tastant-related molecules in the CSF. Dr. Sen Qiao has shown by mRNA sequencing that bitter taste receptors are indeed expressed in TRPM5 tanycytes, proving that tanycytes have the necessary machinery to respond to bitter substances. It is not known where the channel is located within the tanycyte. If the channel is located in the endfoot it can respond downstream of GPCRs activated by signalling molecules in the basement membrane. If the channel is located in the cell body it is more likely that it is activated downstream of CSF-

bourne cues. It might also be a combination of both. Indeed, work from Dr. Igor Gamayun showed in GCaMP reporter mice that Ca^{2+} signals in the TRPM5 tanyctes are bidirectional, indicating that the channel might be expressed in endfeet and in the somata. As observed in the iDISCO pictures, one process of a single tanycyte is branching into multiple thinner processes the closer it is located to the blood vessel. As growing of endfeet is a Ca^{2+}-dependent process, TRPM5 might be responsible for the opening of voltage gated channels which would increase Ca^{2+}-concentrations subsequent to CSF borne molecules to initiate endfoot growth.
The functional role of TRPM5 tanycytes in body homeostasis has been investigated by Qiang Yu in his phd thesis in collaboration with Dr. Timo Mueller (Institute for Diabetes and Obesity, Helmholtz Diabetes Center, Helmholtz Zentrum München, Neuherberg, Germany; German Center for Diabetes Research (DZD), Neuherberg, Germany). After acute ablation of TRPM5 tanycytes with DT, animals on high fat diet showed an impaired glucose tolerance, an increased insulin tolerance and lower blood insulin levels. This phenotype is not due to a lack of TRPM5 in the islets, as ablation of these cells is limited to the tanycytes. One possible explanation for the impaired glucose tolerance in the ablated mice is the disturbed communication between the brain and pancreatic β-cells. The hypothalamus is communicating through the nucleus solitary tract (NTS) with the pancreatic islets and the islets are sending feedback to the brain through the vagus nerve NTS connection (Makhmutova *et al.*, 2020) to maintain the glucose homeostasis of the body. The brain is sensing glucose levels in the blood through portal vein sensors located in close proximity to the portal blood system in the ME. These cells are most likely tanycytes forming endfeet onto the vessels. These findings indicate that TRPM5 tanycytes play a role in regulation of insulin secretion.

4.2 TRPM6 regulates Mg^{2+} homeostasis in the CNS

Studies indicate an essential role of TRPM6 in Mg^{2+} resorption in the kidney and the intestine. The organ mapping revealed TRPM6 is mainly expressed in epithelial cells of the distal convoluted tubule, where the channel potentially participates in Mg^{2+} resorption (G. A. Quamme *et al.*, 2000). We only observed very few τGFP+ cells in the intestine, despite the fact that TRPM6 was shown to be the cause of HSH. Most Mg^{2+} uptake in the intestine is through a paracellular mechanism and is channel independent (Gary A. Quamme, 2008). This might explain the low amount of TRPM6 cells in the intestine, as Mg^{2+} uptake though TRPM6 plays a minor role under physiological conditions. TRPM7 has the same function in the intestine and most studies do not separate between the two channels, making it hard to predict the role of TRPM6 alone.
In the salivary gland τGFP expression was observed only in cells of the glandula sublingualis, responsible for most of saliva production. It is tempting to speculate that TRPPM6 plays a role in the Mg^{2+} regulation of saliva production, as these cells are close to the duct system. Ca^{2+} influx through TRPM7 is involved in the volume regulation of the gland (J. M. Kim *et al.*, 2017) and TRPM6 might have a similar function in mediating these effects. TRPM6 is regulated by parathyroid hormone (PTH) and calcification (Blanchard *et al.*, 2016). We found formerly unknown TRPM6 expression in the thyroid gland. These cells might be regulated by calcitonin released on site and TRPM6 activation leads to subsequent calcitonin release and regulation of TRPM6 in other organs. Investigation of TRPM6IC/e*R26*-τGFP lungs confirmed previously reported TRPM6 expression. Cellular resolution was lacking from these studies and we identified cells resembling leukocytes and epithelial cells to be τGPF positive. Mg^{2+}-absorption might occur in the lung, supported by the fact that dietary Mg^{2+} intake is related to lung function and airway activity (Britton *et al.*, 1994).
TRPM6 and TRPM7 are expressed in the brain, where they play a role in the regulation of vascular proliferation

and Mg^{2+} transport in vascular smooth muscle cells. Most studies have focused on the ubiquitously expressed TRPM7 in vascular Mg^{2+} function (Earley and Brayden, 2015). In iDISCO-cleared brains of TRPM6 reporter mice I revealed the presence of this channel throughout most of the vascular system of the brain. Interestingly, in the ME I did not observe any reporter gene expression in the vascular system. Whole body organ mapping revealed no expression in other vascular structures. These findings identified TRPM6 as the potential sole channel responsible for controlling Mg^{2+} homeostasis in the vascular system of the BBB, a claudin-dependent mechanism (Vink *et al.*, 2011). TRPM6 and TRPM7 are interacting with claudins in other organs to maintain Mg^{2+} homeostasis and a similar mechanism might now have been identified in the brain. TRPM7 expression data with cellular resolution are lacking but channel function in Mg^{2+} homeostasis in the vascular system has been shown outside the brain. These facts might indicate that TRPM6 is responsible for this mechanism in the CNS and TRPM7 in the periphery. To confirm this hypothesis, more detailed TRPM7 mapping data are needed. TRPM6 KO animals die at E12.5 due to a defect in neuronal tube closure (Komiya *et al.*, 2017). Normal tube closure also depends on the establishment of the vascular system in the brain. Neuronal cells release vessel patterning signals and this triggers blood vessels to differentiate and migrate to the surface of the neural tube (James *et al.*, 2011). TRPM6 might be an essential channel in the blood vessel to mediate this process. Future studies need to investigate the expression onset in the brain during embryonic development to reveal the role of TRPM6 in this process. The absence of τGFP signal in the ME indicated that these proposed roles are in BBB vessels only. To investigate the potential role of TRPM6 in Mg^{2+} homeostasis in the brain and controlling Mg^{2+} uptake in the BBB the R26-cas9 mouse bred to the TRPM6 cre-driver should help in answering this role. An AAV with a guide-RNA directed against TRPM6 can be injected into the tailvein of these animals. Due to this injection the virus will be delivered into the blood vessels of the BBB and will knock-out TRPM6. As we did not observe TRPM6 in blood vessels in the periphery this approach is BBB blood vessel specific. If TRPM6 plays a role in the Mg^{2+} uptake in the CNS, these animals should show signs of oxidative stress in the CNS due to high Mg^{2+} levels.

The other cell type in the brain expressing TRPM6 is ependymal cells in the wall of the ventricles and iDISCO-cleared brains indicate that the vast majority of the population are expressing this channel. TRPM6 function in these cells might be involved in regulation of Mg^{2+} uptake from the CSF and controlling Mg^{2+}-dependent signalling from the CSF into the brain. To investigate their role in CNS Mg^{2+} homeostasis, ablation of these cells with DT, injected into the ventricular system in R26-iDTR animals and subsequent investigation of neuronal function will shed light on the function of TRPM6 in ependymal cells.

4.3 TRPV6 is expressed in Ca^{2+} sensitive tissue

TRPV6 functions to regulate Ca^{2+} concentrations. The channel has an important function in male fertility through controlling Ca^{2+} absorption. TRPV6 male KO animals are infertile due to high Ca^{2+}-concentrations in the epididymis. We identified τGFP expression in the vast majority of epithelial cells in the epididymis, revealing that these cells are ideally placed for maintaining low Ca^{2+} levels. In juvenile animals we did not observe any TRPV6, highlighting the function of the channel in sperm maturation which is not required in these animals having not yet undergone puberty. We observed TRPV6 expression in other reproductive organs. We identified large numbers of τGFP+ epithelial cells in the prostate. Increased Ca^{2+} uptake in the prostate is associated with increased risk of prostate cancer (Giovannucci *et al.*, 2006). In the uterus, Ca^{2+} concentrations need to be tightly regulated for uterine contraction and embryo implantation. TRPV6 mRNA levels increase in

the uterus during pregnancy (Lee *et al.*, 2009). In contrast to these findings, we observed only few epithelial cells in the uterus which expressed τGFP and we did not observe an increase in cell number in pregnant animals. To further characterize these uterine cells, investigation of Ca^{2+} responses in the TRPV6IC/eR26-GCaMP3 mice during different cycle stages and also during pregnancy are needed. Depending on the hormonal status of the animals, these cells might respond to external stimuli like oestrogen or progesterone differently.
The secretion of digestive enzymes and fluids is a Ca^{2+}-dependent mechanism in the pancreatic acinar cells (Low *et al.*, 2010). We found TRPV6 in adult animals to be expressed in nearly all acinar cells. This indicates that the channel might be responsible for the increase in Ca^{2+} levels required for the endocytotic release of digestive enzymes. The fact that only a few acinar cells are positive in juvenile animals might indicate, that a different amount of Ca^{2+}-dependent exocytosis from acinar cells is needed during suckling. As for TRPM5 in the taste buds, future experiments investigating whether weaning and intake of solid food increases acinar TRPV6 expression are necessary to confirm this hypothesis. Investigation of Ca^{2+} responses after hormonal activation of acinar cells in WT and TRPV6 KO animals will help elucidate the role of TRPV6 in pancreatic acinar cells.
Interestingly, TRPV6 was not detected in the brain. This shows that Ca^{2+} homeostasis in the CNS is not regulated by TRPV6, in contrast to many tissues in the periphery.

4.4 TRPML3 is mainly expressed in immune cells

TRPML3 is mainly involved in lysosomal exocytosis in a wide variety of cells types, including chemosensing cells. In the nose the channel is expressed in OSNs and VSNs, where it is involved in the trafficking of vesicles which might serve as Ca^{2+} storage (Castiglioni *et al.*, 2011). We confirmed this expression in the olfactory system and identified the channel also in another sensory organ, the taste buds. This expression could not be detected by antibody or *in situ* hybridisation by others (Castiglioni *et al.*, 2011), most likely due to low expression levels. The channel might have a similar function in the taste buds as it has in the olfactory system. Endosomes and lysosomes are involved in immune cell function, such as phagocytosis, antigen presentation and processing by antigen-presenting cells, release of pro-inflammatory mediators or secretion of the pore-forming protein perforin by cytotoxic T lymphocytes (Spix *et al.*, 2020). TRPML1 was shown to have a function during lysosomal exocytosis in a subset of neurons and blood vessels (S. Park *et al.*, 2016). I observed TRPML3-driven τGFP expression in a subset of neurons in the hypothalamus and blood vessels in the CNS and in the ME. The channels might have a similar function during lysosomal exocytosis in these cells. With the use of DT in R26-iDTR mice this subset of cells can be ablated and their impact on compound uptake investigated. It has been shown that wheat germ agglutinin (WGA) injected in the ME is internalized by axon terminals in the ME and then accumulates in lysosomes in the neuronal cell body (Peruzzo *et al.*, 2004). This suggest a possible function of TRPML3 in neurons. Lysosomes filled with unwanted or toxic molecules need to be cleared from the cell by exocytosis and TRML3 may be the channel required for this process in a subset of neurons. Ablation of these cells might result in impaired clearance of such molecules, an effect which could be further investigated by injection of such molecules in the ME or in the CSF in intact or ablated animals. Because exocytosis is a Ca^{2+}-dependent process, GCaMP reporter mice bred to the TRPML3IC mice could be used for the investigation of this process. If these neurons come in contact with molecules that need to be cleared out of the cell, an increase in the Ca^{2+} signal should be observed.

4.5 TRPA1 and TRPC5 as cold sensors

TRPA1 is expressed in enterochromaffin cells, epithelial cells and sensory neurons. Many of these cells have sensory functions and communicate with neighbouring nociceptors. We observed τGFP expression in the TRPA1IC/eR26τGFP animals in OSNs and in the taste buds, both sensory cell types. It is likely that TRPA1 is activated in these cells by one of its many endogenous agonists, such as mustard and garlic, and TRPA1 activation leads to depolarization. Because TRPA1 has been described as a cold sensor, the channel might also work as a cold sensor in the tongue.

TRPA1 was shown to be expressed in the brain, but cellular resolution was lacking. I found TRPA1 expression in a subset of cortical neurons and small neuronal populations in the VMHVL (ventrolateral hypothalamic nucleus ventrolateral part), DM (dorsomedial hypothalamic nuecleus) and ArcMP (arcuate hypothalamic nucleus, medial posterior part). In addition, reporter gene expression was identified in a subset of astrocytes and in blood vessels. Older TRAP1 KO animals display improved learning compared to younger animals (Borbély *et al.*, 2019) a phenomenon which may involve the TRPA1-expressing cortical neurons population. TRPA1 has been shown to be necessary for the increase in intracellular Ca^{2+} depolarization in these cells (Kheradpezhouh *et al.*, 2017). Ablating these cells with DT in R26-iDTR animals, followed by investigation of learning behaviour is essential to define the precise role of these neurons during memory formation. To only knock out the channel, injecting an AAV containing a guide-RNA directed against TRPA1 in TRPCA1IC/eR26-cas9 animals will help to understand not only the role of the cell but the role of TRPA1 itself in this process. To test whether activation of these neurons leads to changes in learning behaviour, DREADD can be used to artificially activate these cells. With the use of the R26-GCaMP mouse and gradient refractive index (GRIN) lenses, the Ca^{2+} activity of these cells could be investigated in the awake animals during learning as the cortex is easily accessible.

Interestingly, τGFP expression in blood vessels was mainly observed in the curvature of the vessels, at least in the cortex. Capillary endothelial cells are important mediators of neurovascular coupling where they sense neuronal activity and generate a signal that dilates upstream arterioles, a process for which TRPA1 is required (Thakore *et al.*, 2020). Thakore *et al.* have shown that Ca^{2+} signalling after TRPA1 agonist application is slow in the capillary bed but rapid in the curvature of the vessel (Figure 45). It is tempting to speculate that this increase in propagation speed is therefore due to higher TRPA1 expression in the curvature. Expression of GCaMP in the TRPA1 vascular endothelial cells and investigation of Ca^{2+} signals following application of TRPA1 agonist will help in explaining these observations.

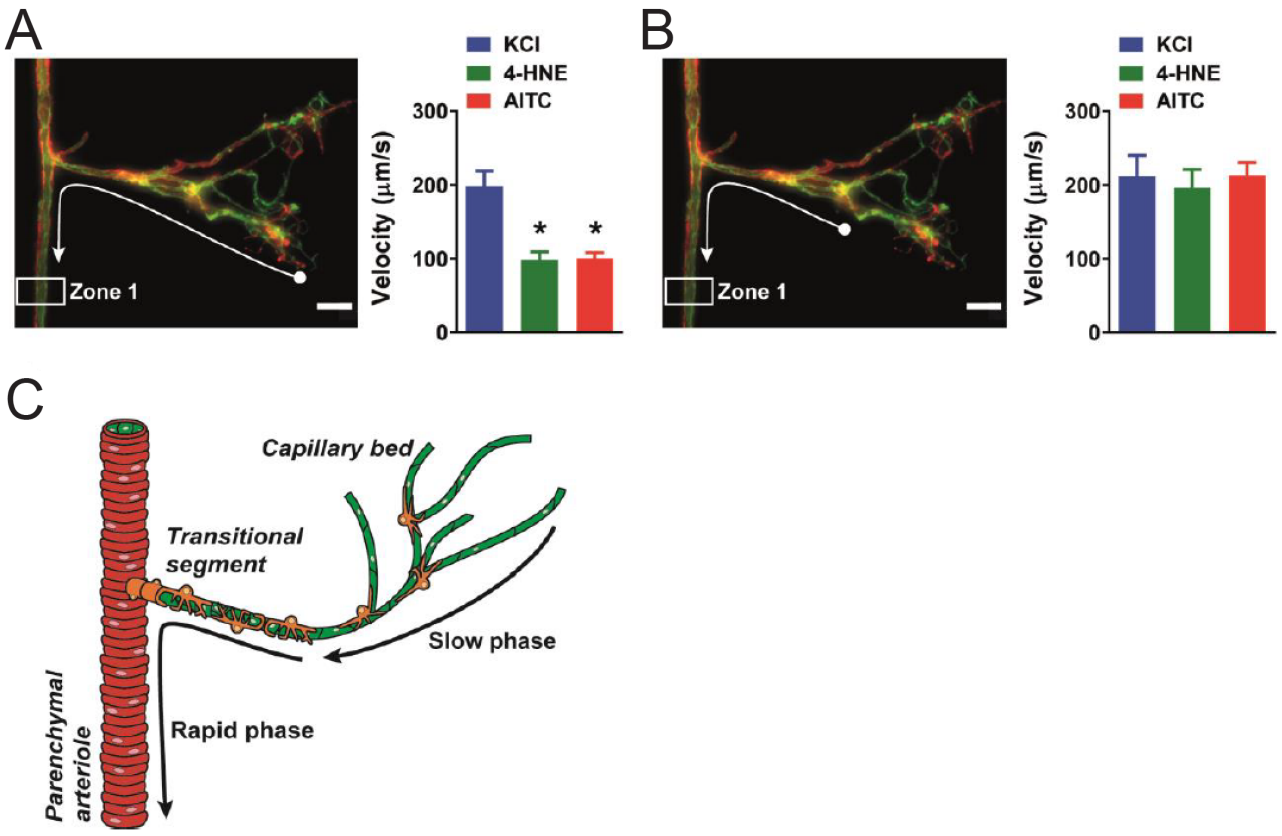

Figure 45: Representative fluorescence image of an ex vivo microvascular preparation obtained from VEC-cre mT/mG mice. Endothelial cells express membrane bound EGFP (green) and all other cell types express tdTomato (red) (A) Left: Conduction velocity of the vasodilator signal was calculated from the time interval and distance travelled to a specific point in the upstream arteriole (Zone 1, white arrow) following application of drugs onto capillary extremities (white ball). Right: Responses to the TRPA1 channel activators AITC (30 μm) and 4-HNE (1 μm) were significantly slower than the response to activation of Kir channels with KCl (10 mM) (B) Left: Velocity measurements were calculated from the post-arteriole transitional segment (adjacent to the capillary bed, white ball) to a point in the upstream arteriole (Zone 1, white arrow). Right: Velocity following AITC (30 μm) or 4-HNE (1 μm) treatment was comparable to that following application of KCl (60 mM) (C) Proposed model showing that activation of TRPA1 channels on capillaries produces a signal that slowly propagates through the capillary network and a faster propagating signal in arterioles and the post-arteriole transitional region. Figure legend and figure reproduced from Thakore *et al.*, 2020.

TRPA1 has been described as a cold sensor in various tissues, highlighting the possibility that the hypothalamic TRPA1 neuron population might be involved in the control of core body temperature in response to cold stimuli. Neurons in the DM are able to control core body temperature in response to cold (Zhao *et al.*, 2017) and TPRM2 channels in the hypothalamus are heat sensors (Song *et al.*, 2016). To test whether the hypothalamic TRPA1 neurons play a role in the control of temperature homeostasis, these cells can be ablated or activated (by DREADD or optogenetic methods) and the change in core body temperature observed. Ca^{2+} imaging in acute brain slices of the hypothalamus under different temperature conditions should show altered Ca^{2+} responses in TRPA1 neurons, if these cells serve as cold sensors in the brain.

We observed τGFP expression in enamel secreting cells and cells in the tooth of TRPA1IC/eR26τGFP reporter mice. A similar staining pattern in the teeth was also observed in the TRPC4 and TRPC5 reporter animals. These findings resulted in a collaboration with Prof. Katharina Zimmermann (University Erlangen-Nürnberg). They identified TRPA1 and TRPC5 expression in odontoblasts and showed that TRPC5, together with TRPA1, mediate cold response in inflamed and healthy teeth in both mice and humans. TRPC4 is also expressed in

odontoblasts but does not play a role in cold sensation in these cells (Bernal *et al.*, 2021). I observed TPRC4 driven τGFP expression in neuronal fibers in the ME and also in cells in close contact with blood vessels. Due to their morphology these cells might be pericytes. Ca^{2+} signalling in pericytes triggers an electrical signal that propagates along the process and controls local blood flow through the vessels (Borysova *et al.*, 2013), forming a network. To test if TRPC4 plays a role in this Ca^{2+} signalling, the electrical properties of τGFP-expressing pericytes in response to TRPC4 agonists should be investigated and the direction and nature of the Ca^{2+} signalling along the projections can be visualized in the GCaMP reporter animals.

I observed τGFP expression in neurons and fibers in the hypothalamus of TRPC5IC/eR26τGFP reporter animals. TRPC5 functions in Arc neurons include regulation of leptin and serotonin effects in pro-opiomelanocortin (Pomc) neurons (Y. Gao *et al.*, 2017) and mediating prolactin-evoked potentials (Blum *et al.*, 2019). In addition to these neurons, I identified a TRPC5-expressing cell type in the pars tuberalis in close contact with the vascular system. The pars tuberalis is located between the pars distalis in the pituitary and the ME. The pars tuberalis can communicate in a retrograde manner with the ME and anterogradely with the pituitary. Cells of the pars tuberalis are connected to the CSF via tanycyte projections. These cells have been described to play a role in melatonin signalling in mammals. TSH is released from these cells and acts on the hypothalamus and on the pituitary to regulate thyroid hormone levels (Yasuo *et al.*, 2011). Besides TRPC5 I also identified TRPA1 and TRPM5-expressing cells in the pars tuberalis, in morphologically similar cells but with varying cell numbers. Multiple experimental approaches can lead to an understanding of the function of these TRP expressing cells. These cells can be ablated by injection of DT in the pars tuberalis in R26-iDTR animals. This can be done in either the single Cre-reporter strains or TRPC5, TRPM5 and TRPA1 Cre-lines can be bred together for manipulation of a bigger cell population and DREADD reporter lines can be injected with CNO for activation. Because the pars tuberalis was described as a linker between the hypothalamus and the pituitary, hormonal measurement of pituitary hormones in the blood after ablation or activation of these cells, either in single lines or combinations of Cre-driver lines, will provide answer for the functional role of the TRP-expressing pars tuberalis cells.

4.6 TRPC2 PVN neurons terminate in the ME

In addition to the τGFP expression in OSNs and VSNs observed in the TRPC2IC/eR26τGFP animals I identified a small population of reporter gene expressing cells in the pituitary and in neurons in the PVN. The TRPC2 pituitary cells are not expressing any of the hormones released by the pituitary. Only very few, negligible reporter gene expressing cells are colocalized with GH. Due to their morphology, these cells might be a subset of folliculo-stellate cells within the pituitary. These cells are not releasing hormones but regulate the endocrine system in a paracrine manner by the release of growth factors such as vascular endothelial growth factor (VEGF) (Inoue *et al.*, 1999). VEGF release is triggered by Ca^{2+} influx (Deyama *et al.*, 2019). One possible role for TRPC2 in these cells is the opening of TRPC2 channels after GPCR activation leading to increased Ca^{2+} influx which is required for VEGF release.
I identified a previously unknown population of TRPC2-expressing neurons with acute TRPC2 expression in the PVN. Fibers from these neurons project through the lateral hypothalamus into the ME and seem to terminate in the posterior part of the ME where they are in close contact to fenestrated blood vessels. This is a feature they share with other hormone realising neurons in the PVN such as those that release CRH, but also with GnRH neurons. Staining against different hormones in the PVN revealed that a subset of TRCP2 neurons expresses CRH, whereas the majority of TRPC2 neurons are negative for all hormones tested. Chronically silencing or ablating these neurons did not have an impact on total ACTH concentrations in the blood. This indicates that the small population of CRH expressing TRPC2 neurons do not have an impact on total ACTH levels. Instead, together with the hormone negative neurons their function might be the modulation of the ME to fine-tune hormone release, as silencing of exocytotic release did not had an effect it might be that compounds are released independent of this mechanism. This would mean that these neurons are rather sensing cells instead of hormone releasing cells, comparable to their function in the olfactory system and also potentially in the pituitary. The PVN is a tightly regulated nucleus and it receives input from many nuclei such as the Arc, the NTS and other interneurons innervating the PVN. Interneurons innervating the PVN mainly release GABA or glutamate to control PVN neurons. Glutamate receptors are G-protein coupled receptors and might be upstream of TRPC2 in the PVN. This would mean that TRPC2 activation leads to an increase in Ca2+ in these neurons, potentially triggering VEGF release. This would implicate that the channel is located in the cell body in the PVN. Another possibility is that the channel is located in the axon in the ME, similar to its localization in the VSNs. In this scenario TRPC2 would be activated downstream of GPCRs which are activated in the ME. Ca2+ imaging in slices of either the ME alone or the PVN in TRPC2IC/eR26-GCaMP3 animals together with activators of TRPC2, such as DAG, can be used to investigate the channels localization. In addition, TRPC2 can be knocked out in the R26-cas9 line in combination with the eR26-GCaMP line to exclude off target effects of DAG. As yet unidentified signalling molecules or transcription factors such as VEGF, from TRPC2 neurons might fine-tune the ME milieu in different ways. One possibility is that they change the permeability of the fenestrated blood vessels and regulate hormone release in this way. An elegant way to test this is the use of R26-iDTR animals in which only the TRPC2 PVN neurons are ablated in adult animals after stereotactic delivery of DT. A benefit of this approach, in contrast to ablation of the cells with DTA, is that no compensation should occur in this short time window. For activation of TRPC2 neurons and investigation of the effects on permeability, CNO can be injected in R26-DREADD animals. To investigate the permeability of the fenestrated blood vessels, Evans Blue can be injected in the tail vein and visualized in sections of the ME with an epifluorescence microscope either after ablation or after CNO administration if the permeability is indeed fine-tuned by the TRPC2 neurons,

one might expect changes in the ability of EvansBlue to enter into the ME. Another factor that can be investigated in these animals is properties of the tanycytic endfeet. Endfeet composition is changing depending on the metabolic status of the animal. Whether factors released by TRPC2 neurons have an impact on endfeet can be investigated in iDSCO cleared MEs with staining against vimentin. These experiments will help to answer the question whether TRPC2 neurons have an indirect effect on hormone release from the ME, by potentially fine-tuning permeability.

It is known that CRH reduces LH release but CRH does not influence GnRH or kisspeptin neurons directly, as CRH administration did not change the electrical properties of either GnRH or kisspetin neurons (Yip, X. Liu, *et al.*, 2021). CRH might however have an impact on the composition of the ME or alternatively may act directly on the pituitary. I observed slightly increased LH and FSH levels one to two hours after CNO activation of TRPC2 neurons. It is tempting to speculate that TRPC2 neurons are modulating the ME in a way that LH and FSH release is enhanced. This could be through an increased permeability of fenestrated blood vessels, subsequent of potential TRPC2 dependent VEGF release, such that more GnRH is reaching the pituitary or it could be a result of retraction of tanycytic endfeet around the GnRH axon terminals leading to an increased GnRH release. Measurement of pituitary hormones in PVN-specific ablated or activated animals will lead to a better understanding of whether TRPC2 neurons play a role in this process. TRPC2 neurons might also regulate other PVN neurons directly via a feedback mechanism. The vasopressin receptors V1R and V2R are GPCRs and Ca^{2+} influx in recpetor-expressing cells is needed for their activation (Birnbaumer, 2000). TRPC2 might be downstream of these GPCRs and mediate the Ca^{2+} influx of the level of the PVN. Indeed, CRH receptors have been shown to be expressed in the PVN (Makino *et al.*, 2005).

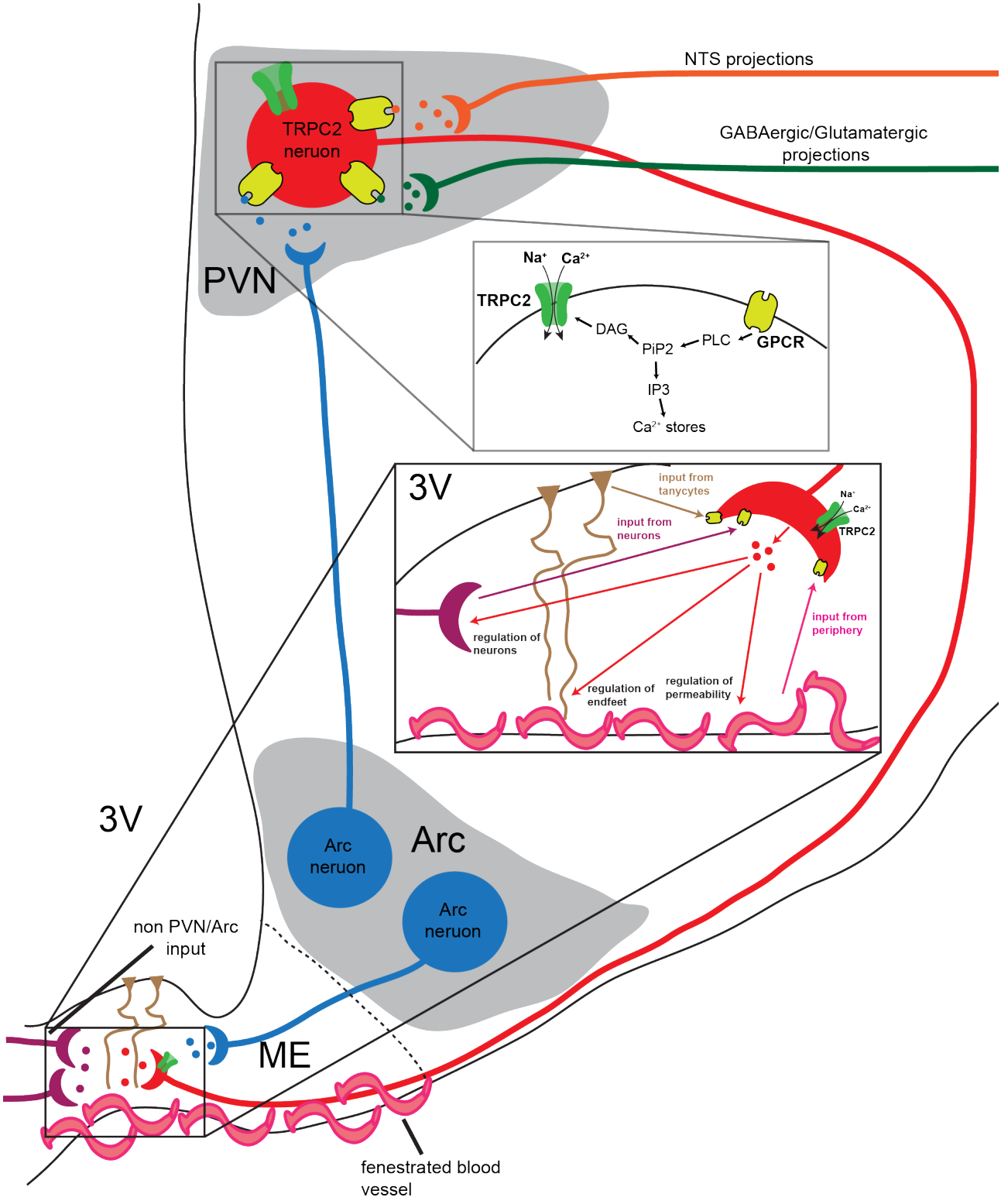

Figure 46: Potential TRPC2 mediated control of the ME. The PVN receives input from the nucleus solitary tract (NTS), the Arc and GABAergic and Glutamatergic input from interneurons. In this proposed model TRPC2 neurons express different GPCRs in the somata, activated by the release of signalling molecules from PVN projecting neurons. Subsequent to GPCR activation PLC is activated and PIP2 is cleaved into IP3 and DAG. DAG is activating TRPC2, triggering Na+ and Ca2+ influx, depolarization and subsequent release of signalling molecules in to the ME. In a second model TRPC2 is located in the membrane near the synapse in the ME, similar to its location in the VSNs. GPCRs are activated either by cues from the blood, tanycytes or other neurons in the ME and subsequently activate TRPC2, triggering release of signalling molecules. Potential mechanisms of this release is control of permeability of fenestrated blood vessels or tanycyte endfeet.

Maternal aggression in females and male-male aggression in males is decreased in TRPC2 KO animals. Hasen and Gammie (Hasen *et al.*, 2009) investigated c-Fos expression in the hypothalamus and vomeronasal amygdala after maternal aggression in WT and KO animals where they compared untested (no intruder) and tested (with intruder) for each genotype. They did not observe an increase in c-Fos expression in the vomeronasal amygdala in KO animals showing that activation of VSNs is drastically reduced. Interestingly, there was also no increase in c-Fos expression in nuclei of the hypothalamus in KO animals after aggression in contrast to WT animals. The PVN, the ventromedial hypothalamus (VMH), the posterior part of the anterior hypothalamus (AHP) and the lateral hypothalamus showed no increase in c-Fos expression. Also I only observed fibers originating from the TRPC2 PVN neurons in the PVN itself and the lateral hypothalamus in the TRPC2IC/eR26-τGFP animals, contact points with the other nuclei might occur in the ME. It is tempting to speculate that these observations in the KO animals are not caused by the disruption of signalling from the VNO but rather from the TRPC2 PVN neurons. To test this hypothesis TRPC2 PVN neurons need to be ablated with DT administration and maternal aggression and also pup-retrieval, followed by c-Fos circuitry mapping, needs to be performed. In this way, it should be possible to differentiate the influence of the VNO and of the PVN neurons on these different brain areas. The circuit mapping was not performed in males but a similar phenotype would be expected as aggressive behaviour is known to be a hard-wired circuit in both genders. The increase in c-Fos expression was only observed after the animals displayed aggressive behaviour. Another experiment to investigate the potential role of TRPC2 neurons in aggressive behaviour and activation of different brain areas is DREADD-mediated activation of these cells. To rule out any influence from the olfactory system, DREADD needs to be exclusively expressed in the PVN neurons. Adeno-associated-viruses (AAVs), bearing a Cre-dependent DREADD construct, injected into the PVN neurons are an alternative to *ROSA26* reporter mice. If TRPC2 PVN neurons are involved in the increase in activity in other brain areas after aggression, these areas should be able to be activated by CNO alone without the display of aggressive behaviour.

4.7 An oestrogenic network is active during embryogenesis

The onset of neuro-oestrogen synthesis and the start of the critical period in mice has previously been investigated, but a conclusive answer regarding localisation at a cellular reolution for aromatase expressing cells during embryonic development remained elusive. With the ArIC/eR26-τGFP reporter mouse, I revealed that the ontogeny of aromatase expression coincides with ERα at E13.5 in few neurons in the hypothalamus, indicating that the brain oestrogen-sensitivity coincides with the potential *de novo* synthesis of neuro-steroids. Without this information, the few aromatase neurons in the embryonic mouse brain are lost in a sea of non-aromatase neurons diluting or watering down (making inconclusive) any previous experimental attempts trying to demonstrate significant steroid hormone production in the brain *in utero*. During embryogenesis the number of oestrogen-producing cells increases and stays restricted to nuclei of the hypothalamus and the amygdala with no major gender differences. Most aromatase-expressing cells do not express ERα, although the two cell populations are rather in close apposition indicating that oestrogen is acting in a paracrine manner. What is the impact of these findings on the understanding of sexual differentiation of the brain? Is there an active role for estradiol, for example in neural differentiation (Toran-Allerand, 1976)? Currently, this is mainly described for between birth and puberty and not *in utero*. One study measured steroid concentrations in the embryonic rat brain from E19 onwards with radio immune assay (RIA) (Konkle *et al.*, 2011). They found no gender difference in oestrogen concentration but RIA lacks cellular resolution. This is in line with my findings that three key enzymes of *de novo* steroid synthesis are already expressed at E13.5 in female mouse brains. This means that long before the known masculinizing and feminizing actions of oestrogen, an aromatase system already develops in both the male and female embryonic brain. The classical aromatization hypothesis claims that the female brain is the default brain and it does not need oestrogen during early development (females are protected by α-fetoprotein) and oestrogenic actions are only needed for masculinization and defeminization. Feminizing actions of oestrogen occur postnatally in females, i.e. when the ovaries start to produce estradiol. In rats, no significant amount of oestrogen was detected before P7 (Zor *et al.*, 1976). Male brains are masculinized and defeminized by oestrogen synthesized from circulating testosterone. Increasing levels of testosterone in the brain originating from the testis in later developmental stages is quite likely increasing the testosterone concentration in the brain on top of hypothetical *de novo* synthesis, in contrast to females. In the classical hypothesis female brains do not need oestrogen until circulating levels from the ovaries increase for normal development. In contrast, my results indicate that the brain needs oestrogenic actions starting with the onset of aromatase expression at E13.5, regardless of gender. I propose that the aromatization hypothesis should be adjusted based on my findings. The fact that there are no gross gender differences *in utero* shows that oestrogen is needed in both genders to develop a 'default' brain status that undergoes sexual differentiation later in development, for example when circulating oestrogen levels rise in females or subsequent to the testosterone surge in males. My proposed adjusted aromatization hypothesis claims that both male and female brains are protected from maternal oestrogen by α-fetoprotein and in contrast to the classical hypothesis, both male and female brains express aromatase and synthesize oestrogen, potentially *de novo* as circulating testosterone in females is not detectable. This oestrogen is acting mainly in a paracrine manner and is needed in the hypothalamus and in the amygdala for normal brain development. This means, that the female brain also needs oestrogenic actions early in development, presumingly without gender differences in contrast to the classical hypothesis. Sexual differentiation occurs due to rising testosterone levels or due to sexually dimorphic regulation of aromatase activity or expression. This shows that before the critical period an oestrogen-dependent neuronal network is

developed and the default status of the brain is neither male or female and oestrogen is required in both genders for normal development (Figure 47 and Figure 48).

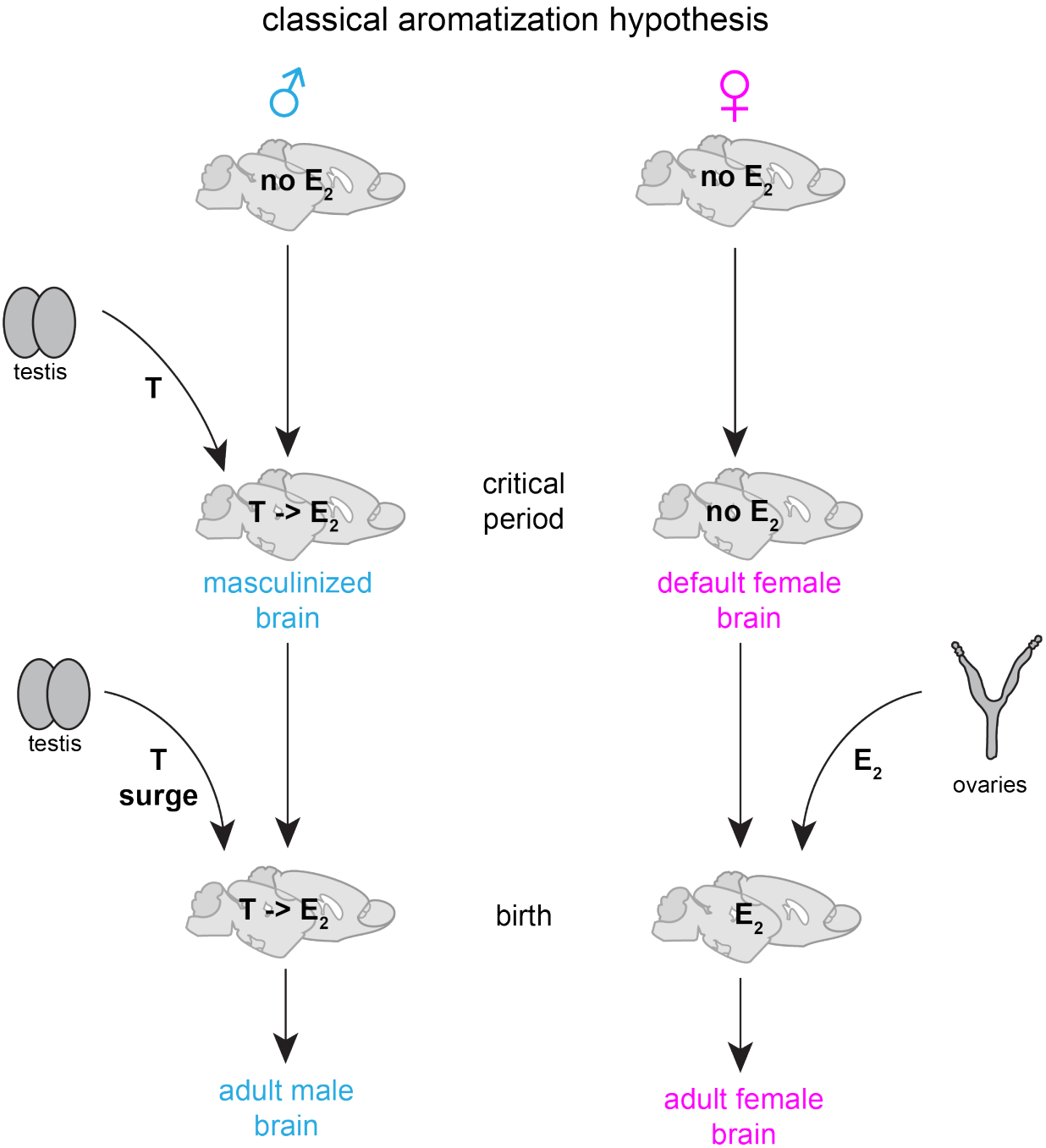

Figure 47: Classical aromatisation hypothesis. In the classical aromatisation hypothesis the female brain is the default status of the brain and is protected from circulating oestrogen by αfeto-protein. The male brain gets masculinized by oestrogen synthesized in the brain from circulating testosterone. During the critical period the female brain is sensitive to oestrogen but under physiological conditions does not have oestrogen in the brain. Shortly after birth males have a testosterone surge that increases the oestrogen levels in the brain and the female brain oestrogen levels rise few days after birth when circulating oestrogen levels increase due to oestrogen synthesis in the ovaries.

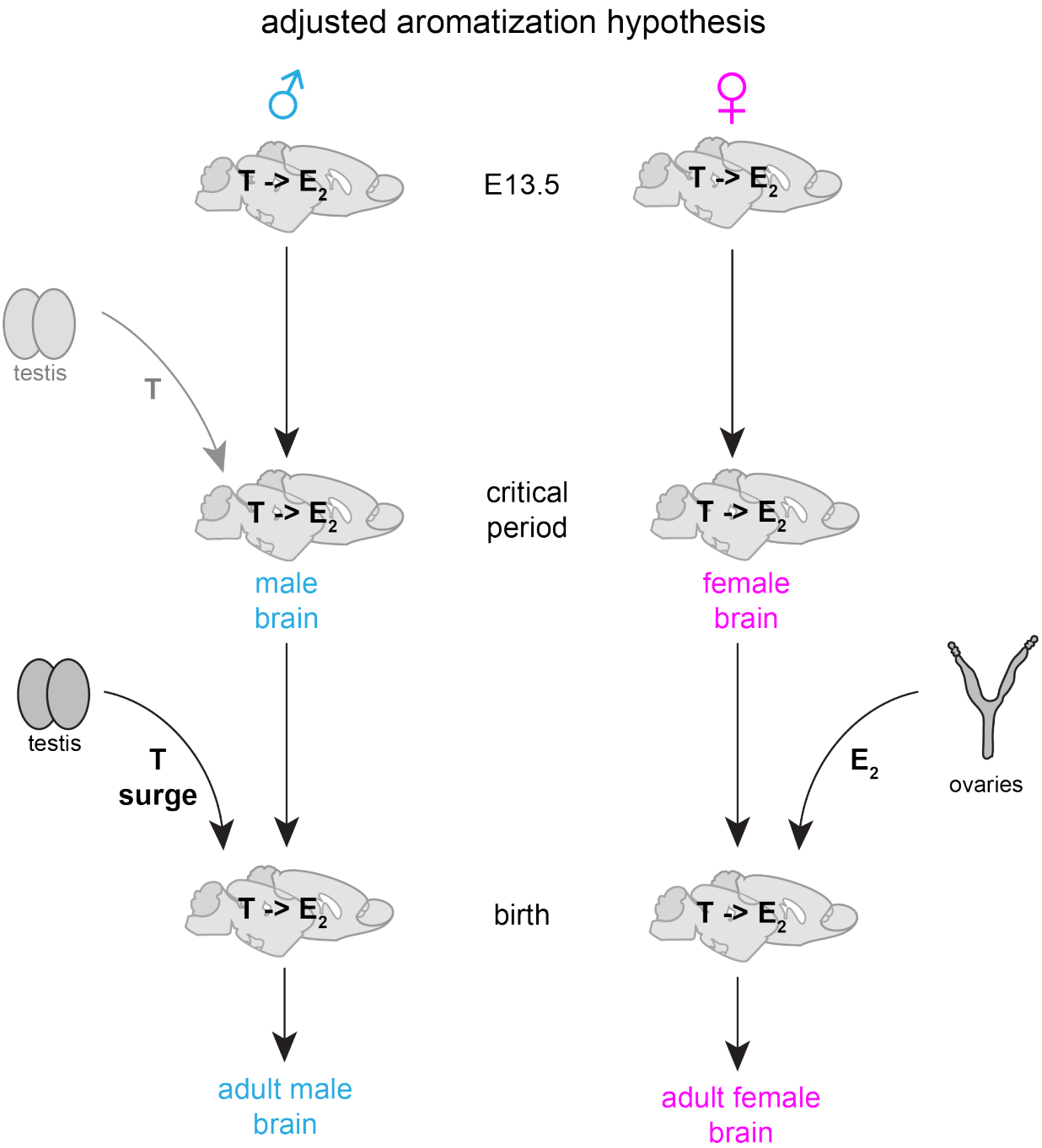

Figure 48: Adjusted aromatisation hypothesis. In the adjusted aromatisation hypothesis both male and female brains synthesis oestrogen from aromatase, possibly *de novo* from cholesterol from E13.5 onwards. The default brain also needs oestrogenic actions in both gender without gross gender differences, in contrast to the classical view in which in female brains oestrogen is not present until produces by the ovaries. Sexual differentiation is potentially established by differences in testosterone levels or by gender specific regulation of aromatase and not just by the absence or presence of oestrogen. The final sexual differentiation is most likely mediated by circulating steroids from the gonads in later developmental stages.

There is still the possibility that gender differences are present before the critical period, not in the cell number of the neuro-oestrogen network but either in expression levels of aromatase, local testosterone levels or gender differences in the oestrogen sensitive cells. I did not observe gross gender differences in the colocalisation of τGFP and ERα cells and the distance between the two populations also did not reveal any gender

differences. The two populations are in close contact, indicating that oestrogen mostly acts in a paracrine manner. This fact raises the exciting possibility that oestrogen is only partially acting as a hormone but rather like a neurotransmitter. Hormones are released far away from their site of action and have long lasting effects, mainly changing expression levels. Neurotransmitter on the other hand are acting close to their release site and their effects occur within the millisecond range. One requirement for oestrogen to act similarly to neurotransmitters is that its release and synthesis need to be regulated over a short time span, much shorter than what could be achieved by regulation through aromatase expression levels. And indeed, aromatase activity can be blocked by phosphorylation of two residues in the aromatase enzyme in a Ca^{2+}-dependent manner. This way, the synthesis of oestrogens can be regulated within milliseconds. My assumption that oestrogen mainly acts in a paracrine manner is in line with this neurotransmitter hypothesis. In rat embryos no gender differences in oestrogen levels were observed in different brain regions. Females display a higher testosterone concentration in the hypothalamus but no increased oestrogen concentrations (Konkle *et al.*, 2011). This makes it tempting to speculate that in females more testosterone is indeed synthesized into higher oestrogen levels but it acts like a neurotransmitter and these transient concentration increases can not be detected with available detection methods. Presuming oestrogen really functions as a neurotransmitter it is important to also take small populations of aromatase-expressing neurons into account, especially early in development. In birds, aromatase was shown to be localized in axon terminals (Balthazart *et al.*, 2006 and Figure 49). I observed dense, nucleus-dependent τGFP fiber networks the ArIC/eR26-τGFP developing brain. If aromatase is also located in the axon terminal in rodents, these fiber networks raise the possibility that aromatase neurons can have neurotransmitter-like oestrogen actions also far away from their cell body. In adult reporter animals, this can be tested with the help of AAVs and the R26-Cas9 mouse. The connectivity map of aromatase neurons can be mapped by injection of Cre-dependent AAVs expressing a red fluorophore. By mapping these patterns the projection pathway of a specific aromatase-expressing nucleus can be differentiated from other aromatase expressing fibers by the co-expression of the red fluorophore. In these areas c-Fos circuitry mapping can be compared between WT animals and animals injected with a guide-RNA targeting the aromatase gene in the R26-Cas9 mouse. In addition, Ca^{2+} imaging approaches will help in understanding of these processes. Either Ca^{2+} is increasing in oestrogen-sensitive cells or Ca^{2+}-signalling plays a role for the phosphorylation of aromatase. With this approach a region specific aromatase KO can be analysed. If aromatase is present in the axon terminals and is acting as a neurotransmitter, differences in c-Fos expression should be observed between the KO and WT animals.

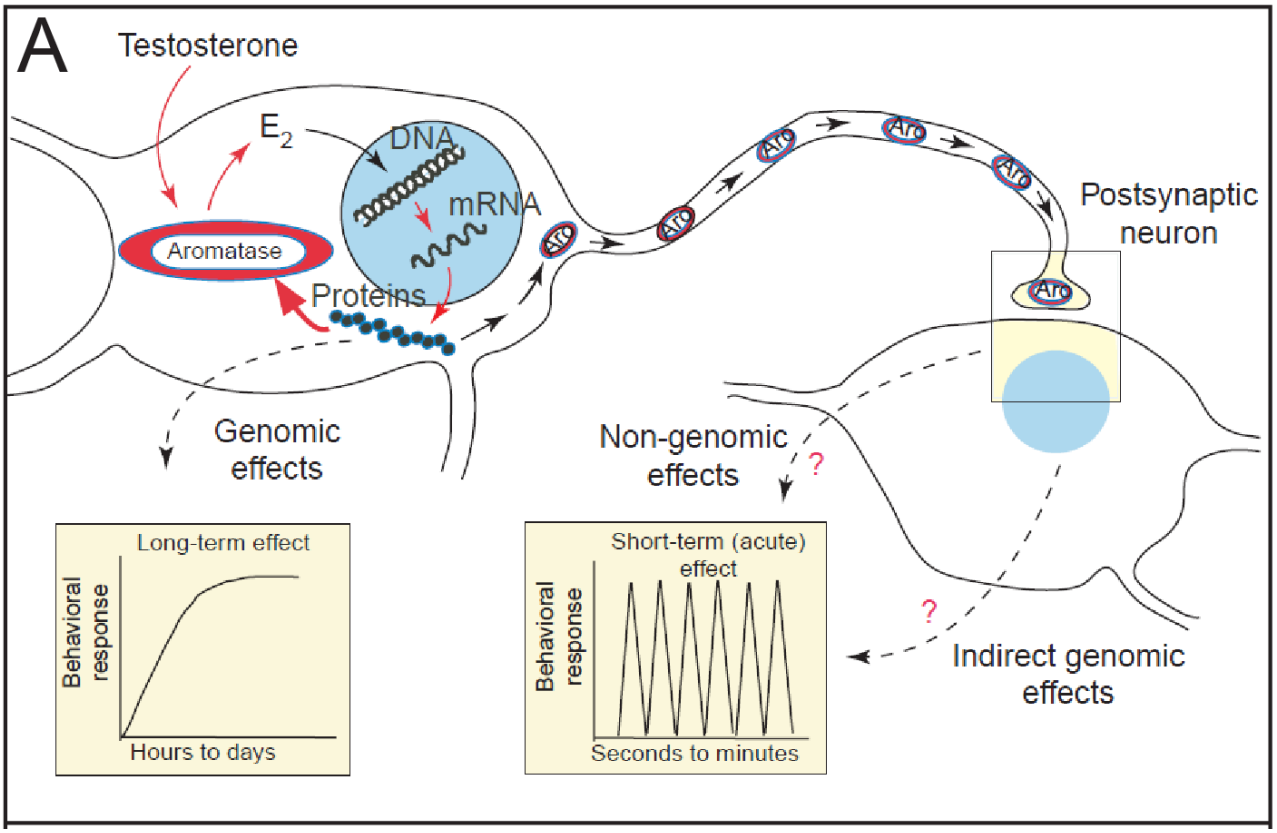

Figure 49: Mechanisms through which rapid changes in oestrogen production presynaptically, caused by phosphorylation and de-phosphorylation of the aromatase enzyme, might modulate neuronal activity in a manner similar to the action of a neurotransmitter or neuromodulator. (A) In the aromatase-expressing neuron, aromatase transcription is enhanced by the action of testosterone or its aromatized metabolite, estradiol (E2). Steroid action also results in the transcription of various other proteins that modify neural activity in the long term and have consequently long-lasting (e.g. seasonal) effects on reproductive behaviours. Aromatase is then transported to presynaptic boutons, as demonstrated by immunocytochemical studies at the electron-microscopic level, where the enzyme catalyses the transformation of testosterone into E2. Red arrows represent metabolic pathways or actual movements of compounds, and black arrows represent control mechanisms. Figure legend and figure reproduced from Balthazart *et al.*, 2006.

I did not observe any gross gender differences *in utero*, not in cell number and not in fiber density and projections. At birth however, I found a profound sexual dimorphism in the Arc. Strikingly, here I observed aromatase expressing cells only in males. This neuron population displays similar properties to the other aromatase-expressing nuclei, including low colocalization with ERα, but the τGFP+ cells are in close apposition to the ERα cells. Kisspeptin neurons are found in the Arc at birth and ERα knock-out in kisspeptin neurons leads to advancement of puberty onset and puberty arrest (Mayer, Acosta-Martinez, *et al.*, 2010). I did not observe aromatase expression in kisspeptin neurons raising the possibility that oestrogen released from aromatase neurons acts in a paracrine manner in kisspeptin neurons. To test the hypothesis that oestrogen acts in a paracrine manner and potentially also as neurotransmitter, Dr. Imre Farkas from the group of Prof. Erik Hrabovszky performed electrophysiological studies in kisspeptin neurons. They observed that testosterone administration in Arc slices inhibits the firing rate of kisspeptin neurons. When an aromatase inhibitor is applied together with testosterone, this inhibition is no longer observed. This shows that oestrogen is acting on kisspeptin neurons by reducing their firing rate. This effect is mediated by ERα, because administering an ERα blocker with testosterone is blocking the reducing effects of oestrogen. This shows that oestrogen is acting in a paracrine manner with, at least some, neurotransmitter properties in juvenile males. Besides its membrane

effect, oestrogen might also influence gene expression in kisspeptin neurons, mediated by ERα acting as transcription factor (Figure 50). The Arc aromatase expression in males is coinciding with the testosterone surge at birth. It might be that in the Arc specifically higher oestrogen concentrations are needed in males, but not in females, indicated by the lack of aromatase neurons in this region.

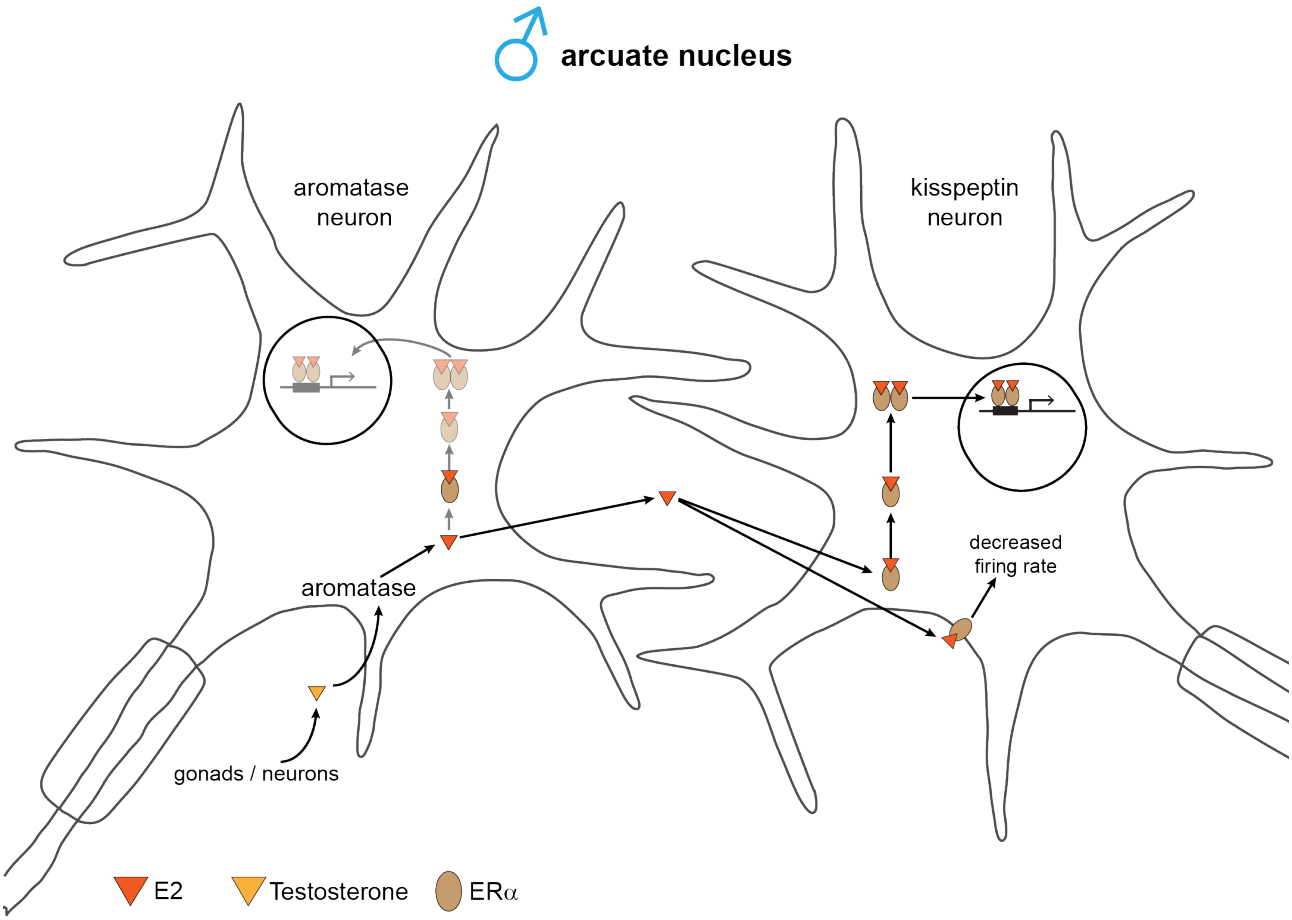

Figure 50: Model of oestrogen action on kisspeptin neurons. Testosterone, either from the gonads or synthesized in the brain is converted to oestrogen in aromatase neurons. These neurons are in close apposition to kisspeptin neurons in the Arc. Through a paracrine mechanism oestrogen reaches the kisspeptin neuron and binds to ERα. After binding the receptor either dimerizes and translocates to the nucleus and acts as a transcription factor. Or the receptor has membrane actions and reduces the firing rate of kisspeptin neurons.

5 References

Abbott, N. J., Rönnbäck, L., & Hansson, E. (2006). Astrocyte-endothelial interactions at the blood-brain barrier. *Nature reviews. Neuroscience*, *7*, 41–53. https://doi.org/10.1038/nrn1824

Alzoubi, A., Almalouf, P., Toba, M., O'Neill, K., Qian, X., Francis, M., Taylor, M. S., Alexeyev, M., McMurtry, I. F., Oka, M., & Stevens, T. (2013). Trpc4 inactivation confers a survival benefit in severe pulmonary arterial hypertension. *The American journal of pathology*, *183*, 1779–1788. https://doi.org/10.1016/j.ajpath.2013.08.016

Amateau, S. K., & McCarthy, M. M. (2004). Induction of pge2 by estradiol mediates developmental masculinization of sex behavior. *Nature neuroscience*, *7*, 643–650. https://doi.org/10.1038/nn1254

Bach, G. (2005). Mucolipin 1: Endocytosis and cation channel–a review. *Pflugers Archiv : European journal of physiology*, *451*, 313–317. https://doi.org/10.1007/s00424-004-1361-7

Baird, D. T., Baker, T. G., McNatty, K. P., & Neal, P. (1975). Relationship between the secretion of the corpus luteum and the length of the follicular phase of the ovarian cycle. *Journal of reproduction and fertility*, *45*, 611–619. https://doi.org/10.1530/jrf.0.0450611

Bakker, J. [J.], Honda, S., Harada, N., & Balthazart, J. (2003). The aromatase knockout (arko) mouse provides new evidence that estrogens are required for the development of the female brain. *Annals of the New York Academy of Sciences*, *1007*, 251–262. https://doi.org/10.1196/annals.1286.024

Bakker, J. [Julie], De Mees, C., Douhard, Q., Balthazart, J., Gabant, P., Szpirer, J., & Szpirer, C. (2006). Alpha-fetoprotein protects the developing female mouse brain from masculinization and defeminization by estrogens. *Nature neuroscience*, *9*, 220–226. https://doi.org/10.1038/nn1624

Balthazart, J., & Ball, G. F. (2006). Is brain estradiol a hormone or a neurotransmitter? *Trends in neurosciences*, *29*, 241–249. https://doi.org/10.1016/j.tins.2006.03.004

Belgorosky, A., Pepe, C., Marino, R., Guercio, G., Saraco, N., Vaiani, E., & Rivarola, M. A. (2003). Hypothalamic-pituitary-ovarian axis during infancy, early and late prepuberty in an aromatase-deficient girl who is a compound heterocygote for two new point mutations of the cyp19 gene. *The Journal of clinical endocrinology and metabolism*, *88*, 5127–5131. https://doi.org/10.1210/jc.2003-030433

Benemei, S., De Logu, F., Li Puma, S., Marone, I. M., Coppi, E., Ugolini, F., Liedtke, W., Pollastro, F., Appendino, G., Geppetti, P., Materazzi, S., & Nassini, R. (2017). The anti-migraine component of butterbur extracts, isopetasin, desensitizes peptidergic nociceptors by acting on trpa1 cation channel. *British journal of pharmacology*, *174*, 2897–2911. https://doi.org/10.1111/bph.13917

Benn, B. S., Ajibade, D., Porta, A., Dhawan, P., Hediger, M., Peng, J.-B., Jiang, Y., Oh, G. T., Jeung, E.-B., Lieben, L., Bouillon, R., Carmeliet, G., & Christakos, S. (2008). Active intestinal calcium transport in the absence of transient receptor potential vanilloid type 6 and calbindin-d9k. *Endocrinology*, *149*, 3196–3205. https://doi.org/10.1210/en.2007-1655

Berghard, A., Buck, L. B., & Liman, E. R. (1996). Evidence for distinct signaling mechanisms in two mammalian olfactory sense organs. *Proceedings of the National Academy of Sciences of the United States of America*, *93*, 2365–2369. https://doi.org/10.1073/pnas.93.6.2365

Berkovitz, G. D., Guerami, A., Brown, T. R., MacDonald, P. C., & Migeon, C. J. (1985). Familial gynecomastia with increased extraglandular aromatization of plasma carbon19-steroids. *The Journal of clinical investigation*, *75*, 1763–1769. https://doi.org/10.1172/JCI111888

Bernal, L., Sotelo-Hitschfeld, P., König, C., Sinica, V., Wyatt, A., Winter, Z., Hein, A., Touska, F., Reinhardt, S., Tragl, A., Kusuda, R., Wartenberg, P., Sclaroff, A., Pfeifer, J., Ectors, F., Dahl, A., Freichel, M., Vlachova, V., Brauchi, S., … Katharina, Z. (2021). Odontoblast trpc5 channels signal cold pain in teeth. *Science Advances*.

Beynon, R. J., Veggerby, C., Payne, C. E., Robertson, D. H. L., Gaskell, S. J., Humphries, R. E., & Hurst, J. L. (2002). Polymorphism in major urinary proteins: Molecular heterogeneity in a wild mouse population. *Journal of chemical ecology*, *28*, 1429–1446. https://doi.org/10.1023/a:1016252703836

Bezençon, C., Fürholz, A., Raymond, F., Mansourian, R., Métairon, S., Le Coutre, J., & Damak, S. (2008). Murine intestinal cells expressing trpm5 are mostly brush cells and express markers of neuronal and inflammatory cells. *The Journal of comparative neurology*, *509*, 514–525. https://doi.org/10.1002/cne.21768

Bianco, S. D. C., Peng, J.-B., Takanaga, H., Suzuki, Y., Crescenzi, A., Kos, C. H., Zhuang, L., Freeman, M. R., Gouveia, C. H. A., Wu, J., Luo, H., Mauro, T., Brown, E. M., & Hediger, M. A. (2007). Marked disturbance of calcium homeostasis in mice with targeted disruption of the trpv6 calcium channel gene. *Journal of bone and mineral research : the official journal of the American Society for Bone and Mineral Research*, *22*, 274–285. https://doi.org/10.1359/jbmr.061110

Biegon, A., Alia-Klein, N., & Fowler, J. S. (2012). Potential contribution of aromatase inhibition to the effects of nicotine and related compounds on the brain. *Frontiers in pharmacology*, *3*, 185. https://doi.org/10.3389/fphar.2012.00185

Birnbaumer, M. (2000). Vasopressin receptors. *Trends in endocrinology and metabolism: TEM*, *11*, 406–410. https://doi.org/10.1016/s1043-2760(00)00304-0

Blanchard, M. G., Kittikulsuth, W., Nair, A. V., de Baaij, J. H. F., Latta, F., Genzen, J. R., Kohan, D. E., Bindels, R. J. M., & Hoenderop, J. G. J. (2016). Regulation of mg2+ reabsorption and transient receptor potential melastatin type 6 activity by camp signaling. *Journal of the American Society of Nephrology : JASN*, *27*, 804–813. https://doi.org/10.1681/ASN.2014121228

Blum, T., Moreno-Pérez, A., Pyrski, M., Bufe, B., Arifovic, A., Weissgerber, P., Freichel, M., Zufall, F., & Leinders-Zufall, T. (2019). Trpc5 deficiency causes hypoprolactinemia and altered function of oscillatory dopamine neurons in the arcuate nucleus. *Proceedings of the National Academy of Sciences of the United States of America*, *116*, 15236–15243. https://doi.org/10.1073/pnas.1905705116

Boehm, U., Zou, Z., & Buck, L. B. (2005). Feedback loops link odor and pheromone signaling with reproduction. *Cell*, *123*, 683–695. https://doi.org/10.1016/j.cell.2005.09.027

Borbély, É., Payrits, M., Hunyady, Á., Mező, G., & Pintér, E. (2019). Important regulatory function of transient receptor potential ankyrin 1 receptors in age-related learning and memory alterations of mice. *GeroScience*, *41*, 643–654. https://doi.org/10.1007/s11357-019-00083-1

Borkum, J. M. (2018). The migraine attack as a homeostatic, neuroprotective response to brain oxidative stress: Preliminary evidence for a theory. *Headache*, *58*, 118–135. https://doi.org/10.1111/head.13214

Borysova, L., Wray, S., Eisner, D. A., & Burdyga, T. (2013). How calcium signals in myocytes and pericytes are integrated across in situ microvascular networks and control microvascular tone. *Cell calcium*, *54*, 163–174. https://doi.org/10.1016/j.ceca.2013.06.001

Britton, J., Pavord, I., Richards, K., Wisniewski, A., Knox, A., Lewis, S., Tattersfield, A., & Weiss, S. (1994). Dietary magnesium, lung function, wheezing, and airway hyperreactivity in a random adult population sample. *Lancet (London, England)*, *344*, 357–362. https://doi.org/10.1016/s0140-6736(94)91399-4

Bröker-Lai, J., Kollewe, A., Schindeldecker, B., Pohle, J., Nguyen Chi, V., Mathar, I., Guzman, R., Schwarz, Y., Lai, A., Weißgerber, P., Schwegler, H., Dietrich, A., Both, M., Sprengel, R., Draguhn, A., Köhr, G., Fakler, B., Flockerzi, V., Bruns, D., & Freichel, M. (2017). Heteromeric channels formed by trpc1, trpc4 and trpc5 define hippocampal synaptic transmission and working memory. *The EMBO journal*, *36*, 2770–2789. https://doi.org/10.15252/embj.201696369

Burek, M. J., Nordeen, K. W., & Nordeen, E. J. (1997). Sexually dimorphic neuron addition to an avian song-control region is not accounted for by sex differences in cell death. *Journal of neurobiology*, *33*, 61–71.

Calizo, L. H., & Flanagan-Cato, L. M. (2000). Estrogen selectively regulates spine density within the dendritic arbor of rat ventromedial hypothalamic neurons. *The Journal of neuroscience : the official journal of the Society for Neuroscience*, *20*, 1589–1596.

Carani, C., Qin, K., Simoni, M., Faustini-Fustini, M., Serpente, S., Boyd, J., Korach, K. S., & Simpson, E. R. (1997). Effect of testosterone and estradiol in a man with aromatase deficiency. *The New England journal of medicine*, *337*, 91–95. https://doi.org/10.1056/NEJM199707103370204

Castiglioni, A. J., Remis, N. N., Flores, E. N., & García-Añoveros, J. (2011). Expression and vesicular localization of mouse trpml3 in stria vascularis, hair cells, and vomeronasal and olfactory receptor neurons. *The Journal of comparative neurology*, *519*, 1095–1114. https://doi.org/10.1002/cne.22554

Chandrashekar, J. [J.], Mueller, K. L., Hoon, M. A., Adler, E., Feng, L., Guo, W., Zuker, C. S., & Ryba, N. J. (2000). T2rs function as bitter taste receptors. *Cell*, *100*, 703–711. https://doi.org/10.1016/s0092-8674(00)80706-0

Chandrashekar, J. [Jayaram], Hoon, M. A., Ryba, N. J. P., & Zuker, C. S. (2006). The receptors and cells for mammalian taste. *Nature*, *444*, 288–294. https://doi.org/10.1038/nature05401

Chubanov, V., Ferioli, S., Wisnowsky, A., Simmons, D. G., Leitzinger, C., Einer, C., Jonas, W., Shymkiv, Y., Bartsch, H., Braun, A., Akdogan, B., Mittermeier, L., Sytik, L., Torben, F., Jurinovic, V., van der Vorst, E. P., Weber, C., Yildirim, Ö. A., Sotlar, K., … Gudermann, T. (2016). Epithelial magnesium transport by trpm6 is essential for prenatal development and adult survival. *eLife*, *5*. https://doi.org/10.7554/eLife.20914

Chung, K., Wallace, J., Kim, S.-Y., Kalyanasundaram, S., Andalman, A. S., Davidson, T. J., Mirzabekov, J. J., Zalocusky, K. A., Mattis, J., Denisin, A. K., Pak, S., Bernstein, H., Ramakrishnan, C., Grosenick, L., Gradinaru, V., & Deisseroth, K. (2013). Structural and molecular interrogation of intact biological systems. *Nature*, *497*, 332–337. https://doi.org/10.1038/nature12107

Clapham, D. E., Julius, D., Montell, C., & Schultz, G. (2005). International union of pharmacology. xlix. nomenclature and structure-function relationships of transient receptor potential channels. *Pharmacological reviews*, *57*, 427–450. https://doi.org/10.1124/pr.57.4.6

Clarkson, J., & Herbison, A. E. (2006). Postnatal development of kisspeptin neurons in mouse hypothalamus; sexual dimorphism and projections to gonadotropin-releasing hormone neurons. *Endocrinology*, *147*, 5817–5825. https://doi.org/10.1210/en.2006-0787

Clasadonte, J., & Prevot, V. (2018). The special relationship: Glia-neuron interactions in the neuroendocrine hypothalamus. *Nature reviews. Endocrinology*, *14*, 25–44. https://doi.org/10.1038/nrendo.2017.124

Colsoul, B., Schraenen, A., Lemaire, K., Quintens, R., Van Lommel, L., Segal, A., Owsianik, G., Talavera, K., Voets, T., Margolskee, R. F., Kokrashvili, Z., Gilon, P., Nilius, B., Schuit, F. C., & Vennekens, R. (2010). Loss of high-frequency glucose-induced ca2+ oscillations in pancreatic islets correlates with

impaired glucose tolerance in trpm5-/- mice. *Proceedings of the National Academy of Sciences of the United States of America*, *107*, 5208–5213. https://doi.org/10.1073/pnas.0913107107

Constantin, S. (2011). Physiology of the gonadotrophin-releasing hormone (gnrh) neurone: Studies from embryonic gnrh neurones. *Journal of neuroendocrinology*, *23*, 542–553. https://doi.org/10.1111/j.1365-2826.2011.02130.x

Cuajungco, M. P., & Samie, M. A. (2008). The varitint-waddler mouse phenotypes and the trpml3 ion channel mutation: Cause and consequence. *Pflugers Archiv : European journal of physiology*, *457*, 463–473. https://doi.org/10.1007/s00424-008-0523-4

DeHaven, W. I., Jones, B. F., Petranka, J. G., Smyth, J. T., Tomita, T., Bird, G. S., & Putney, J. W. (2009). Trpc channels function independently of stim1 and orai1. *The Journal of physiology*, *587*, 2275–2298. https://doi.org/10.1113/jphysiol.2009.170431

Demartini, C., Tassorelli, C., Zanaboni, A. M., Tonsi, G., Francesconi, O., Nativi, C., & Greco, R. (2017). The role of the transient receptor potential ankyrin type-1 (trpa1) channel in migraine pain: Evaluation in an animal model. *The journal of headache and pain*, *18*, 94. https://doi.org/10.1186/s10194-017-0804-4

Deyama, S., Bang, E., Wohleb, E. S., Li, X.-Y., Kato, T., Gerhard, D. M., Dutheil, S., Dwyer, J. M., Taylor, S. R., Picciotto, M. R., & Duman, R. S. (2019). Role of neuronal vegf signaling in the prefrontal cortex in the rapid antidepressant effects of ketamine. *The American journal of psychiatry*, *176*, 388–400. https://doi.org/10.1176/appi.ajp.2018.17121368

Di Palma, F., Belyantseva, I. A., Kim, H. J., Vogt, T. F., Kachar, B., & Noben-Trauth, K. (2002). Mutations in mcoln3 associated with deafness and pigmentation defects in varitint-waddler (va) mice. *Proceedings of the National Academy of Sciences of the United States of America*, *99*, 14994–14999. https://doi.org/10.1073/pnas.222425399

Doerner, J. F., Gisselmann, G., Hatt, H., & Wetzel, C. H. (2007). Transient receptor potential channel a1 is directly gated by calcium ions. *The Journal of biological chemistry*, *282*, 13180–13189. https://doi.org/10.1074/jbc.M607849200

Dubois, S. L., Acosta-Martínez, M., DeJoseph, M. R., Wolfe, A., Radovick, S., Boehm, U., Urban, J. H., & Levine, J. E. (2015). Positive, but not negative feedback actions of estradiol in adult female mice require estrogen receptor α in kisspeptin neurons. *Endocrinology*, *156*, 1111–1120. https://doi.org/10.1210/en.2014-1851

Earley, S. (2013). Trpm4 channels in smooth muscle function. *Pflugers Archiv : European journal of physiology*, *465*, 1223–1231. https://doi.org/10.1007/s00424-013-1250-z

Earley, S., & Brayden, J. E. (2015). Transient receptor potential channels in the vasculature. *Physiological reviews*, *95*, 645–690. https://doi.org/10.1152/physrev.00026.2014

Enklaar, T., Esswein, M., Oswald, M., Hilbert, K., Winterpacht, A., Higgins, M., Zabel, B., & Prawitt, D. (2000). Mtr1, a novel biallelically expressed gene in the center of the mouse distal chromosome 7 imprinting cluster, is a member of the trp gene family. *Genomics*, *67*, 179–187. https://doi.org/10.1006/geno.2000.6234

Fleetwood, L., Shu-rong, Z., Eneroth, P., & Landgren, B. M. (1983). Evaluation of a rapid method for determination of total urinary estrogens in morning samples from normally menstruating women. [TJ: CONTRACEPTION.]. *Contraception*, *27*, 329–338. https://doi.org/10.1016/s0010-7824(83)80013-4

Fonfria, E., Murdock, P. R., Cusdin, F. S., Benham, C. D., Kelsell, R. E., & McNulty, S. (2006). Tissue distribution profiles of the human trpm cation channel family. *Journal of receptor and signal transduction research*, *26*, 159–178. https://doi.org/10.1080/10799890600637506

Gao, C., Wang, Y., Tian, W., Zhu, Y., & Xue, F. (2014). The therapeutic significance of aromatase inhibitors in endometrial carcinoma. *Gynecologic oncology*, *134*, 190–195. https://doi.org/10.1016/j.ygyno.2014.04.060

Gao, Y., Yao, T., Deng, Z., Sohn, J.-W., Sun, J., Huang, Y., Kong, X., Yu, K.-J., Wang, R.-T., Chen, H., Guo, H., Yan, J., Cunningham, K. A., Chang, Y., Liu, T., & Williams, K. W. (2017). Trpc5 mediates acute leptin and serotonin effects via pomc neurons. *Cell reports*, *18*, 583–592. https://doi.org/10.1016/j.celrep.2016.12.072

Giovannucci, E., Liu, Y., Stampfer, M. J., & Willett, W. C. (2006). A prospective study of calcium intake and incident and fatal prostate cancer. *Cancer epidemiology, biomarkers & prevention : a publication of the American Association for Cancer Research, cosponsored by the American Society of Preventive Oncology*, *15*, 203–210. https://doi.org/10.1158/1055-9965.EPI-05-0586

Glidewell-Kenney, C., Hurley, L. A., Pfaff, L., Weiss, J., Levine, J. E., & Jameson, J. L. (2007). Nonclassical estrogen receptor alpha signaling mediates negative feedback in the female mouse reproductive axis. *Proceedings of the National Academy of Sciences of the United States of America*, *104*, 8173–8177. https://doi.org/10.1073/pnas.0611514104

Godfrey, P. A., Malnic, B., & Buck, L. B. (2004). The mouse olfactory receptor gene family. *Proceedings of the National Academy of Sciences of the United States of America*, *101*, 2156–2161. https://doi.org/10.1073/pnas.0308051100

Gottsch, M. L., Navarro, V. M., Zhao, Z., Glidewell-Kenney, C., Weiss, J., Jameson, J. L., Clifton, D. K., Levine, J. E., & Steiner, R. A. (2009). Regulation of kiss1 and dynorphin gene expression in the murine brain by classical and nonclassical estrogen receptor pathways. *The Journal of neuroscience : the official journal of the Society for Neuroscience*, *29*, 9390–9395. https://doi.org/10.1523/JNEUROSCI.0763-09.2009

Groenestege, W. M. T., Hoenderop, J. G., van den Heuvel, L., Knoers, N., & Bindels, R. J. (2006). The epithelial mg2+ channel transient receptor potential melastatin 6 is regulated by dietary mg2+ content and estrogens. *Journal of the American Society of Nephrology : JASN*, *17*, 1035–1043. https://doi.org/10.1681/ASN.2005070700

Guinamard, R., Sallé, L., & Simard, C. (2011). The non-selective monovalent cationic channels trpm4 and trpm5. *Advances in experimental medicine and biology*, *704*, 147–171. https://doi.org/10.1007/978-94-007-0265-3_8

Halpern, M. (1987). The organization and function of the vomeronasal system. *Annual review of neuroscience*, *10*, 325–362. https://doi.org/10.1146/annurev.ne.10.030187.001545

Hasen, N. S., & Gammie, S. C. (2009). Trpc2 gene impacts on maternal aggression, accessory olfactory bulb anatomy and brain activity. *Genes, brain, and behavior*, *8*, 639–649. https://doi.org/10.1111/j.1601-183X.2009.00511.x

Hemsell, D. L., Edman, C. D., Marks, J. F., Siiteri, P. K., & MacDonald, P. C. (1977). Massive extranglandular aromatization of plasma androstenedione resulting in feminization of a prepubertal boy. *The Journal of clinical investigation*, *60*, 455–464. https://doi.org/10.1172/JCI108796

Hidema, S., Fukuda, T., Hiraoka, Y., Mizukami, H., Hayashi, R., Otsuka, A., Suzuki, S., Miyazaki, S., & Nishimori, K. (2016). Generation of oxtr cdna(ha)-ires-cre mice for gene expression in an oxytocin

receptor specific manner. *Journal of cellular biochemistry*, *117*, 1099–1111. https://doi.org/10.1002/jcb.25393

Hiller-Sturmhöfel, S., & Bartke, A. (1998). The endocrine system: An overview. *Alcohol health and research world*, *22*, 153–164.

Howitt, M. R., Lavoie, S., Michaud, M., Blum, A. M., Tran, S. V., Weinstock, J. V., Gallini, C. A., Redding, K., Margolskee, R. F., Osborne, L. C., Artis, D., & Garrett, W. S. (2016). Tuft cells, taste-chemosensory cells, orchestrate parasite type 2 immunity in the gut. *Science (New York, N.Y.)*, *351*, 1329–1333. https://doi.org/10.1126/science.aaf1648

Inoue, K., Couch, E. F., Takano, K., & Ogawa, S. (1999). The structure and function of folliculo-stellate cells in the anterior pituitary gland. *Archives of histology and cytology*, *62*, 205–218. https://doi.org/10.1679/aohc.62.205

James, J. M., & Mukouyama, Y.-s. (2011). Neuronal action on the developing blood vessel pattern. *Seminars in cell & developmental biology*, *22*, 1019–1027. https://doi.org/10.1016/j.semcdb.2011.09.010

Jeong, K.-H., & Kaiser, U. B. (2006). Chapter 31 - gonadotropin-releasing hormone regulation of gonadotropin biosynthesis and secretion. In J. D. Neill (Ed.), *Knobil and neill's physiology of reproduction (third edition)* (Third Edition, pp. 1635–1701). Academic Press. https://doi.org/https://doi.org/10.1016/B978-012515400-0/50036-1

Jia, C., Goldman, G., & Halpern, M. (1997). Development of vomeronasal receptor neuron subclasses and establishment of topographic projections to the accessory olfactory bulb. *Brain research. Developmental brain research*, *102*, 209–216. https://doi.org/10.1016/s0165-3806(97)00097-7

Jones, M. E. E., Boon, W. C., McInnes, K., Maffei, L., Carani, C., & Simpson, E. R. (2007). Recognizing rare disorders: Aromatase deficiency. *Nature clinical practice. Endocrinology & metabolism*, *3*, 414–421. https://doi.org/10.1038/ncpendmet0477

Jong, T. R. d., Menon, R., Bludau, A., Grund, T., Biermeier, V., Klampfl, S. M., Jurek, B., Bosch, O. J., Hellhammer, J., & Neumann, I. D. (2015). Salivary oxytocin concentrations in response to running, sexual self-stimulation, breastfeeding and the tsst: The regensburg oxytocin challenge (roc) study. *Psychoneuroendocrinology*, *62*, 381–388. https://doi.org/10.1016/j.psyneuen.2015.08.027

Jordt, S.-E., Bautista, D. M., Chuang, H.-H., McKemy, D. D., Zygmunt, P. M., Högestätt, E. D., Meng, I. D., & Julius, D. (2004). Mustard oils and cannabinoids excite sensory nerve fibres through the trp channel anktm1. *Nature*, *427*, 260–265. https://doi.org/10.1038/nature02282

Kawamoto, T., & Kawamoto, K. (2014). Preparation of thin frozen sections from nonfixed and undecalcified hard tissues using kawamot's film method (2012). *Methods in molecular biology (Clifton, N.J.)*, *1130*, 149–164. https://doi.org/10.1007/978-1-62703-989-5_11

Ke, M.-T., Fujimoto, S., & Imai, T. (2013). Seedb: A simple and morphology-preserving optical clearing agent for neuronal circuit reconstruction. *Nature neuroscience*, *16*, 1154–1161. https://doi.org/10.1038/nn.3447

Kheradpezhouh, E., Choy, J. M. C., Daria, V. R., & Arabzadeh, E. (2017). Trpa1 expression and its functional activation in rodent cortex. *Open biology*, *7*. https://doi.org/10.1098/rsob.160314

Kim, D. W., Washington, P. W., Wang, Z. Q., Lin, S. H., Sun, C., Ismail, B. T., Wang, H., Jiang, L., & Blackshaw, S. (2020). The cellular and molecular landscape of hypothalamic patterning and differentiation from embryonic to late postnatal development. *Nature communications*, *11*, 4360. https://doi.org/10.1038/s41467-020-18231-z

Kim, H. J., Soyombo, A. A., Tjon-Kon-Sang, S., So, I., & Muallem, S. (2009). The ca(2+) channel trpml3 regulates membrane trafficking and autophagy. *Traffic (Copenhagen, Denmark)*, *10*, 1157–1167. https://doi.org/10.1111/j.1600-0854.2009.00924.x

Kim, J. M., Choi, S., & Park, K. (2017). Trpm7 is involved in volume regulation in salivary glands. *Journal of dental research*, *96*, 1044–1050. https://doi.org/10.1177/0022034517708766

Kimchi, T., Xu, J., & Dulac, C. (2007). A functional circuit underlying male sexual behaviour in the female mouse brain. *Nature*, *448*, 1009–1014. https://doi.org/10.1038/nature06089

Knoll, J. G., Clay, C. M., Bouma, G. J., Henion, T. R., Schwarting, G. A., Millar, R. P., & Tobet, S. A. (2013). Developmental profile and sexually dimorphic expression of kiss1 and kiss1r in the fetal mouse brain. *Frontiers in endocrinology*, *4*, 140. https://doi.org/10.3389/fendo.2013.00140

Komiya, Y., Bai, Z., Cai, N., Lou, L., Al-Saadi, N., Mezzacappa, C., Habas, R., & Runnels, L. W. (2017). A nonredundant role for the trpm6 channel in neural tube closure. *Scientific reports*, *7*, 15623. https://doi.org/10.1038/s41598-017-15855-y

Konkle, A. T. M., & McCarthy, M. M. (2011). Developmental time course of estradiol, testosterone, and dihydrotestosterone levels in discrete regions of male and female rat brain. *Endocrinology*, *152*, 223–235. https://doi.org/10.1210/en.2010-0607

Koopman, P., Gubbay, J., Vivian, N., Goodfellow, P., & Lovell-Badge, R. (1991). Male development of chromosomally female mice transgenic for sry. *Nature*, *351*, 117–121. https://doi.org/10.1038/351117a0

Krasteva-Christ, G., Soultanova, A., Schütz, B., Papadakis, T., Weiss, C., Deckmann, K., Chubanov, V., Gudermann, T., Voigt, A., Meyerhof, W., Boehm, U., Weihe, E., & Kummer, W. (2015). Identification of cholinergic chemosensory cells in mouse tracheal and laryngeal glandular ducts. *International immunopharmacology*, *29*, 158–165. https://doi.org/10.1016/j.intimp.2015.05.028

Kremeyer, B., Lopera, F., Cox, J. J., Momin, A., Rugiero, F., Marsh, S., Woods, C. G., Jones, N. G., Paterson, K. J., Fricker, F. R., Villegas, A., Acosta, N., Pineda-Trujillo, N. G., Ramírez, J. D., Zea, J., Burley, M.-W., Bedoya, G., Bennett, D. L. H., Wood, J. N., & Ruiz-Linares, A. (2010). A gain-of-function mutation in trpa1 causes familial episodic pain syndrome. *Neuron*, *66*, 671–680. https://doi.org/10.1016/j.neuron.2010.04.030

Kruse, M., Schulze-Bahr, E., Corfield, V., Beckmann, A., Stallmeyer, B., Kurtbay, G., Ohmert, I., Schulze-Bahr, E., Brink, P., & Pongs, O. (2009). Impaired endocytosis of the ion channel trpm4 is associated with human progressive familial heart block type i. *The Journal of clinical investigation*, *119*, 2737–2744. https://doi.org/10.1172/JCI38292

Kumar, D., Candlish, M., Periasamy, V., Avcu, N., Mayer, C., & Boehm, U. (2015). Specialized subpopulations of kisspeptin neurons communicate with gnrh neurons in female mice. *Endocrinology*, *156*, 32–38. https://doi.org/10.1210/en.2014-1671

Kumar, D., Freese, M., Drexler, D., Hermans-Borgmeyer, I., Marquardt, A., & Boehm, U. (2014). Murine arcuate nucleus kisspeptin neurons communicate with gnrh neurons in utero. *The Journal of neuroscience : the official journal of the Society for Neuroscience*, *34*, 3756–3766. https://doi.org/10.1523/JNEUROSCI.5123-13.2014

Kumar, D., Periasamy, V., Freese, M., Voigt, A., & Boehm, U. (2015). In utero development of kisspeptin/gnrh neural circuitry in male mice. *Endocrinology*, *156*, 3084–3090. https://doi.org/10.1210/EN.2015-1412

Kusumakshi, S., Voigt, A., Hübner, S., Hermans-Borgmeyer, I., Ortalli, A., Pyrski, M., Dörr, J., Zufall, F., Flockerzi, V., Meyerhof, W., Montmayeur, J.-P., & Boehm, U. (2015). A binary genetic approach to characterize trpm5 cells in mice. *Chemical senses*, *40*, 413–425. https://doi.org/10.1093/chemse/bjv023

Lechan, R. M., Wu, P., Jackson, I. M., Wolf, H., Cooperman, S., Mandel, G., & Goodman, R. H. (1986). Thyrotropin-releasing hormone precursor: Characterization in rat brain. *Science (New York, N.Y.)*, *231*, 159–161. https://doi.org/10.1126/science.3079917

Lee, B.-M., Lee, G.-S., Jung, E.-M., Choi, K.-C., & Jeung, E.-B. (2009). Uterine and placental expression of trpv6 gene is regulated via progesterone receptor- or estrogen receptor-mediated pathways during pregnancy in rodents. *Reproductive biology and endocrinology : RB&E*, *7*, 49. https://doi.org/10.1186/1477-7827-7-49

Lephart, E. D. (1996). A review of brain aromatase cytochrome p450. *Brain research. Brain research reviews*, *22*, 1–26.

Leypold, B. G., Yu, C. R., Leinders-Zufall, T., Kim, M. M., Zufall, F., & Axel, R. (2002). Altered sexual and social behaviors in trp2 mutant mice. *Proceedings of the National Academy of Sciences of the United States of America*, *99*, 6376–6381. https://doi.org/10.1073/pnas.082127599

Li, Q., & Liberles, S. D. (2015). Aversion and attraction through olfaction. *Current biology : CB*, *25*, R120–R129. https://doi.org/10.1016/j.cub.2014.11.044

Liedtke, W. B., & Heller, S. (2007). Trp ion channel function in sensory transduction and cellular signaling cascades.

Liman, E. R. [E. R.], Corey, D. P., & Dulac, C. (1999). Trp2: A candidate transduction channel for mammalian pheromone sensory signaling. *Proceedings of the National Academy of Sciences of the United States of America*, *96*, 5791–5796. https://doi.org/10.1073/pnas.96.10.5791

Liman, E. R. [Emily R.]. (2010). A trp channel contributes to insulin secretion by pancreatic β-cells. *Islets*, *2*, 331–333. https://doi.org/10.4161/isl.2.5.12973

Liu, Y.-C., & Chiang, A.-S. (2003). High-resolution confocal imaging and three-dimensional rendering. *Methods (San Diego, Calif.)*, *30*, 86–93. https://doi.org/10.1016/s1046-2023(03)00010-0

Low, J. T., Shukla, A., & Thorn, P. (2010). Pancreatic acinar cell: New insights into the control of secretion. *The international journal of biochemistry & cell biology*, *42*, 1586–1589. https://doi.org/10.1016/j.biocel.2010.07.006

Makhmutova, M., Weitz, J., Tamayo, A., Pereira, E., Boulina, M., Almaça, J., Rodriguez-Diaz, R., & Caicedo, A. (2020). Pancreatic β-cells communicate with vagal neurons. *Gastroenterology*. https://doi.org/10.1053/j.gastro.2020.10.034

Makino, S., Tanaka, Y., Nazarloo, H. P., Noguchi, T., Nishimura, K., & Hashimoto, K. (2005). Expression of type 1 corticotropin-releasing hormone (crh) receptor mrna in the hypothalamic paraventricular nucleus following restraint stress in crh-deficient mice. *Brain research*, *1048*, 131–137. https://doi.org/10.1016/j.brainres.2005.04.065

Martin, R. M., Lin, C. J., Nishi, M. Y., Billerbeck, A. E. C., Latronico, A. C., Russell, D. W., & Mendonca, B. B. (2003). Familial hyperestrogenism in both sexes: Clinical, hormonal, and molecular studies of two siblings. *The Journal of clinical endocrinology and metabolism*, *88*, 3027–3034. https://doi.org/10.1210/jc.2002-021780

Mayer, C., Acosta-Martinez, M., Dubois, S. L., Wolfe, A., Radovick, S., Boehm, U., & Levine, J. E. (2010). Timing and completion of puberty in female mice depend on estrogen receptor alpha-signaling in

kisspeptin neurons. *Proceedings of the National Academy of Sciences of the United States of America*, *107*, 22693–22698. https://doi.org/10.1073/pnas.1012406108

Mayer, C., & Boehm, U. (2011). Female reproductive maturation in the absence of kisspeptin/gpr54 signaling. *Nature neuroscience*, *14*, 704–710. https://doi.org/10.1038/nn.2818

Mazzuca, M. (1974). Letter: Detection of luteinizing hormone-releasing hormone in the guinea pig median eminence with an immunohistoenzymatic technique. *The journal of histochemistry and cytochemistry : official journal of the Histochemistry Society*, *22*, 993–996. https://doi.org/10.1177/22.10.993

McEwen, B. S. (2007). Physiology and neurobiology of stress and adaptation: Central role of the brain. *Physiological reviews*, *87*, 873–904. https://doi.org/10.1152/physrev.00041.2006

Minke, B., Wu, C., & Pak, W. L. (1975). Induction of photoreceptor voltage noise in the dark in drosophila mutant. *Nature*, *258*, 84–87. https://doi.org/10.1038/258084a0

Mittapalli, R. K., Manda, V. K., Adkins, C. E., Geldenhuys, W. J., & Lockman, P. R. (2010). Exploiting nutrient transporters at the blood-brain barrier to improve brain distribution of small molecules. *Therapeutic delivery*, *1*, 775–784. https://doi.org/10.4155/tde.10.76

Mullier, A., Bouret, S. G., Prevot, V., & Dehouck, B. (2010). Differential distribution of tight junction proteins suggests a role for tanycytes in blood-hypothalamus barrier regulation in the adult mouse brain. *The Journal of comparative neurology*, *518*, 943–962. https://doi.org/10.1002/cne.22273

Mullis, P. E., Yoshimura, N., Kuhlmann, B., Lippuner, K., Jaeger, P., & Harada, H. (1997). Aromatase deficiency in a female who is compound heterozygote for two new point mutations in the p450arom gene: Impact of estrogens on hypergonadotropic hypogonadism, multicystic ovaries, and bone densitometry in childhood. *The Journal of clinical endocrinology and metabolism*, *82*, 1739–1745. https://doi.org/10.1210/jcem.82.6.3994

Nadler, M. J., Hermosura, M. C., Inabe, K., Perraud, A. L., Zhu, Q., Stokes, A. J., Kurosaki, T., Kinet, J. P., Penner, R., Scharenberg, A. M., & Fleig, A. (2001). Ltrpc7 is a mg.atp-regulated divalent cation channel required for cell viability. *Nature*, *411*, 590–595. https://doi.org/10.1038/35079092

Naftolin, F., Ryan, K. J., Davies, I. J., Reddy, V. V., Flores, F., Petro, Z., Kuhn, M., White, R. J., Takaoka, Y., & Wolin, L. (1975). The formation of estrogens by central neuroendocrine tissues. *Recent progress in hormone research*, *31*, 295–319. https://doi.org/10.1016/b978-0-12-571131-9.50012-8

Nagata, K., Zheng, L., Madathany, T., Castiglioni, A. J., Bartles, J. R., & García-Añoveros, J. (2008). The varitint-waddler (va) deafness mutation in trpml3 generates constitutive, inward rectifying currents and causes cell degeneration. *Proceedings of the National Academy of Sciences of the United States of America*, *105*, 353–358. https://doi.org/10.1073/pnas.0707963105

Nilius, B. [B.], Vennekens, R., Prenen, J., Hoenderop, J. G., Droogmans, G., & Bindels, R. J. (2001). The single pore residue asp542 determines ca2+ permeation and mg2+ block of the epithelial ca2+ channel. *The Journal of biological chemistry*, *276*, 1020–1025. https://doi.org/10.1074/jbc.M006184200

Nilius, B. [Bernd], & Flockerzi, V. (2014). *Mammalian transient receptor potential (trp) cation channels: Volume i* (Vol. 222). https://doi.org/10.1007/978-3-642-54215-2

Nilius, B. [Bernd], & Owsianik, G. (2011). The transient receptor potential family of ion channels. *Genome biology*, *12*, 218. https://doi.org/10.1186/gb-2011-12-3-218

Ohtaki, T., Shintani, Y., Honda, S., Matsumoto, H., Hori, A., Kanehashi, K., Terao, Y., Kumano, S., Takatsu, Y., Masuda, Y., Ishibashi, Y., Watanabe, T., Asada, M., Yamada, T., Suenaga, M., Kitada, C., Usuki,

S., Kurokawa, T., Onda, H., … Fujino, M. (2001). Metastasis suppressor gene kiss-1 encodes peptide ligand of a g-protein-coupled receptor. *Nature*, *411*, 613–617. https://doi.org/10.1038/35079135

Omura, M., & Mombaerts, P. (2014). Trpc2-expressing sensory neurons in the main olfactory epithelium of the mouse. *Cell reports*, *8*, 583–595. https://doi.org/10.1016/j.celrep.2014.06.010

Ortiz de Montellano, P. R., & De Voss, J. J. (2002). Oxidizing species in the mechanism of cytochrome p450. *Natural product reports*, *19*, 477–493. https://doi.org/10.1039/b101297p

O'Shaughnessy, P. J. (2014). Hormonal control of germ cell development and spermatogenesis. *Seminars in cell & developmental biology*, *29*, 55–65. https://doi.org/10.1016/j.semcdb.2014.02.010

Oshimoto, A., Wakabayashi, Y., Garske, A., Lopez, R., Rolen, S., Flowers, M., Arevalo, N., & Restrepo, D. (2013). Potential role of transient receptor potential channel m5 in sensing putative pheromones in mouse olfactory sensory neurons. *PloS one*, *8*, e61990. https://doi.org/10.1371/journal.pone.0061990

Ostrowski, R., Wang, R., Tu, S., Zhang, J., & Shao, A. (2020). Roles of trp channels in neurological diseases. *Oxidative Medicine and Cellular Longevity*, *2020*, 7289194. https://doi.org/10.1155/2020/7289194

Park, C.-K., Kim, M. S., Fang, Z., Li, H. Y., Jung, S. J., Choi, S.-Y., Lee, S. J., Park, K., Kim, J. S., & Oh, S. B. (2006). Functional expression of thermo-transient receptor potential channels in dental primary afferent neurons: Implication for tooth pain. *The Journal of biological chemistry*, *281*, 17304–17311. https://doi.org/10.1074/jbc.M511072200

Park, S., Ahuja, M., Kim, M. S., Brailoiu, G. C., Jha, A., Zeng, M., Baydyuk, M., Wu, L.-G., Wassif, C. A., Porter, F. D., Zerfas, P. M., Eckhaus, M. A., Brailoiu, E., Shin, D. M., & Muallem, S. (2016). Fusion of lysosomes with secretory organelles leads to uncontrolled exocytosis in the lysosomal storage disease mucolipidosis type iv. *EMBO reports*, *17*, 266–278. https://doi.org/10.15252/embr.201541542

Parkash, J., Messina, A., Langlet, F., Cimino, I., Loyens, A., Mazur, D., Gallet, S., Balland, E., Malone, S. A., Pralong, F., Cagnoni, G., Schellino, R., De Marchis, S., Mazzone, M., Pasterkamp, R. J., Tamagnone, L., Prevot, V., & Giacobini, P. (2015). Semaphorin7a regulates neuroglial plasticity in the adult hypothalamic median eminence. *Nature communications*, *6*, 6385. https://doi.org/10.1038/ncomms7385

Pérez, C. A., Huang, L., Rong, M., Kozak, J. A., Preuss, A. K., Zhang, H., Max, M., & Margolskee, R. F. (2002). A transient receptor potential channel expressed in taste receptor cells. *Nature neuroscience*, *5*, 1169–1176. https://doi.org/10.1038/nn952

Pérez, C. A., Margolskee, R. F., Kinnamon, S. C., & Ogura, T. (2003). Making sense with trp channels: Store-operated calcium entry and the ion channel trpm5 in taste receptor cells. *Cell calcium*, *33*, 541–549. https://doi.org/10.1016/s0143-4160(03)00059-9

Peruzzo, B., Pastor, F. E., Blázquez, J. L., Amat, P., & Rodríguez, E. M. (2004). Polarized endocytosis and transcytosis in the hypothalamic tanycytes of the rat. *Cell and tissue research*, *317*, 147–164. https://doi.org/10.1007/s00441-004-0899-1

Philippaert, K., Pironet, A., Mesuere, M., Sones, W., Vermeiren, L., Kerselaers, S., Pinto, S., Segal, A., Antoine, N., Gysemans, C., Laureys, J., Lemaire, K., Gilon, P., Cuypers, E., Tytgat, J., Mathieu, C., Schuit, F., Rorsman, P., Talavera, K., … Vennekens, R. (2017). Steviol glycosides enhance pancreatic beta-cell function and taste sensation by potentiation of trpm5 channel activity. *Nature communications*, *8*, 14733. https://doi.org/10.1038/ncomms14733

PHOENIX, C. H., R W, G. O. Y., GERALL, A. A., & YOUNG, W. C. (1959). Organizing action of prenatally administered testosterone propionate on the tissues mediating mating behavior in the female guinea pig. *Endocrinology*, *65*, 369–382. https://doi.org/10.1210/endo-65-3-369

Pyrski, M., Eckstein, E., Schmid, A., Bufe, B., Weiss, J., Chubanov, V., Boehm, U., & Zufall, F. (2017). Trpm5 expression in the olfactory epithelium. *Molecular and cellular neurosciences*, *80*, 75–88. https://doi.org/10.1016/j.mcn.2017.02.002

Quamme, G. A. [G. A.], & de Rouffignac, C. (2000). Epithelial magnesium transport and regulation by the kidney. *Frontiers in bioscience : a journal and virtual library*, *5*, D694–D711. https://doi.org/10.2741/quamme

Quamme, G. A. [Gary A.]. (2008). Recent developments in intestinal magnesium absorption. *Current opinion in gastroenterology*, *24*, 230–235. https://doi.org/10.1097/MOG.0b013e3282f37b59

Rhees, R. W., Shryne, J. E., & Gorski, R. A. (1990). Onset of the hormone-sensitive perinatal period for sexual differentiation of the sexually dimorphic nucleus of the preoptic area in female rats. *Journal of neurobiology*, *21*, 781–786. https://doi.org/10.1002/neu.480210511

Richardson, D. S., & Lichtman, J. W. (2015). Clarifying tissue clearing. *Cell*, *162*, 246–257. https://doi.org/10.1016/j.cell.2015.06.067

Rizzoti, K., & Lovell-Badge, R. (2017). Pivotal role of median eminence tanycytes for hypothalamic function and neurogenesis [Stem cells of endocrine glands]. *Molecular and Cellular Endocrinology*, *445*, 7–13. https://doi.org/https://doi.org/10.1016/j.mce.2016.08.020

Robertson, D. H., Hurst, J. L., Bolgar, M. S., Gaskell, S. J., & Beynon, R. J. (1997). Molecular heterogeneity of urinary proteins in wild house mouse populations. *Rapid communications in mass spectrometry : RCM*, *11*, 786–790. https://doi.org/10.1002/(SICI)1097-0231(19970422)11:7⟨786::AID-RCM876⟩3.0.CO;2-8

Rodríguez, E. M., Blázquez, J. L., & Guerra, M. (2010). The design of barriers in the hypothalamus allows the median eminence and the arcuate nucleus to enjoy private milieus: The former opens to the portal blood and the latter to the cerebrospinal fluid. *Peptides*, *31*, 757–776. https://doi.org/10.1016/j.peptides.2010.01.003

Roper, S. D. (2007). Signal transduction and information processing in mammalian taste buds. *Pflugers Archiv : European journal of physiology*, *454*, 759–776. https://doi.org/10.1007/s00424-007-0247-x

Samie, M. A., Grimm, C., Evans, J. A., Curcio-Morelli, C., Heller, S., Slaugenhaupt, S. A., & Cuajungco, M. P. (2009). The tissue-specific expression of trpml2 (mcoln-2) gene is influenced by the presence of trpml1. *Pflugers Archiv : European journal of physiology*, *459*, 79–91. https://doi.org/10.1007/s00424-009-0716-5

Sawada, Y., Hosokawa, H., Hori, A., Matsumura, K., & Kobayashi, S. (2007). Cold sensitivity of recombinant trpa1 channels. *Brain research*, *1160*, 39–46. https://doi.org/10.1016/j.brainres.2007.05.047

Schaefer, M., Plant, T. D., Obukhov, A. G., Hofmann, T., Gudermann, T., & Schultz, G. (2000). Receptor-mediated regulation of the nonselective cation channels trpc4 and trpc5. *The Journal of biological chemistry*, *275*, 17517–17526. https://doi.org/10.1074/jbc.275.23.17517

Schlingmann, K. P., Waldegger, S., Konrad, M., Chubanov, V., & Gudermann, T. (2007). Trpm6 and trpm7–gatekeepers of human magnesium metabolism. *Biochimica et biophysica acta*, *1772*, 813–821. https://doi.org/10.1016/j.bbadis.2007.03.009

Seminara, S. B., Messager, S., Chatzidaki, E. E., Thresher, R. R., Acierno, J. S., Shagoury, J. K., Bo-Abbas, Y., Kuohung, W., Schwinof, K. M., Hendrick, A. G., Zahn, D., Dixon, J., Kaiser, U. B., Slaugenhaupt, S. A., Gusella, J. F., O'Rahilly, S., Carlton, M. B. L., Crowley, W. F., Aparicio, S. A. J. R., & Colledge,

W. H. (2003). The gpr54 gene as a regulator of puberty. *The New England journal of medicine*, *349*, 1614–1627. https://doi.org/10.1056/NEJMoa035322

Shepro, D., & Morel, N. M. (1993). Pericyte physiology. *FASEB journal : official publication of the Federation of American Societies for Experimental Biology*, *7*, 1031–1038. https://doi.org/10.1096/fasebj.7.11.8370472

Simerly, R. B., Zee, M. C., Pendleton, J. W., Lubahn, D. B., & Korach, K. S. (1997). Estrogen receptor-dependent sexual differentiation of dopaminergic neurons in the preoptic region of the mouse. *Proceedings of the National Academy of Sciences of the United States of America*, *94*, 14077–14082. https://doi.org/10.1073/pnas.94.25.14077

Simpson, E. R. [E. R.], Mahendroo, M. S., Means, G. D., Kilgore, M. W., Hinshelwood, M. M., Graham-Lorence, S., Amarneh, B., Ito, Y., Fisher, C. R., & Michael, M. D. (1994). Aromatase cytochrome p450, the enzyme responsible for estrogen biosynthesis. *Endocrine reviews*, *15*, 342–355. https://doi.org/10.1210/edrv-15-3-342

Simpson, E. R. [Evan R.]. (2004). Models of aromatase insufficiency. *Seminars in reproductive medicine*, *22*, 25–30. https://doi.org/10.1055/s-2004-823024

Smith, J. T., Popa, S. M., Clifton, D. K., Hoffman, G. E., & Steiner, R. A. (2006). Kiss1 neurons in the forebrain as central processors for generating the preovulatory luteinizing hormone surge. *The Journal of neuroscience : the official journal of the Society for Neuroscience*, *26*, 6687–6694. https://doi.org/10.1523/JNEUROSCI.1618-06.2006

Sofikitis, N., Giotitsas, N., Tsounapi, P., Baltogiannis, D., Giannakis, D., & Pardalidis, N. (2008). Hormonal regulation of spermatogenesis and spermiogenesis. *The Journal of steroid biochemistry and molecular biology*, *109*, 323–330. https://doi.org/10.1016/j.jsbmb.2008.03.004

Song, K., Wang, H., Kamm, G. B., Pohle, J., Reis, F. d. C., Heppenstall, P., Wende, H., & Siemens, J. (2016). The trpm2 channel is a hypothalamic heat sensor that limits fever and can drive hypothermia. *Science (New York, N.Y.)*, *353*, 1393–1398. https://doi.org/10.1126/science.aaf7537

Spix, B., Chao, Y.-K., Abrahamian, C., Chen, C.-C., & Grimm, C. (2020). Trpml cation channels in inflammation and immunity. *Frontiers in immunology*, *11*, 225. https://doi.org/10.3389/fimmu.2020.00225

Stan, R. V., Kubitza, M., & Palade, G. E. (1999). Pv-1 is a component of the fenestral and stomatal diaphragms in fenestrated endothelia. *Proceedings of the National Academy of Sciences of the United States of America*, *96*, 13203–13207. https://doi.org/10.1073/pnas.96.23.13203

Stowers, L., Holy, T. E., Meister, M., Dulac, C., & Koentges, G. (2002). Loss of sex discrimination and male-male aggression in mice deficient for trp2. *Science (New York, N.Y.)*, *295*, 1493–1500. https://doi.org/10.1126/science.1069259

Stratakis, C. A., Vottero, A., Brodie, A., Kirschner, L. S., DeAtkine, D., Lu, Q., Yue, W., Mitsiades, C. S., Flor, A. W., & Chrousos, G. P. (1998). The aromatase excess syndrome is associated with feminization of both sexes and autosomal dominant transmission of aberrant p450 aromatase gene transcription. *The Journal of clinical endocrinology and metabolism*, *83*, 1348–1357. https://doi.org/10.1210/jcem.83.4.4697

Susaki, E. A., & Ueda, H. R. (2016). Whole-body and whole-organ clearing and imaging techniques with single-cell resolution: Toward organism-level systems biology in mammals. *Cell chemical biology*, *23*, 137–157. https://doi.org/10.1016/j.chembiol.2015.11.009

Suzuki, Y., Kovacs, C. S., Takanaga, H., Peng, J.-B., Landowski, C. P., & Hediger, M. A. (2008). Calcium channel trpv6 is involved in murine maternal-fetal calcium transport. *Journal of bone and mineral research : the official journal of the American Society for Bone and Mineral Research*, *23*, 1249–1256. https://doi.org/10.1359/jbmr.080314

Tainaka, K., Kuno, A., Kubota, S. I., Murakami, T., & Ueda, H. R. (2016). Chemical principles in tissue clearing and staining protocols for whole-body cell profiling. *Annual review of cell and developmental biology*, *32*, 713–741. https://doi.org/10.1146/annurev-cellbio-111315-125001

Tang, Q., Guo, W., Zheng, L., Wu, J.-X., Liu, M., Zhou, X., Zhang, X., & Chen, L. (2018). Structure of the receptor-activated human trpc6 and trpc3 ion channels. *Cell research*, *28*, 746–755. https://doi.org/10.1038/s41422-018-0038-2

Tanner, J. M., Whitehouse, R. H., & Takaishi, M. (1966). Standards from birth to maturity for height, weight, height velocity, and weight velocity: British children, 1965. ii. *Archives of disease in childhood*, *41*, 613–635. https://doi.org/10.1136/adc.41.220.613

Thakore, P., Alvarado, M. G., Ali, S., Mughal, A., Pires, P. W., Yamasaki, E., Pritchard, H. A. T., Isakson, B. E., Tran, C. H. T., & Earley, S. (2020). Brain endothelial cell trpa1 channels initiate neurovascular coupling. *bioRxiv*. https://doi.org/10.1101/2020.09.14.295600

Thyagarajan, B., Lukacs, V., & Rohacs, T. (2008). Hydrolysis of phosphatidylinositol 4,5-bisphosphate mediates calcium-induced inactivation of trpv6 channels. *The Journal of biological chemistry*, *283*, 14980–14987. https://doi.org/10.1074/jbc.M704224200

Tizzano, M., Cristofoletti, M., Sbarbati, A., & Finger, T. E. (2011). Expression of taste receptors in solitary chemosensory cells of rodent airways. *BMC pulmonary medicine*, *11*, 3. https://doi.org/10.1186/1471-2466-11-3

Todd, B. J., Schwarz, J. M., & McCarthy, M. M. (2005). Prostaglandin-e2: A point of divergence in estradiol-mediated sexual differentiation. *Hormones and behavior*, *48*, 512–521. https://doi.org/10.1016/j.yhbeh.2005.07.011

Tomás, J., Santos, C. R. A., Quintela, T., & Gonçalves, I. (2016). "tasting" the cerebrospinal fluid: Another function of the choroid plexus? *Neuroscience*, *320*, 160–171. https://doi.org/10.1016/j.neuroscience.2016.01.057

Toran-Allerand, C. D. (1976). Sex steroids and the development of the newborn mouse hypothalamus and preoptic area in vitro: Implications for sexual differentiation. *Brain research*, *106*, 407–412. https://doi.org/10.1016/0006-8993(76)91038-6

Tsunematsu, T., Fu, L.-Y., Yamanaka, A., Ichiki, K., Tanoue, A., Sakurai, T., & van den Pol, A. N. (2008). Vasopressin increases locomotion through a v1a receptor in orexin/hypocretin neurons: Implications for water homeostasis. *The Journal of neuroscience : the official journal of the Society for Neuroscience*, *28*, 228–238. https://doi.org/10.1523/JNEUROSCI.3490-07.2008

Ullrich, N. D., Voets, T., Prenen, J., Vennekens, R., Talavera, K., Droogmans, G., & Nilius, B. (2005). Comparison of functional properties of the ca2+-activated cation channels trpm4 and trpm5 from mice. *Cell calcium*, *37*, 267–278. https://doi.org/10.1016/j.ceca.2004.11.001

Vannier, B., Peyton, M., Boulay, G., Brown, D., Qin, N., Jiang, M., Zhu, X., & Birnbaumer, L. (1999). Mouse trp2, the homologue of the human trpc2 pseudogene, encodes mtrp2, a store depletion-activated capacitative ca2+ entry channel. *Proceedings of the National Academy of Sciences of the United States of America*, *96*, 2060–2064. https://doi.org/10.1073/pnas.96.5.2060

Vigouroux, R. J., Belle, M., & Chédotal, A. (2017). Neuroscience in the third dimension: Shedding new light on the brain with tissue clearing. *Molecular brain*, *10*, 33. https://doi.org/10.1186/s13041-017-0314-y

Vink, R., & Nechifor, M. (2011). Magnesium in the central nervous system.

Vreeburg, J. T., van der Vaart, P. D., & van der Schoot, P. (1977). Prevention of central defeminization but not masculinization in male rats by inhibition neonatally of oestrogen biosynthesis. *The Journal of endocrinology*, *74*, 375–382. https://doi.org/10.1677/joe.0.0740375

Walder, R. Y., Yang, B., Stokes, J. B., Kirby, P. A., Cao, X., Shi, P., Searby, C. C., Husted, R. F., & Sheffield, V. C. (2009). Mice defective in trpm6 show embryonic mortality and neural tube defects. *Human molecular genetics*, *18*, 4367–4375. https://doi.org/10.1093/hmg/ddp392

Wang, L., Vanacker, C., Burger, L. L., Barnes, T., Shah, Y. M., Myers, M. G., & Moenter, S. M. (2019). Genetic dissection of the different roles of hypothalamic kisspeptin neurons in regulating female reproduction (J. K. Elmquist, C. Dulac, & V. Prevot, Eds.). *eLife*, *8*, e43999. https://doi.org/10.7554/eLife.43999

Watts, A. G., Tanimura, S., & Sanchez-Watts, G. (2004). Corticotropin-releasing hormone and arginine vasopressin gene transcription in the hypothalamic paraventricular nucleus of unstressed rats: Daily rhythms and their interactions with corticosterone. *Endocrinology*, *145*, 529–540. https://doi.org/10.1210/en.2003-0394

Weissgerber, P., Kriebs, U., Tsvilovskyy, V., Olausson, J., Kretz, O., Stoerger, C., Vennekens, R., Wissenbach, U., Middendorff, R., Flockerzi, V., & Freichel, M. (2011). Male fertility depends on ca²+ absorption by trpv6 in epididymal epithelia. *Science signaling*, *4*, ra27. https://doi.org/10.1126/scisignal.2001791

Westergaard, E., & Brightman, M. W. (1973). Transport of proteins across normal cerebral arterioles. *The Journal of comparative neurology*, *152*, 17–44. https://doi.org/10.1002/cne.901520103

Whalen, R. E., & Olsen, K. L. (1981). Role of aromatization in sexual differentiation: Effects of prenatal atd treatment and neonatal castration. *Hormones and behavior*, *15*, 107–122. https://doi.org/10.1016/0018-506x(81)90022-2

Williams, J. A. (2010). Regulation of acinar cell function in the pancreas. *Current opinion in gastroenterology*, *26*, 478–483. https://doi.org/10.1097/MOG.0b013e32833d11c6

Wissenbach, U., Niemeyer, B. A., Fixemer, T., Schneidewind, A., Trost, C., Cavalie, A., Reus, K., Meese, E., Bonkhoff, H., & Flockerzi, V. (2001). Expression of cat-like, a novel calcium-selective channel, correlates with the malignancy of prostate cancer. *The Journal of biological chemistry*, *276*, 19461–19468. https://doi.org/10.1074/jbc.M009895200

Wu, Y., Miyamoto, T., Li, K., Nakagomi, H., Sawada, N., Kira, S., Kobayashi, H., Zakohji, H., Tsuchida, T., Fukazawa, M., Araki, I., & Takeda, M. (2011). Decreased expression of the epithelial ca2+ channel trpv5 and trpv6 in human renal cell carcinoma associated with vitamin d receptor. *The Journal of urology*, *186*, 2419–2425. https://doi.org/10.1016/j.juro.2011.07.086

Wyatt, A., Wartenberg, P., Candlish, M., Krasteva-Christ, G., Flockerzi, V., & Boehm, U. (2017). Genetic strategies to analyze primary trp channel-expressing cells in mice. *Cell calcium*, *67*, 91–104. https://doi.org/10.1016/j.ceca.2017.05.009

Xu, H., Delling, M., Li, L., Dong, X., & Clapham, D. E. (2007). Activating mutation in a mucolipin transient receptor potential channel leads to melanocyte loss in varitint-waddler mice. *Proceedings of the National Academy of Sciences of the United States of America*, *104*, 18321–18326. https://doi.org/10.1073/pnas.0709096104

Yang, F., Ruan, Y.-C., Yang, Y.-j., Wang, K., Liang, S.-s., Han, Y.-b., Teng, X.-M., & Yang, J.-Z. (2015). Follicular hyperandrogenism downregulates aromatase in luteinized granulosa cells in polycystic ovary syndrome women. *Reproduction (Cambridge, England)*, *150*, 289–296. https://doi.org/10.1530/REP-15-0044

Yasuo, S., & Korf, H.-W. (2011). The hypophysial pars tuberalis transduces photoperiodic signals via multiple pathways and messenger molecules. *General and comparative endocrinology*, *172*, 15–22. https://doi.org/10.1016/j.ygcen.2010.11.006

Yip, S. H., Boehm, U., Herbison, A. E., & Campbell, R. E. (2015). Conditional viral tract tracing delineates the projections of the distinct kisspeptin neuron populations to gonadotropin-releasing hormone (gnrh) neurons in the mouse. *Endocrinology*, *156*, 2582–2594. https://doi.org/10.1210/en.2015-1131

Yip, S. H., Liu, X., Hessler, S., Cheong, I., Porteous, R., & Herbison, A. E. (2021). Indirect suppression of pulsatile lh secretion by crh neurons in the female mouse. *Endocrinology*, *162*. https://doi.org/10.1210/endocr/bqaa237

Yoshimura, M., Nishimura, K., Nishimura, H., Sonoda, S., Ueno, H., Motojima, Y., Saito, R., Maruyama, T., Nonaka, Y., & Ueta, Y. (2017). Activation of endogenous arginine vasopressin neurons inhibit food intake: By using a novel transgenic rat line with dreadds system. *Scientific reports*, *7*, 15728. https://doi.org/10.1038/s41598-017-16049-2

Zeevi, D. A., Frumkin, A., Offen-Glasner, V., Kogot-Levin, A., & Bach, G. (2009). A potentially dynamic lysosomal role for the endogenous trpml proteins. *The Journal of pathology*, *219*, 153–162. https://doi.org/10.1002/path.2587

Zhang, Y., Hoon, M. A., Chandrashekar, J., Mueller, K. L., Cook, B., Wu, D., Zuker, C. S., & Ryba, N. J. P. (2003). Coding of sweet, bitter, and umami tastes: Different receptor cells sharing similar signaling pathways. *Cell*, *112*, 293–301. https://doi.org/10.1016/s0092-8674(03)00071-0

Zhao, Z.-D., Yang, W. Z., Gao, C., Fu, X., Zhang, W., Zhou, Q., Chen, W., Ni, X., Lin, J.-K., Yang, J., Xu, X.-H., & Shen, W. L. (2017). A hypothalamic circuit that controls body temperature. *Proceedings of the National Academy of Sciences of the United States of America*, *114*, 2042–2047. https://doi.org/10.1073/pnas.1616255114

Zor, U., Lamprecht, S. A., Misulovin, Z., Koch, Y., & Lindner, H. R. (1976). Refractoriness of ovarian adenylate cyclase to continued hormonal stimulation. *Biochimica et biophysica acta*, *428*, 761–765. https://doi.org/10.1016/0304-4165(76)90206-3

Zufall, F., Ukhanov, K., Lucas, P., Liman, E. R., & Leinders-Zufall, T. (2005). Neurobiology of trpc2: From gene to behavior. *Pflugers Archiv : European journal of physiology*, *451*, 61–71. https://doi.org/10.1007/s00424-005-1432-4

6 Appendix

Table 8: Summary of τGFP expression in TRPM5IC/eR26-τGFP animals. - = no cells, + = low cell number, ++ = moderate cell number, +++ = high cell number.

organ	adult female	adult male	juvenile female	juvenile male
brain	+ tanycytes +++ choroid plexus	+ tanycytes +++ choroid plexus	+ tanycytes +++ choroid plexus	+ tanycytes +++ choroid plexus
pituitary	++	++	+	+
VNO	++	++	+	+
MOE	++ olfactory sensory neurons +++ Bowman glands	++ olfactory sensory neurons +++ Bowman glands	++ olfactory sensory neurons +++ Bowman glands	++ olfactory sensory neurons +++ Bowman glands
tongue	+++ taste buds ++ lamina propria	+++ taste buds ++ lamina propria	+ taste buds ++ lamina propria	+ taste buds ++ lamina propria
salivary gland	+	+	+	+
trachea	+	+	+	+
larynx	+	+	+	+
thymus	+	+	+	+
heart	+	+	+	+
lung	+	+	+	+
spleen	+	+	+	+
pancreas	+ exocrine pancreas +++ endocrine pancreas	+ exocrine pancreas +++ endocrine pancreas	+ exocrine pancreas +++ endocrine pancreas	+ exocrine pancreas +++ endocrine pancreas
stomach	+	+	+	+
liver	+	+	+	+
gallbladder	+	+	+	+
duodenum	+	+	+	+
ileum	+	+	+	+
jejunum	++	++	+	+
ceacum	+	+	+	+
colon	++	++	+	+
kidney	+	+	+	+
adrenal gland	+	+	+	+
urethra	+	+	+	+
bladder	+	+	+	+
prostate		++		+

continued on next page

continued from previous page

organ	adult female	adult male	juvenile female	juvenile male
testis		++		++
epididymis			++	++
ovary	+++		+++	

Table 9: Summary of τGFP expression in TRPV6IC/eR26-τGFP animals. - = no cells, + = low cell number, ++ = moderate cell number, +++ = high cell number.

organ	adult female	adult male	juvenile female	juvenile male
brain	-	-	-	-
pituitary	+	+	+	+
VNO	-	-	-	-
MOE	-	-	-	-
teeth	++	++	+	+
tongue	+	+	+	+
salivary gland	+++	+++	+++	+++
trachea	+	+	+	+
thymus	-	-	-	-
heart	-	-	-	-
lung	+	+	+	+
spleen	-	-	-	-
pancreas	+++	+++	++	++
liver	-	-	-	-
gallbladder	-	-	-	-
stomach	+ parietal cells + epethilial cells	+ parietal cells + epethilial cells	+ parietal cells + epethilial cells	+ parietal cells + epethilial cells
duodenum	+	+	+	+
jejunum	-	-	-	-
ileum	-	-	-	-
ceacum	+	+	+	+
colon	+	+	+	+
kidney	+	+	+	+
bladder	-	-	-	-
adrenal gland	-	-	-	-
bone	-	-	-	-
ovary	-		not investigated	
uterus	+		not investigated	
testis		+		-

continued on next page

continued from previous page

organ	adult female	adult male	juvenile female	juvenile male
epididymis		+++		-
prostate		+++		++

Table 10: Summary of τGFP expression in TRPA1IC/eR26-τGFP animals. - = no cells, + = low cell number, ++ = moderate cell number, +++ = high cell number.

organ	adult female	adult male
brain	+ neurons + astrocytes + blood vessels ++ fiber in bulb	+ neurons + astrocytes + blood vessels ++ fiber in bulb
pituitary	+ anterior pituitary	+ anterior pituitary
VNO	-	-
MOE	+ olfactory sensory neurons	+ olfactory sensory neurons
teeth	+++	+++
tongue	++ taste buds	++ taste buds
salivary gland	++	++
trachea	-	-
thyriod gland	+++	+++
thymus	+	+
heart	+	+
lung	-	-
spleen	+	+
pancreas	+ islet of Langerhans	+ islet of Langerhans
liver	-	-
gallbladder	-	-
stomach	+	+
duodenum	+++	+++
ileum	+++	+++
jejunum	+++	+++
ceacum	++	++
colon	+++	+++
kidney	+ medulla	+ medulla
adrenal gland	+	+
bladder	+	+
prostate		-
testis		++

continued on next page

continued from previous page

organ	adult female	adult male
epididymis		+
ovary	+	
uterus	++	

Table 11: Summary of τGFP expression in TRPML3IC/eR26-τGFP animals. - = no cells, + = low cell number, ++ = moderate cell number, +++ = high cell number.

organ	adult female	adult male
brain	+ neurons + blood vessels +++ fiber in bulb	+ neurons + blood vessels +++ fiber in bulb
pituitary	+++ anterior pituitary + neuro pituitary	+++ anterior pituitary + neuro pituitary
VNO	+++	+++
MOE	+++ olfactory sensory neurons	+++ olfactory sensory neurons
tongue	+++ taste buds	+++ taste buds
salivary gland	++	++
trachea	++ mucus secreting cells	++ mucus secreting cells
thyriod gland	+++	+++
thymus	+++	+++
heart	+	+
lung	+++	+++
spleen	+++	+++
pancreas	++ islet of Langerhans	++ islet of Langerhans
liver	++	++
gallbladder	+	+
stomach	+	+
duodenum	+++	+++
ileum	+++	+++
jejunum	+++	+++
ceacum	+	+
colon	+	+
kidney	+ cortex +++ medulla	+ cortex +++ medulla
adrenal gland	-	-
bladder	+	+
prostate		+

continued on next page

continued from previous page

organ	adult female	adult male
testis		++
epidydymis		++
ovary	+	
uterus	+++	

Table 12: Summary of τGFP expression in TRPM6IC/eR26-τGFP animals. - = no cells, + = low cell number, ++ = moderate cell number, +++ = high cell number.

organ	adult female	adult male
brain	++ blood vessels ++ ependymal cells	++ blood vessels ++ ependymal cells
pituitary	-	-
VNO	-	-
MOE	-	-
tongue	-	-
salivary gland	++ glandula sublingualis	++ glandula sublingualis
trachea	-	-
thyriod gland	++	++
thymus	+	+
heart	-	-
lung	+++ epithelial cells +++ small, round cells	+++ epithelial cells +++ small, round cells
spleen	-	-
pancreas	-	-
liver	-	-
gallbladder	-	-
stomach	-	-
duodenum	-	-
ileum	+	+
jejunum	+	+
ceacum	+	+
colon	-	-
kidney	++	++
adrenal gland	-	-
bladder	-	-
prostate		-
testis		++

continued on next page

continued from previous page

organ	adult female	adult male
epididymis		-
ovary	-	
uterus	+	

Table 13: Summary of τGFP expression in TRPC2IC/eR26-τGFP animals. - = no cells, + = low cell number, ++ = moderate cell number, +++ = high cell number.

organ	adult female	adult male
brain	+ neurons (only in PVN) + Glia and Astrocytes	+ neurons (only in PVN) + Glia and Astrocytes
pituitary	+	+
VNO	++++	++++
MOE	+++ olfactory sensory neurons	+++ olfactory sensory neurons
tongue	-	-
salivary gland	-	-
trachea	-	-
thyriod gland	-	-
larynx	-	-
thymus	-	-
heart	-	-
lung	-	-
spleen	-	-
pancreas	-	-
liver	-	-
gallbladder	-	-
stomach	-	-
duodenum	-	-
ileum	-	-
jejunum	-	-
ceacum	-	-
colon	-	-
kidney	-	-
adrenal gland	-	-
bladder	-	-
prostate	-	-
testis	++	++
epididymis	-	-

continued on next page

continued from previous page

organ	adult female	adult male
ovary	-	-

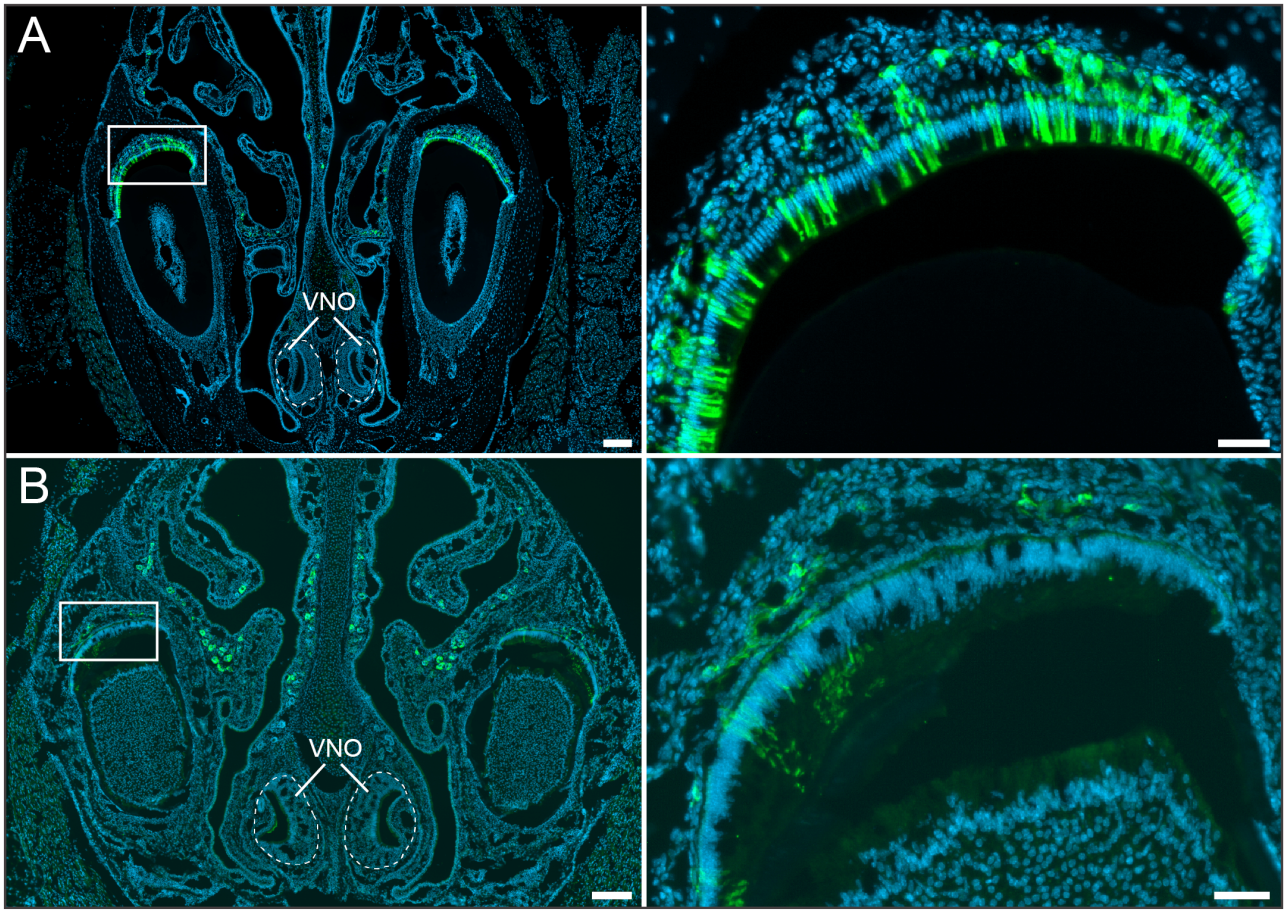

Figure 51: TRPV6 is expressed in enamel secreting epithelial cells. (A) Reporter gene expression was found in enamel secreting epithelial cells in adult TRPV6 reporter animals. No τGFP expression was found in the VNO but few τGFP+ cells were observed in the mucosa. (B) In juvenile animals the same pattern was found but enamel secreting cells were fewer in number. Scalebars: 200 μm overview, 50 μm inset.

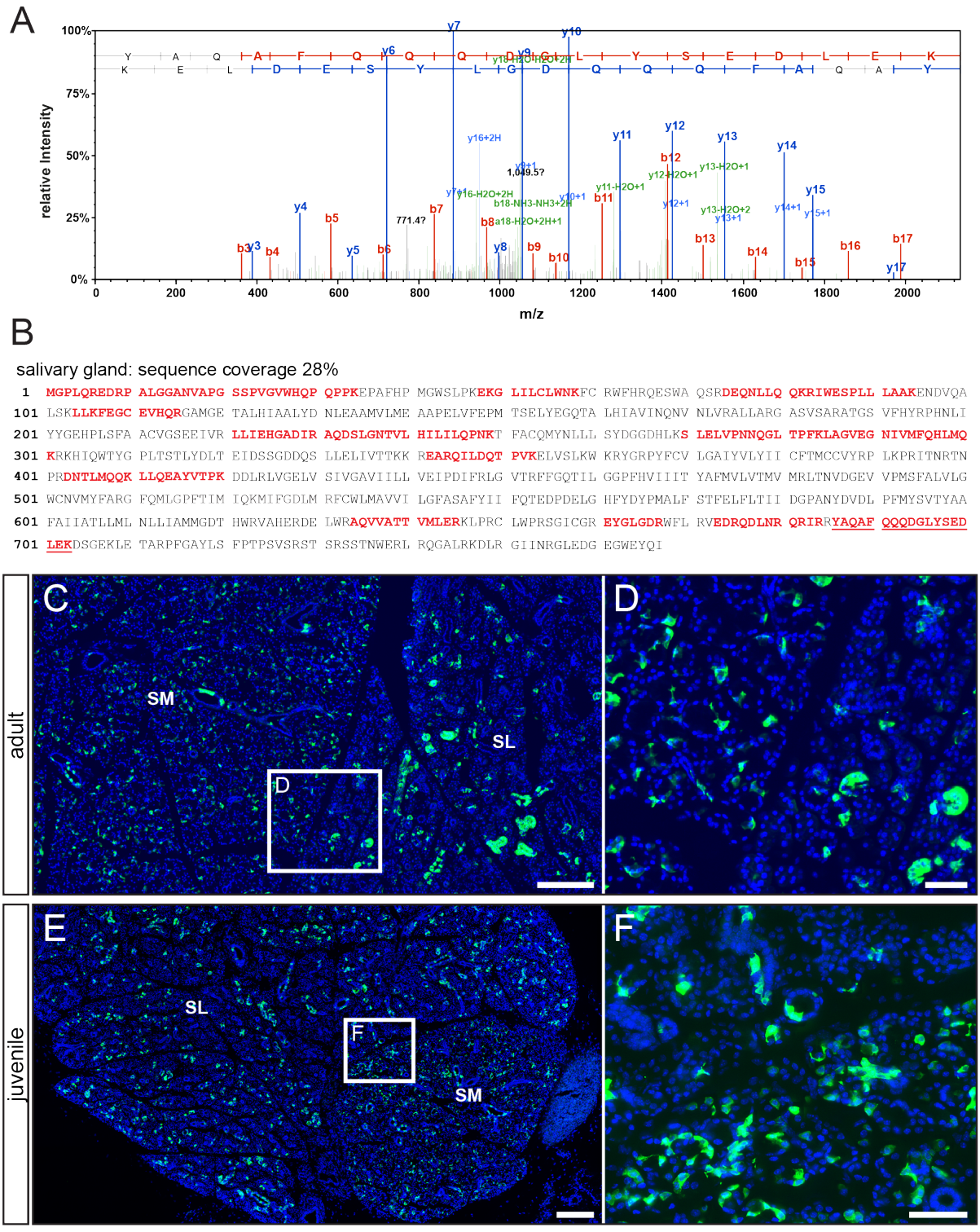

Figure 52: TRPV6 expression was found in a subset of granular convoluted duct cells in the salivary gland. (A) Example of collision induced damage (CID) MS/MS fragmentation spectra (blue, y-ions, red, b-ions) derived from a tryptic mouse TRPV6 peptide analyzed by nano-LC ESI-MS/MS technique in the elute after TRPV6 enrichment from adult WT salivary glands. (B) Predicted protein sequence of mouse TRPV6 (SwissProt: Q91WD2) is shown in black. Amino acids (aa) identified by MS/MS fragmentation are shown in red, covering 28% of TRPV6 protein sequence, the underlined tryptic TRPV6 peptide is shown in (A). (C) τGFP-reporter gene expression in the adult salivary gland. TRPV6 is expressed in the submandibular part (SM) and in the sublingual part (SL) of the adult salivary gland. τGFP+ cells in the SL part seems to be more clustered compared to the SM part. (D) Magnified image of the area indicated in (C). (E) τGFP-reporter gene expression in the juvenile salivary gland. A similar staining was observed compared to the adult salivary gland but overall fewer τGFP+ cells were found. (F) Magnified image of the area indicated in (E). Nuclearstain in blue. Scalebars: 200 μm (C) and (E), 50 μm (D) and (F).

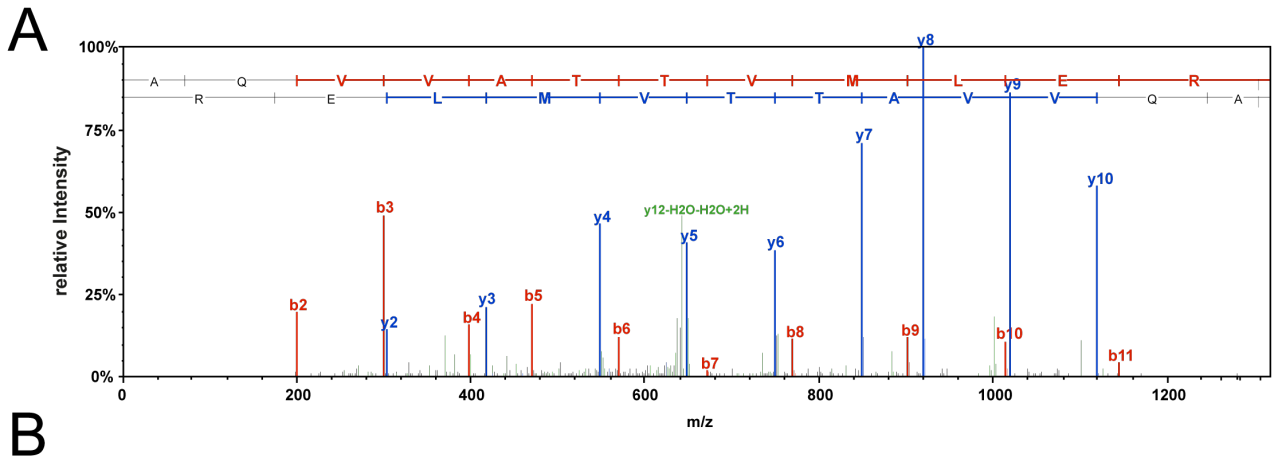

B

caecum: sequence coverage 20%

```
  1 MGPLQREDRP ALGGANVAPG SSPVGVWHQP QPPKEPAFHP MGWSLPKEKG LILCLWNKFC RWFHRQESWA QSRDEQNLLQ QKRIWESPLL LAAKENDVQA
101 LSKLLKFEGC EVHQRGAMGE TALHIAALYD NLEAAMVLME AAPELVFEPM TSELYEGQTA LHIAVINQNV NLVRALLARG ASVSARATGS VFHYRPHNLI
201 YYGEHPLSFA ACVGSEEIVR LLIEHGADIR AQDSLGNTVL HILILQPNKT FACQMYNLLL SYDGGDHLKS LELVPNNQGL TPFKLAGVEG NIVMFQHLMQ
301 KRKHIQWTYG PLTSTLYDLT EIDSSGDDQS LLELIVTTKK REARQILDQT PVKELVSLKW KRYGRPYFCV LGAIYVLYII CFTMCCVYRP LKPRITNRTN
401 PRDNTLMQQK LLQEAYVTPK DDLRLVGELV SIVGAVIILL VEIPDIFRLG VTRFFGQTIL GGPFHVIIIT YAFMVLVTMV MRLTNVDGEV VPMSFALVLG
501 WCNVMYFARG FQMLGPFTIM IQKMIFGDLM RFCWLMAVVI LGFASAFYII FQTEDPDELG HFYDYPMALF STFELFLTII DGPANYDVDL PFMYSVTYAA
601 FAIIATLLML NLLIAMMGDT HWRVAHERDE LWRAQVVATT VMLERKLPRC LWPRSGICGR EYGLGDRWFL RVEDRQDLNR QRIRRYAQAF QQQDGLYSED
701 LEKDSGEKLE TARPFGAYLS FPTPSVSRST SRSSTNWERL RQGALRKDLR GIINRGLEDG EGWEYQI
```

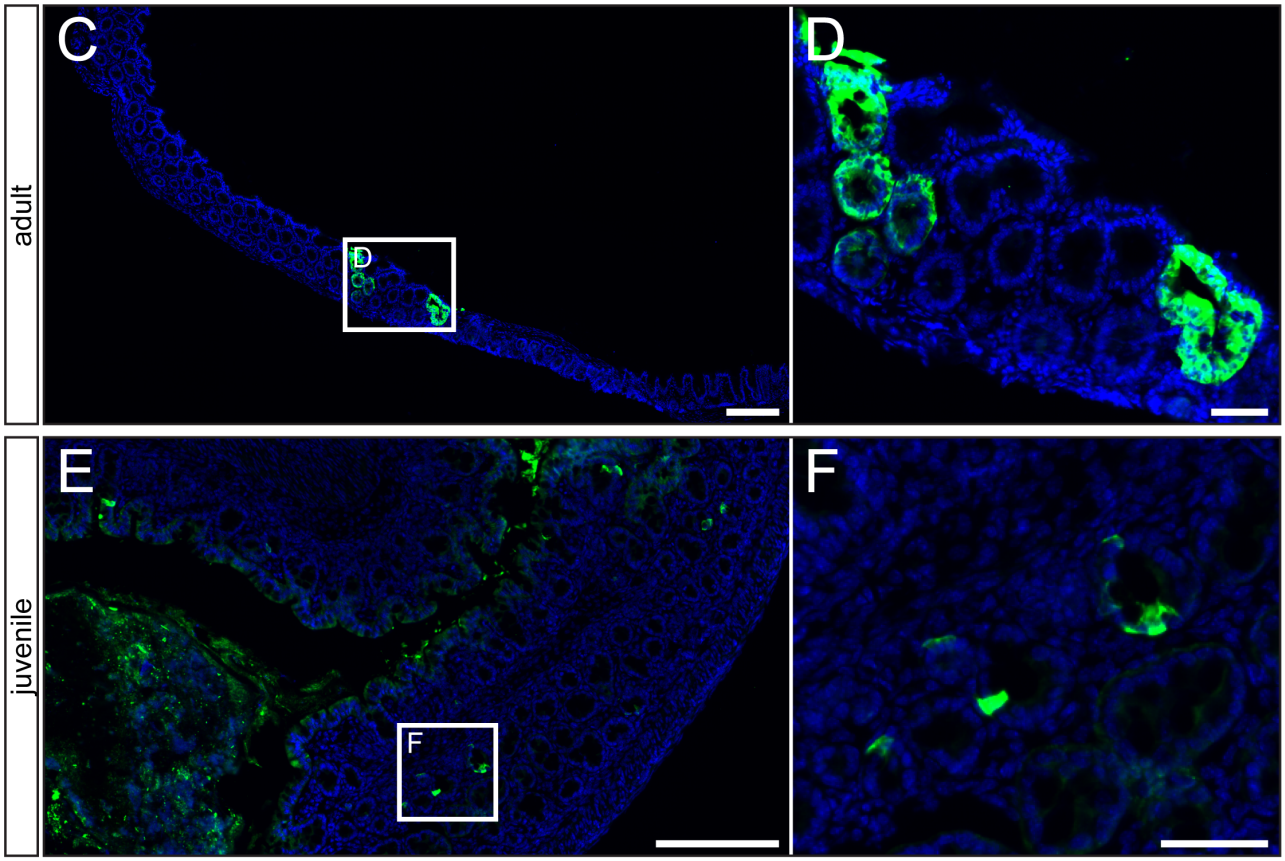

Figure 53: Example of CID fragmented MS/MS spectra derived from a tryptic TRPV6 peptide enrichment from adult mouse WT caecum by TRPV6 antibodies and analyzed by nano-LC ESI-MS/MS technique. (B) Predicted primary protein sequence of mouse TRPV6 is shown in black. Amino acids identified by MS2 fragmentation are shown in red, covering 20% of TRPV6 protein sequence, the underlined tryptic TRPV6 peptide is shown in (A). (C) Low number of TRPV6-expressing cells in the mucosa of the adult caecum. (D) Magnified image of the area indicated in (C). (E) Similar staining pattern in the juvenile caecum. (F) Magnified image of the area indicated in (E). Nuclearstain in blue. Scalebars: 200 μm (C) and (E), 50 μm (D) and (F).

A

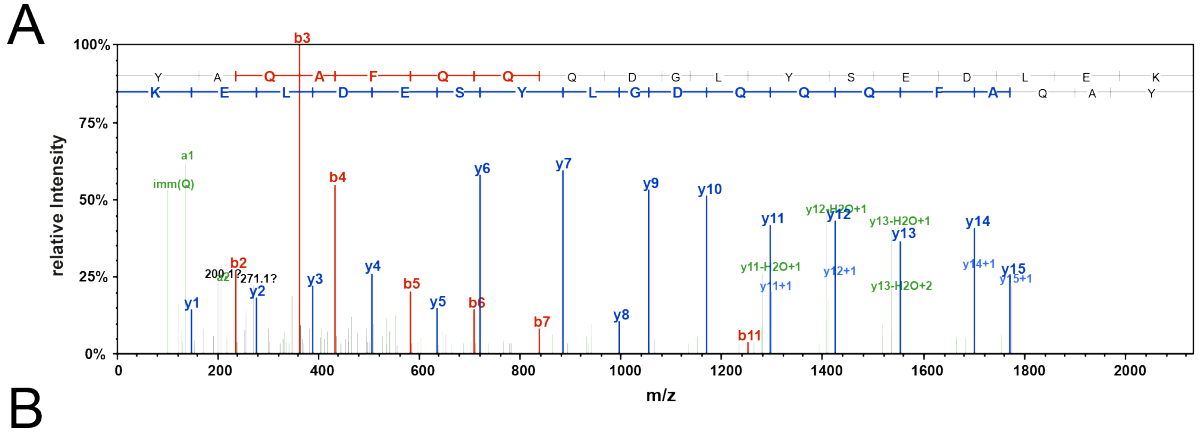

B

Pancreas: sequence coverage 27%

```
  1 MGPLQREDRP ALGGANVAPG SSPVGVWHQP QPPKEPAFHP MGWSLPKEKG LILCLWNKFC RWFHRQESWA QSRDEQNLLQ QKRIWESPLL LAAKENDVQA
101 LSKLLKFEGC EVHQRGAMGE TALHIAALYD NLEAAMVLME AAPELVFEPM TSELYEGQTA LHIAVINQNV NLVRALLARG ASVSARATGS VFHYRPHNLI
201 YYGEHPLSFA ACVGSEEIVR LLIEHGADIR AQDSLGNTVL HILILQPNKT FACQMYNLLL SYDGGDHLKS LELVPNNQGL TPFKLAGVEG NIVMFQHLMQ
301 KRKHIQWTYG PLTSTLYDLT EIDSSGDDQS LLELIVTTKK REARQILDQT PVKELVSLKW KRYGRPYFCV LGAIYVLYII CFTMCCVYRP LKPRITNRTN
401 PRDNTLMQQK LLQEAYVTPK DDLRLVGELV SIVGAVIILL VEIPDIFRLG VTRFFGQTIL GGPFHVIIIT YAFMVLVTMV MRLTNVDGEV VPMSFALVLG
501 WCNVMYFARG FQMLGPFTIM IQKMIFGDLM RFCWLMAVVI LGFASAFYII FQTEDPDELG HFYDYPMALF STFELFLTII DGPANYDVDL PFMYSVTYAA
601 FAIIATLLML NLLIAMMGDT HWRVAHERDE LWRAQVVATT VMLERKLPRC LWPRSGICGR EYGLGDRWFL RVEDRQDLNR QRIRRYAQAF QQQDGLYSED
701 LEKDSGEKLE TARPFGAYLS FPTPSVSRST SRSSTNWERL RQGALRKDLR GIINRGLEDG EGWEYQI
```

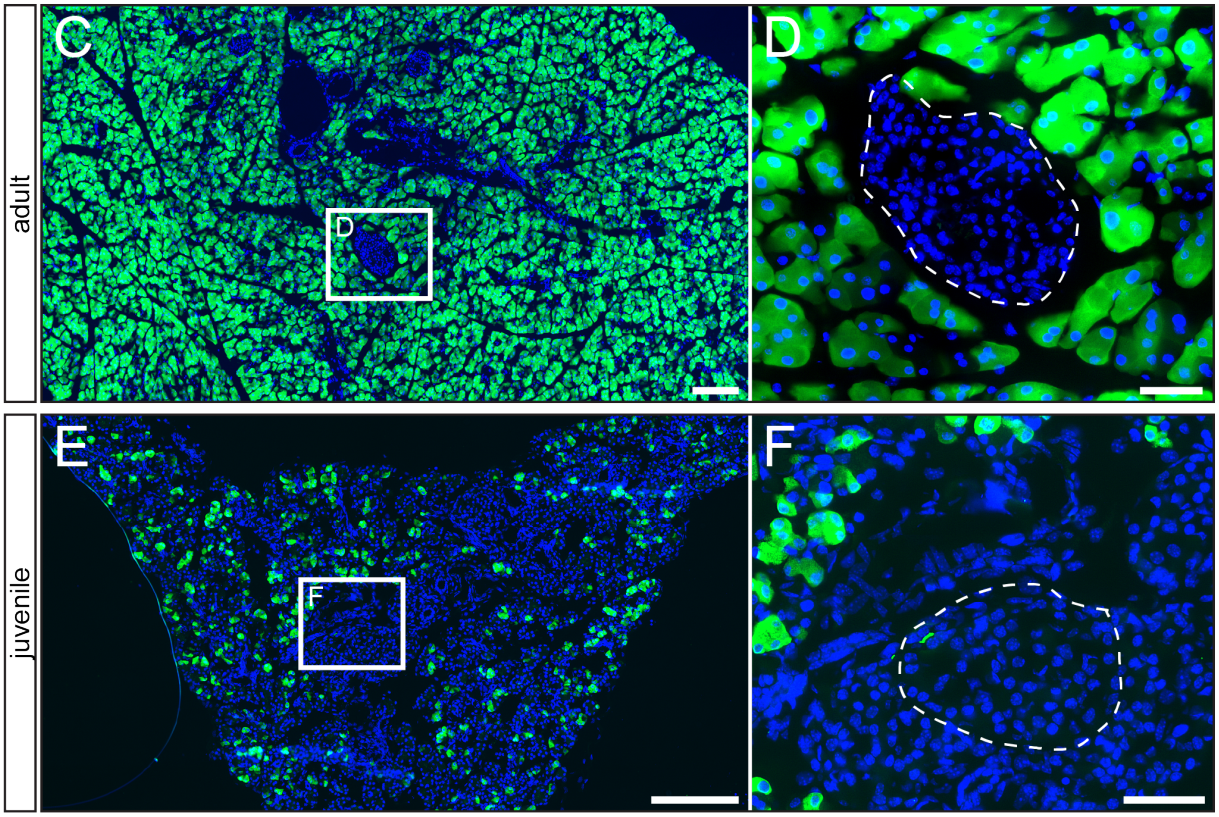

Figure 54: TRPV6 is exclusively found in acinar cells in the pancreas. (A) Example of CID fragmented MS/MS spectra derived from a tryptic TRPV6 peptide enrichment from adult mouse WT pancreas by TRPV6 antibodies and analyzed by nano-LC ESI-MS/MS technique. (B) Predicted primary protein sequence of mouse TRPV6 is shown in black. Amino acids identified by MS2 fragmentation are shown in red, covering 27% of TRPV6 protein sequence, the underlined tryptic TRPV6 peptide is shown in (A). (C) Mostly all acinar cells in the adult exocrine pancreas express τGFP. The islets of Langerhans were found negative for TRPV6. (D) Magnified image of the area indicated in (C). Dashed line indicates islets of Langerhans. (E) In the juvenile pancreas, TRPV6-expression was also only observed in the acinar cells of the exocrine pancreas. The number of GFP+ cells is drastically reduced compared to adults. (F) Magnified image of the area indicated in (E). Dashed line indicates islets of Langerhans. Nuclearstain in blue. Scalebars: 200 μm (C) and (E), 50 μm (D) and (F).

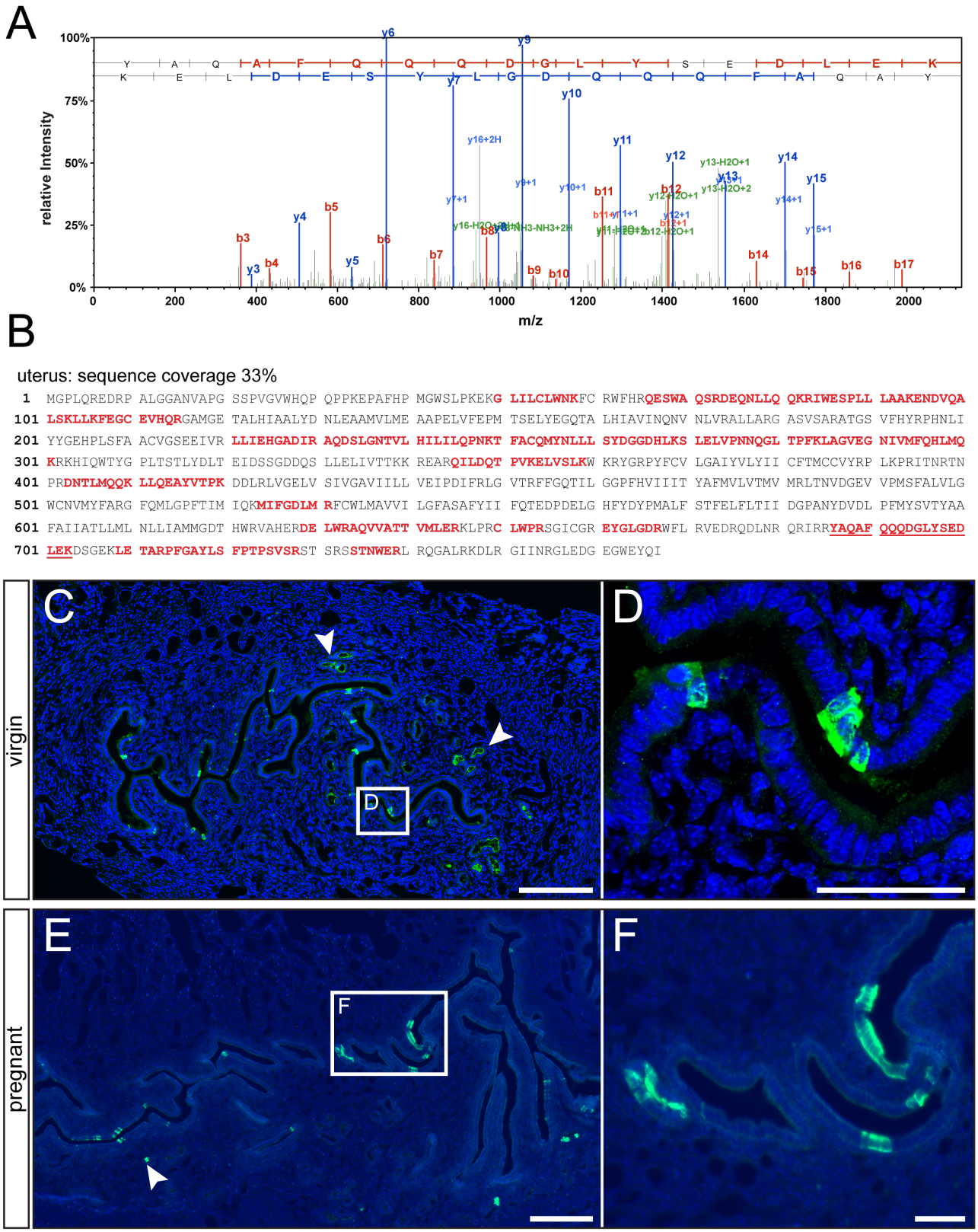

Figure 55: Example of CID fragmented MS/MS spectra derived from a tryptic TRPV6 peptide enrichment from pregnant wt uterus using TRPV6-specific antibodies and analyzed by nano-LC ESI-MS/MS technique. (B) Predicted primary protein sequence of mouse TRPV6 is shown in black. Amino acids identified by MS2 fragmentation are shown in red, covering 27% of TRPV6 protein sequence, the underlined tryptic TRPV6 peptide is shown in (A). (C) τGFP+ cells were detected in small subset of epithelium cells and tubular glands (arrowheads) of the virgin endometrium. (D) Magnified image of the area indicated in (C). (E) The same expression profile was observed in the endometrium of pregnant mice (F) Magnified image of the area indicated in (E). Nuclearstain in blue. Scalebars: 200 μm (C) and (E), 50 μm (D) and (F).

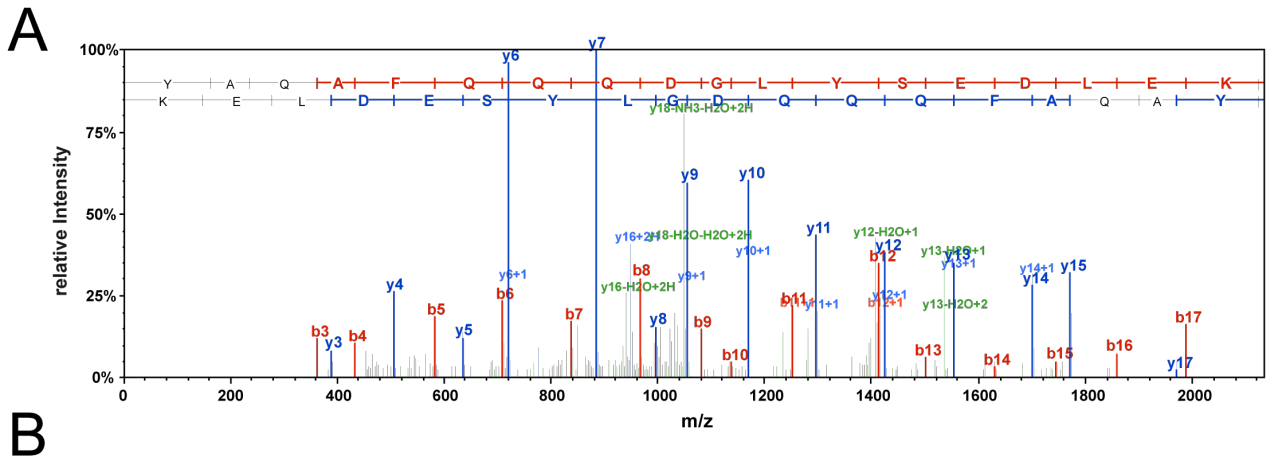

B

epididymis: sequence coverage 44%

```
  1 MGPLQREDRP ALGGANVAPG SSPVGVWHQP QPPKEPAFHP MGWSLPKEKG LILCLWNKFC RWFHRQESWA QSRDEQNLLQ QKRIWESPLL LAAKENDVQA
101 LSKLLKFEGC EVHQRGAMGE TALHIAALYD NLEAAMVLME AAPELVFEPM TSELYEGQTA LHIAVINQNV NLVRALLARG ASVSARATGS VFHYRPHNLI
201 YYGEHPLSFA ACVGSEEIVR LLIEHGADIR AQDSLGNTVL HILILQPNKT FACQMYNLLL SYDGGDHLKS LELVPNNQGL TPFKLAGVEG NIVMFQHLMQ
301 KRKHIQWTYG PLTSTLYDLT EIDSSGDDQS LLELIVTTKK REARQILDQT PVKELVSLKW KRYGRPYFCV LGAIYVLYII CFTMCCVYRP LKPRITNRTN
401 PRDNTLMQQK LLQEAYVTPK DDLRLVGELV SIVGAVIILL VEIPDIFRLG VTRFFGQTIL GGPFHVIIIT YAFMVLVTMV MRLTNVDGEV VPMSFALVLG
501 WCNVMYFARG FQMLGPFTIM IQKMIFGDLM RFCWLMAVVI LGFASAFYII FQTEDPDELG HFYDYPMALF STFELFLTII DGPANYDVDL PFMYSVTYAA
601 FAIIATLLML NLLIAMMGDT HWRVAHERDE LWRAQVVATT VMLERKLPRC LWPRSGICGR EYGLGDRWFL RVEDRQDLNR QRIRRYAQAF QQQDGLYSED
701 LEKDSGEKLE TARPFGAYLS FPTPSVSRST SRSSTNWERL RQGALRKDLR GIINRGLEDG EGWEYQI
```

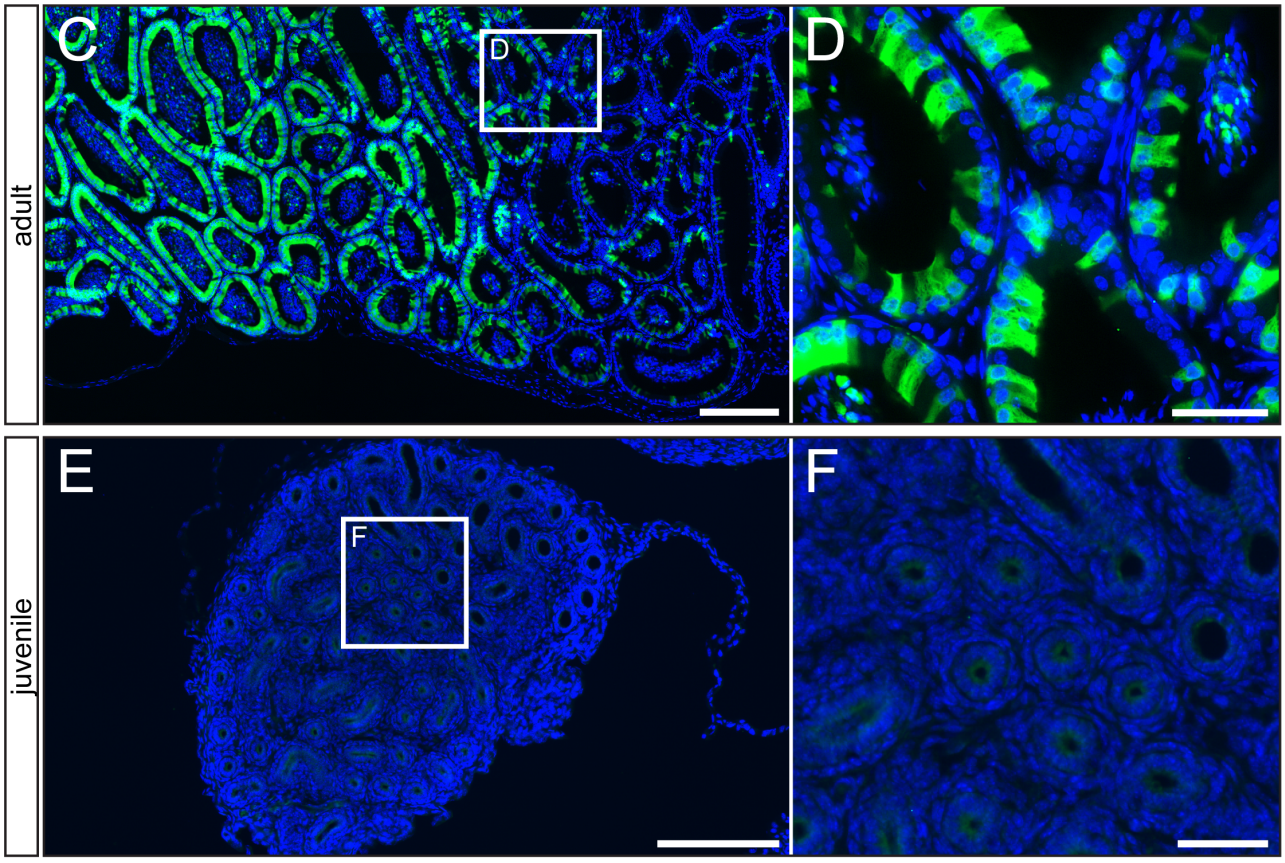

Figure 56: Example of CID fragmented MS/MS spectra derived from a tryptic TRPV6 peptide enrichment from adult mouse wt epididymis by TRPV6 antibodies and analyzed by nano-LC ESI-MS/MS technique. (B) Predicted primary protein sequence of mouse TRPV6 is shown in black. Amino acids identified by MS2 fragmentation are shown in red, covering 44% of TRPV6 protein sequence, the underlined tryptic TRPV6 peptide is shown in (A). (C) Large numbers of TRPV6 expressing cells were found in the epithelial cells of the adult epididymal tubes. (D) Magnified image of the area indicated in (C). (E) No reporter gene expression was detected in the juvenile epididymis. (F) Magnified image of the area indicated in (E). Nuclearstain in blue. Scalebars: 200 μm (C) and (E), 50 μm (D) and (F).

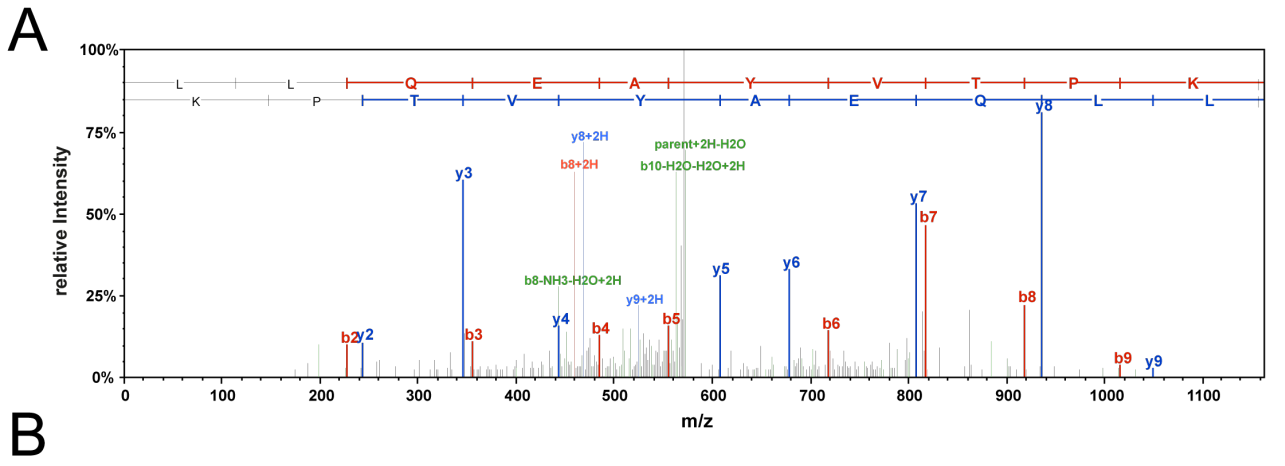

B

prostate: sequence coverage 16%

```
  1 MGPLQREDRP ALGGANVAPG SSPVGVWHQP QPPKEPAFHP MGWSLPKEKG LILCLWNKFC RWFHRQESWA QSRDEQNLLQ QKRIWESPLL LAAKENDVQA
101 LSKLLKFEGC EVHQRGAMGE TALHIAALYD NLEAAMVLME AAPELVFEPM TSELYEGQTA LHIAVINQNV NLVRALLARG ASVSARATGS VFHYRPHNLI
201 YYGEHPLSFA ACVGSEEIVR LLIEHGADIR AQDSLGNTVL HILILQPNKT FACQMYNLLL SYDGGDHLKS LELVPNNQGL TPFKLAGVEG NIVMFQHLMQ
301 KRKHIQWTYG PLTSTLYDLT EIDSSGDDQS LLELIVTTKK REARQILDQT PVKELVSLKW KRYGRPYFCV LGAIYVLYII CFTMCCVYRP LKPRITNRTN
401 PRDNTLMQQK LLQEAYVTPK DDLRLVGELV SIVGAVIILL VEIPDIFRLG VTRFFGQTIL GGPFHVIIIT YAFMVLVTMV MRLTNVDGEV VPMSFALVLG
501 WCNVMYFARG FQMLGPFTIM IQKMIFGDLM RFCWLMAVVI LGFASAFYII FQTEDPDELG HFYDYPMALF STFELFLTII DGPANYDVDL PFMYSVTYAA
601 FAIIATLLML NLLIAMMGDT HWRVAHERDE LWRAQVVATT VMLERKLPRC LWPRSGICGR EYGLGDRWFL RVEDRQDLNR QRIRRYAQAF QQQDGLYSED
701 LEKDSGEKLE TARPFGAYLS FPTPSVSRST SRSSTNWERL RQGALRKDLR GIINRGLEDG EGWEYQI
```

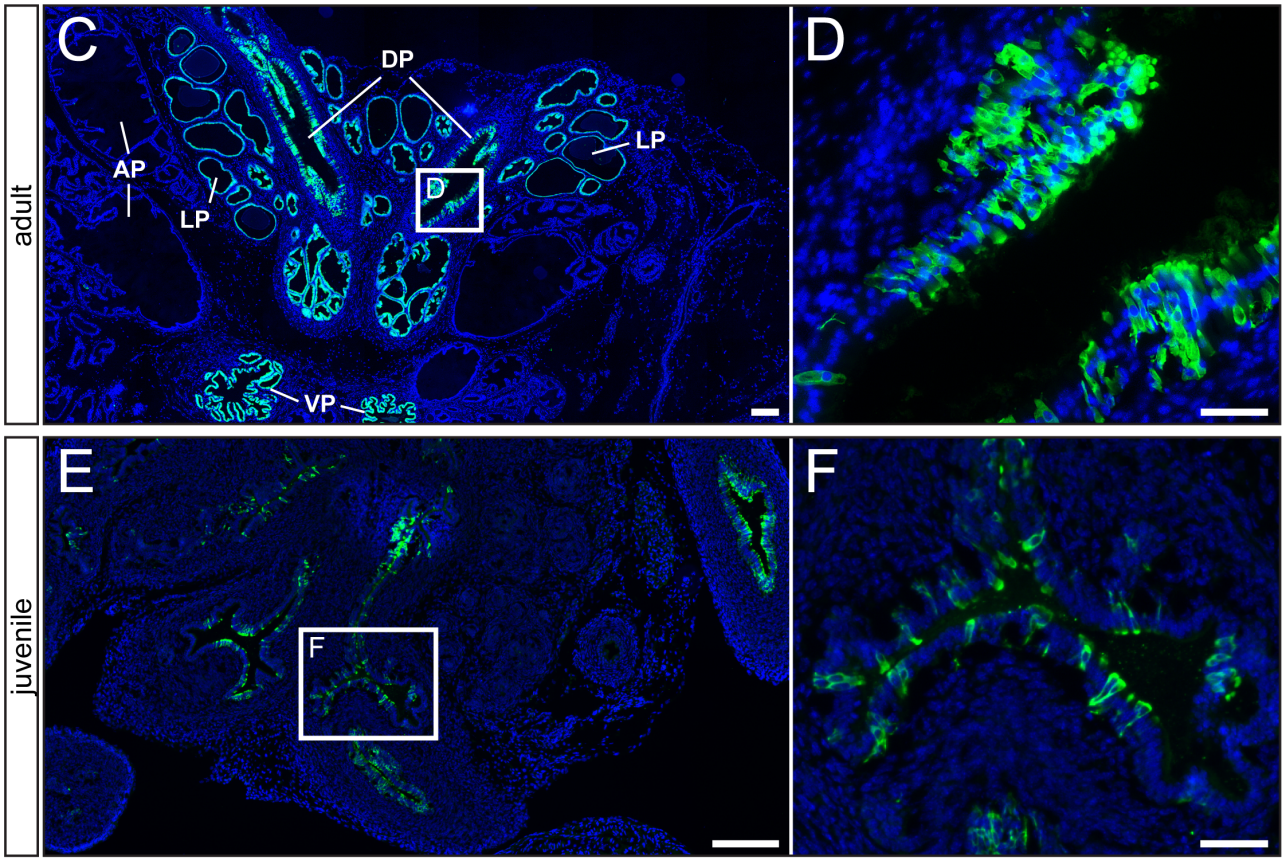

Figure 57: Example of CID fragmented MS/MS spectra derived from a tryptic TRPV6 peptide enrichment from adult mouse WT prostate by TRPV6 antibodies and analyzed by nano-LC ESI-MS/MS technique. (B) Predicted primary protein sequence of mouse TRPV6 is shown in black. Amino acids identified by MS2 fragmentation are shown in red, covering 16% of TRPV6 protein sequence, the underlined tryptic TRPV6 peptide is shown in (A). (C) TRPV6 expression was found in the epithelial cells of the dorsal (DP), lateral (LP) and ventral (VP) lobes of the adult prostate. AP = anterior lobe. (D) Magnified image of the area indicated in (C). (E) A similar expression pattern was detected in the juvenile prostate, although the number of GFP+ cells was lower (F). Magnified image of the area indicated in (E). Nuclearstain in blue. Scalebars: 200 μm (C) and (E), 50 μm (D) and (F).

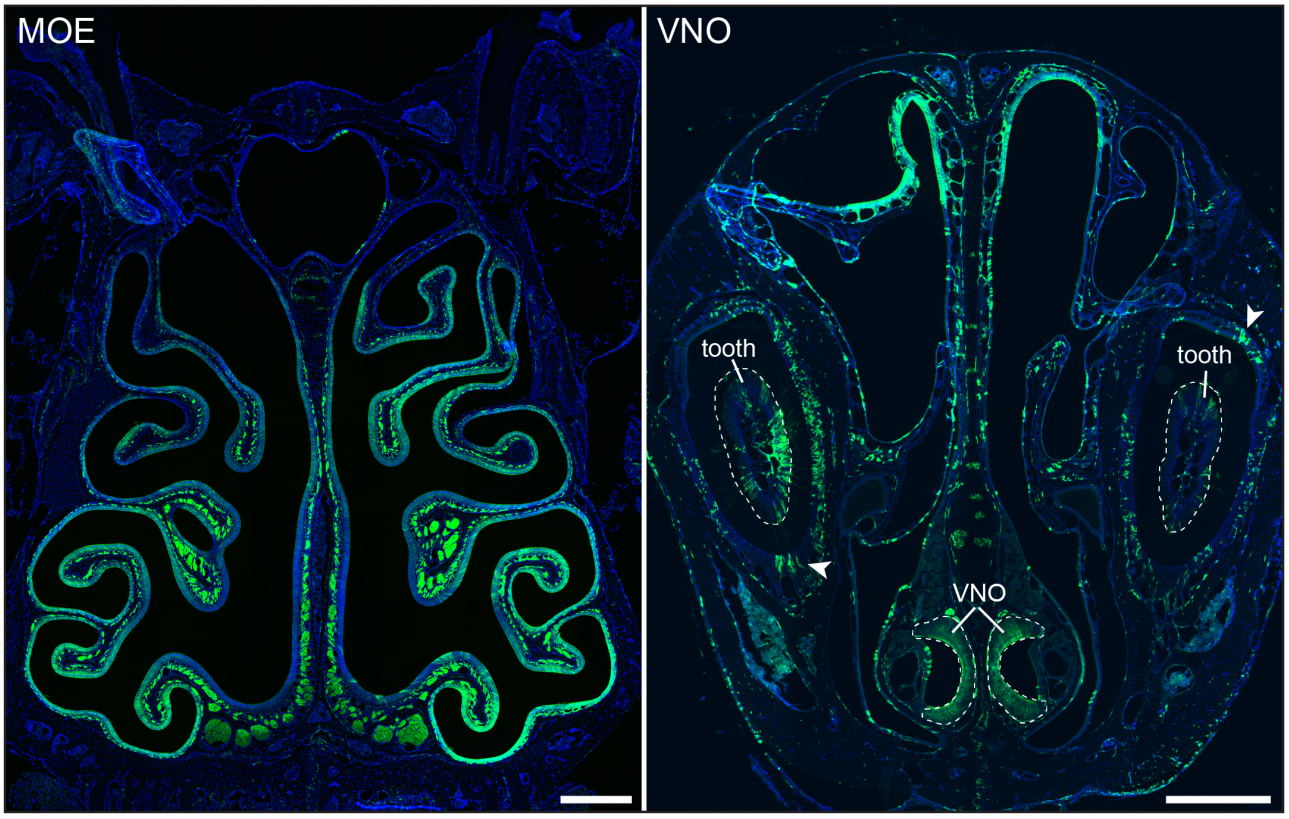

Figure 58: TRPML3 is expressed in olfactory sensory neurons. In the MOE, the vast majority of OSNs were expressing τGFP in the TRPML3 reporter mouse. A subset of VSNs were found τGFP+. Reporter gene expression was observed in teeth and in a small fraction of enamel secreting cell. Mucus secreting cells in the olfactory tissue were also positive for the reporter gene. Nuclearstain in blue. Scalebars: 500 μm.

Table 14: Summary of τGFP expression in the embryonic E13.5 brain of ArIC/eR26-τGFP animals. + for fibers. +: very few.

E13.5	female (n = 4)	male (n = 5)	p-value
Structure	τGFP+	τGFP+	
stria terminalis	23.13 ± 6.15	17.50 ± 4.18	n.s. (0.4564)
medial preoptic area	48.75 ± 14.88 (+)	46.00 ± 5.58 (+)	n.s. (0.8551)

Table 15: Summary of τGFP expression in the embryonic E16.5 brain of ArIC/eR26-τGFP animals. + for fibers. +: very few, ++: moderate dense, +++: dense, ++++: very dense.

E16.5	female (n = 3)	male (n = 3)	p-value
Structure	τGFP+	τGFP+	
cortical amygdaloid nucleus	150.83 ± 3.00 (+)	125.00 ± 19.93 (+)	n.s. (0.2693)
medial amygdaloid nucleus	839.25 ± 83.33 (++++)	1047.50 ± 88.80 (++++)	n.s. (0.1490)

continued on next page

continued from previous page

E16.5	female (n = 3)	male (n = 3)	p-value
Structure	τGFP+	τGFP+	
optic tract	379.25 ± 61.00 (+++)	471.75 ± 72.25 (+++)	n.s. (0.3807)
stria terminalis	279.25 ± 27.63 (++++)	388.75 ± 69.88 (++++)	n.s. (0.2185)
bed nucleus of stria terminalis	165.83 ± 30.33 (++)	284.50 ± 41.10 (++)	n.s. (0.0807)
lateral preoptic area	33.33 ± 9.60 (+)	45.83 ± 5.43 (+)	n.s. (0.3205)
lateral hypothalamic area	37.50 ± 17.50 (+)	24.18 ± 9.03 (+)	n.s. (0.5354)
medial tuberal nucleus	62.50 ± 20.48 (+)	65.43 ± 12.35 (+)	n.s. (0.9087)
medial preoptic area	996.75 ± 70.25 (+++)	1070.75 ± 178.00 (+++)	n.s. (0.7181)
dorsomedial nucleus	216.68 ± 12.24 (++)	105.43 ± 9.80 (++)	* (0.0258)
ventromedial nucleus	78.33 ± 44.73 (++)	144.58 ± 15.68 (++)	n.s. (0.2347)
paraventricular nucleus	95.83 ± 18.18 (++)	± 11.73 (++)	n.s. (0.0872)

Table 16: Summary of τGFP expression in the embryonic E18.5 brain of ArIC/eR26-τGFP animals. + for fibers. +: very few, ++: moderate dense, +++: dense, ++++: very dense.

E18.5	female (n = 3)	male (n = 3)	p-value
Structure	τGFP+	τGFP+	
amygdalo hippocampal area	150.00 ± 45.08 (+)	135.83 ± 39.33 (+)	n.s. (0.8244)
cortical amygdaloid nucleus	73.33 ± 48.65 (+)	110.00 ± 7.10 (++)	n.s. (0.4973)
medial amygdaloid nucleus	1075.00 ± 217.38 (++++)	1060.75 ± 103.30 (++++)	n.s. (0.9559)
optic tract	279.25 ± 64.33 (+++)	416.75 ± 41.68 (+++)	n.s. (0.1471)
stria terminalis	754.25 ± 123.53 (++++)	435.75 ± 86.23 (++++)	n.s. (0.1021)
bed nucleus of stria terminalis	274.25 ± 41.58 (+++)	308.75 ± 15.63 (+++)	n.s. (0.5388)
lateral preoptic area	123.33 ± 68.83 (+)	55.83 ± 6.48 (+)	n.s. (0.3842)
lateral hypothalamic area	81.68 ± 13.10 (+)	43.75 ± 11.63 (+)	n.s. (0.0962)
medial tuberal nucleus	85.83 ± 22.38 (+)	107.93 ± 9.85 (+)	n.s. (0.4175)
medial preoptic area	2885.00 ± 132.18 (+++)	2745.00 ± 123.50 (+++)	n.s. (0.4187)
dorsomedial nucleus	359.25 ± 13.10 (+++)	214.18 ± 44.05 (+++)	* (0.0344)
ventromedial nucleus	234.18 ± 29.48 (+++)	177.08 ± 2.20 (+++)	n.s. (0.1257)

continued on next page

continued from previous page

E18.5	female (n = 3)	male (n = 3)	p-value
Structure	τGFP+	τGFP+	
paraventricular nucleus	282.50 ± 76.65 (+++)	145.00 ± 59.80 (+++)	n.s. (0.2302)

Table 17: Summary of τGFP expression in the P0 brain of ArIC/eR26-τGFP animals. + for fibers. +: very few, ++: moderate dense, +++: dense, ++++: very dense.

P0	female (n = 3)	male (n = 4)	p-value
Structure	τGFP+	τGFP+	
accumbens nucleus, shell	31.66 ± 15.70 (+)	25.63 ± 9.55 (+)	n.s. (0.7923)
bed nucleus of stria terminalis			
medial division, anterior part	54.18 ± 10.65 (+++)	58.75 ± 19.28 (+++)	n.s. (0.8588)
medial division, ventral part	26.68 ± 15.90 (+)	17.50 ± 10.00 (+)	n.s. (0.6284)
medial division, posteromedial part	920.00 ± 34.60 (++++)	627.25 ± 101.95 (++++)	n.s. (0.0931)
medial division, posterior part	192.50 ± 82.70 (+++)	243.45 ± 73.68 (+++)	n.s. (0.4749)
posterointermediate part	0.00 ± 0.00 (++++)	0.00 ± 0.00 (++++)	
supracapsular part	0.00 ± 0.00 (++++)	0.00 ± 0.00 (++++)	
anteroventral periventricular nucleus	99.18 ± 34.23 (+)	123.13 ± 42.63 (+)	n.s. (0.6967)
median preoptic area	50.00 ± 9.03 (+)	39.08 ± 4.55 (+)	n.s. (0.2908)
medial preoptic nucleus			
medial part	1040.00 ± 161.45 (+++)	625.75 ± 109.93 (+++)	n.s. (0.1200)
lateral part	73.33 ± 16.23 (++)	63.45 ± 24.28 (++)	n.s. (0.7680)
medial preoptic area	120.83 ± 25.50 (++)	60.95 ± 4.60 (++)	* (0.0418)
ventromedial nucleus	77.50 ± 17.50 (++)	121.25 ± 33.43 (++)	n.s. (0.3471)
paraventricular hypothalamic nucleus			
anterior parvicellular part	523.30 ± 80.43 (+++)	360.75 ± 61.08 (+++)	n.s. (0.1521)
medial parvicellular part	60.00 ± 34.65 (++)	97.20 ± 22.53 (++)	n.s. (0.3883)

continued on next page

continued from previous page

P0	female (n = 3)	male (n = 4)	p-value
Structure	τGFP+	τGFP+	
anterior hypothalamic area			
central	0.00 ± 0.00 (++)	0.00 ± 0.00 (++)	
anterior	0.00 ± 0.00 (++)	0.00 ± 0.00 (++)	
caudate putamen (striatum)	89.18 ± 56.75 (+)	99.08 ± 43.20 (+)	n.s. (0.8928)
internal capsule	119.18 ± 53.08 (+)	103.13 ± 52.43 (+)	n.s. (0.8417)
medial amygdaloid nucleus			
anterior dorsal part	273.25 ± 48.68 (+)	264.00 ± 52.90 (+)	n.s. (0.9147)
anteroventral part	55.00 ± 46.40 (+)	94.38 ± 23.55 (+)	n.s. (0.4474)
posterodorsal part	1559.25 ± 272.50 (++++)	1047.50 ± 194.45 (++++)	n.s. (0.1747)
posteroventral part	307.50 ± 48.88 (++)	320.25 ± 30.55 (++)	n.s. (0.8237)
dorsomedial hypothalamic nucleus	861.75 ± 63.15 (+++)	667.00 ± 115.95 (+++)	n.s. (0.3032)
arcuate hypothalamic nucleus	0.00 ± 0.00	175.95 ± 64.13 (+)	
penduncular part of lateral hypothalamus	32.50 ± 20.05 (+)	82.83 ± 37.10 (+)	n.s. (0.5857)
medial tuberal nucleus	97.50 ± 12.58 (++)	124.08 ± 34.13 (++)	n.s. (0.5524)
amygdalohippocampal area			
anterolateral part	28.33 ± 18.28 (+)	33.13 ± 7.85 (+)	n.s. (0.7995)
posteromedial part	76.68 ± 12.45 (+)	49.70 ± 7.15 (+)	n.s. (0.1055)
posteromedial cortical amygdaloid nucleus	110.00 ± 63.75 (+)	82.20 ± 16.73 (+)	n.s. (0.5816)

Table 18: Summary of τGFP and ERα double positive neurons in the E13.5 brain of ArIC/eR26-τGFP animals.

E13.5	female (n = 4)	male (n = 5)	p-value
Structure	τGFP+/ERα+	τGFP+/ERα+	
stria terminalis	0.00 ± 0.00	0.00 ± 0.00	
medial preoptic area	0.00 ± 0.00	0.00 ± 0.00	

Table 19: Summary of τGFP and ERα double positive neurons when compared to the toal number of τGFP neurons in the E13.5 brain of ArIC/eR26-τGFP animals.

E13.5	female (n = 4)	male (n = 5)	p-value
Structure	(τGFP+/ERα+)/τGFP only	(τGFP+/ERα+)/τGFP only	
stria terminalis	0.00 ± 0.00	0.00 ± 0.00	
medial preoptic area	0.00 ± 0.00	0.00 ± 0.00	

Table 20: Summary of τGFP and ERα double positive neurons in the E16.5 brain of ArIC/eR26-τGFP animals.

E16.5	female (n = 3)	male (n = 3)	p-value
Structure	τGFP+/ERα+	τGFP+/ERα+	
cortical amygdaloid nucleus	3.33 ± 0.83	5.00 ± 0.00	
medial amygdaloid nucleus	215.00 ± 32.63	180.00 ± 36.08	n.s. (0.5117)
optic tract	95.00 ± 22.40	117.50 ± 54.15	n.s. (0.7205)
stria terminalis	58.33 ± 7.95	60.00 ± 2.90	n.s. (0.8534)
bed nucleus of stria terminalis	15.83 ± 7.28	25.83 ± 3.00	n.s. (0.2723)
lateral preoptic area	0.00 ± 0.00	1.68 ± 1.68	
lateral hypothalamic area	0.00 ± 0.00	0.00 ± 0.00	
medial tuberal nucleus	25.68 ± 6.83	37.50 ± 9.48	n.s. (0.4057)
medial preoptic area	75.83 ± 13.65	120.00 ± 3.90	* (0.0339)
dorsomedial nucleus	0.83 ± 0.83	4.18 ± 3.00	n.s. (0.6453)
ventromedial nucleus	0.00 ± 0.00	0.83 ± 0.83	
paraventricular nucleus	0.83 ± 0.83	0.83 ± 0.83	n.s. (1.0000)

Table 21: Summary of τGFP and ERα double positive neurons when compared to the toal number of τGFP neurons in the E16.5 brain of ArIC/eR26-τGFP animals.

E16.5	female (n = 3)	male (n = 3)	p-value
Structure	(τGFP+/ERα+)/τGFP only	(τGFP+/ERα+)/τGFP only	
cortical amygdaloid nucleus	3.32% ± 0.07%	3.70% ± 1.52%	n.s. (0.8167)
medial amygdaloid nucleus	25.38% ± 1.24%	18.70% ± 2.37%	n.s. (0.0672)
optic tract	24.41% ± 2.23%	23.50% ± 5.90%	n.s. (0.8919)
stria terminalis	21.26% ± 2.11%	17.25% ± 1.90%	n.s. (0.2298)
bed nucleus of stria terminalis	8.90% ± 4.12%	10.86% ± 2.22%	n.s. (0.6962)
lateral preoptic area	0.00% ± 0.00%	0.00% ± 0.00%	
lateral hypothalamic area	0.00% ± 0.00%	0.00% ± 0.00%	
medial tuberal nucleus	44.67% ± 3.17%	57.09% ± 11.96%	n.s. (0.3721)
medial preoptic area	7.57% ± 3.17%	11.37% ± 1.58%	n.s. (0.1162)
dorsomedial nucleus	0.00% ± 0.00%	0.00% ± 0.00%	
ventromedial nucleus	0.00% ± 0.00%	0.00% ± 0.00%	
paraventricular nucleus	0.00% ± 0.00%	0.00% ± 0.00%	

Table 22: Summary of τGFP and ERα double positive neurons in the E18.5 brain of ArIC/eR26-τGFP animals.

E18.5	female (n = 3)	male (n = 3)	p-value
Structure	τGFP+/ERα+	τGFP+/ERα+	
amygdalo hippocampal area	5.83 ± 0.83	10.83 ± 1.35	n.s. (0.1012)
cortical amygdaloid nucleus	0.00 ± 0.00	5.83 ± 0.83	
medial amygdaloid nucleus	260.75 ± 52.48	196.68 ± 40.45	n.s. (0.3876)
optic tract	100.00 ± 34.65	115.83 ± 6.50	n.s. (0.6765)
stria terminalis	249.18 ± 12.45	109.18 ± 13.73	* (0.0293)
bed nucleus of stria terminalis	44.18 ± 12.45	60.00 ± 12.83	n.s. (0.4257)
lateral preoptic area	0.00 ± 0.00	0.00 ± 0.00	

continued on next page

continued from previous page

E18.5	female (n = 3)	male (n = 3)	p-value
Structure	τGFP+/ERα+	τGFP+/ERα+	
lateral hypothalamic area	5.83 ± 3.00	0.00 ± 0.00	
medial tuberal nucleus	44.18 ± 9.60	68.33 ± 9.40	n.s. (0.1465)
medial preoptic area	365.00 ± 44.23	270.75 ± 18.85	n.s. (0.1217)
dorsomedial nucleus	7.50 ± 1.45	0.00 ± 0.00	
ventromedial nucleus	16.68 ± 7.95	5.00 ± 1.45	n.s. (0.2222)
paraventricular nucleus	6.68 ± 3.63	0.00 ± 0.00	

Table 23: Summary of τGFP and ERα double positive neurons when compared to the toal number of τGFP neurons in the E18.5 brain of ArIC/eR26-τGFP animals.

E18.5	female (n = 3)	male (n = 3)	p-value
Structure	(τGFP+/ERα+)/τGFP only	(τGFP+/ERα+)/τGFP only	
amygdalo hippocampal area	5.74% ± 3.14%	9.39% ± 2.16%	n.s. (0.3917)
cortical amygdaloid nucleus	0.00% ± 0.00%	5.24% ± 0.36%	
medial amygdaloid nucleus	24.69% ± 2.12%	19.14% ± 3.35%	n.s. (0.2348)
optic tract	32.18% ± 8.72%	21.00% ± 1.52%	n.s. (0.2532)
stria terminalis	34.19% ± 3.14%	26.65% ± 4.53%	n.s. (0.2434)
bed nucleus of stria terminalis	15.53% ± 1.67%	22.13% ± 3.73%	n.s. (0.1818)
lateral preoptic area	1.32% ± 1.32%	0.00% ± 0.00%	
lateral hypothalamic area	6.55% ± 3.29%	4.17% ± 4.17%	n.s. (0.6758)
medial tuberal nucleus	52.80% ± 5.13%	59.80% ± 5.13%	n.s. (0.2464)
medial preoptic area	12.66% ± 1.41%	9.57% ± 1.51%	n.s. (0.2099)
dorsomedial nucleus	1.78% ± 0.89%	0.22% ± 0.22%	n.s. (0.1649)
ventromedial nucleus	8.09% ± 4.14%	3.88% ± 1.85%	n.s. (0.4049)
paraventricular nucleus	3.15% ± 1.65%	0.00% ± 0.00%	

Table 24: Summary of τGFP and ERα double positive neurons in the P0 brain of ArIC/eR26-τGFP animals.

P0	female (n = 3)	male (n = 3)	p-value
Structure	τGFP+/ERα+	τGFP+/ERα+	
accumbens nucleus, shell	0.00 ± 0.00	0.00 ± 0.00	
bed nucleus of stria terminalis			
medial division, anterior part	2.50 ± 1.45	0.63 ± 0.63	n.s. (0.8513)
medial division, ventral part	0.00 ± 0.00	0.00 ± 0.00	
medial division, posteromedial part	236.68 ± 41.78	16.88 ± 9.10	** (0.0018)
medial division, posterior part	13.33 ± 13.33	3.75 ± 2.40	n.s. (0.5385)
posterointermediate part	0.00 ± 0.00	0.00 ± 0.00	
supracapsular part	0.00 ± 0.00	0.00 ± 0.00	
anteroventral periventricular nucleus	25.83 ± 18.40	29.38 ± 7.80	n.s. (0.8513)
median preoptic area	0.00 ± 0.00	0.00 ± 0.00	
medial preoptic nucleus			
medial part	93.33 ± 36.25	58.75 ± 22.58	n.s. (0.4312)
lateral part	8.33 ± 2.20	11.25 ± 5.83	n.s. (0.6993)
medial preoptic area	15.00 ± 10.40	3.13 ± 1.88	n.s. (0.2436)
ventromedial nucleus	5.83 ± 5.83	8.75 ± 3.40	n.s. (0.1874)
paraventricular hypothalamic nucleus			
anterior parvicellular part	15.00 ± 12.58	10.00 ± 2.50	n.s. (0.3048)
medial parvicellular part	0.00 ± 0.00	0.00 ± 0.00	
anterior hypothalamic area			
central	0.00 ± 0.00	0.00 ± 0.00	
anterior	0.00 ± 0.00	0.00 ± 0.00	
caudate putamen (striatum)	0.00 ± 0.00	0.00 ± 0.00	
internal capsule	1.68 ± 1.68	0.00 ± 0.00	

continued on next page

continued from previous page

P0	female (n = 3)	male (n = 3)	p-value
Structure	τGFP+/ERα+	τGFP+/ERα+	
medial amygdaloid nucleus			
anterior dorsal part	4.18 ± 0.83	10.00 ± 2.18	n.s. (0.8814)
anteroventral part	1.68 ± 0.83	7.50 ± 1.88	n.s. (0.9321)
posterodorsal part	670.75 ± 180.55	127.50 ± 56.60	* (0.0218)
posteroventral part	19.18 ± 2.20	23.75 ± 6.95	n.s. (0.6104)
dorsomedial hypothalamic nucleus	41.68 ± 14.23	15.63 ± 13.18	n.s. (0.3262)
arcuate hypothalamic nucleus	0.00 ± 0.00	88.13 ± 37.23	
penduncular part of lateral hypothalamus	6.70 ± 4.40	44.38 ± 19.18	n.s. (0.1620)
medial tuberal nucleus	65.00 ± 6.28	59.38 ± 15.30	n.s. (0.7773)
amygdalohippocampal area			
anterolateral part	2.50 ± 1.45	6.25 ± 2.98	n.s. (0.3599)
posteromedial part	15.00 ± 9.48	3.13 ± 1.20	n.s. (0.1999)
posteromedial cortical amygdaloid nucleus	10.00 ± 2.50	2.50 ± 1.45	* (0.0390)

Table 25: Summary of τGFP and ERα double positive neurons when compared to the toal number of τGFP neurons in the P0 brain of ArIC/eR26-τGFP animals.

P0	female (n = 3)	male (n = 3)	p-value
Structure	(τGFP+/ERα+)/τGFP only	(τGFP+/ERα+)/τGFP only	
medial division, anterior part	5.28% ± 3.74%	1.67% ± 1.67%	n.s. (0.3737)
medial division, ventral part	0.00% ± 0.00%	0.00% ± 0.00%	
medial division, posteromedial part	26.64% ± 4.14%	3.81% ± 2.23%	** (0.0034)
medial division, posterior part	6.93% ± 6.93%	2.02% ± 1.35%	n.s. (0.4517)
posterointermediate part	0.00% ± 0.00%	0.00% ± 0.00%	
supracapsular part	0.00% ± 0.00%	0.00% ± 0.00%	

continued on next page

continued from previous page

P0	female (n = 3)	male (n = 3)	p-value
Structure	(τGFP+/ERα+)/τGFP only	(τGFP+/ERα+)/τGFP only	
anteroventral periventricular nucleus	31.58% ± 19.72%	39.17% ± 10.17%	n.s. (0.7523)
median preoptic area	0.00% ± 0.00%	0.00% ± 0.00%	
medial preoptic nucleus			
medial part	9.90% ± 4.98%	9.81% ± 2.91%	n.s. (0.9863)
lateral part	11.32% ± 1.02%	22.86% ± 13.06%	n.s. (0.4896)
medial preoptic area	10.41% ± 7.33%	3.52% ± 2.05%	n.s. (0.3440)
ventromedial nucleus	7.67% ± 3.84%	19.31% ± 4.87%	n.s. (0.1382)
paraventricular hypothalamic nucleus			
anterior parvicellular part	2.67% ± 2.02%	2.56% ± 2.56%	n.s. (0.9444)
medial parvicellular part	0.00% ± 0.00%	0.00% ± 0.00%	
anterior hypothalamic area			
central	0.00% ± 0.00%	0.00% ± 0.00%	
anterior	0.00% ± 0.00%	0.00% ± 0.00%	
caudate putamen (striatum)	0.00% ± 0.00%	0.00% ± 0.00%	
internal capsule	1.71% ± 1.71%	0.00% ± 0.00%	
medial amygdaloid nucleus			
anterior dorsal part	1.55% ± 0.30%	0.99% ± 0.44%	n.s. (0.3718)
anteroventral part	33.90% ± 33.05%	1.03% ± 1.03%	n.s. (0.2884)
posterodorsal part	43.83% ± 8.66%	9.52% ± 3.13%	** (0.0084)
posteroventral part	6.72% ± 1.56%	7.13% ± 2.04%	n.s. (0.8880)
dorsomedial hypothalamic nucleus	5.13% ± 2.52%	2.44% ± 2.01%	n.s. (0.4347)
arcuate hypothalamic nucleus	0.00% ± 0.00%	40.83% ± 4.81%	
penduncular part of lateral hypothalamus	23.56% ± 14.51%	46.33% ± 5.50%	n.s. (0.1591)
medial tuberal nucleus	67.61% ± 6.33%	57.39% ± 3.53%	n.s. (0.1902)

continued on next page

continued from previous page

P0	female (n = 3)	male (n = 3)	p-value
Structure	(τGFP+/ERα+)/τGFP only	(τGFP+/ERα+)/τGFP only	
amygdalohippocampal area			
anterolateral part	6.37% ± 3.31%	16.35% ± 9.06%	n.s. (0.4091)
posteromedial part	16.58% ± 9.39%	7.56% ± 3.45%	n.s. (0.3551)
posteromedial cortical amygdaloid nucleus	11.80% ± 4.59%	2.66% ± 1.60%	n.s. (0.0856)

7 Abbreviations

ACTH adrenocorticotropin

Arc Arcuate nucleus

AVP arginine-vasopressin

AVPV anteroventral periventricular nucleus

BBB blood brain barrier

CNO Clozapine N-oxide

CNS central nervous system

CRH corticotropin-releasing hormone

CSF cerebrospinal fluid

DAG diacylglycerol

DREADD designer receptor exclusively activated by designer drug

DT diphtheria toxin

DTA diphtheria toxin A

E embryonic day

ER oestrogen receptor

ERE oestrogen response element

FSH follicle-stimulating hormone

GH growth hormone

GnRH gonadotropin-releasing hormone

GPCR G-protein coupled receptor

hpg-axis hypothalamic-pituitary-gonadal axis

IP3 inositol-1,4,5-triphosphate

LH luteinizing hormone

ME median eminence

OSNs olfactory sensory neurons

OXT oxytocin

P postnatal day

PIP2 phosphatidylinositol 4,5-biphosphate

PVN paraventricular nucleus

SST somatostatin

TH tyrosin hydroxylase

TRH thyrotropin-releasing hormone

TRP transient receptor potential

TSH thyroid-stimulating hormone

VSNs vomeronasal sensory neurons

8 List of Figures

9 List of Tables

10 Acknowledgements

My deepest gratitude goes to Prof. Ulrich Boehm for giving me the opportunity to work in his research group and for his constant support and guidance from the beginning until the end of my PhD.

I would like to thank Prof. Frank Kirchhoff for being the second supervisor of this thesis.

I am thankful to be able to collaborate with different scientist during my PhD. Dr. Imre Farkas and Prof. Erik Hrabovszky from Hungary, Dr. Paolo Giacobini and Gaetan Ternier from France, Anna Erbacher and Barbara Spix from Munich and multiple people from Homburg. I want to thank especially Dr. Claudia-Fecher Trost and Femke Lux for their work on the TRPV6 mapping together with me and the lab of Prof. Veit Flockerzi for helping me out so many times during my PhD. Prof. Krasteva-Christ for guiding me during the start of the organ mapping and always helping me with my anatomy questions. My special thanks go to Barbara Wardas for being a great friend and also for being able to discuss our projects and non-scientific topics during my PhD.

I thank all members of the animal facility of Dr. Petra Weißgerber. Tanja, Tom, Nadine, Johannes, Miriam, Jaqueline and all other animal care takers for taking care of our animals and also for all their effort. Thank you all very, very much.

I also want to thank Martin and Kathrin for their technical support and always fixing all the small and big things around the lab.

I am also deeply thankful to all present and former members of AG Boehm. Devesh and Soumya taught me everything when I first joined the lab. Roberto, Vicky, Qiao, Mike, Sarah, Igor, Qiang, Deb, Mari, Amanda and Mona, thank you all for making the lab such a great place to work in.

I need to thank especially thank Amanda and Mona for their technical support and their work they do for the lab.

My special thanks go to Qiao Sen and Kai Busch for not only being great friends, helping by just being there and listening to me. Thank you so much!

Without the constant help and patience of my parents nothing would have been possible. I am deeply thankful to have them.

Finally, I thank my wife Sandra. Without her constant encouragement this work would not have been completed.

11 Publications

1. **Wartenberg, P.**; Farkas, I.; Csillag, V.; Shah, N.; Colledge, W. H.; Hrabovszky, E. & Boehm, U. (2021) Neurosteroid synthesis by aromatase neurons regulates neuronal activity in the developing murine brain. *Submitted.*

2. **Wartenberg, P.**[*]; Lux, F.[*]; Busch, K.; Boehm, U. & Weißgerber, P. (2021) A TRPV6 atlas for the mouse. *Submitted.*

3. Yu, Q.[*]; Gamayun, I.[*]; **Wartenberg, P.**; Zhang, Q.; Qiao, S.; Kusumakshi, S.; Candlish, S.; Götz, V.; Wen, S.; Ternier, G.; Philipp, S.; Giacobini, P.; Ciofi, P.; Müller, T. D. & Boehm, U. (2021). Bitter taste cells in the ventricular walls of the brain modulate energy homeostasis. *In preparation.*

4. Spix, B.; Butz, E. S.; Chen C.; Plesch E.; **Wartenberg, P.**; Rosato, A. S.; Arlt, E.; Briukhovetska D.; Jeridi, A.; Wyatt, A.; Kissing, S.; Teupser, D.; Holdt, L. M.; Boehm, U.; Garcia-Anoveros, J.; Saftig, P.; Schiller, H. B.; Kobold, S.; Boekhoff, I.; Zierler, S.; Wahl-Schott, C.; Gudermann, T.; Bracher, F.; Yildirim A.; Biel, M. & Grimm C. (2021) Impaired MMP-12 clearance and emphysema-like phenotype in mucolipin 3 deficient mice. *Under review.*

5. Bernal, L.; Sotelo-Hitschfeld, P.; König, C.; Sinica, V.; Wyatt, A.; Winter, Z.; Hein, A.; Touska, F.; Reinhardt, S.; Tragl, A.; Kusuda, R.; **Wartenberg, P.**; Sclaroff, A.; Pfeifer, J.; Ectors, F.; Dahl, A.; Freichel, M.; Vlachova, V.; Brauchi, S.; Roza, C.; Boehm, U.; Clapham, D. E.; Lennerz, J. K. & Katharina, Z. (2021). Odontoblast TRPC5 Channels Signal Cold Pain in Teeth. *Science Advances, in press.*

6. Toufaily, C.; Schang, G.; Zhou, X.; **Wartenberg, P.**; Boehm, U.; Lydon, J. P.; Roelfsema, F. & Bernard, D. J. (2020). Impaired LH surge amplitude in gonadotrope-specific progesterone receptor knockout mice. *The Journal of Endocrinology*, *244*, 111-122

7. Aoki, M.; **Wartenberg, P.**; Grünewald, R.; Phillipps, H. R.; Wyatt, A.; Grattan, D. R. & Boehm, U. (2019). Widespread Cell-Specific Prolactin Receptor Expression in Multiple Murine Organs. *Endocrinology, 160*, 2587-2599.

8. Kaiser, E.; Tian, Q.; Wagner, M.; Barth, M.; Xian, W.; Schröder, L.; Ruppenthal, S.; Kaestner, L.; Boehm, U.; **Wartenberg, P.**; Lu, H.; McMillin, S. M.; Bone, D. B. J.; Wess, J. & Lipp, P. (2019). DREADD technology reveals major impact of Gq signalling on cardiac electrophysiology. *Cardiovascular Research, 115*, 1052-1066

9. Candlish, M.; **Wartenberg, P.** & Boehm, U. (2018). Genetic Strategies Examining Kisspeptin Regulation of GnRH Neurons. *The GnRH Neuron and its Control (chapter 11), John Wiley and Sons, Ltd*, 259-287.

10. Wyatt, A.*; **Wartenberg, P***.; Candlish, M.; Krasteva-Christ, G.; Flockerzi, V. & Boehm, U. (2017). Genetic strategies to analyze primary TRP channel-expressing cells in mice. *Cell Calcium, 67*, 91-104.

[*] = contributed equally

12 Curriculum Vitae

For data protection reasons, the curriculum vitae is not published in the electronic version of the dissertation.